



Technische Universität München

Lehrstuhl für Entwicklungsgenetik

Pathogenic Mutation of *Lrrk2* – a mouse model for
pre-motor Parkinson's disease

Florian H. H. Giesert

Vollständiger Abdruck der von der Fakultät Wissenschaftszentrum
Weihenstephan für Ernährung, Landnutzung und Umwelt der Technischen
Universität München zur Erlangung des akademischen Grades eines

Doktors der Naturwissenschaften

genehmigten Dissertation.

Vorsitzender: Univ.-Prof. Dr. K. Schneitz
Prüfer der Dissertation: 1. Univ.-Prof. Dr. W. Wurst
2. Univ.-Prof. Dr. A. Kapurniotu

Die Dissertation wurde am 24.10.2011 bei der Technischen Universität München eingereicht und durch die Fakultät Wissenschaftszentrum Weihenstephan für Ernährung, Landnutzung und Umwelt am 27.02.2012 angenommen.

1 Table of contents

1	TABLE OF CONTENTS	I
2	ABSTRACT / ZUSAMMENFASSUNG	1
3	INTRODUCTION	4
3.1	Parkinson's Disease	4
3.1.1	The characteristics of Parkinson's Disease	4
3.1.2	The basal ganglia circuit	5
3.2	The genetic aspects of Parkinson's Disease	9
3.3	Common pathways in Parkinson's disease	11
3.4	PARK8: <i>Lrrk2</i> – the Leucine-rich repeat kinase 2	12
3.4.1	The structure of the <i>Lrrk2</i> gene and its protein	13
3.4.2	The genetic basis of <i>Lrrk2</i> -linked PD	17
3.4.3	What is known about the function of LRRK2?	20
3.5	Mouse models for Parkinson's Disease	22
3.5.1	Genetic rodent models of PD	23
3.5.2	Mouse models of <i>LRRK2</i> -linked PD.....	24
4	AIM OF THE STUDY	27
5	RESULTS	28
5.1	Comparative Expression Analysis of <i>Lrrk1</i> and <i>Lrrk2</i>	28
5.1.1	Expression during embryonic development	28
5.1.2	Expression in the postnatal and adult brain	33
5.1.3	LRRK2 protein expression in the adult CNS	37
5.1.4	<i>Lrrk2</i> -expressing neuronal subtypes in the striatum	40
5.2	Generation of the <i>Lrrk2</i> R1441C knock-in mouse line	41
5.2.1	The <i>Lrrk2</i> R1441C knock-in targeting strategy	42
5.2.2	Generation of <i>Lrrk2</i> R1441C transgenic ES cells	43
5.2.3	Generation of the <i>Lrrk2</i> R1441C knock-in mouse line	45
5.3	The <i>Lrrk2</i> knockdown mouse line	46
5.4	Functional analysis of the Leucine-rich repeat kinase 2	48
5.4.1	Analysis of <i>Lrrk2</i> R1441C mouse embryonic fibroblasts	48
5.4.2	The cytoskeleton in <i>Lrrk2</i> R1441C cells.....	50
5.4.2.1	Basal stability of the cytoskeleton network.....	51
5.4.2.2	Neurite outgrowth in R1441C neurons	52
5.4.2.3	Tubulin hyperacetylation in R1441C neurons can be further enhanced by HDAC-6 inhibition	60
5.4.2.4	LRRK2 and the cold-stability of the microtubular network	62

5.4.3	LRRK2 function at the synapse.....	64
5.4.3.1	LRRK2 protein colocalizes with NSF in synaptosomes	64
5.4.3.2	Synaptic function: Exocytosis and endocytosis cycles in R1441C neurons .	66
5.5	The morphological analysis of the <i>Lrrk2</i> R1441C line.....	69
5.5.1	The development of the CNS in <i>Lrrk2</i> R1441C mice.....	69
5.5.2	Pathology of mid-aged <i>Lrrk2</i> R1441C mice	71
5.5.3	Pathology of fully aged <i>Lrrk2</i> R1441C mice.....	73
5.6	Behavioural analysis.....	76
5.6.1	Analysis of young <i>Lrrk2</i> R1441C and <i>Lrrk2</i> knockdown mice	76
5.6.1.1	Motor behaviour of the <i>Lrrk2</i> mouse lines	77
5.6.1.2	Cognition and memory in the <i>Lrrk2</i> mouse lines	79
5.6.1.3	Depression- and anxiety-like behaviour	81
5.6.2	Odour discrimination in aged <i>Lrrk2</i> R1441C and <i>Lrrk2</i> knockdown mice.....	84
5.6.3	Gait analysis of aged <i>Lrrk2</i> R1441C and <i>Lrrk2</i> knockdown mice	87
6	DISCUSSION	91
6.1	Analysis of <i>Lrrk1</i> and <i>Lrrk2</i> expression	91
6.1.1	Expression during embryogenesis	91
6.1.2	<i>Lrrk2</i> mRNA expression in the adult CNS.....	93
6.1.3	LRRK2 protein expression in the adult CNS	96
6.1.4	<i>Lrrk2</i> expression in the adult striatum	98
6.2	Generation of the <i>Lrrk2</i> R1441C knock-in mouse model	101
6.3	Functional analysis	102
6.4	Dopaminergic system, histological analysis.....	112
6.5	Behavioural analysis.....	115
6.6	Concluding remarks.....	122
7	MATERIALS AND METHODS	125
7.1	Materials	125
7.1.1	Chemicals.....	125
7.1.2	Enzymes.....	128
7.1.3	Commercial kits.....	128
7.1.4	Solutions.....	129
7.1.5	Instrumentation.....	133
7.1.6	Antibodies.....	135
7.2	Methods	136
7.2.1	Methods in Molecular biology.....	136
7.2.1.1	General methods working with DNA	136
7.2.1.2	General methods working with RNA	138
7.2.1.3	General methods working with bacteria	139
7.2.1.4	The polymerase chain reaction	139
7.2.1.5	Southern blot analysis	142
7.2.1.6	Western blot analysis	144
7.2.1.7	Protein fractionation.....	146
7.2.1.8	HPLC analysis	148
7.2.2	Histological methods	149
7.2.2.1	Perfusion and cutting.....	149
7.2.2.2	<i>In situ</i> hybridisation on paraffin sections (radioactive)	150

7.2.2.3	<i>In situ</i> hybridisation on paraffin sections (DIG-labelled probes).....	153
7.2.2.4	Immunohistochemistry on paraffin sections	155
7.2.2.5	Immunohistochemistry on frozen sections (free floating).....	156
7.2.2.6	Documentation of histological results.....	157
7.2.3	Methods in cell culture	157
7.2.3.1	Mouse embryonic fibroblasts.....	157
7.2.3.2	Primary neuronal cultures from mouse tissue.....	160
7.2.4	Methods in ES cell culture.....	164
7.2.4.1	Embryonic stem cells.....	164
7.2.4.2	Preparation of feeder cells.....	165
7.2.4.3	Splitting of ES cells.....	165
7.2.4.4	Freezing and thawing of ES cells	166
7.2.4.5	Electroporation of ES cells	166
7.2.4.6	Selection of recombinant ES cell clones	167
7.2.4.7	Screening for correctly recombined ES cell clones.....	168
7.2.5	Animal husbandry.....	168
7.2.5.1	Animal facilities.....	168
7.2.5.2	Blastocyst injection and embryo transfer.....	169
7.2.5.3	Establishment of new genetically modified mouse lines	170
7.2.6	Behavioural analysis	170
7.2.6.1	Tail suspension test.....	170
7.2.6.2	Accelerating rotarod	170
7.2.6.3	Forced swim test	171
7.2.6.4	Open field test	171
7.2.6.5	Object recognition test.....	171
7.2.6.6	Social discrimination test.....	172
7.2.6.7	Odour preference test.....	172
7.2.6.8	Odour discrimination test-battery	173
7.2.6.9	Gait analysis.....	174
8	REFERENCES	176
9	APPENDIX	205
9.1	The <i>Lrrk2</i> R1441C Targeting Vector	205
9.2	Primer Sequences	206
9.3	General abbreviations.....	207
9.4	Curriculum vitae.....	209
9.5	Acknowledgments.....	211
10	SELBSTSTÄNDIGKEITSERKLÄRUNG.....	212

2 Abstract / Zusammenfassung

Abstract

The aim of the present study was to create a Parkinson's disease (PD) mouse model for further exploring the aetiology of PD and to get closer insights into the physiological roles of the *Leucine-rich repeat kinase 2 (Lrrk2)*-gene, which is mutated in certain familial forms of PD. We performed a detailed analysis of the murine expression pattern of both *Lrrk2* and its paralog *Lrrk1* in *Mus musculus* on mRNA and protein level. By this we demonstrated, that *Lrrk2* is predominately expressed in the target areas of dopaminergic projection and has no bias to the direct or indirect pathway of the *basal ganglia circuit*. Next we generated a mouse model harbouring the disease-associated point mutation R1441C in the GTPase domain of the endogenous murine *Lrrk2* gene. No overt motor dysfunction or pathological signs of neurodegeneration can be observed both in young and fully aged animals. Nevertheless, on the behavioural level we could identify several alterations reminiscent of pre-motor symptoms observed in PD patients. *Lrrk2* R1441C animals not only show alterations of depression- and anxiety-related behaviour, but also reduced olfaction and subtle gait alterations. Interestingly, also the analysis of a *Lrrk2* knockdown mouse line with almost complete depletion of LRRK2 protein did show nearly identical behavioural alterations.

In addition, we used both mouse models as a resource to investigate the cellular functions of *Lrrk2*. Both *mouse embryonic fibroblasts* (MEF) and primary hippocampal neurons have been utilized in this regard. We could provide hints for a role of the protein in cytoskeleton organisation as well as synaptic transmission, albeit the constitutive expression of pathogenic LRRK2 on an endogenous level seems to be compensated to a large extend. Interestingly on the functional level, altered LRRK2 function in R1441C cells rather leads to opposing trends compared to the *Lrrk2* knockdown situation. Strikingly on the behavioural level both lines performed in a similar manner and did show a high overlap in regard to the identified phenotypes. This indicates that both the dysfunction and loss of LRRK2 alters distinct cellular processes in a contrary way, but the general impairment of these processes

results in a similar dysfunction on the systemic level. In summary, both lines nicely recapitulate early, non-motor symptoms observed in PD patients and can therefore be seen as valid mouse models of presymptomatic Parkinson's disease.

Zusammenfassung

Die Zielsetzung der vorliegenden Arbeit war die Herstellung und Analyse eines Mausmodells der Parkinson'schen-Krankheit -*Morbus Parkinson*- um Aufschlüsse über die Ätiologie dieser Krankheit und über die physiologische Rolle des mit familiären Formen von *Morbus Parkinson* assoziierten Gens *Leucine-rich repeat kinase 2 (Lrrk2)* zu gewinnen. Zunächst untersuchten wir im Detail die Expressionsmuster, sowohl von *Lrrk2*, als auch von seinem Paralog *Lrrk1*, während der Entwicklung und im adulten Gehirn der Maus. Dabei konnten wir zeigen, dass *Lrrk2* überwiegend in den Zielregionen dopaminergischer Projektionen exprimiert wird und gleichermaßen im direkten als auch im indirekten Basalganglien-Signalweg vertreten ist.

Im Weiteren generierten wir ein Mausmodell, welches die in *Morbus Parkinson* Patienten entdeckte Punktmutation R1441C in der GTPase-Domäne des endogenen *Lrrk2*-Gens der Maus enthält. Sowohl in jungen, als auch in hochbetagten Mäusen lassen sich keine offenkundigen Bewegungsstörungen oder pathologischen Zeichen von Neurodegeneration nachweisen. Doch in bestimmten Verhaltensaspekten konnten wir einige Veränderungen bei dieser Mauslinie beobachten, die man als prämotorische Symptome auch bei *Morbus Parkinson* Patienten diagnostiziert. Die *Lrrk2* R1441C Mäuse zeigen nicht nur Änderungen im angst- und depressionsassoziiertem Verhalten, sondern auch einen stark eingeschränkten Geruchssinn und Veränderungen im Gangmuster. Interessanterweise zeigte die Analyse einer *Lrrk2* knockdown Mauslinie, die nahezu kein LRRK2 Protein mehr exprimiert, sehr ähnliche Verhaltensänderungen.

Zusätzlich wurden aus beiden Mausmodellen embryonale Fibroblasten (MEF) und hippocampale Primärneurone gewonnen, um die zellulären Funktionen von *Lrrk2* zu erforschen. Dadurch haben wir Hinweise erhalten, das *Lrrk2* eine

Rolle bei der Organisation des Zytoskeletts, sowie in der synaptischen Signalübertragung spielt. Jedoch scheint die konstitutive Expression von pathogenem *Lrrk2* auf endogenem Level rasch kompensiert zu werden. Im Vergleich beider Linien ist es bemerkenswert, dass auf zellulärem Niveau die Effekte von *Lrrk2* R1441C und dem Verlust des LRRK2-Proteins eher in entgegengesetzte Richtungen tendieren, während sich die Phänotypen im Verhalten der Tiere stark ähneln. Das könnte bedeuten, dass in diesem Fall dieselben zellulären Prozesse auf konträre Art verändert werden, die allgemeine Beeinträchtigung dieser Prozesse aber in ähnlichen Funktionsstörungen auf systemischem Niveau resultieren. Insgesamt rekapitulieren beide Linien frühe, nicht-motorische Symptome, wie man sie bei Patienten diagnostiziert nach, und könne deshalb als funktionierende Mausmodelle für die präsymptomatische Phase von *Morbus Parkinson* angesehen werden.

3 Introduction

3.1 Parkinson's Disease

3.1.1 The characteristics of Parkinson's Disease

Already in the ancient Greece, anatomists like Erasistratos have reported about movement disorders characterized by rigidity and akinesia, but it took more than 2000 years, until James Parkinson in 1817 defined and scientifically described this disease. In his publication "An Essay on the Shaking Palsy", he termed the disorder - *paralysis agitans* (Parkinson, 2002) - which was later on referred to as *Morbus Parkinson* or *Parkinson's disease* (PD). Like Alzheimer's disease (AD) also PD, as the second most common neurodegenerative disorder, is highly age related and therefore becomes more and more a severe and widespread problem in our ageing society. The *Rotterdam study* documented an increased of PD prevalence from 0.3% in the group of 55 to 64 years old participants to 4.3% in the group from 85 to 94 years old participants (de Rijk *et al.*, 1995; de Lau *et al.*, 2005). The mean age of onset is 55 (Dauer and Przedborski, 2003), marked by the appearance of the classical clinical features of PD: tremor at rest, rigidity of the skeletal muscles, bradykinesia (or akinesia) and postural instability (Shulman *et al.*, 1996; Bloem *et al.*, 2001; Berardelli *et al.*, 2001). Besides these main features and some other motor symptoms like postural deformities and sudden freezing during movement, also many non-motor symptoms have been observed in patients: neurobehavioral abnormalities like depression, apathy, anxiety and hallucinations; abnormalities of the vegetative system; sleep disturbance and sensory abnormalities like olfactory dysfunction (Jankovic, 2008). On the pathological level, the major motor-symptoms are caused by the loss of nigrostriatal dopaminergic neurons, whereas the pathoaetiology of the non-motor symptoms is not yet fully understood. The loss of dopaminergic neurons is often but not always accompanied by cytoplasmic protein aggregations or inclusions - the so called *Lewy Bodies* (LBs) - in remaining neurons of the Substantia Nigra pars compacta (SNc) as well as in various other regions of the nervous system (Marsden, 1983; Forno, 1996; Spillantini, 1997, Braak

et al. 2003). Interestingly, this very distinct cytopathological characteristic is not limited to PD but can also be found in disorders like *dementia with Lewy bodies* (DLB) or Alzheimer's disease (Gibb, *et al.* 1989). Besides this, some PD patient's brains show also features of other related disorders. For example neurofibrillary tangles (NFT) composed out of hyper-phosphorylated tau protein (MAPT or microtubule-associated protein Tau), which originally is rather a hallmark for AD and some other neurodegenerative diseases (grouped as tauopathies), can be found (Avila, *et al.* 2004).

Taken together, PD is a very complex and heterogeneous disorder, characterized by miscellaneous clinical and pathological features which partially can also be found in other related neurodegenerative diseases. Since the severe motor symptoms arise relatively late in the course of the disease when already gross parts of the dopaminergic system have been destroyed (Terzioglu and Galter, 2008), an early, presymptomatic diagnosis is still impossible. All these factors do not only hinder the precise diagnosis and classification (Jankovic, 2008), but renders the research about the aetiology of this progressive movement disorder complex and difficult.

3.1.2 The basal ganglia circuit

As already mentioned, the major hallmark of PD is the degeneration of dopaminergic neurons in the substantia nigra pars compacta (SNc) which is located in the ventral part of the midbrain and represents an essential part of the so called *basal ganglia circuit*. The disruption of SNc function classifies PD into the group of basal ganglia diseases (Albin *et al.*, 1989) like e.g. Huntington's disease (HD). Going from rostral to caudal, this circuitry is composed out of the forebrain structures caudate nucleus and putamen - which are also, together with the nucleus accumbens referred to as the striatum (Zeiss, 2005) - the globus pallidus (GP), the subthalamic nucleus and the substantia nigra of the midbrain (Blandini *et al.*, 2000). As an element of the extrapyramidal motor system, different areas of the basal ganglia circuit get their input from various motor regions of the cortex. Subsequently, these information are getting processed and are sent back to the same cortical regions via the thalamus resulting in motor output (DeLong and Wichmann, 2007). In

brief, cortical input reaching the SNc via the subthalamic nucleus (STN) will be sent back all the way to the forebrain by the dopaminergic neurons of the nigrostriatal pathway to the striatum (**Fig.1**). 95% of all striatal neurons are the so called *medium-sized spiny neurons* (MSN), and are expressing either the dopamine receptor D1 or D2 or both forms (Mallet *et al.*, 2006). While older studies suggested that nearly half of the MSN coexpress both forms of the receptor (Surmeier *et al.*, 1996), the recent analysis of BAC-reporter mice suggest that only a small proportion of about 5-17% coexpress both D1 and D2, while 47-52% express only D1 and 26-43% only the D2 dopamine receptor (Matamales *et al.*, 2009; Valjent *et al.*, 2009). The neurons of the direct striatonigral pathway express a high amount of the D1 receptor and are projecting back to the output nuclei substantia nigra pars reticulata (SNr) and the internal globus pallidus (GPin) (DeLong and Wichmann, 2007) where they inhibit their activity. The reduced activity of these nuclei leads to the disinhibition of the thalamic projections exciting the motor regions of the cortex and therefore leading to an increase in motor activity (Kreitzer and Malenka, 2008). On the other hand, the neurons of the indirect striatopallidal pathway

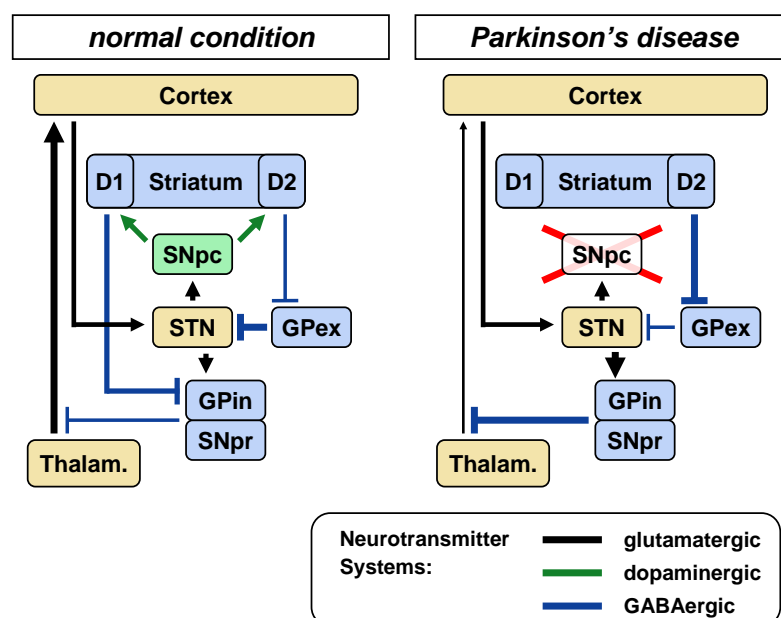


Figure 1: Parkinson's disease (PD) is determined by the disruption of the basal ganglia circuit. Schematic representation of the basal ganglia circuit function (left) and its alterations in PD (right). The thickness of the arrows indicates the relative level of activation (modified from Blandini *et al.*, 2000). **Abbr.:** D1/2, dopamine receptor D1/2; GPex, external globus pallidus; GPin, internal globus pallidus; SNpc, substantia nigra pars compacta; SNpr, substantia nigra pars reticulata; STN, subthalamic nucleus.

are expressing high amounts of the D2 receptor, which - in contrast to D1 - is inhibited in the presence of dopamine. These neurons are connected to the external globus pallidus (GP_{ex}) by GABAergic inhibitory synapses. Therefore, the indirect pathway leads, via the STN and subsequent activation of the output nuclei (SN_r, medial GP) to an enhanced inhibition of the thalamo-cortical projections (**Fig.1**). Taken together, the activation of the D1 receptors in the striatum enhances motor activity, whereas activation of the D2 receptor inhibits the motor activity (Surmeier *et al.*, 2007). This admittedly simplified functional model of the basal ganglia circuit is used to explain mainly aspects of the motor deficits observed in PD. The progressive loss of neurons in the SN_c implicates a reduction of dopaminergic nerve terminals in the striatum and finally to a reduction of physiological active, extracellular dopamine in the synaptic clefts of the striatum.

The nearly total loss of dopaminergic input in the symptomatic phase of PD results in the increase of GABAergic signalling from the output nuclei (**Fig.1**) and therefore in an increased inhibition of the motor output (Blandini *et al.*, 2000). In more detail, two effects can be discriminated. In the striatum, the output of the direct pathway, mediated by the dopamine receptor D1 is decreased if not abolished (Obeso *et al.*, 2000). This leads to difficulties in initiating and performing movements (e.g. bradykinesia), since this pathway under normal conditions selects appropriate movements. The indirect pathway normally inhibits inappropriate movements. Because of the antagonistic mechanism of the D2 receptor which is inhibited in the presence of dopamine (Surmeier *et al.*, 2007) this pathway leads to an increase in unwanted movement (e.g. tremor at rest or the often observed dyskinesia) when dopamine is depleted (Kreitzer and Malenka, 2008). Even though it is tempting to apply this model also to the non-motor symptoms of PD, it is not sufficient to explain all of them (for review: Lewis and Barker 2009).

Problems in treating PD do not only arise by its clinical heterogeneity but also by the fact, that the major symptoms only occur when about 50-70% of the dopaminergic neurons have already been lost (Terzioglu and Galter, 2008). Minor loss of nigrostriatal innervations during the early phase of the disease can be compensated by multiple mechanisms. Since these neurons are

present in the two states - spontaneously firing and quiescent (Grace, 2008), the system can handle this reduction by activating more and more quiescent nerves until a certain threshold is reached. On the molecular level, different modifications can keep up the required dopaminergic signalling for example by an increase in the amount of both D1 and D2 receptors, which has been shown in the brain of untreated PD patients (Guttman, 1992). Another compensatory mechanism is the downregulation of the dopamine transporter (DAT), which is involved in terminating the dopamine signalling by the reuptake of the transmitter into the presynaptic neuron (Adams *et al.*, 2005; Storch *et al.*, 2004). It is worthwhile to mention, that there is still a debate whether dopamine is neurotoxic or neuroprotective. It seems that extracellular dopamine rather mediates neuroprotection via the activation of the dopamine D2 receptor (Bozzi and Borrelli, 2006), whereas excessive amounts of intracellular dopamine are associated with increased ROS (reactive oxygen species) production and cytotoxicity (Chen *et al.*, 2008). These compensations, together with an increased activity of other cholinergic transmitter systems may explain why the first manifestations of the classical motor features of PD come up, when the dopamine level in the striatum already dropped to 30% and more than 50% of the dopaminergic neurons (Fearnley and Lees, 1991; Terzioglu and Galter, 2008) in the SNc are lost (**Fig.2**). This relative late onset but steep increase in symptomatic allows so far only a very late initial diagnosis and therefore prevents a neuroprotective treatment in early phases of the disease.

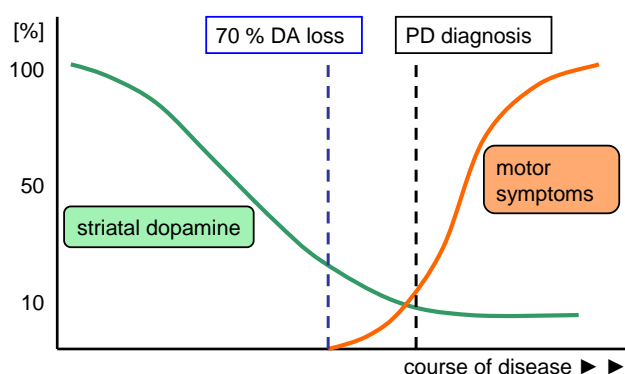


Figure 2: In Parkinson's disease major motor symptoms appear when already about 50-70% dopaminergic neurons in the SNc have been lost. Schematic representation of the relationship between loss of dopamine caused by the degeneration of dopaminergic neurons, onset of PD motor symptoms and PD diagnosis in the course of the disease. **Abbr.:** DA, dopaminergic neurons.

Taken together, the functional model of the basal ganglia circuit can describe the neurological implications of the neuronal cell loss in the SNc and other

brain regions, but can not shed light on the cellular and molecular backgrounds of the disease.

3.2 The genetic aspects of Parkinson's Disease

A major step forward in identifying cellular and molecular mechanisms of PD was achieved in the last decade by the identification of several loci involved in inheritable forms of PD. In contrast to the sporadic form, familial PD - which contributes for about 10% to 15% (Nussbaum and Polymeropoulos, 1997) of all PD cases - exhibits a mendelian pattern of inheritance. Up to now 16 different PARK loci associated to familial PD (Simón-Sánchez *et al.*, 2009; Paisán-Ruiz *et al.*, 2010; Tan *et al.*, 2010) have been identified and in most of the cases also the responsible gene has been mapped (**Fig. 3**). It is not clear, to what extent some or all of these genes also contribute to the more common sporadic form of PD in a mechanistic or causative sense (Hardy *et al.*, 2006; Thomas and Beal, 2007). Rareness and relative low penetrance of the identified mutations makes it hard to classify them from common gene variants and susceptibility factors, to polygenic or monogenic disease genes. Nevertheless, pathogenic mutations in at least five of these genes - *SNCA*, *parkin*, *DJ-1*, *PINK1* and *Lrrk2* - have been clearly identified to cause monogenic forms of familial PD (Abeliovich and Flint Beal, 2006).

PARK loci	position	gene	form of PD mutations	probable function
PARK1/4	4q21	<i>SNCA</i>	AD; A30P, E46K, A53T, duplication and triplication	lipid-membrane associated protein
PARK2	6q25.2–q27	<i>Parkin</i>	AR, J; various mutations, exonic deletions, duplications and triplication	ubiquitin E3 ligase
PARK3	2p13	unknown	AD	unknown
PARK5	4p14	<i>UCHL1</i>	AD and idiopathic; I93M and S18Y	ubiquitin C-terminal hydrolase
PARK6	1p35–p36	<i>PINK1</i>	AR; G309D, exonic deletions	mitochondrial kinase

PARK loci	position	gene	form of PD mutations	probable function
PARK7	1p36	<i>DJ-1</i>	AR and EO; homozygous exon, deletion, L166P	chaperone, antioxidant
PARK8	12q12	<i>LRRK2</i>	AD and idiopathic; R1441C/G/H, Y1699C, G2019S, I2020T, G2385R	cytosolic kinase
PARK9	1p36	<i>ATP13A2</i>	Kufor–Rakeb syndrome and EO-PD; loss-of-function mutations	P-type ATPase
PARK10	1p32	unknown	Idiopathic	unknown
PARK11	2q36–q37	unknown	AD and idiopathic	unknown
PARK12	Xq21-q25	unknown	familial	unknown
PARK13	2p13	<i>Omi/</i> <i>HTRA2</i>	Idiopathic A141S, G399S	mitochondrial serine protease
PARK14	22q13	<i>PLA2G6</i>	AR, L545T	phospholipase
PARK15	22q12-q13	<i>FBX07</i>	Parkinsonian-Pyramidal syndrome, T22M	ubiquitin E3 ligase
PARK16	1q32	unknown	susceptibility	unknown
–	17q21	<i>MAPT/tau</i>	susceptibility	microtubule-associated protein
–	2q22-q23	<i>NR4A2/</i> <i>Nurr1</i>	familial, downregulation	transcription factor
–	5q23.1-q23.3	<i>SNCAIP/</i> <i>Synphilin</i>	susceptibility	SNCA-interactor

Figure 3: During the last decade, several genomic loci have been identified to be involved in inheritable forms of PD referred to as *familial Parkinson's disease*. List of PARK loci linked to various forms of familial PD and related neurodegenerative diseases (adapted from Thomas and Beal, 2007 and Belin and Westerlund, 2008; extended with data from Paisán-Ruiz *et al.*, 2010 and Tan *et al.*, 2010). **Abbr.:** AD, autosomal dominant; AR, autosomal recessive; J, juvenile; EO, early onset.

The question arises, if it is possible to identify common pathways which can not only link different genetic forms of PD but also could contribute to the understanding of sporadic PD. This in turn, would allow the development of novel protective and therapeutic strategies for the treatment of PD (Gasser, 2007). Up to now, no unifying pathway for the aetiology of PD is known, but by studying the function of the PARK genes so far, several cellular scenes

and mechanisms have been shown to be involved. In the following, these fundamental knowledge and findings are reviewed on the basis of findings from the four major PD-related genes besides *Lrrk2*.

3.3 Common pathways in Parkinson's disease

Since mutations in the *Parkin* gene have been associated with autosomal-recessive early-onset PD (Kitada *et al.*, 1998; Lücking *et al.*, 2002), proteasomal degradation arose as one cellular mechanism affected in PD. The *Parkin* gene encodes a protein-ubiquitin E3 ligase with two hotspots for pathogenic mutations - an ubiquitin-like domain and a RING finger domain (Giasson and Lee, 2001). In the process of proteasomal protein degradation, target proteins are marked by polyubiquitination to be transported into the proteasome for subsequent degradation. The ubiquitination is carried out by a complex of different proteins; amongst them E3 ligases which are mediating the specificity to the targeted protein. The effects of pathogenic mutations in the *Parkin* gene can be either the loss of substrate specificity or impair the ability of the protein for self-ubiquitination (Zhang *et al.*, 2000). Besides others, also the PARK7-associated gene *DJ-1* has been shown to be a target of Parkin-mediated polyubiquitination. Bound to the dynein-dynactin complex utilizing HDAC-6 as an adaptor protein, DJ-1 will be transported into aggregate for degradation via microtubular transport (Olzmann *et al.*, 2007).

Functional interaction of Parkin with the gene responsible for PARK6-linked early-onset PD named *PINK1* or PTEN induced kinase 1 (Valente *et al.*, 2004) highlights another main cellular scene – the mitochondria. PINK1 has been shown to accumulate specifically on depolarized mitochondria whereas Parkin was recruited to those same damaged mitochondria (Jones, 2010). A role of mitochondrial function in the aetiology of PD, either under basal conditions or oxidative stress has been proposed since *Drosophila* knock-out models of both *Parkin* and *PINK1* exhibit similar mitochondrial-related phenotypes, which can be rescued by PINK1 in case of Parkin-deficiency; these results are interpreted that both proteins act in a common pathway for regulating mitochondrial physiology and cell survival - at least in *Drosophila* (Yang *et al.*, 2008; Shiba *et al.*, 2009). Interestingly, also the mitochondrial protease

Omi/HtrA2 interacts with PINK1 and it has been suggested, that both molecules act in the same stress-sensing pathway. Due to the activation of the mitogen-activated protein kinase (MAPK) P38, Omi/HtrA2 can be released into the cytosol and subsequently activate caspase-dependent apoptosis. The specific phosphorylation of Omi/HtrA2 by PINK1 could regulate this mechanism and thereby mediate neuroprotection (Plun-Favreau *et al.*, 2007). A further group of Parkin substrates leads to another interesting mechanism involved in the aetiology of PD – to the regulation of transport and release of synaptic vesicles. In this regard, the synaptic vesicle-associated protein CDCrel-1, synphilin-1, the alpha-synuclein-interacting protein and alpha-synuclein (*SNCA*) itself, have to be mentioned (Zhang *et al.*, 2000; Chung *et al.*, 2001; Polymeropoulos *et al.*, 1997). The endogenous function of *SNCA* is until now not completely understood. *SNCA* protein is located in presynaptic nerve terminals; there it can bind to synaptic vesicles and therefore a role in synaptic vesicles trafficking and synaptic transmission but also in several other cellular processes has been proposed (Chandra *et al.*, 2004; Gasser *et al.*, 2007; Shen, 2010 Gasser *et al.*, 2007). This idea is supported by the interaction of *SNCA* with the cysteine-string protein (CSP), which is involved in the assembly of the SNARE complex (Chandra *et al.*, 2005). Membrane fusion in cells is carried out by a complex mechanism under the participation of N-ethylmaleimide-sensitive factor (NSF) and different SNARE proteins like VAMP or syntaxin (Malhotra *et al.*, 1988).

In sum, the diversity of molecular mechanisms and pathways (proteasome dysfunction, mitochondrial dysfunction, transport dysfunction, autophagy) which have been shown to be involved in the aetiology of PD so far, reflect the complexity and heterogeneity of the clinical and pathological features. One exclusive disease-relevant pathway, integrating all previous observations can not (yet) be postulated.

3.4 PARK8: *Lrrk2* – the Leucine-rich repeat kinase 2

In 2002, with PARK8 a new locus linked to familial PD has been identified by a linkage analysis in a Japanese family suffering from autosomal dominant PD with classical clinical features (Funayama *et al.*, 2002). Patients suffering from

PARK8-linked PD exhibit a whole variety of pathological hallmarks, not only of PD but also of other neurodegenerative diseases like AD. While some patients only show neuronal loss and gliosis in the SNc, in other patients Lewy bodies and even Tau inclusions could be detected (Wszolek *et al.*, 2004). Two years later, the gene which is the focus of this thesis - *Leucine-Rich Repeat Kinase 2* (abbr.: **LRRK2**, pronounced *Lark-two*) – was identified to be responsible for PARK8 linked PD (Zimprich *et al.*, 2004; Paisán-Ruíz *et al.*, 2004). It encodes for the huge multidomain protein LRRK2, which is also sometimes referred to as dardarin, derived from the Basque term “dardare” for “to tremble”.

3.4.1 The structure of the *Lrrk2* gene and its protein

LRRK2 in *Homo sapiens* is located on chromosome 12 (**Fig.4, A**); in the vicinity of the gene in region 12q12, no other PD related genes can be found. In *Mus musculus*, *Lrrk2* is located on chromosome 15 (15F1) in a syntenic order sharing the same neighbouring genes very similar to the situation in humans. The locus of *LRRK2* itself spans a region of 144 kb and consists out of 51 exons (**Fig.4, B**) encoding for a large protein with a molecular weight of 286 kDa (2,527 amino acids). Since so many functional protein domains could be identified in the sequence, LRRK2 is often referred to as a multidomain protein. Especially the C-terminal half of the protein exhibits protein-protein binding domains, a GTPase and a kinase domain (**Fig.4, C**). This special array classifies LRRK2, together with its highly similar paralog LRRK1 (Taylor JN *et al.*, 2007), into the group of ROCO proteins (Bosgraaf and Van Haastert, 2003).

The Ras/GTPase domain termed *Ras of complex* or Roc domain is a member of a new subfamily of small GTPases belonging to the Ras superfamily of small GTPases which are involved in a variety of cellular processes (Wennerberg *et al.*, 2005). The adjacent characteristic motive is called the COR domain, or *C-terminal of Roc*. Together, Roc and COR provide the guiding motive for the newly defined subfamily referred to as the ROCO protein family (Bosgraaf and Van Haastert, 2003). ROCO proteins are highly conserved throughout evolution and can be found even in primitive prokaryotes like *archaeae*. Hence it has been speculated whether eukaryotic

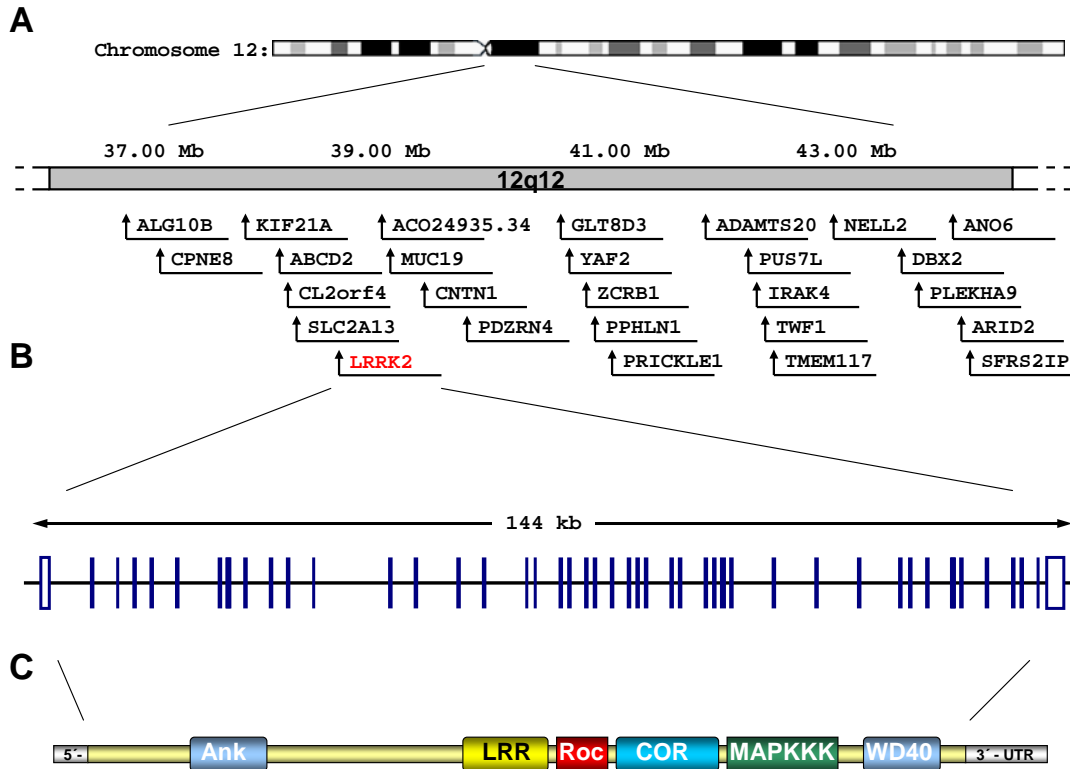


Figure 4: Leucine-Rich Repeat Kinase 2 (*LRRK2*) has been identified to be the gene responsible for PARK8 linked autosomal dominant PD. Schematic drawing of genomic, transcript and protein structure of the human *LRRK2* gene: **A)** Genomic vicinity of *LRRK2* on chromosome 12, (region 12q12) based on the ensembl genome browser (Hubbart *et al.*, 2007). **B)** Intron-exon structure of *LRRK2*. **C)** Protein architecture of *LRRK2* with its multi-domain structure. **Abbr.:** **Ank**, ankyrin repeats; **LRR**, leucine-rich repeats; **Roc**, Ras of complex GTPase; **COR**, C-terminal of Roc; **MAPKKK**, mitogen-activated protein kinase kinase kinase; **WD40**, WD-40 or beta-transducin repeats.

ROCO proteins do have a symbiotic, mitochondrial origin (Marín, 2007). The central Roc and COR motive provides the general characteristic of all ROCO proteins, but also various other domains can be added. In case of *LRRK2*, 3' and to adjacent to COR, a serine/threonine kinase domain similar to mitogen-activated protein kinase kinase kinase (MAPKKK) represents the second catalytic domain of this multi-domain protein (Paisán-Ruíz *et al.*, 2004; Guo *et al.*, 2007). This MAPKKK domain exhibits high similarity with the group of mixed-lineage kinases (MLK) which have been shown to mediate cell-death in neurodegenerative disorders via the phosphorylation and activation of the transcription factor C-Jun (Manning *et al.*, 2002; West *et al.*, 2005; Silva *et al.*, 2005). The functionality of the kinase domain has been revealed by autophosphorylation and MBP- (myelin basic protein) assays (West *et al.*, 2005; Gloeckner *et al.*, 2006), also the overall activity is conspicuously low

(Gloeckner *et al.*, 2009). The fact, that the activity of the MAPKKK domain seems to be dependent on GTP binding to the Roc (GTPase) domain (Ito *et al.*, 2007; Guo *et al.*, 2007), suggests a mechanism of intramolecular regulation. In general, dimerization and following autophosphorylation can serve as a mechanism to regulate the catalytic activities of kinases, as it has been already shown for other MAPKKKs (Leung and Lassam, 1998). Indeed for LRRK2, the formation of homodimers, presumably by dimerization of two Roc-GTPase domains (Gloeckner *et al.*, 2006; Deng *et al.*, 2008) could be shown. In addition not only homo- but also heterodimerization is possible and has been suggested to occur with Dapk1 (death-associated protein kinase 1) or other members of the ROCO protein family like Lrrk1 (Klein *et al.*, 2009; Dächsel *et al.*, 2010).

Altogether, the following could be proposed as a model for the molecular regulation of LRRK2 activity (**Fig.5**): In its inactive state, LRRK2 is dimerized at its Roc-GTPase domain while bound to GDP. The exchange of GDP with

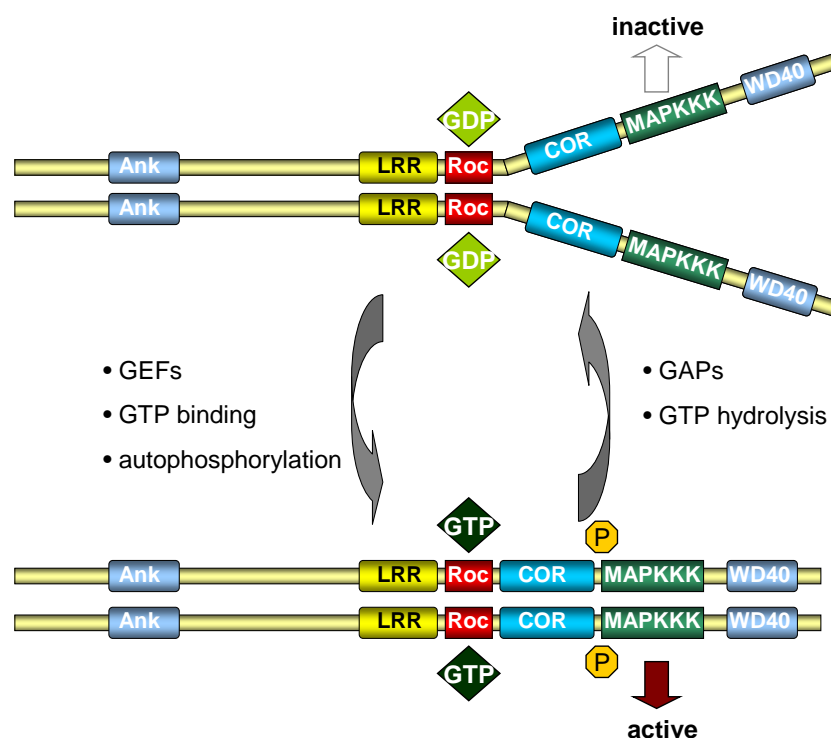


Figure 5: Homodimerized LRRK2 activates itself by autophosphorylation subsequent to a conformational shift induced by GTP-binding. Scheme of the probable intramolecular regulation of LRRK2 kinase activity (based on and modified from Mata *et al.*, 2006; West *et al.*, 2007; Gloeckner *et al.*, 2006 and Deng *et al.*, 2008). **Abbr.:** see Fig.4.

GTP, catalyzed by certain GEFs (guanine nucleotide exchange factor proteins) like ARHGEF7 (Haebig *et al.*, 2010), causes a conformational change. This brings the kinase domains in close proximity to each other, induces autophosphorylation and subsequently the activation of the MAPKKK. Deactivation is achieved by the hydrolysis of GTP to GDP by the Roc-GTPase domain, probably supported by certain GAPs (GTPase activating proteins) (Mata *et al.*, 2006; West *et al.*, 2007; Gloeckner *et al.*, 2006; Deng *et al.*, 2008). But it is also possible, that GEFs and GAPs are substituted by the dimerization of the Roc domain itself (Gasper *et al.*, 2009). This uncommon regulatory property of this ROCO protein can be concentrated into the slogan: *one protein - two enzymes*.

LRRK2 protein contains more functional domains, which are all mediating protein-protein interactions (Mata *et al.*, 2006): First of all a stretch of several leucine-rich repeats (Lrr) is building up the domain which contributes to the name of *LRRK2*. Each repeat is typically 20 to 30 amino acids long and unusually rich in the hydrophobic amino acid leucine with an 11-residue hallmark sequence LxxLxLxxNxL (Bella *et al.*, 2008). This widespread motive can be found in hundreds of proteins with various functions like cell adhesion and signalling, platelet aggregation, disease resistance, neuronal development or RNA processing; in all these cases, the Lrr domain is involved in protein-protein interactions (Buchanan and Gay, 1996). Also the other two conserved protein domains are involved in protein-protein binding and interaction: Several ankyrin repeats (Ank) can be found N-terminal of the Roc domain. Proteins bearing such repeats have been shown to be involved in cell–cell signaling, cytoskeleton integrity, intracellular transport, inflammatory response and other mechanisms (Mosavi *et al.*, 2004). At the C-terminus, a domain of WD-40 repeats, also known as WD or beta-transducin repeats (WD40) can be identified. The propeller-like structure of this protein-protein binding motive (Chen *et al.*, 2004) can be found in numerous proteins involved in cytoskeletal assembly, vesicle formation and trafficking, transcriptional regulation and RNA processing (Yu *et al.*, 2000).

3.4.2 The genetic basis of *Lrrk2*-linked PD

Mutations in the *LRRK2* gene can be found in up to 10% of autosomal dominant familial PD and in up to 3.6% of sporadic Parkinsonism (Berg *et al.*, 2005; Xiromerisiou *et al.*, 2007; Lesage and Brice, 2009). The first pathogenic mutations in the *LRRK2* gene have been identified in families with PARK8-linked PD by two independent groups in 2004. The missense mutation R1441C could be identified in a family from Nebraska; mutation Y1699C in a German-Canadian family (Zimprich *et al.*, 2004). The mutations R1441G and again Y1699C have been identified in five families with Basque ancestry (Paisán-Ruiz *et al.*, 2004).

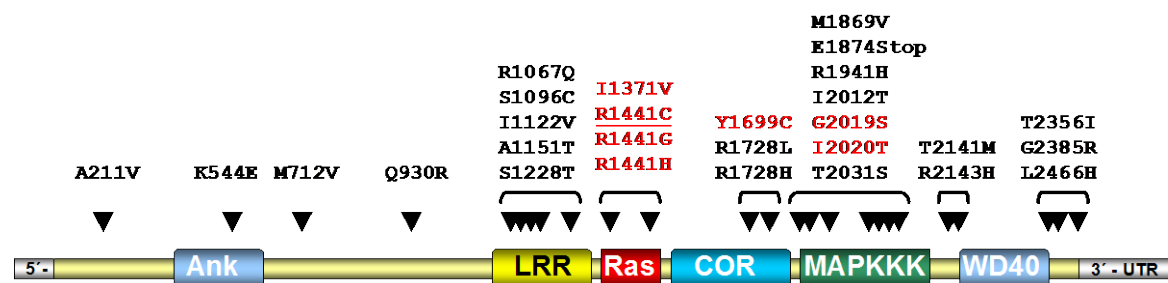


Figure 6: The functional domains of *LRRK2* are the hotspots for pathogenic missense mutations associated with PARK8-linked PD. Schematic representation of mutations identified in PD patients in the multidomain protein *LRRK2*. Confirmed pathogenic mutations are depicted in red (adapted and unified from Paisán-Ruiz *et al.*, 2008; Giasson and Van Deerlin, 2008; Lesage and Brice, 2009). **Abbr.:** see Fig.4.

By degrees, more and more missense-mutations have been reported by numerous groups (Fig.6) and until now, seven of them (I1371V, R1441C/G/H, Y1699C, G2019S and I2020T) have been confirmed as being clearly pathogenic (Lesage and Brice, 2009). These pathogenic mutations can be classified into three groups in regard to their localisation: mutations in the MAPKKK domain, mutations in the Roc GTPase domain and mutations in the different protein-protein interaction domains; In genome wide association studies, also common variability proximal to the *LRRK2* locus has been linked to PD which suggest a role of the protein also in the sporadic form of the disease (Simón-Sánchez *et al.*, 2009).

On the clinical level, patients with *LRRK2*-linked PD do exhibit similar features to sporadic patients (Haugarvoll *et al.*, 2008). The pathology in contrast, is discussed to be more pleiomorphic than in other familial PD cases (Taylor JN *et*

al., 2006); it has reported that even patients with identical mutations can exhibit diverse pathological features (Giasson and Van Deerlin, 2008). Classical nigrostriatal degeneration has been reported for all, the presence of Lewy bodies (LB) for many of the patients. Interestingly the very common G2019S patients do show a rather classical PD pathology, whereas the pathology in patients with quite rare mutations like R1441C can show higher degree of variation (Biskup and West, 2008). For example Wszolek and colleagues have reported in one of the first pathological analysis of *LRRK2*-linked PD patients, that only about 50% of R1441C patients do exhibit Lewy bodies (LBs) and Lewy neurites (LNs) (Wszolek *et al.*, 2004). Due to conflicting data, it has to be doubted whether *LRRK2* protein can be found in alpha-synuclein positive inclusion bodies like LBs or LNs in PD or other neurodegenerative diseases (Santpere and Ferrer, 2009). Remarkable is the fact, that also rare cases of Tau-pathology have been diagnosed in *LRRK2*-linked PD patients (Rajput *et al.*, 2006; Devine and Lewis, 2008). The neuronal expressed Tau-protein stabilizes microtubules and is involved in axonal outgrowth but can also aggregate to toxic oligomers. In tauopathies like for example *Alzheimer's disease* (AD), these aggregates form inclusion bodies referred to as neurofibrillary tangles (Ballatore *et al.*, 2007). Recently, also the *MAPT* (microtubule-associated protein Tau) locus has been linked to PD as a susceptibility factor (**Fig.3**) (Simón-Sánchez *et al.*, 2009). Until now, neither a direct linkage to AD or any other neurodegenerative diseases, nor higher susceptibility rates could be observed in carriers of *LRRK2* mutations (Lee E *et al.*, 2007; Lesage and Brice, 2009).

The general penetrance of *LRRK2*-linked PD is assumed to be in the range of 30% by the age of fifty, and around 80% at an age over eighty (Goldwurm *et al.*, 2007; Healy *et al.*, 2008). Notably, homozygote carriers of single mutations are indistinguishable from heterozygote carriers in regard to the clinical phenotype (Ishihara *et al.*, 2006).

But what are the possible molecular consequences of these missense-mutations, in particular with respect to the proposed model of the intra-molecular regulation of *LRRK2* activity? The most prominent, prevalent and best studied of all, the G2019S missense mutation in the MAPKKK domain, is located in the activation segment of the kinase domain (Nolen *et al.*, 2004). It has been

shown by several groups, that this amino acid substitution does enhance the kinase activity in autophosphorylation assays and in phosphorylation of the generic kinase substrate MBP (myelin basic protein) *in vitro* (West *et al.*, 2005; Jaleel *et al.*, 2007). Of course, this gain-of-function effect of the mutation fits very well to its dominant mode of inheritance. Therefore, it has been speculated whether all identified pathogenic mutations finally result in elevated kinase activity. Findings, that cytotoxicity induced by the *in vitro* overexpression of human LRRK2 protein is dependent on the kinase activity (Smith *et al.*, 2006; Greggio *et al.*, 2006), supported this idea. But unexpectedly for no other pathogenic mutation this finding could be confirmed - at least in autophosphorylation assays. For the adjacent mutation I2020T both an increase and a decreases of the kinase activity has been reported (Gloeckner *et al.*, 2006; Jaleel *et al.*, 2008), for others like I1371V, R1441C/G/H and Y1699C, alterations could not be confirmed. In the case of Roc-GTPase missense mutation R1441C – which is in the focus of this work - some groups did detect a slightly higher rate of autophosphorylation by overexpressing R1441C mutated LRRK2 *in vitro* (Smith *et al.*, 2006; West *et al.*, 2007; Guo *et al.*, 2007); in more recent publications, other report that there are no such differences compared to wild-type LRRK2 (Lewis *et al.*, 2007; Jaleel *et al.*, 2007; Greggio *et al.*, 2008, Gloeckner *et al.*, 2008). To date it is widely accepted, that only G2019S and I2020T do lead to enhanced autophosphorylation activity (Biskup and West, 2008; Santpere and Ferrer, 2009), also due to the fact that an increase could also be observed in the phosphorylation of moesin - one putative substrate of LRRK2 (Jaleel *et al.*, 2008).

The most prominent mutation in the Roc-GTPase domain R1441C is located outside the GTP binding pocket and therefore does not alter the binding of GTP but decreases the GTP hydrolysis activity (Lewis *et al.*, 2007; Li X *et al.*, 2007). This would imply that R1441C mutated LRRK2 will stay longer in the GTP-bound state which represents the active form of the protein according to the putative model of the intramolecular regulation of LRRK2 activity (**see 3.4.1 and Fig.5**), but further studies are required to fully elucidate that mechanism. So far, other basic biochemical properties of LRRK2 as for example the localization and stability of the protein seem not to be changed by any pathogenic mutation (Biskup and West, 2008).

3.4.3 What is known about the function of LRRK2?

To get a first idea about the physiological role of LRRK2 protein it is useful to look in detail onto the available functional data from LRRK2 orthologs and other ROCO proteins from different species.

For instance *Lrk-1* of *Caenorhabditis elegans*, a homolog of the human *LRRK* genes, has been identified to be involved in the transport and sorting of synaptic vesicles. In the nervous system of this nematode, this kinase is located in the soma but not in the axons or dendrites of neurons and is showing an overlap with certain markers for the Golgi apparatus. *Lrk-1* seems to act together with the AP-1 clathrin adaptor complex to exclude synaptic vesicles proteins from the dendrites and thus direct them into the axon (Sakaguchi-Nakashima *et al.*, 2007). Loss of *Lrk-1* protein induces a higher sensitivity to the ER (endoplasmic reticulum) stressor tunicamycin. Loss of the *C.elegans* homologue of pink-1, which results in mitochondrial alterations, can rescue the *Lrk-1* phenotype and vice versa (Sämann *et al.*, 2009). This indicates a possible common role for both genes in functions like stress response and regulation of vesicular transport at least in nematodes.

The fruit fly *Drosophila melanogaster* has been widely used not only to study genetics and developmental biology, but also neurodegenerative diseases. For many PARK genes, this is the only model organism, where central phenotypical aspects of PD like degeneration of dopaminergic neurons can be observed (Bilen and Bonini, 2005). While PD-like phenotypes like dopaminergic degeneration and locomotion defects, but also loss of fertility in female flies can be seen in a model in which the endogenous *LRRK2* ortholog *dLRRK* is knocked out (Lee SB *et al.*, 2007), other do not detect any phenotype in another loss-of-function model where the kinase activity of *dLRRK* is abolished by truncation of the protein (Wang D *et al.*, 2008). Initially, no phenotype could be observed when either wild-type or R1441C mutated human LRRK2 protein gets overexpressed in *Drosophila* (Lee SB *et al.*, 2007). But some months later, Liu and colleagues reported that the overexpression of either wild-type or the G2019S mutated form of hLRRK2 in neurons does induce degeneration of dopaminergic neurons, locomotor

dysfunction and early mortality (Liu *et al.*, 2008). These discrepancies may be explained by differences in the experimental approaches and the use of different pathogenic mutations (Lewis, 2009). With 4E-BP (*eIF4E*-binding protein), the first putative substrate for *dLRRK* in *Drosophila* has been identified. This initiation factor is a key component of the eIF4F complex that is required for cap-dependent protein synthesis and necessary for cellular stress-response; its deregulated phosphorylation by *dLRRK* might lead to enhanced cell sensitivity for different stressors (Imai *et al.*, 2008). Controversially, recent studies report that the specific phosphorylation activity of LRRK2 is quite low and 4E-BP phosphorylation might be seen as a general stress response caused by overexpression (Kumar *et al.*, 2010).

Of course also *in vitro* analyses in different animal and human cell lines or primary cells did contribute to the fundamental understanding of *Lrrk2* function to a great extent. Like indicated before, some groups observed cytotoxicity when they ectopically overexpress human LRRK2 in various established cell lines like HEK-293, SH-SY5Y, HeLa or COS-7, but also in primary neurons. In addition, also the *in vitro* formation of inclusion bodies has been described (Greggio *et al.*, 2006; MacLeod *et al.*, 2008). For this toxic effect, both the kinase as well as the GTPase activity is required (Smith *et al.*, 2006; West *et al.*, 2006). But it is questionable whether PD-associated mutations do remarkably enhance cytotoxicity compared to wild-type LRRK2, or if toxicity is simply dependent on the grade of LRRK2 overexpression (Santpere and Ferrer, 2009). In primary cortical rat neurons, exogenous human LRRK2 with the mutations G2019S and I2020T leads to a dramatic reduction in neurite length and branching (minor effects in R1441G and Y1699C), whereas knockdown of endogenous *Lrrk2* leads to increased neurite elongation (MacLeod *et al.*, 2008). In differentiated SH-SY5Y cells, the G2019S-LRRK2 induced subtle shortening of primary neurites has been associated with an increase of autophagy probably via the MAPK/Erk pathway (Plowey *et al.*, 2008). Using HEK293 cells, further studies observed a slight increase of SNCA expression following Erk-activation by mutated LRRK2 overexpression (Carballo-Carbajal *et al.*, 2010).

More information about the cellular roles of LRRK2 is derived from the identification of interaction partners and substrates. In general, the majority of

identified but not yet confirmed interaction partners can be grouped into four functional classes: cytoskeleton, synaptic transmission, kinases and chaperones (Dächsel *et al.*, 2007; Meixner *et al.*, 2011; Piccoli *et al.*, 2011). Except for parkin (Smith *et al.*, 2005), LRRK2 seems not to interact directly with any other of the PD-linked genes. The mechanism of endocytosis as a role for LRRK2 was suggested by the identification of Rab5b as an LRRK2-interacting protein. The small GTPases Rab5b is not only involved in endocytosis and recycling of cell surface molecules like receptors, but also has been shown to play a role in neurodegenerative diseases (Baskys *et al.*, 2007). Accordingly, Shin and colleagues could not only demonstrate the colocalisation of both proteins in synaptosomal fractions, but also an impairment of synaptic vesicle endocytosis after overexpression or knock-down of *Lrrk2* in primary rat neurons which can be rescued by Rab5b overexpression (Shin *et al.*, 2008).

The first putative substrates for LRRK2 have been identified by a KESTREL screen (kinase substrate tracking and elucidation), showing the phosphorylation of moesin and two near relatives (Jaleel *et al.*, 2007). The members of the ERM (ezrin, radixin, moesin) protein family are involved in linking the actin cytoskeleton with membrane structures (Bretscher *et al.*, 2000). But also the microtubular network seems to be involved in LRRK2-function since the direct interaction of beta-tubulin with the Roc-GTPase domain could be demonstrated by another group (Gandhi *et al.*, 2008). Further substrate molecules are members of the Jun amino-terminal kinase (JNK) and p38 MAPK which is activated in response to different nonmitogenic signals proinflammatory cytokines and environmental stress (Nebreda and Porras, 2000). Gloeckner and colleagues could show that LRRK2 can phosphorylate MKK3/6 and MKK4/7 and that only the LRRK2 mutations G2019S and I2020T lead to an increase of their phosphorylation (Gloeckner *et al.*, 2009).

3.5 Mouse models for Parkinson's Disease

During the last 25 years, a whole variety of different *in vivo* model systems have been developed to study the aetiology of PD. Prior to the identification of genetic factors involved in PD, only toxin-induced lesion models were

available. Following is a recapitulation of existing mouse models for Parkinson's disease, of their individual properties and which insights they have given into the aetiology of PD.

3.5.1 Genetic rodent models of PD

With identification of the PARK genes, the quest for transgenic models recapitulating as many motor and non-motor features of PD as possible has started. Up to now, several rodent knockout models for the three most common genes inherited in an autosomal recessive form, namely *Parkin*, *DJ-1* and *PINK1*, have been reported. Mice, deficient for functional Parkin protein do show a slight increase in extracellular dopamine in the striatum but no degeneration of nigrostriatal, dopaminergic neurons. Only one model has been published to show a loss of TH positive neurons – not in the SN but in the locus coeruleus (Goldberg *et al.*, 2003). Except for this model, which is showing a reduction of startle response, on the behavioural level just subtle motor and non-motor behavioural changes could be observed (von Coelln *et al.*, 2004). On a cellular level, the loss of Parkin protein leads to mitochondrial dysfunction and extraordinary increase of oxidative stress.

Up to now three different mouse models for *DJ-1* linked PD have been published (Melrose *et al.*, 2006/2). Likewise to parkin, also these mice do not show significant nigrostriatal neurodegeneration. Nevertheless, the *DJ-1* genetrapped mouse, created and analysed in our laboratory, exhibits a mild, age-independent loss of TH-positive cells in the ventral tegmental area of the midbrain in the range of about 10% (Pham *et al.*, 2010). Further on, changes in striatal dopamine reuptake accompanied by slight changes in motor and non-motor behaviour has been reported. *DJ-1*-deficient mice are hypoactive in the open field and depict a higher susceptibility for environmental toxins like paraquat (Yang *et al.*, 2007, Chandran *et al.*, 2008). On the cellular level, slight impairments in several complexes of the mitochondrial respiratory chain can be observed (Pham *et al.*, 2010).

For *PINK1*, up to now two mouse models have been published so far. Once again, the depletion of PINK1 protein does not cause severe alterations or nigrostriatal degeneration. Likewise, also the behaviour of these animals

exhibit only minor changes. The only systemic changes are alterations in striatal dopamine reuptake, similar to those observed in *DJ-1* (Harvey *et al.*, 2008).

The situation is quite different for models dealing with autosomal dominant inherited PD, since the knockout or knockdown of the corresponding gene may be not sufficient to fully mimic the situation in the patients. In the case of alpha-synuclein (*SNCA*) were not only missense but in particular gene duplications and triplications have been identified, various models overexpressing wild-type or mutated forms of *SNCA* have been reported (Polymeropoulos *et al.*, 1997). The use of different promoters results in varying levels of transgene expression and tissue specificities. Nevertheless also different loss-of function models have been generated for *SNCA*. Not surprisingly only minor changes like a small reduction of striatal dopamine has been reported (Abeliovich *et al.*, 2000). The double knockout of both alpha- and beta-synuclein leads to a reduction in the reserve pool of synaptic vesicles. This observation in the hippocampus approves the role of these proteins in the synaptic function (Chandra *et al.*, 2004). While these models rather aim to elucidate the endogenous function of the protein, overexpression of wild-type or mutated *SNCA* is used for modelling the aetiology of PD. The first published mouse overexpressing wild-type *SNCA* for example shows age-dependent reduction in TH-positive cells of the midbrain and intranuclear inclusions in various regions of the adult rodent brain (Masliah *et al.*, 2000). Instead mice overexpressing the human *SNCA* bearing the mutations A30P or A53T did show some other pathological features of PD like the accumulation of insoluble *SNCA*, a reduction in TH-positive nerve terminals in the striatum and hyperphosphorylation of tau-protein (Kahle *et al.*, 2001; Manning-Bog and Langston, 2007). In this regard, *SNCA* overexpressing mice are up to now unique in the group of rodent *PARK* models (Terzioglu *et al.*, 2008).

3.5.2 Mouse models of *LRRK2*-linked PD

A couple of groups have started to establish various gain-of-function and loss-of-function mouse models to elucidate the physiological and pathological role of *Lrrk2* (Sen and West, 2009). Early publications, dealing with the molecular

function of LRRK2, did use *LRRK2* mouse models to some respect. Data from Li and colleagues confirmed both the binding of GTP to FLAG-tagged murine *Lrrk2* overexpressed in BAC-transgenic mice and its hydrolysis (Li *et al.*, 2007). Knock-out mouse models have been used as negative controls for the co-immunoprecipitation of CHIP with LRRK2 (Ko *et al.*, 2009) or for the confirmation of antibodies used in Western blot and immunohistochemistry (IHC) experiments (Biskup *et al.*, 2006). Overexpression of human G2019S LRRK2 controlled by tetracycline-responsive promoter in the murine forebrain does not evoke any phenotype except the retardation of axonal outgrowth in primary prepared neurons (Wang *et al.*, 2008; C. Xie, unpublished data). Melrose and colleagues gave a preliminary comment in regard to a phenotype by reporting that a BAC mouse (Bacterial Artificial Chromosome), expressing human wild-type LRRK2 approximately 20-fold higher than the endogenous levels do not exhibit any overt phenotype up to the age of 24 month (Melrose, 2008).

In contrast to these preliminary information, one year later the first published mouse model overexpressing hLRRK2 has been reported to recapitulate cardinal features of PD. In this analysis, BAC transgenic mice have been utilized which overexpress human LRRK2, carrying the pathogenic R1441G point mutation, on a level at least 5- to 10-fold higher than endogenous murine LRRK2. These mice exhibit subtle motor symptoms like an age-dependent reduction of rearing activity which could be partially rescued by administration of the dopamine precursor levodopa (L-DOPA). On a functional level, microdialysis experiments suggest a reduced striatal dopamine release. Also minor pathological alterations like morphological abnormalities of TH-positive dendrites could be observed (Li Y *et al.*, 2009).

Later on, Tong and colleagues published a far more physiological model, similar to the knock-in mouse model described later in this study. Also here, the pathogenic R1441C point mutation is introduced into the endogenous murine *Lrrk2* gene. Up to an age of 2 years, no pathological signs of PD like degeneration of the dopaminergic system, inclusion bodies or alterations in the basal dopamine release could be observed in these mice. On the behavioural level, in contrast to the wild-type controls, R1441C mice failed to respond to amphetamine treatment. Since this psycho-stimulant has been

shown to modulate the transport and release of dopaminergic vesicles (Robertson *et al.*, 2009), the authors looked closer into stimulated catecholamine release in these mice and identified an alteration in the dopamine autoreceptor D2 function. Quinpirol, a D2 receptor agonist, fails to inhibit firing of DA-neurons *in vitro* and causes less reduced locomotor activity *in vivo*, which suggests a general role of LRRK2 in dopaminergic neurotransmission and especially in D2 receptor function (Tong *et al.*, 2009). These findings were supported by the most recent publications from Li and colleagues, which compared transgenic BAC mice overexpressing either wild-type hLRRK2 or the G2019S mutated form of hLRRK2. Both lines did show differential alterations in regard to behaviour and dopaminergic transmission. Nevertheless, also these mice did not display any pathological signs of neurodegeneration (Li *et al.*, 2010). Nevertheless, for the kidneys of 20 month old *Lrrk2*-deficient mice, Tong and colleagues recently did report perturbations of the autophagy-lysosomal pathway (Tong *et al.*, 2010).

Taken together, none genetically modified rodent models do recapitulate virtually all features of PD. The desired key features would be the slow and progressive loss of nigrostriatal dopaminergic neurons attended by progressive motor dysfunctions; furthermore inclusion body pathology (Lewy bodies, Lewy neurites, tau-pathology, neurofibrillar tangles). Until now, all models are usefully to shed light on distinct features and mechanisms of the disease, but up to this point no unifying disease model is available.

4 Aim of the Study

The general scope of the present study was to create an additional PD disease model for further exploring the aetiology of Parkinson's disease and to get closer insights into the physiological roles of the Leucine-rich repeat kinase 2.

First of all, the murine expression pattern of both *Lrrk2* and its paralog *Lrrk1* was comprehensively analysed throughout the development from early embryonic stages until in particular in the adult brain.

To exactly simulate the pathological mutation observed in Parkinson's disease patients, the corresponding c>t transition has been inserted into the endogenous murine *Lrrk2* gene. After correct homologous recombination, the wild-type exon 31 has been exchanged by the mutated and *loxP*-flanked form. The generated mouse line was analyzed at different ages in regard to behavioural, morphological and pathological changes. This initial analysis was mainly focused on impairments, correlating to clinical motor and non-motor symptoms observed in Parkinson's disease patients. Referring to this, parameters like motor functions but also depression and anxiety-like behaviour or olfaction has been studied comprehensively. Since in PD, mainly the dopaminergic system is affected, the histology was focused on that; nevertheless, also some other routes have been followed in this analysis.

Furthermore, an existing knockdown mouse line, expressing a short hairpin RNA directed against *Lrrk2* has been utilized to analyze the effects of an almost complete loss of LRRK2 protein *in vivo*. Also this mouse line, focusing rather on the physiological functions of the protein, has been initially analyzed in a similar way as the generated disease model. In addition, both mouse models have been used as a source to investigate the cellular functions of LRRK2. Both mouse embryonic fibroblasts (MEF) and primary cortical or hippocampal neurons allowed studying *in vitro* distinct aspects like cytoskeletal stability, neurite outgrowth or exo- and endocytosis on a cellular level.

5 Results

5.1 Comparative Expression Analysis of *Lrrk1* and *Lrrk2*

5.1.1 Expression during embryonic development

In the initial stage of this PhD project, virtually nothing was known about *Lrrk2* except the structure of the mRNA, the composition of its conserved domains and of course its association with Parkinson's disease (PD) (Zimprich *et al.*, 2004; Paisán-Ruíz *et al.*, 2004). The pattern of expression is suggestive for the physiological role of a protein. Therefore, a comparative expression analysis was performed for *Lrrk2* and also for its highly conserved paralog *Lrrk1* (Marín, 2006) in order to evaluate the possibility of redundancy of these two proteins. Since we were interested particular in the role of *Lrrk2* in PD, we put the main emphasis on the expression in the brain of adult mice, but also the embryonic development was taken into account. Because no high specific antibodies suitable for immunohistochemistry (IHC) were available, we utilized the technique of *in situ* hybridisation (ISH) with radioactive labelled RNA probes (see 7.2.2.2). A set of different cDNA fragments based on the mRNA of *Lrrk1* and *Lrrk2* was designed and cloned via RT-PCR (Fig.7). To achieve a maximum of specificity of these probes, overlapping stretches of about 800bp were placed into the less conserved 5' region of the *Lrrk2* coding sequence, avoiding cross reactivity with *Lrrk1* and other ROCO proteins (see 3.4.1). The longer 5' and 3' UTRs of *Lrrk1* allowed placing the probes mostly in these

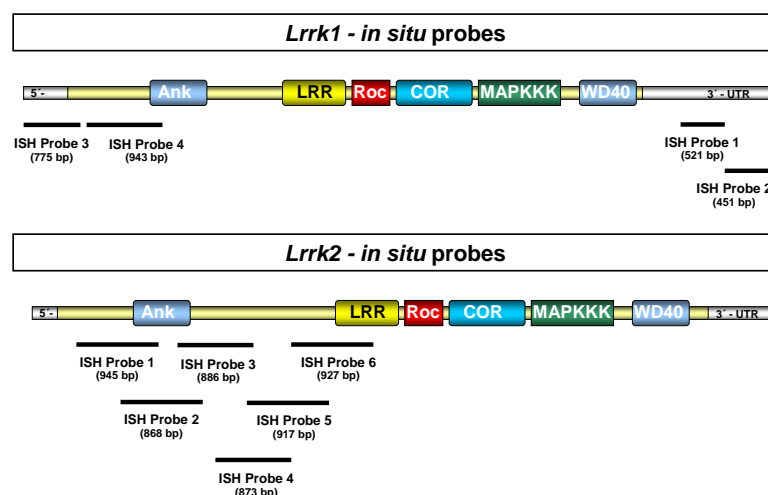


Figure 7: The high degree of conservation between *Lrrk1* and *Lrrk2* mRNA requires a careful design of ISH probes to ensure their specificity. Schematic representation of the *Lrrk1* and *Lrrk2* ISH-probe localisation on the mRNA. Sequences are based on the NCBI accession numbers NM_146191 for *Lrrk1* and NM_025730 for *Lrrk2*.

completely unconserved parts of the transcript. For both genes respectively, all probes exhibited a similar pattern of expression and regions where only *Lrrk1* and not *Lrrk2* (and vice versa) is expressed, indicate that the probes are highly specific.

In early embryonic stages, the expression of *Lrrk2* was additionally checked via RT-PCR using primer pairs for *Lrrk2* ISH probe 1 (see 9.2); postnatal brain and adult kidney served as positive control. In virtually all stages and organs beginning from ES cells till adulthood, qualitative expression of *Lrrk2* mRNA could be detected (Fig.8).

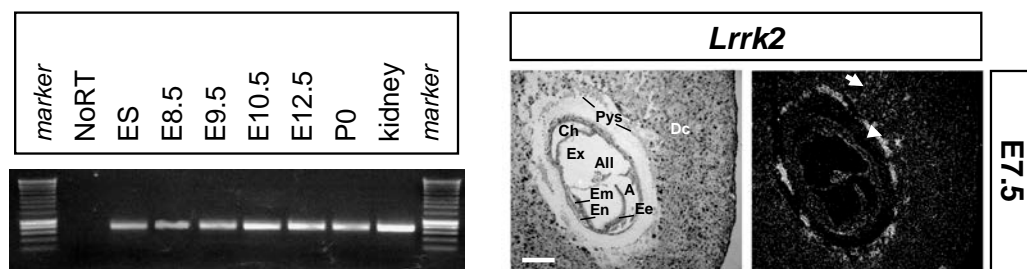


Figure 8: Qualitative expression of *Lrrk2* mRNA can be detected from early embryonic stages onwards but on levels below the detection limit of radioactive *in situ* hybridisation (ISH). Expression of *Lrrk2* mRNA during early murine development. Semiquantitative RT-PCR for *Lrrk2* mRNA on different embryos and adult tissues (left). ISH for *Lrrk2* mRNA in the early gestation embryo at stage E7.5 (right). Both a brightfield picture (left) for anatomical orientation as well as a darkfield picture (right) representing the ISH signal in white is depicted. Strong *Lrrk2* mRNA expression can be observed in the parietal yolk sac (**white arrowhead**) and in the decidua (**white arrow**). Scale bar represents 200 μ m. **Abbr.:** A, amniotic cavity; All, allantois; Ch, chorion; Dc, decidua; Ee, embryonic ectoderm; Em, embryonic mesoderm; En, embryonic endoderm; ES, murine embryonic stem cell; Ex, exocoelomic cavity; NoRT, negative control; Pys, parietal yolk sac.

The earliest embryonic stage analyzed by *in situ* hybridisation was E7.5 (embryonic day 7.5). At this developmental stage only the surrounding maternal tissue shows robust *Lrrk2* expression (parietal yolk sac, decidua), whereas in the embryonic tissue the expression is too weak to be detected even by the highly sensitive radioactive *in situ* hybridisation (Fig.8). From E9.0 till E11.5 weak expression can be observed nearly ubiquitously embryo but rather not in the neuroepithelium of the developing central nervous system (CNS). The only stronger expression domain during these stages can be found in the urogenital ridge (Fig.9, C, D).

Lrrk1 expression at E10.5 was shown at E10.5 by *in situ* hybridisation at E10.5 and by RT-PCR (data not shown). Also in case of *Lrrk1*, the early

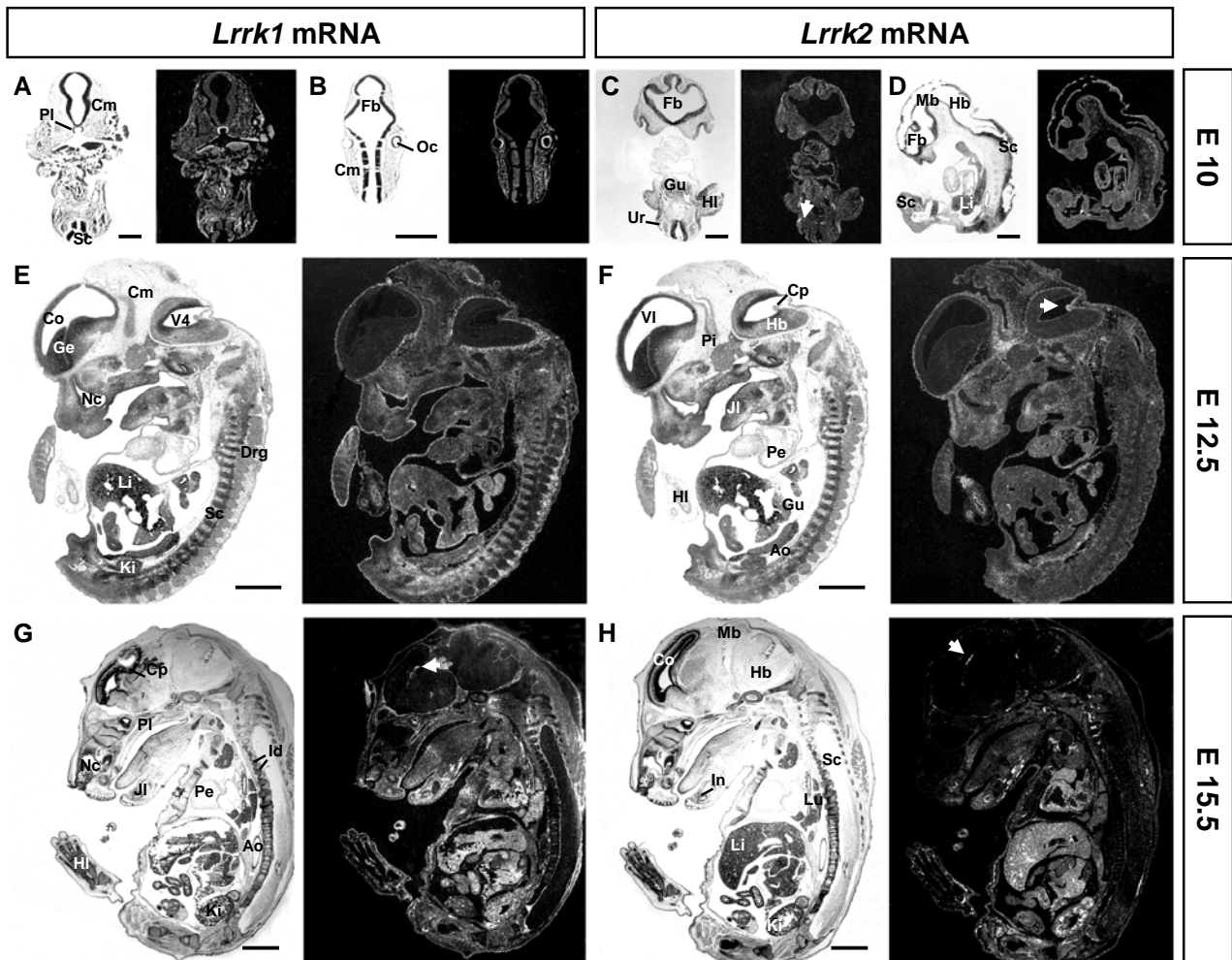


Figure 9: Both *Lrrk1* and *Lrrk2* exhibit a largely overlapping albeit not similar expression pattern during embryogenesis in many different organs and structures from mid- to late-gestation. *Lrrk1* and *Lrrk2* mRNA expression in the developing embryo of various mid-gestation stages illustrated by radioactive *in situ* hybridisation (ISH). For each embryo, both brightfield pictures (left) for anatomical orientation as well as darkfield pictures (right) representing the ISH signal in white are depicted: Stronger *Lrrk1* mRNA levels at E10 can be observed in the cephalic mesenchyme tissue in the inner layer of the optic cup (**A**, coronal; **B**, horizontal), whereas *Lrrk2* mRNA can be found predominately in the urogenital ridge (**white arrow** in **C**, coronal) but is, like *Lrrk1*, nearly absent from the developing CNS (**D**, sagittal). At the embryonic stage E12.5, additional domains of high *Lrrk1* expression are the epithelia of nose and mouth and the inner epithelium of the intestine (**E**, sagittal); for *Lrrk2* the choroid plexus (**white arrow**) and the pituitary gland have to be mentioned (**F**, sagittal). Around E15.5 both *Lrrk1* and *Lrrk2* are heavily expressed in the cephalic mesenchyme surrounding the neuronal tissue of the CNS (**G**, **H**, sagittal), as well as in the choroid plexus (**white arrows** in **G** and **H**). Also the lower jaw shows strong expression domains of both genes. **Abbr.:** Ao, aorta; Cm, cephalic mesenchyme; Co, cortex; Cp, choroid plexus; Drg, dorsal root ganglia; Fb, forebrain; Fl, forelimb; Ge, ganglionic eminence; Gu, gut; Hb, hindbrain; Hl, hind limb; Id, intervertebral disc; In, incisor; JI, lower jaw; Ki, kidney; Li, liver; Lu, lung; Mb, midbrain; Nc, nasal cavity; Oc, optic cup; Pe, pericardium; Pi, pituitary gland; Pl, palate; Sc, spinal cord; V4, fourth ventricle; VI, lateral ventricle. Scale bars represent 500µm (A-D) and 1mm (E-H).

embryonic expression is widespread but the overall level seems to be higher. The intensity of the lower-degree, more ubiquitous expression is comparable to the *Lrrk2* *in situ* hybridisation but you can find more regions with elevated

levels of *Lrrk1* mRNA: the inner layer of the optic cup (the future nervous layer of retina), the cephalic mesenchyme tissue, the epithelia of nose and mouth and the epithelium of the intestine (**Fig.9, A, B**).

By E12.5, besides the weak till moderate ubiquitous expression, *Lrrk2* starts to be strongly expressed in the pituitary gland, developing incisors, in chondral structures of the vertebrae, in the nasal bone, and in distal limbs. Furthermore, robust expression in parts of the developing kidney can be detected especially in the medulla and around the distal excretory ductules. Interestingly, no expression was observed in the embryonic nervous system; however, starting from E12 onwards the choroid plexus displays a conspicuously strong expression (**Fig.9, F**).

Similar to *Lrrk2*, *Lrrk1* can not be detected in the developing central nervous system except at a very low level in the choroid plexus. Misleading is the strong expression of both genes in the tissue directly surrounding the CNS which will build up the three layers of the meninges (dura mater, arachnoid mater and pia mater), but these are no neural elements of the CNS. In contrast to *Lrrk2*, strong *Lrrk1* expression levels can be detected in the developing inner ear, in and around the bronchia of the lung and transiently in the pituitary gland (**Fig.9, E**).

Two days later, in developmental stage E14.5 the ubiquitous expression of *Lrrk2* is slightly diminished (**Fig.10, A**). The strongest expression can be detected in the choroid plexus, around the nasal capsule, in the primordium of upper and lower incisor tooth and in the chondral structures of the vertebrae (**Fig.10, B**). Also very strong is the expression in the metanephric vesicles of the kidney (**Fig.10, C**) and moderate expression in all other parts of the developing kidney and in the lung. In the kidney, the high expression level of *Lrrk2* sustains until adulthood (data not shown). The strong expression in the mesenchyme surrounding the forming distal limbs can also be seen from this stage onwards; even better at around E15.5 (**Fig.9, H**). At that stage heart and liver begin to exhibit signal which is probably caused by unspecific probe-trapping in blood cells often observed using radioactive *in situ* hybridisations. The general level of the *Lrrk1 in situ* hybridisation signal exceeds the corresponding *Lrrk2* level in these stages clearly. Expression in the choroid plexus gets stronger till E15.5; the expression in the cephalic mesenchyme

tissue, visible at E12.5, is still there but not so well defined as it is for *Lrrk2*. At around E14.5 strong expression of *Lrrk1* in the meninges surrounding the developing brain and spinal cord is still present and continues to be expressed until adulthood. At E15.5 strongest expression can be observed in the epithelia of nose and mouth, especially in the region of the forming palate (Fig.9, G). Furthermore at this stage, strong *Lrrk1* expression can be detected in the lung, in distal limbs and in the primordia of the teeth; one day later also in tongue and kidney similar to *Lrrk2*. Interestingly, the tissue expression patterns are similar, but distinct within the tissues. In the developing kidney for example, *Lrrk2* mRNA is more restricted to certain structures like the metanephric vesicles than *Lrrk1*. The same holds true for the expression in the limbs, where *Lrrk2* expression is more or less restricted to the area around the forming bones (Fig.10).

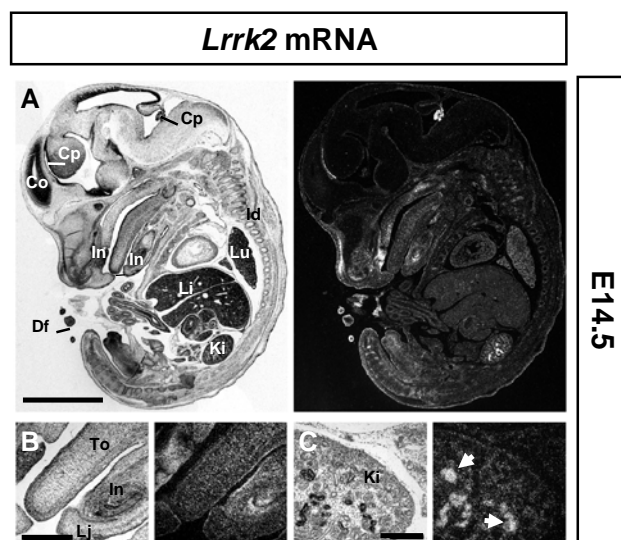


Figure 10:

A detailed view onto the late-gestation embryo reveals that *Lrrk2* shows strong and distinct expression in various regions of organogenesis. ISH for *Lrrk2* mRNA expression in the E14.5 embryo: **A)** The overview sagittal section is depicting strong expression in the choroid plexus, in chondral structures of the nasal capsule and intervertebral discs as well as in the mesenchyme surrounding the forming digits. **B)** Detailed view of the lower jaw reveals strong *Lrrk2* expression in the primordium of upper and lower incisive tooth. **C)** Detailed view of the developing kidney with strong expression in

the metanephric vesicles (white arrow). **Abbr.:** Co, cortex; Cp, choroid plexus; Df, forelimb digit; Id, intervertebral disc; In, incisive; Ki, kidney; Li, liver; Lu, lung; Pi, pituitary gland; To, tongue. Scale bars represent 2mm (A) and 250µm (B, C).

Taken together, the expression of both genes, *Lrrk1* and *Lrrk2* exhibit a largely overlapping expression pattern during embryogenesis in many different organs and structures. Interestingly, both genes are not expressed in high or even moderate amounts in the developing CNS, indicating that they may not play major roles in the overall embryonic development of the murine nervous system.

5.1.2 Expression in the postnatal and adult brain

The first broad and robust *Lrrk2* expression in neuronal tissue can be observed in the murine brain around birth (postnatal day 0 or P0). Not only RT-PCR can detect notable *Lrrk2* mRNA expression (Fig.8), but also distinct *in situ* hybridisation signal becomes visible in the CNS for the first time. The levels of ubiquitous expression is not too prominent, but some domains, specifically in the developing cortex, in the cerebellum and in the brain stem show stronger expression (Fig.11, A). At P7, the overall expression level, but also the levels in some distinct regions of the brain like in the striatum or, transiently in the olfactory bulb, increases notably. During these first weeks, on the one side, the expression domain in the cortex gets dorsoventral extended and stronger, whereas the level of *Lrrk2* expression in the olfactory bulb decreases slightly but is still higher compared to adulthood. Furthermore, in the developing cerebellum, the widespread *Lrrk2* expression narrows down to the Purkinje cell layer. The expression in the caudate putamen (striatum) is rather low, compared with the cortical domain (Fig.11, B).

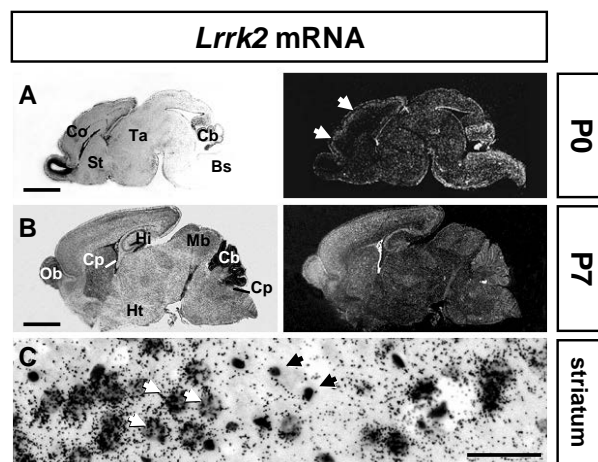


Figure 11:

Lrrk2 mRNA expression in neuronal tissue can be observed for the first time in the murine CNS around birth. The ISH signal is increasing during the postnatal development and shows a predominately neuronal association. Expression of *Lrrk2* mRNA depicted by ISH from earliest postnatal stages onwards: **A)** At birth (P0) weak *Lrrk2* expression is detected ubiquitously; only the developing cortex (**white arrows**), cerebellum and brainstem show moderate to stronger expression. **B)** At stage P7, levels in forebrain structures like cortex, striatum and olfactory bulb increases. Strong signal in the non-neuronal tissue of the choroid plexus persists throughout development. **C)** A high magnification bright-field picture demonstrates the association of ISH signal (black grains) predominately with the larger neuronal nissl bodies (nuclei and ER) (**white arrows**) instead of the smaller glial nuclei (**black arrows**).

Abbr.: Bs, brain stem; Cb, cerebellum; Co, cortex; Cp, choroid plexus; Hi, hippocampus; Mb, midbrain; Ob, olfactory bulb; Sc, spinal cord; St, striatum; Th, thalamus; Scale bars represent 2mm (A, B) and 50 μ m (C).

After three weeks, at postnatal day 21 the striatal expression has outrun the cortical expression and is now one of the most outstanding expression domain in the central nervous system besides the ones of in the piriform and

visual cortices, olfactory tubercle, cerebellum and brainstem. To this time point almost all expression domains have reached their adult levels. Only in the olfactory bulb the amount of *Lrrk2* mRNA is still slightly higher than observed in adulthood (**Fig.13, C**).

In the adult mouse brain (older than 6 weeks), positive *in situ* hybridisation signal can be detected ubiquitously in virtually all brain regions. Strongest expression is found in the forebrain and cerebellum. Conspicuously high expression is found in the piriform and visual cortex, olfactory tubercle, striatum and amygdala (**Fig.12, E, F** and **Fig.13, D**). Interestingly the cortex exhibits an area-specific expression of *Lrrk2*, with highest expression in the piriform and visual

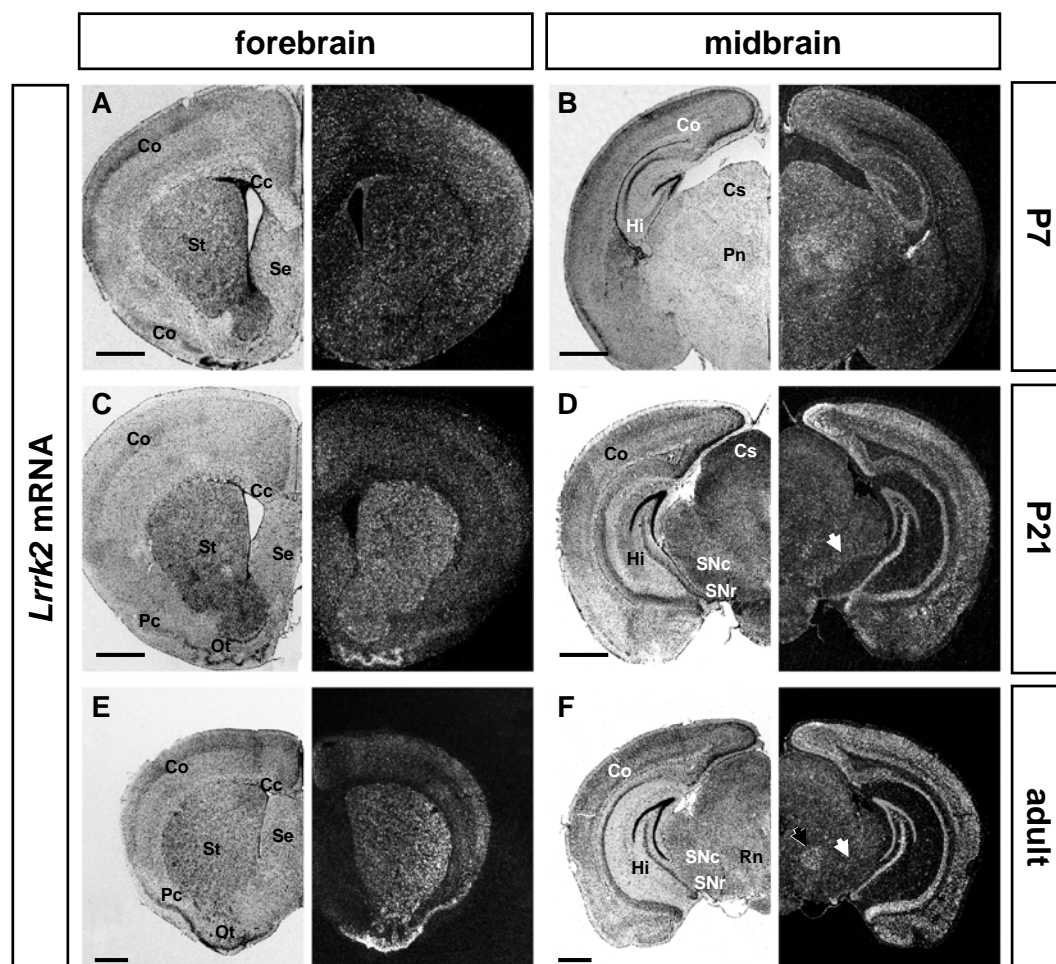


Figure 12: The expression of *Lrrk2* in the postnatal forebrain is highly dynamic. In the striatum, mRNA levels increase markedly in comparison to the cortex during postnatal development. On the contrary, the substantia nigra in the midbrain depicts constantly a quite low degree of expression (white arrows). *Lrrk2* expression depicted by ISH on coronal brain sections from postnatal and adult mice. **Abbr.:** Cc, corpus callosum; Co, cortex; Cs, superior colliculus; Hi, hippocampus; Mb, midbrain; Ot, olfactory tubercle; Pc, piriform cortex; Pn, parafascicular nucleus; Rn, red nucleus; Se, septum; SNc, substantia nigra pars compacta; SNr, substantia nigra pars reticulata; St, striatum; Scale bars represent 1 mm.

cortex; however, strong expression can also be observed in the motor, somatosensory, auditory and visual cortex (**Fig.13, D**). Furthermore, the anterior olfactory nucleus as well as the hippocampus displays strong *Lrrk2* expression. Herein, specifically the pyramidal cells of the hippocampus proper (CA1,2, and 3) are strongly labelled, whereas the dentate gyrus displays less expression (**Fig.12, F**). *Lrrk2* expression can also be found in the subventricular zone (data not shown) - the second region of neurogenesis in the adult

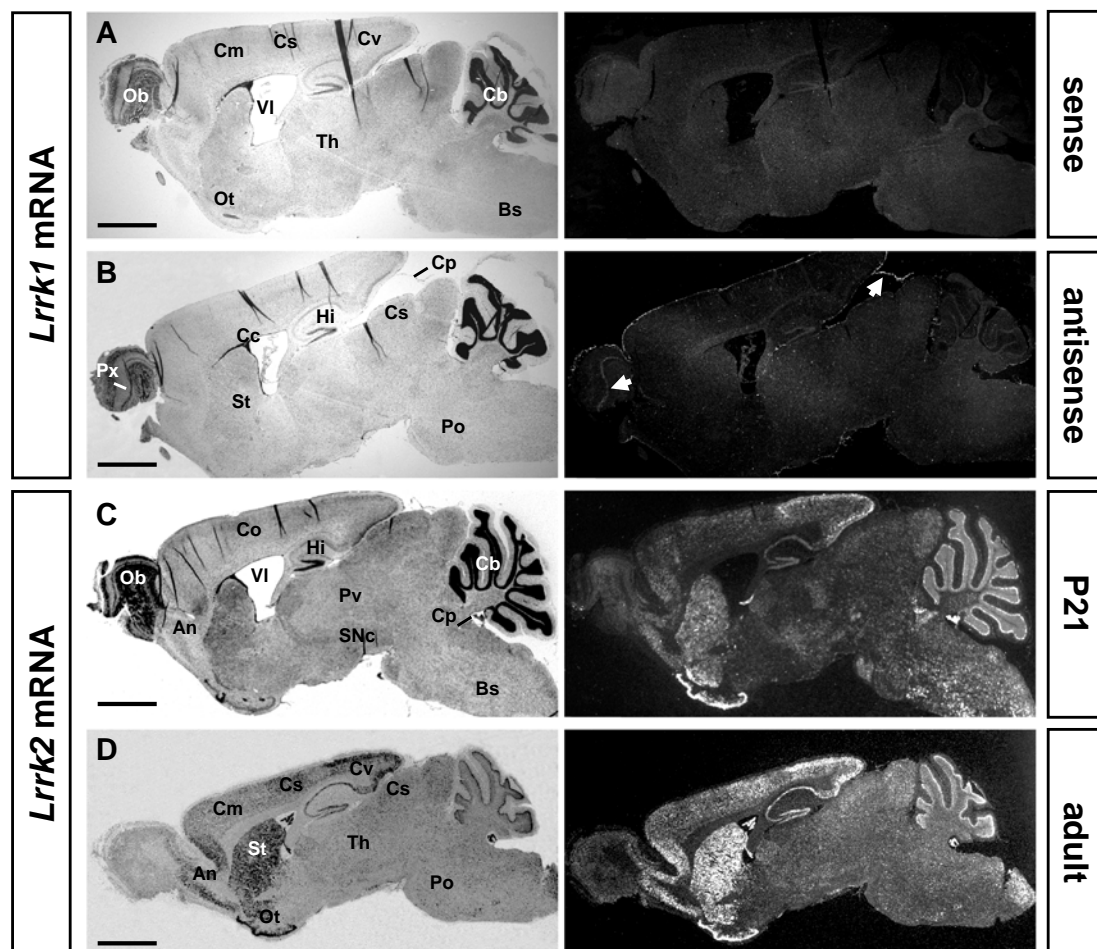


Figure 13: Expression of the *Lrrk2*-paralog *Lrrk1* is barely detectable in the postnatal and adult mouse brain. Besides the non-neuronal meninges, only the olfactory bulb depicts *Lrrk1* mRNA expression. In contrast, on consecutive sections strong *Lrrk2* expression can be detected in various regions throughout the postnatal and adult CNS. *Lrrk1* and *Lrrk2* ISH in the 21 day old (A-C) and adult (D) murine brain: **A**) The according sense-probe is used as a negative control in ISH experiments. **B**) Various *Lrrk1*-specific ISH probes only detect mRNA expression restricted to the mitral cell layer and the meninges (white arrows). **C, D**) Overview of *Lrrk2* expression in the postnatal and adult murine brain. **Abbr.:** An, anterior olfactory nucleus; Bs, brain stem; Cc, corpus callosum; Co, cortex; Com, motor cortex; Cos, somatosensory cortex; Cov, visual cortex; Hi, hippocampus; Mb, midbrain; Ot, olfactory tubercle; Pc, piriform cortex; Px, plexiform layer; Pn, parafascicular nucleus; Po, pons; Rn, red nucleus; Se, septum; SNc, substantia nigra pars compacta; St, striatum; Th, thalamus; VI, lateral ventricle. Scale bars represent 2mm.

rodent brain besides the hippocampus.

Going caudal from the thalamus to the midbrain, two very distinct domains with high expression are the parafascicular nucleus and the red nucleus. The area of the superior colliculus displays moderate expression. The dopaminergic system of the midbrain, built up by the substantia nigra pars compacta and pars reticulata as well as by the ventral tegmental area show only moderate to lower levels of *Lrrk2* expression (**Fig.12, D, F and Fig.13, C**). In the hindbrain, we find the strongest *in situ* hybridisation signals in the Purkinje cell layer of the cerebellum and in the pontine nuclei. Moderate expression can be detected in the median raphe nucleus, reticulotegmental nucleus of the pons and in the facial nucleus (data not shown). Altogether, the ubiquitous level of *Lrrk2* mRNA in the hindbrain is slightly higher than in midbrain. This general pattern of expression sustains stable during adulthood; also in the brains of aged wild-type mice up to 24 month, no significant differences neither in regard to the pattern, nor to the level of expression could be observed (data not shown).

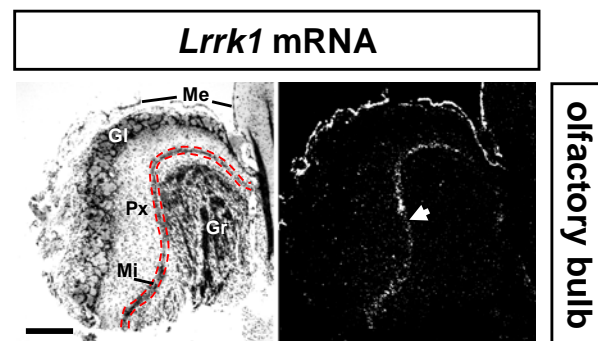


Figure 14:

A detailed view onto the adult olfactory bulb depicts the only neuronal expression of *Lrrk1* in the mitral cell layer (white arrow). *Lrrk1* mRNA expression detected by radio-active ISH in the adult CNS. **Abbr.:** **Gl**, glomerular layer; **Gr**, granular layer; **Me**, meninges; **Mi**, mitral layer; **Px**, plexiform layer. Scale bar represents 500µm.

In contrast to *Lrrk2*, *Lrrk1* mRNA can not be detected in the early postnatal brain. Only the meninges, surrounding the CNS exhibit a strong *in situ* hybridisation signal. The rest of the CNS depicts if at all background staining similar to the sense probe which serves as negative control (**Fig.13, A, B**). This holds true until adulthood. Confirmation via RT-PCR from adult brain tissue reveals almost no products in regions like striatum or ventral midbrain. Only in the sample derived from cortical RNA, *Lrrk1* mRNA could be detected (data not shown); it has to be assumed, that at least partially the strongly *Lrrk1* expressing meninges were accidentally dissected together with the rest of the tissue. Later on, at around postnatal day 21 (P21) a single expression domain is

showing up - the mitral cell layer of the olfactory bulb (**Fig.13, B and Fig.14**); this holds true until adulthood.

Taken together, after birth the expression of *Lrrk2* becomes detectable within neuronal tissue in the CNS and increases during the early postnatal development of the rodent brain. Conspicuous is the strong increase in expression in the striatum and cortex and the remaining low expression in the midbrain - specifically within the substantia nigra and the ventral tegmental area. In contrast to *Lrrk2*, *Lrrk1* is barely detectable in the adult mouse brain and limited to a cell layer in the olfactory bulb where no prominent *Lrrk2* expression can be found.

5.1.3 LRRK2 protein expression in the adult CNS

In the course of this work, a whole variety of different commercial and non-commercial antibodies directed against LRRK1 and LRRK2 protein were tested in different immunohistochemistry (IHC). Despite of using several different modi of tissue preparation, antigen retrieval and detection, nearly all antibodies depicted either no or ubiquitous protein distribution in the adult murine brain and thereby failed to proof their specific binding to LRRK2 in histochemistry (**Fig.15**). Weak cellular staining in *Lrrk2* mRNA expressing regions of the adult CNS could be obtained by using the commercial polyclonal antibody NB300-267. On knockdown tissue, IHCs resulted in moderate reduction of the staining suggesting at least partial specificity (data not shown); nevertheless, these results could not be confirmed with later batches of the antibody.

However, to determine the expression of LRRK2 in the adult brain also on the protein level, we used instead Western blot analysis on total protein lysates prepared from different brain regions. For this, the polyclonal antibody 1E11 (produced by Elisabeth Kremmer) which has been shown to be highly specific in Western blot analysis (Gloeckner *et al.*, 2009) was used on total cell lysates prepared from nine regions of the adult brain. Subsequent quantification and normalization to beta-tubulin levels revealed that the pattern of protein expres-

Antibody:				Tested in:	Staining on Tissue:		Specificity:
name	protein	epitope	provider		wild-type	knockdown	
AP7098a	Hs-LRRK1	n-terminus	Abgent Antibodies	IHC-P, IHC-Fr	no	<i>n.d.</i>	no
AP7098b	Hs-LRRK1	c-terminus	Abgent Antibodies	IHC-P, IHC-Fr	no	<i>n.d.</i>	no
1E11	Hs-LRRK2	n/a	E. Kremmer (HMGU)	IHC-Fr	no	<i>n.d.</i>	no
SC-48736	Mm-Lrrk2	n-terminus	Santa Cruz Biotechnology	IHC-P, IHC-Fr, ICC	yes	yes	no
NB300-267	Hs-LRRK2	aa 900-1000	Novus Biologicals	IHC-P, IHC-Fr, ICC	yes	reduced	partially
ab60154	Hs-LRRK2	aa 260-300	Abcam®	IHC-P, IHC-Fr	no	<i>n.d.</i>	no
4A7	Hs-LRRK2	n/a	E. Kremmer (HMGU)	IHC-Fr	no	no	no
NoB7	Hs-LRRK2	n/a	E. Kremmer (HMGU)	IHC-Fr	no	no	no
4D1	Hs-LRRK2	n/a	E. Kremmer (HMGU)	IHC-Fr	yes	yes	no
11D7	Hs-LRRK2	n/a	E. Kremmer (HMGU)	IHC-Fr	no	no	no
3F1	Hs-LRRK2	n/a	E. Kremmer (HMGU)	IHC-Fr	yes	yes	no
13G5	Hs-LRRK2	n/a	E. Kremmer (HMGU)	IHC-Fr	yes	yes	no
12H2	Hs-LRRK2	n/a	E. Kremmer (HMGU)	IHC-Fr	no	no	no
LS-C96473	Hs-LRRK2	aa 2200-2500	LifeSpan Biosciences	ICC	no	<i>n.d.</i>	no
MJFF-1 (C5-8)	Hs-LRRK2	aa 970-2527	G. Piccoli (IHG, HMGU)	IHC-Fr	no	no	no
MJFF-2 (C41-2)	Hs-LRRK2	aa 970-2527	G. Piccoli (IHG, HMGU)	IHC-Fr	no	no	no
MJFF-3 (C69-6)	Hs-LRRK2	aa 970-2527	G. Piccoli (IHG, HMGU)	IHC-Fr	no	no	no
MJFF-4 (C81-8)	Hs-LRRK2	aa 970-2527	G. Piccoli (IHG, HMGU)	IHC-Fr	no	no	no

Figure 15: A variety of commercial and non-commercial antibodies failed to detect LRRK1 and LRRK2 protein on their endogenous levels in immunohistochemistry (IHC). List of antibodies tested for IHC in the course of this work. Only the LRRK2-directed antibody NB300-267 did show a moderate reduction on knockdown tissue suggesting at least partial specificity. Any cellular staining on wild-type tissue (adult brain; in some cases also embryonic tissue) is indicated in green; similar and non-reduced staining on LRRK2 knockdown tissue is indicated in red. **Abbr.:** aa, amino acid position in the LRRK2 protein; **HMGU**, Helmholtz-Zentrum München; **ICC**, immunocytochemistry on primary neurons; **IHC** Immunohistochemistry on **-Fr**, free floating cryo sections (**-Fr**) or on paraffin sections (**-P**); **n/a**, not applicable; **n.d.** not determined.

sion fits quite well to the pattern observed by radioactive *in situ* hybridisation (ISH). The highest levels of *Lrrk2* mRNA and protein could be detected in cortex and striatum by both approaches. But strikingly, while ISH did show a higher relative level of *Lrrk2* mRNA in the striatum compared to cortex (e.g. **Fig.12, F**), on the protein level it was the other way around. To obtain quantitative data in regard to mRNA levels, we performed quantitative real-time PCR. Therefore, for preparing total RNA, we were utilizing the contralateral site of the very same brain samples which have been used for Western blot analysis. The levels of *Lrrk2* mRNA measured by qPCR did also match quite well to the ISH data. Nevertheless, by comparing the relative percentages of mRNA and protein, we detected a big discrepancy between these levels in the striatum where 32.9% ($\pm 6.2\%$) of the total *Lrrk2* mRNA but only 17.6% ($\pm 4.0\%$) of LRRK2 protein of the adult CNS is expressed. This indicates an excess of 1.8-fold of mRNA if we assume a close to 1:1 correlation of the relative protein and mRNA levels throughout the brain. A higher mRNA excess could only be observed in the brain-stem (2.25-fold) but on a far lower

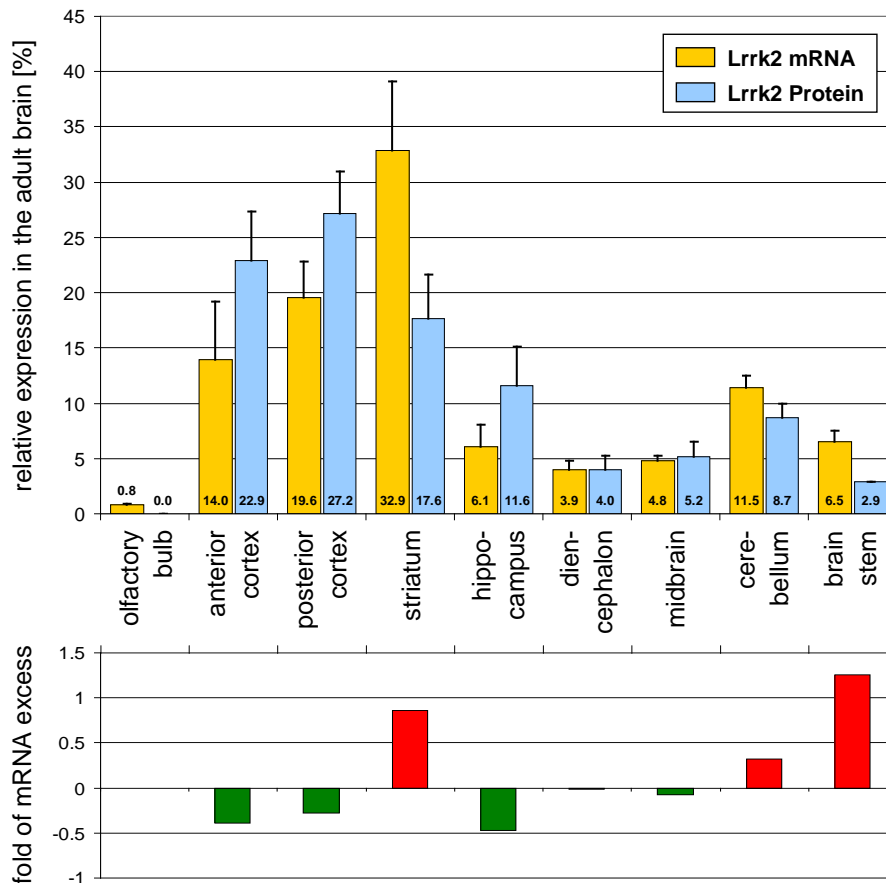


Figure 16: Relative *Lrrk2* mRNA and protein levels correspond in most regions of the adult mouse brain; nevertheless, especially in the adult striatum and brain stem, a conspicuous excess of mRNA could be observed. This was taken as a hint for a possible posttranscriptional regulation of *Lrrk2* expression in distinct regions of the CNS. Results from quantitative real-time PCR and Western blot quantifications in various brain regions. To allow the comparison of both LRRK2 mRNA and protein, in both cases the sum of all individual levels were set to 100%. The fold of mRNA excess (mRNA/protein [both in percentage of total brain levels]) of each brain region is indicated below. For detecting *Lrrk2* mRNA and protein respectively, the anti-LRRK2 antibody 1E11 and the TaqMan® gene expression assay for murine *Lrrk2* (Mm00481934_m1) have been used.

level ($6.5\% \pm 1.0\%$ of mRNA, compared to $2.9\% \pm 0.1\%$ of protein). Since the population of the medium spiny neurons (MSNs) in the striatum do exhibit rather local projections compared for example with the long projecting dopaminergic or serotonergic neurons of the midbrain, a possible transport of LRRK2 protein out of the striatum seems to be unlikely to explain the observed discrepancies. Instead we assume a posttranscriptional regulation of *Lrrk2* in the striatum via specific microRNAs and are currently working to prove this hypothesis.

5.1.4 *Lrrk2*-expressing neuronal subtypes in the striatum

Focusing on the most interesting and pronounced *Lrrk2* expression domain - expressed. The radioactive *in situ* hybridisation allows discriminating between neuronal, glial and endothelial cells by their different morphology in the Nissl counterstaining (Love *et al.*, 2008). Based on this, we observed *Lrrk2* to be expressed predominantly in neurons and to a small amount in glial cells (Fig.11, C). Since the striatum is the major target of the dopaminergic neurons in the substantia nigra affected in PD, the identification of dopaminoceptive neurons expressing *Lrrk2* in this region is of relevance. To get more information about the actual subtypes of neurons, we performed nonradioactive *in situ* hybridisation, either with a fluorescent or a nonfluorescent precipitate as signal, followed by fluorescent immunohistochemistry for different marker genes of the dopaminoceptive neurons (see 7.2.2.3 and 7.2.2.4). This more elaborate technical set-up was necessary since we could not perform double immunohistochemistry (see 5.1.3, Fig.15).

First of all we could confirm the predominant neuronal expression of *Lrrk2* by showing a very high, but not total overlap of strong *Lrrk2* mRNA expressing cells with the broad neuronal marker NeuN (Neuronal Nuclei antigen) in the

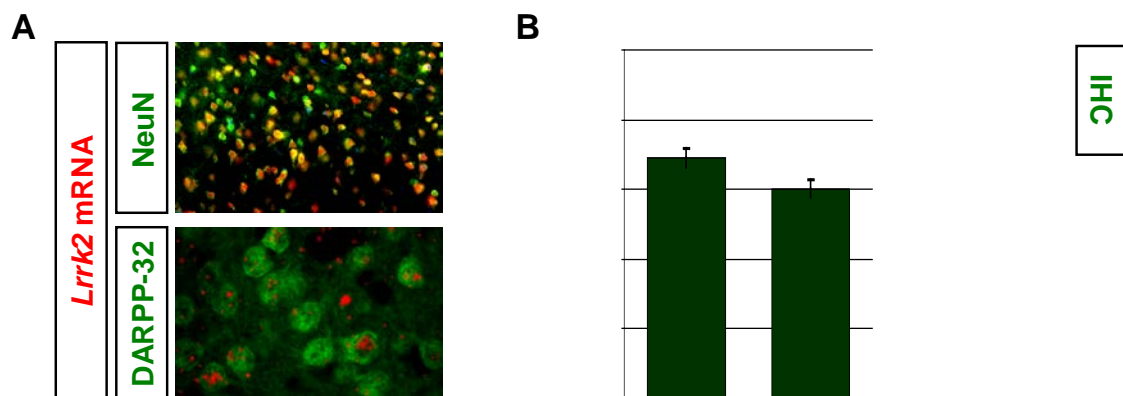


Figure 17: *Lrrk2* mRNA in the striatum is expressed in the dopaminoceptive medium spiny neurons. Furthermore, *Lrrk2* mRNA expression colocalizes only partially with dopamine receptor-D1 (DR-D1) or DR-D2-positive neurons respectively, indicating a role in both the direct as well as the indirect pathway of the basal ganglia circuit. **A)** Double *in situ* - and immunohistochemistry (ISH-IHC) results: **A)** ISHs using a fluorescent precipitate to depict *Lrrk2* mRNA in red followed by IHCs either against the pan-neuronal marker NeuN or the medium spiny neuron (MSN) marker DARPP-32. **B)** ISHs using a non-fluorescent precipitate to depict *Lrrk2* mRNA in black followed by IHCs against the two main dopamine receptors. Quantification revealed that $69.02\% \pm 0.4\%$ DR-D1 positive and $60.3\% \pm 3.7\%$ DR-D2 positive cells heavily coexpress *Lrrk2* mRNA.

adult cortex (**Fig.17**). The dopamine and cAMP regulated phosphoprotein 32 (DARPP-32) also named PPP1R1B was used as a marker for the medium spiny neurons (MSNs) in the striatum (Hemmings and Greengard, 1986) which are the main target cells for the dopaminergic neurons of the nigro-striatal pathway. Virtually all striatal cells which highly express *Lrrk2* mRNA are positive for this integrator of dopamine signalling, indicating that in dopaminoceptive neurons the level of LRRK2 is conspicuously elevated. This notion was supported by double *in situ* - and immunohistochemistry (ISH-IHC) using antibodies against the two predominant dopamine receptors DR-D1 and DR-D2.

For quantification we used an approach with a nonfluorescent precipitate as an *in situ* hybridisation signal, which is less sensitive but gives also less background (**Fig.17**). High, but interestingly not complete overlap of expression is found for striatal neurons with high *Lrrk2* mRNA expression. 69.02% ($\pm 0.4\%$) of all DR-D1 positive cells and 60.3% ($\pm 3.7\%$) of all DR-D2 positive cells are heavily expressing *Lrrk2* mRNA. From this, we can conclude that indeed *Lrrk2* is expressed in both dopaminoceptive populations of the medium spiny neurons in the striatum, thereby possibly affecting both the direct and indirect pathway within the basal ganglia circuitry.

5.2 Generation of the *Lrrk2* R1441C knock-in mouse line

The idea behind this mutant mouse line is to create a model for Parkinson's disease by inserting the first in patients identified pathological point mutation R1441C into the endogenous murine *Lrrk2* gene. This missense mutation in the Roc-GTPase domain is leading to an amino acid substitution from basic arginine to hydrophilic cystein.

LRRK2 <i>Mus musculus</i> (NM_025730.3)	KLMIVGNTGSGKTTLLQQLMKMKPELGMQGATVGDVDRDWSIQIRGKRRKDLVLNVWDFAGR	1398
LRRK2 <i>Homo sapiens</i> (NM_198578.3)	KLMIVGNTGSGKTTLLQQLMKTKKSDLGMQSATVGDVVDWPIQIRDKRKRDLVLNVWDFAGR	1398
	*****.*****.*****.*****.*****.*****.*****.*****.*****.*****	
LRRK2 <i>Mus musculus</i> (NM_025730.3)	EEFYSTHPHFMTQRALYLAVYDLSKGGQAEVDAMKPWLFNFKARASSSPVILVGTSLDVSDEKQ	1461
LRRK2 <i>Homo sapiens</i> (NM_198578.3)	EEFYSTHPHFMTQRALYLAVYDLSKGGQAEVDAMKPWLFNFKARASSSPVILVGTSLDVSDEKQ	1461
	*****.*****.*****.*****.*****.*****.*****.*****.*****.*****	

Figure 18: The vicinity of the R1441C mutation site is completely conserved between *Homo sapiens* and *Mus musculus*. Protein alignment (*ClustalW2*) of the human LRRK2 Roc-GTPase domain with its murine homologue (amino acids 1335 to 1461 based on the specified transcripts). The PD-associated arginine-residue 1441 is indicated in orange.

The LRRK2 protein is highly conserved between mouse and human (Marín, 2006) and especially the vicinity of residue 1441 is 100% identical between those two species (**Fig.18**). Therefore, it is possible to simulate the molecular effects of this point mutation in the endogenous locus, avoiding the exogenous expression or overexpression of a mutated human transgene.

5.2.1 The *Lrrk2* R1441C knock-in targeting strategy

The strategy to insert the transition $c>t$ in the first position of the second codon of exon 31 leading to the pathogenic missense mutation R1441C was planned and designed in a collaboration with Dr. Holger Prokisch from the institute of human genetics of the Helmholtz Zentrum München. The targeting construct was generated by the DNA engineering company Gene Bridges[©] utilizing Red[®]/ET[®] recombination out of a BAC clone into the targeting vector.

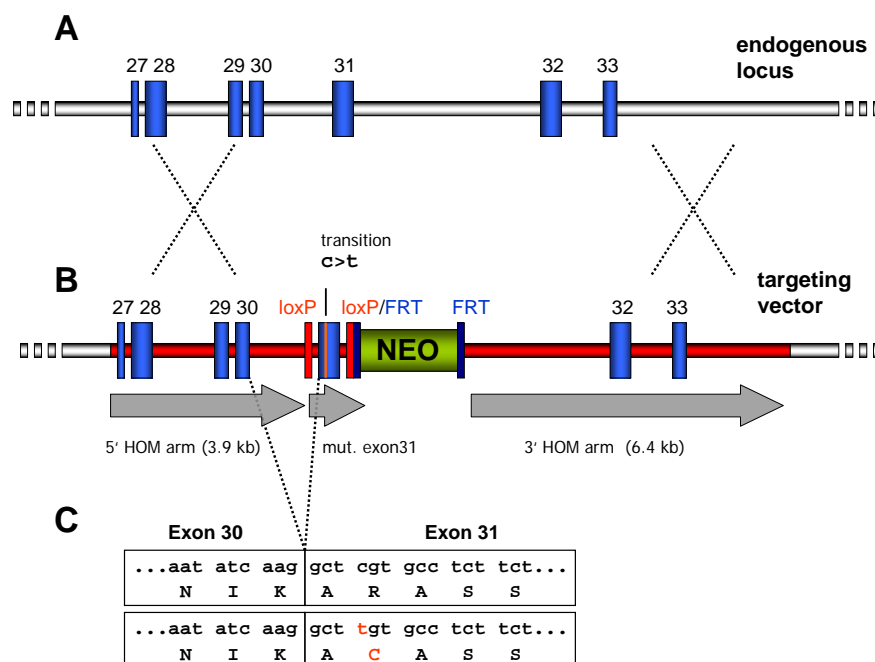


Figure 19: The *Lrrk2* R1441C knock-in targeting strategy is based on the homologous recombination of the point-mutated *loxP*-flanked exon 31 followed by a selection marker into the endogenous *Lrrk2* locus. **A)** Part of the endogenous genomic *Lrrk2* locus with its exons 27-33. **B)** The genomic locus after integration of the targeting construct (red) consisting of the 5'- and 3'-homology arm (HOM arm), the *loxP*-flanked exon 31 bearing the transition $c > t$, followed by the *FRT*-flanked neomycin resistance cassette. **C)** The wild-type and mutated mRNA and protein sequences indicating the resultant missense mutation R1441C.

The resulting vector *pKnock-In Park8* (see 9.1, Fig.59) consists of the 5'-homology arm of about 3.9 kb length spanning the *Lrrk2* genomic region from introns 26 till 30; then follows exon 31 with the single nucleotide substitution inserted by site-directed mutagenesis and flanked by two *loxP* (locus x-over P1)-sites in the adjacent intronic sequences. Subsequently follows a FRT site flanked neomycin resistance cassette and the approximately 6.4 kb long 3' homology arm which ends in intron 33 (Fig.19).

After correct homologous recombination, the endogenous wild-type exon 31 is exchanged with the mutated and *loxP*-flanked form. In addition, the length of intron 31 increases by approximately 2 kb due to the insertion of the neomycin resistance cassette (Fig.19, B). By means of *FLP-FRT* recombination it would be possible to remove the inserted neomycin resistance cassette after it is utilized as selection marker in the procedure of ES clone screening (Zhu & Sadowski, 1995). The *loxP* sites in contrast allows removing the whole exon 31 site- and time-specific by *Cre-lox* recombination (Metzger & Chambon, 2001). Since it is composed out of 219 bases, the removal of this exon will not lead to a frameshift but to the deletion of the C-terminal part of the ROC-GTPase domain and in consequence to the disruption of the GTPase activity of the protein.

5.2.2 Generation of *Lrrk2* R1441C transgenic ES cells

Prior to the electroporation of the construct, the targeting vector has to be linearized to support its recombination. For this, the restriction enzyme *Ppi I* was used in most cases (see 9.1, Fig.59). Altogether four electroporations into cells from the embryonic stem cell line TBV2 derived from 129SV/J mice, were performed. Therefore, $1 \cdot 10^8$ cells were mixed with 120 μg of the linearized plasmid *pLrrk2-knock-in* and electroporated with a single electric pulse for 0.1 msec with 0.8 kV and 3 μF . After every successful run, the cells were positively selected by the Neomycin analogue Geneticin (G418). Clones surviving the treatment with 150 – 200 $\mu\text{g}/\text{ml}$ of the antibiotics in ES culturing medium for six to eight days, were picked and expanded, now again without selection, on multi-well dishes. Several copies of these plates were generated for both genomic DNA isolation and transient storage of the cells in liquid

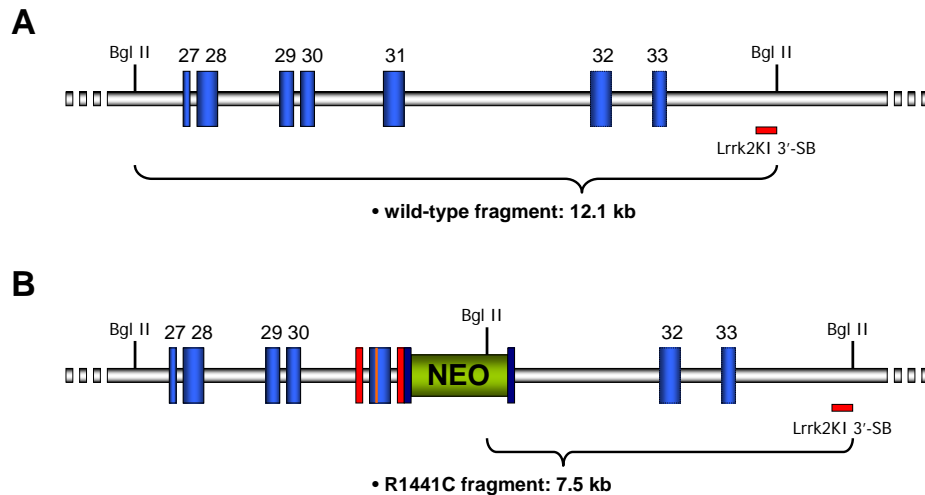


Figure 20: Schematic illustration of the *Lrrk2* R1441C 3'-Southern blot principle used to verify correct recombination in ES cell clones. A) The probe *Lrrk2KI 3'-SB* (red) does recognize a 12.1kb big fragment created by *Bgl II* digestion. B) After insertion of the *Lrrk2* knock-in construct, an additional *Bgl II* restriction site in the neomycine resistance cassette shortens this fragment to 7.5 kb, which allows to discriminate between the wild-type and R1441C allele. The corresponding 5' Southern blot principle is illustrated in 7.2.1.5, Fig.55.

nitrogen. The prepared DNA of the clones were then screened via Southern blot analysis for homologous integration of the targeting vector using *Bgl II* to digest the genomic DNA, and by using the Southern blot probe *Lrrk2KI 3'-SB* located upstream of the 3' homology arm (Fig.20).

Altogether seven ES cell clones out of about 600 to 700 screened clones could be identified to be correctly recombinant (Fig. 21). Checking the recombination via 3'-Southern blot, only the correct integration of those parts of the vector between the 3' end of the homology arm and the *Bgl II* restriction site

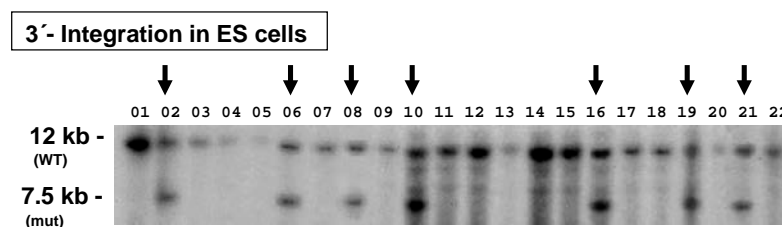


Figure 21: In total seven ES cell clones have been identified for positive 3'-integration. For four of the clones, a complete homologous recombination could be verified and were used for blastocyst injection. Identification of transgenic ES cells via Southern blot using the probe *Lrrk2KI 3'-SB*. Positive heterozygous clones (arrows) do show both wild-type (12 kb) and mutant bands (7.5 kb) at a comparable level of intensity indicating a true-positive result. Principle and fragment sizes are depicted in Fig.20.

can be verified. To ensure, that no crucial parts of the construct are missing due to incomplete recombination, all positive clones had to be checked also for correct 5'-integration by another Southern blot assay. For four out of seven clones, this 5'-Southern blot (see 7.2.1.5, Fig.55), using the probe *Lrrk2KI* 5'-SB on *Spe I* digested DNA (data not shown), confirmed correct integration. Those four recombinant embryonic stem cell clones have then been thawed, expanded and prepared for blastocyst injection.

5.2.3 Generation of the *Lrrk2* R1441C knock-in mouse line

Embryonic stem cells from all these four clones were injected into C57BL/6 derived blastocysts and transferred into pseudopregnant CD-1 foster mothers. Three of the clones gave rise to in total four chimeric mice (C1-4). They have been classified on the basis of their fur colour being between 30% and 100% chimeric (C1^{cloneC7}: 30%; C2^{cloneC7}: 30%; C3^{cloneG9/2}: 90%; C4^{cloneF6}: 100%). Every hair follicle which arise from a wild-type cell, will create a black (a/a), every follicle from a transgenic cell an agouti (A^w/a) coloured hair. Since more agouti fur colour indicates, that more transgenic cells contributed to this particular mouse, the probability that a high-degree chimera will give birth to a transgenic offspring is higher respectively. This germ line transmission, standing for the event that an embryo originates from either a transgenic sperm- or egg-cell, occurred for three of the four chimeras and was confirmed not only by Southern blot but also by PCR and sequencing (Fig.22). Genotyping via PCR, in this case was based on three different reactions. With at least one wild-type allele as template, reaction *Exon31-WT* will generate a 900bp product stretching from intron 30 to intron 31. In case of integration, the size would have to increase to more than 3 kb, since it now contains the neomycin cassette. Due to the competition with the much shorter wild-type fragment (Raeymaekers, 2000), this product can efficiently only be amplified in homozygote state - like here in the positive control using the vector p*Lrrk2*-knock-in (=p*Knock-In Park8*) as template. *Exon31-Neo* uses the very same 5' primer but now in combination with a 3' primer located in the neomycin cassette giving rise to a 1 kb product. The amplification of the 800 bp product

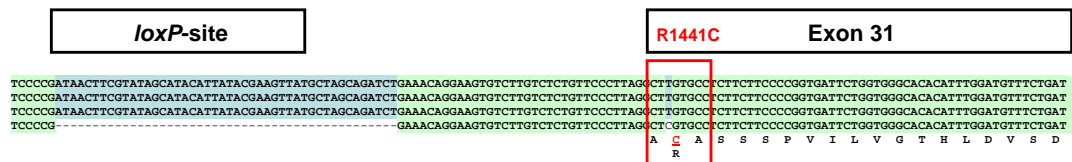


Figure 22: The final verification via PCR and sequencing of the first obtained *Lrrk2* R1441C knock-in mice could demonstrate the perfect accuracy of the integration and confirms the germ-line transmission event. **A)** Schematic illustration of the *Lrrk2* R1441C locus in wild-type (upper) and mutated form (lower). The different amplicons used for genotyping are indicated in red. **B)** The corresponding PCR results using either wild-type DNA, the targeting vector *pKnock-In Park8*, DNA of the identified ES cell clone F6 or DNA from the first 4 animals (B1-4) as template, confirmed the germ-line transmission event. **C)** Sequencing results from two mutant mice (B1 and B4) in comparison with the sequences of the targeting vector *pKnock-In Park8* and of the wild-type *Lrrk2* locus confirms the correct integration of the construct (see 9.1, Fig.60).

Neo served as additional control. Figure 22 b demonstrates germline transmission for the mice B1, B3 and B4. The PCR products *Exon31-WT* and *Exon31-Neo* respectively, were used for sequencing. Thereby, the presence of the point mutation and the total integrity of both *loxP* sites could be confirmed (Fig.22, C).

The R1441C *Lrrk2* knock-in mice display no obvious initial phenotype. Heterozygote and homozygote carriers of the R1441C point mutation can not be discriminated from their wild-type littermates in respect to size, viability and home cage behaviour. Breeding heterozygote males and females, the genotypes of the animals display a normal Mendelian ratio (n=230) Thus, viability of mutant mice is not reduced. Fertility of the mutant mice, litter size and gender distribution is also not altered (data not shown).

5.3 The *Lrrk2* knockdown mouse line

In addition to the R1441C knock-in mouse line, Doctor Ralf Kühn provided us with a further *Lrrk2* mouse model – the *Lrrk2* knockdown mouse utilizing RNAi-mediated gene silencing of the target gene (Kühn *et al.*, 2007; Delić *et*

al., 2008). Initially, a pgk-promoter driven hygromycin cassette, flanked by attP recognition sites for Φ C31 integrase (Groth *et al.*, 2000) has been integrated into the ROSA26 locus by homologous recombination to obtain the ROSA26 acceptor. The thereby modified cell line could be easily modified to generate the *Lrrk2* knockdown line, by exchanging the hygromycin resistance cassette with the short hairpin directed against *Lrrk2* (shLrrk2) (Fig.23, a), which is also flanked by attP sites, via receptor mediated cassette exchange (RMCE) (Hitz *et al.*, 2007).

Selection for recombinant clones could be performed through the newly added Neomycin resistance. The expression of the shLrrk2 construct is driven by the RNA polymerase III promoter U6. The short hairpin consists of a 23 base pair long sense-, followed by a short spacer and the antisense motive, complementary to the target region of the *Lrrk2* mRNA. After transcription, the RNA folds into a stem-loop and forms a short hairpin. Just like the endogenous microRNAs (miRNA), also the shRNA is processed by the enzyme Dicer into double stranded siRNA. In this conformation, it will be incorporated into the RISC complex (RNA-induced silencing complex) together with the target mRNA, leading to its rapid degradation (Lee *et al.*, 2002; Meister and Tuschl 2004).

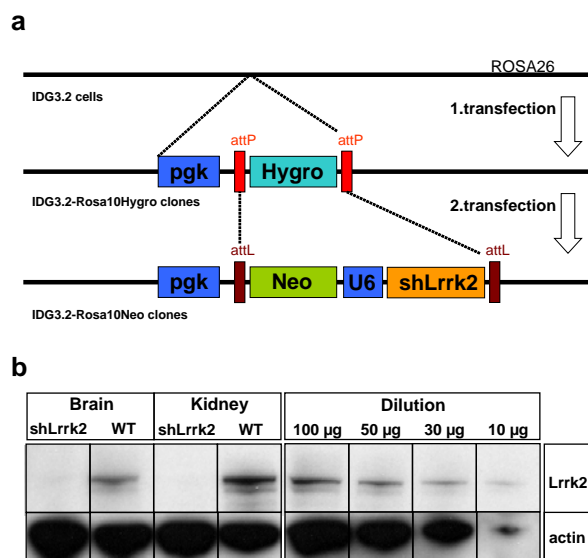


Figure 23:

As a loss-of function model, the *Lrrk2* knockdown mouse line has been used. This short hairpin RNA (shRNA) expressing line displays a LRRK2 reduction by more than 95% on the protein level. Strategy and verification of the *Lrrk2* knockdown mouse: a) Integration of a pgk-promoter driven Hygromycin cassette (Hygro), flanked by attP recognition sites into the ROSA26 locus (upper line) by homologous recombination generates the ROSA26 acceptor (mid-line). Exchanging this cassette with the short hairpin directed against *Lrrk2* (shLrrk2) by RMCE to generate the *Lrrk2* knockdown line (lower line). b)

Verification of the knockdown efficiency in the adult mouse brain and kidney via Western blot analysis using the LRRK2-directed antibody 1E11 (courtesy of Dr. Ralf Kühn).

The *in vivo* functionality and efficiency of the *Lrrk2* knockdown mice has been verified by Western blot analysis of brain and kidney lysates derived from both young and one year old *Lrrk2* knockdown animals (**Fig.23, b**). The knockdown efficiency in the brain exceeds 90% to 95% on the protein level in heterozygous mice carrying one allele the *Lrrk2* targeting shRNA in the ROSA-26 locus (Delić *et al.*, 2008).

This mouse line gave us the opportunity to study complementary to the putative gain-of function effect of a pathogenic point mutation, also the effects of an almost complete loss of LRRK2 protein *in vivo*. Just as well as the R1441C *Lrrk2* knock-in mice, also the *Lrrk2* knockdown animals display no obvious initial phenotype. Neither the size, viability and home cage behaviour of the mutant mice seems to be altered nor the fertility and litter size (data not shown).

5.4 Functional analysis of the Leucine-rich repeat kinase 2

Genetically modified mouse models are not only useful to study the effects of these alterations *in vivo* in the context of a complex animal, but also to analyze isolated tissue or single cells *ex vitro* or *in vivo*. Since basically nothing was known about the physiological function of LRRK2 protein, we decided to start an *in vitro* analysis, looking for cellular and molecular changes in different cell lines derived from our *Lrrk2* R1441C knock-in mouse model as well as from *Lrrk2* knockdown mice.

5.4.1 Analysis of *Lrrk2* R1441C mouse embryonic fibroblasts

Murine embryonic fibroblast cells (MEF) are a suitable system for basic approaches, since they are easy to handle in regard to preparation, immortalization and long-term cultivation. After having confirmed that *Lrrk2* mRNA is expressed in fibroblasts (data not shown) embryonic fibroblasts from wild-type, heterozygote and homozygote E12.5 littermates were prepared and immortalized using the 3T3 protocol, which is based on the continuous passaging of the cells until after 20 to 30 generations a spontaneous immortalized cell line is established (see 7.2.3.1).

Genotyping of the lines was performed from DNA prepared from the cells itself by southern blot. In addition, we studied and compared the expression of wild-type and R1441C point mutated *Lrrk2* by RT-PCR based on RNA prepared from the different fibroblast lines. An amplified cDNA stretch of 730bp, containing exon 31, can be digested by the restriction enzyme *BssSI* into two fragments (480 bp and 250 bp) if the recognition site is not mutated by the R1441C mutation. In the heterozygote state (**Fig.24; A, b**), both the mutated 730 bp fragment and the two wild-type fragments are present in comparable quantity. This result indicates that the inserted point-mutation has no effect onto the expression level and stability of the *Lrrk2* mRNA.

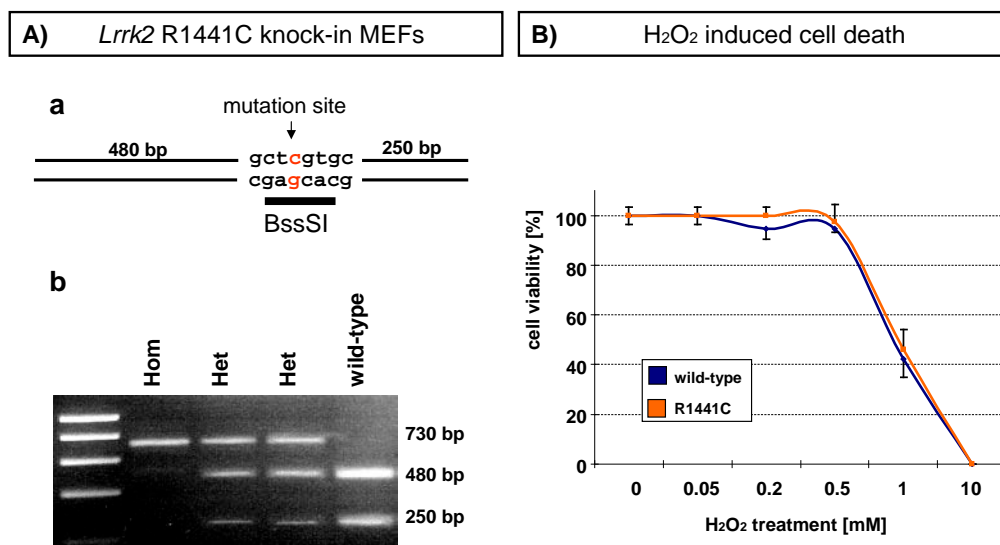


Figure 24: The *Lrrk2* R1441C mouse embryonic fibroblast (MEF) lines correctly express the wild-type and mutated alleles of *Lrrk2* on comparable levels and do not show significant differences in regard to general cell viability and oxidative stress-resistance. **A)** Verification of the *Lrrk2* R1441C knock-in MEF cell lines: **a)** The inserted c>t transition in the first position of the second codon of exon 31 disrupts a *BssSI* restriction site within a 730bp long cDNA amplicon. **b)** Digestion of the cDNA subsequent to RT-PCR results either in complete digestion of both alleles into a 250bp and a 480bp fragment in the wild-type situation (WT), no digestion in the homozygote (HOM) or a partial digestion in the heterozygote (Het) situation. **B)** Viability of wild-type and *Lrrk2* knock-in MEF cells under oxidative stress. Cells were treated with a gradient of hydrogen peroxide for 16 hours: Viability at 0.05 mM H₂O₂: wild-type 100.0% ± 3.5%, R1441C 100.0% ± 3.6%; 0.2 mM: wild-type 94.7% ± 4.2%, R1441C 100.0% ± 3.6%; 0.5 mM: wild-type 94.7% ± 1.4%, R1441C 97.4% ± 7.0%; 1 mM: wild-type 42.1% ± 7.1%, R1441C 46.2% ± 7.0%.

Already during the course of establishing these cell lines, no overt differences in regard to cellular morphology, and general viability could be observed (data not shown). Therefore we applied an additional challenge in order to detect possible slight differences with respect to viability. Hydrogen peroxide is often

used to mimic oxidative stress and to study the resistance of cells to oxidative stress induced cell death *in vitro* (Takahashi-Niki *et al.*, 2004, Görner *et al.*, 2007). We quantified the rate of cell death, induced by rising levels of H₂O₂ over a time period of 16 hours. Viability was assessed by reduction of adherent cells compared to untreated control and by morphological changes like disruption of the cytoskeleton network, rounded shape of the cell or fragmentation of the nucleus. In these conditions, until a hydrogen peroxide concentration of 500 µM both wild-type and *Lrrk2* knock-in MEF cells showed only a slight decrease of relative viability in the range of 5% with a slight but nonsignificantly higher viability in the R1441C knock-in cells especially pronounced at a concentration of 200 µM (wild-type 94.7% ± 4.2%, R1441C 100.0% ± 3.6%; Student's t-test: p=0.19). Subsequently, the viability dropped dramatically around 1 mM H₂O₂; a higher degree of variability within the cultures but no significant differences between the two genotypes could be observed. (Fig.24, B).

Recently published data indeed suggest a higher vulnerability to oxidative stress of different cellular systems by the overexpression of *Lrrk2* bearing the pathogenic mutation G2019S. Toxicity and ROS (reactive oxygen species) production is slightly increased by the mutated kinase domain compared to wild-type protein (Heo *et al.*, 2010, Saha *et al.*, 2010). Thereby, since our data could not proof an enhanced vulnerability to oxidative stress, distinct mechanisms of the G2019S mutation in the kinase domain and of the R1441C mutation in the GTPase domain or a general effect of the LRRK2 expression level has to be assumed.

5.4.2 The cytoskeleton in *Lrrk2* R1441C cells

Based on this initial result which indicates rather distinct roles of the different pathogenic forms of LRRK2, we concentrated our functional analysis onto unique features of the Roc-GTPase domain which is affected by the R1441C point mutation. One of the first published interactions of LRRK2 protein showed the putative binding of alpha- and beta-tubulin heterodimers to the Roc domain of LRRK2 (Gandhi *et al.*, 2008). In addition, it is known that the cytoskeleton structure is highly affected in several neurodegenerative

diseases (Benitez-King *et al.*, 2008). Therefore we decided to take a deeper look onto the cytoskeleton and in particular onto the microtubular network in *Lrrk2* knock-in cells.

5.4.2.1 Basal stability of the cytoskeleton network

Immunocytochemistry for different cytoskeletal marker like beta actin and alpha tubulin did not reveal any differences in the network architecture between wild-type and *Lrrk2* knock-in MEF cells in untreated conditions (**Fig.25, A**). Qualitatively the density of either actin or tubulin polymeric fibres, the length of individual fibres or their distribution within the cell seemed to be normal. Also under mild oxidative stress, induced by hydrogen peroxide (500 μ M for 16hours), no prominent differences in the reaction of the microtubular network could be observed (see **5.4.1**; data not shown).

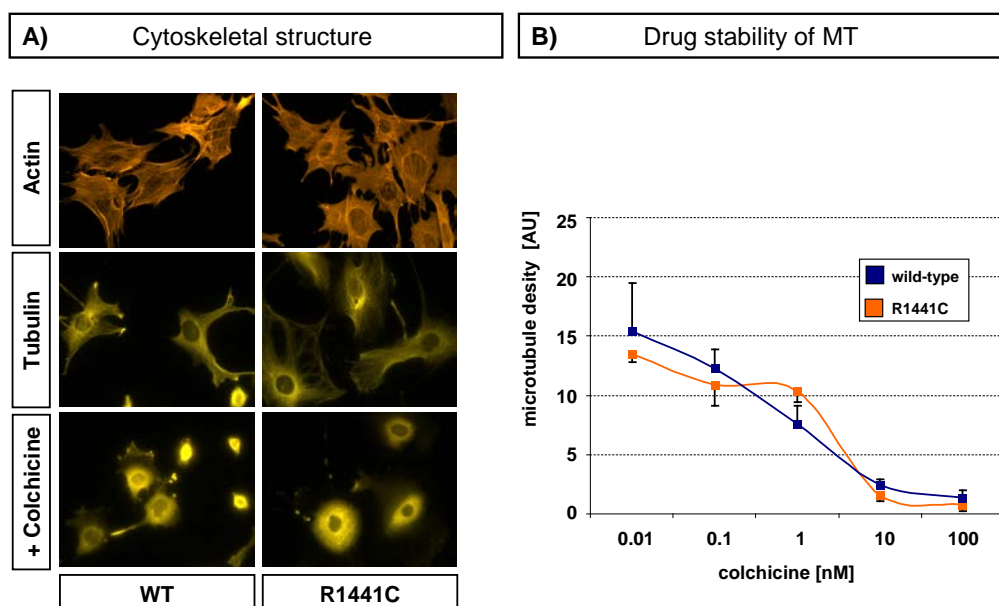


Figure 25: The analysis of the cytoskeletal architecture in *Lrrk2* R1441C mouse embryonic fibroblasts (MEFs) exhibit no significant alterations in the drug-stability of the microtubular cytoskeleton. **A)** The cytoskeleton structure in MEF cells: Actin and Tubulin network in untreated cells do not show genotype differences. Also the colchicine-induced collapses of the microtubular network seems to be similar between wild-type and R1441C cells after treatment with 10 nM colchicine. **B)** Quantitative measurement of polymeric tubulin fibre density after colchicine treatment in arbitrary units (AU). Density at **0.01nM colchicine:** wild-type 15.43 ± 4.06 , R1441C 13.47 ± 0.65 ; **0.1nM:** wild-type 12.24 ± 1.68 , R1441C 10.86 ± 1.74 ; **1.0nM:** wild-type 7.59 ± 1.56 , R1441C 10.38 ± 0.92 ; **10nM:** wild-type 2.48 ± 0.47 , R1441C 1.60 ± 0.51 ; **100nM:** wild-type 1.37 ± 0.63 , R1441C 0.73 ± 0.51 .

The treatment of wild-type as well as *Lrrk2* knock-in cells with 10 nM colchicine is sufficient to induce the almost complete collapse of the microtubular network in both genotypes (**Fig.25, A**). The toxic alkaloid colchicine specifically inhibits the polymerization of tubulins by capping the plus-end of the growing microtubules (Mareel and De Mets *et al*, 1984) leading to the slow but continuous disintegration of the fibres.

A quantitative assay was performed, by treating fibroblast cells of both genotypes with different concentrations of this destabilizing substance for 16 hours. Subsequent fixation, an immunocytochemistry (ICC) using anti alpha-tubulin antibody depicted a clear density reduction of polymeric tubulin fibres up to a complete elimination of the microtubular network. For quantification, major microtubule fibres of single cells have been traced manually and quantified by *ImageJ* (Abramoff *et al.*, 1984) in regard to length and density. For both cell lines, a concentration-dependent reduction of microtubular fibres could be observed. Neither the threshold of colchicine concentration capable to influence the cytoskeleton stability, nor the gradient of concentration-dependent reduction (gradient of regression lines of wild-type: -3.79 and R1441C: -3.47) revealed any clear-cut differences between wild-type and *Lrrk2* R1441C knock-in cells. Along the gradient, wild-type values tend to be slightly increased (**Fig.25, B**) except at data point 1 nM, where a non-significant tendency (Student's t-test: $p=0.09$) towards a higher drug-stability (1.0 nM: wild-type 7.59 ± 1.56 , R1441C 10.38 ± 0.92) in mutant fibroblasts can be observed.

Taken together, this elementary assay to determine the drug-stability of the microtubular cytoskeleton seemed to be not to be appropriate or sensitive enough to reveal putative small differences in microtubular dynamics.

5.4.2.2 Neurite outgrowth in R1441C neurons

Dividing fibroblast may serve as a starting point, but to study disease-relevant processes, it is crucial to look for LRRK2 function in postmitotic neurons. Instead of artificial overexpression of wild-type or mutated LRRK2 in neurons, like it has been done by other groups (Wang *et al.*, 2008; Shin *et al.*, 2008), it was possible to utilise the existing mouse models to prepare genetically modified primary neurons.

To ensure robust levels of endogenous LRRK2 protein, only brain regions with strong expression like the hippocampus, cortex and striatum were used for preparation. Since neuronal expression of *Lrrk2* mRNA starts relatively late in development between E17.5 and P0, only embryos in this range of age have been used to ensure that also initial observations made in the first days of cultivation are dependent on *Lrrk2* expression. Preparation and cultivation of the cells was performed using a self-established protocol which is based on different published protocols (Banker and Goslin, 1998) as described in

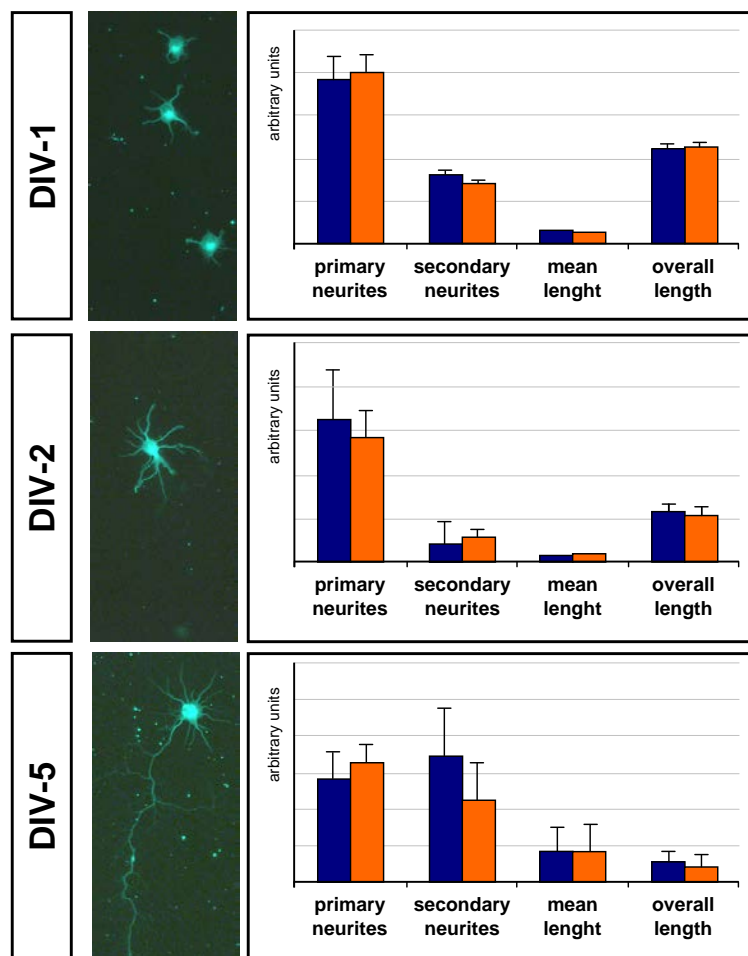


Figure 26: In primary hippocampal neurons derived from *Lrrk2* R1441C embryos, no significant alteration in neurite branching and complexity could be observed. The reported neurite shortening seen in neurons overexpressing LRRK2 could not be confirmed by these results.

Results of the initial neurite outgrowth assay in *Lrrk2* R1441C primary hippocampal neurons evaluated after different time-points in culture (DIV-1, -2 and -5). **DIV-1:** wild-type 3.68 ± 1.03 , R1441C 4.02 ± 0.84 ; sec. neurites: wild-type 2.61 ± 0.19 , R1441C 2.43 ± 0.18 ; mean length: wild-type 0.26 ± 0.03 , R1441C 0.24 ± 0.03 ; overall length: wild-type 2.27 ± 0.13 , R1441C 2.29 ± 0.14 . **DIV-2:** wild-type 6.68 ± 2.16 , R1441C 5.81 ± 1.24 ; sec. neurites: wild-type 0.96 ± 0.94 , R1441C 1.14 ± 0.36 ; mean length: wild-type 0.28 ± 0.03 , R1441C 0.32 ± 0.05 ; overall length: wild-type 2.34 ± 0.23 , R1441C 2.12 ± 0.16 . **DIV-5:** wild-type 8.65 ± 2.69 , R1441C 9.92 ± 1.62 ; sec. neurites: wild-type 10.28 ± 3.24 , R1441C 6.64 ± 3.06 ; mean length: wild-type 2.78 ± 2.43 , R1441C 2.74 ± 2.55 ; overall length: wild-type 1.68 ± 1.40 , R1441C 1.46 ± 1.35 (expressed in arbitrary units).

materials and methods (see 7.2.3.2). Mutant and wild-type primary hippocampal neurons derived from littermates were seeded on poly-D-lysine coated coverslips and cultivated in Neurobasal[®] medium without serum to restrain glial proliferation. Immediately after the round-shaped cells attach to the ground, they start to develop small, filipodia like extension which will be elongated into neurites. These neurites will then be specified into dendrites and axons during the next days in culture (days *in vitro*; DIV) leading to the assembly of a complex network. Although not all mechanisms of initial neurite outgrowth are fully understood, it is well known that the cytoskeleton plays a crucial role in this process (da Silva and Dotti, 2002). The actin filaments have to be destabilized at the site of out-growth; microtubule have to invade the growing filipodia; branching of dendrites requires coordinated interplay of actin and tubulin; (Georges *et al.*, 2008); the extension of processes requires an effective transport of tubulin monomers/oligomers and of membrane compounds (Tsaneva-Atanasova *et al.*, 2008). Due to this, any disturbance in the build-up or dynamics not only of the tubulin-, but also in the actin-cytoskeleton, could influence the course of the initial neurite outgrowth. We studied different aspects of neurite outgrowth in primary neurons, prepared from the hippocampus of wild-type, hetero-zygote and homozygote *Lrrk2* R1441C knock-in embryos at stage E16.5: initial phase of outgrowth (DIV1,2) and maturing neurons (DIV5).

For the initial phase of neurite outgrowth within the first two days of cultivation, the numbers of primary (DIV1 wild-type 3.68 ± 1.03 , R1441C 4.02 ± 0.84 ; DIV2 wild-type 6.68 ± 2.16 , R1441C 5.81 ± 1.24) and secondary neurites (DIV1 wild-type 2.61 ± 0.19 , R1441C 2.43 ± 0.18 ; DIV2: wild-type 0.96 ± 0.94 , R1441C 1.14 ± 0.36) were nearly identical between wild-type and R1441C neurons (the results for heterozygote and homozygote carriers were pooled). Also the mean and overall length of the neurites are the same between the two genotypes (**Fig. 26**) and the same holds true for the length of the longest process, defined as the axon (data not shown).

More mature neurons at DIV5 show a higher degree of heterogeneity which results in an increase of the variation. The mean length of processes remains unaltered (wild-type 2.78 ± 2.43 , R1441C 2.74 ± 2.55) and also the total length is the same between both genotypes, since the loss of secondary

neurites is partially compensated by the fact that R1441C cells show in turn a slight and nonsignificant increase in primary neurites (wild-type 8.65 ± 2.69 , R1441C 9.92 ± 1.62). Altogether, the neurite outgrowth assay did not show any significant deficits. The reported neurite shortening in neurons over-expressing *Lrrk2* R1441C and a potential decrease in neurite branching and complexity could not be confirmed by this assay (MacLeod *et al.*, 2006).

4.4.3.3 Neurite outgrowth in *Lrrk2* knockdown neurons

Previous studies have shown the antagonistic effect of *Lrrk2* knockdown compared to the expression of pathogenic LRRK2 in regard to neurite outgrowth (MacLeod *et al.*, 2006). Therefore, we carried out an initial neurite outgrowth assay using primary neurons prepared from the hippocampus of wild-type and *Lrrk2* knockdown embryos. The assay was performed similar to the *Lrrk2* R1441C knock-in line except the fact, that only neurons at the stage DIV2.5, corresponding to the initial phase of outgrowth have been used. The mean, maximal and overall length of the neurites did not show significant changes. But intriguingly, all of these general parameters are slightly elevated in *Lrrk2* knockdown neurons (**Fig.27**); in particular the mean neurite length of mutant neurons ($57,819 \pm 8149$) is increased by nearly 25% compared to the wild-type control ($47,122 \pm 7117$). From that it can be concluded, that the trend in knockdown cells goes slightly towards elongated processes. Also the

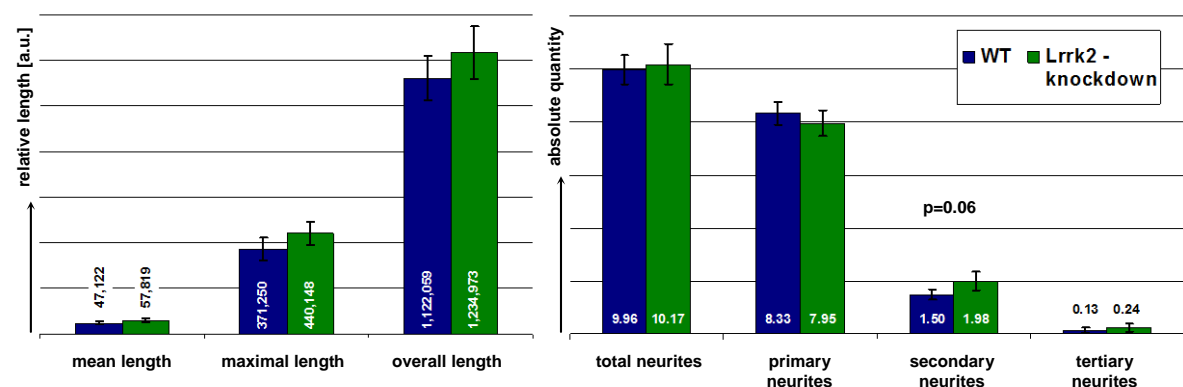


Figure 27: In primary hippocampal neurons derived from *Lrrk2* knockdown embryos, a tendency towards an increase in branching and network complexity due to the higher number of secondary neurites could be observed. Initial neurite outgrowth of *Lrrk2* knock-out neurons at DIV2.5. Neurite length is depicted in arbitrary units (left). Altogether three independent cultures per genotype group have been analyzed (number of secondary neurites: t-Test: $p=0,0618$, data is expressed as mean \pm SEM).

numbers of the tertiary neurites (0.134 ± 0.10 in wild-type to 0.242 ± 0.15 in mutant) points towards a slightly higher complexity and increased branching. The numbers of secondary neurites (1.50 ± 0.20 in wild-type to 1.98 ± 0.36 in mutant) exhibit a clear tendency (Student's t-test: $p=0.0618$) for having more secondary neurites in *Lrrk2* knockdown neurons (**Fig.27**).

The later development of the neuronal network at around DIV5 unfortunately was not analysed since also in highly diluted neuronal cultures not enough neurons without any cell-to-cell contact could be found in later stages. Analysis of neurons contacting each other, would not allow any comparison with the results of the R1441C knock-in line.

In summary, this neurite outgrowth assay could show a tendency towards an increase in branching and network complexity due to the higher number of secondary neurites. A potential marginal increase in neurite length can not be excluded.

4.4.3.4 Neuronal morphology in the striatum of aged *Lrrk2* knockdown mice

To examine whether *Lrrk2* has a physiological role in controlling dendritic morphology *in vivo* we analysed brains of *Lrrk2* knockdown mice and their wild-type using the FD Rapid GolgiStain™ staining. By this classical technique, randomly entire single neurons are getting stained, which allows studying the complete dendritic arbour (**Fig.28, A**). After 3-D reconstruction neurons using the Neurolucida® system, a variety of different parameters related to dendritic arborisation can be assessed. Due to the high expression of *Lrrk2* mRNA and its central role in the basal ganglia circuit, we have chosen the dopaminergic medium spiny neurons (MSNs) of the striatum, to perform this *in vivo* analysis of the neuronal morphology.

Qualitatively, no striking differences in the morphology of the neurons could be seen between wild-type and LRRK2-depleted animals. But again, slight increases in *Lrrk2* knockdown neurons could be observed in nearly all general parameters like neurite quantity (24.19 ± 1.69 in wild-type to 30.44 ± 3.67 in mutant) and endings per cell (43.75 ± 3.60 in wild-type to 55.94 ± 6.10 in mutant), branching points or nodes (17.56 ± 1.71 in wild-type to 23.31 ± 2.52 in mutant) and overall neurite length (65.18 ± 2.65 in wild-type to 69.83 ± 3.03

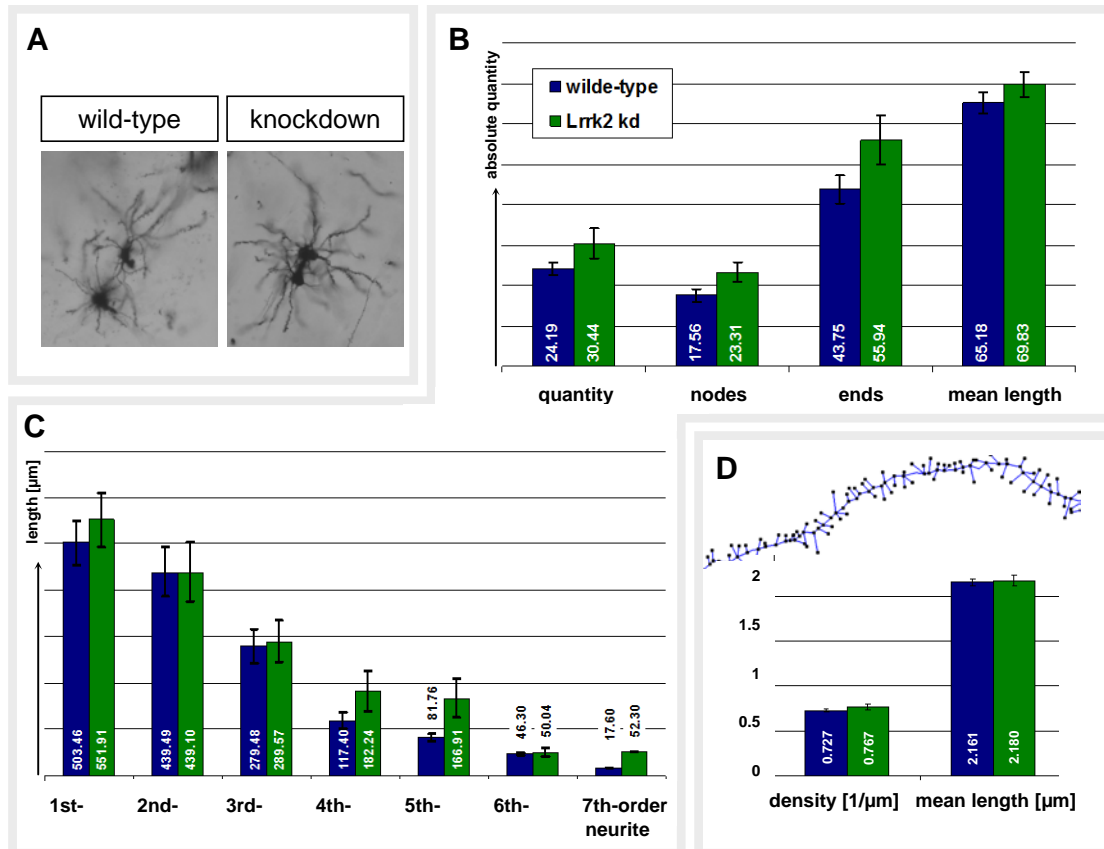


Figure 28: Medium spiny neurons (MSN) in the striatum of aged *Lrrk2* knockdown mice show only slight tendencies towards an increase in branching and network complexity marked by subtle increasing numbers of higher order neurites. The morphology of medium spiny neurons in aged *Lrrk2* knockdown mice were visualized by Golgi-staining and quantified subsequent to 3-D reconstruction. **A)** MSN example pictures. **B)** Quantity, Number of nodes and ends are depicted in absolute numbers. **C)** The mean length and total length of the 1st- till 7th-order neurites are depicted in μm (right). **D)** The length and density of the spines are not altered in *Lrrk2* knockdown MSNs. Depicted is an exemplified 3-D reconstruction (top) and the results of the quantification in μm and $1/\mu\text{m}$ respectively (for A-D: $n=25$, data is expressed as mean \pm SEM)

in mutant) (**Fig.28, B-C**). Also like already observed *in vitro*, in particular the dendrites of higher branching order seem to be affected: In particular the neurites of the 4th- and 5th-order are longer in knockdown neurons ($182\mu\text{m} \pm 43\mu\text{m}$ and $167\mu\text{m} \pm 42\mu\text{m}$) compared to the wild-type neurons ($117\mu\text{m} \pm 18\mu\text{m}$ and $82\mu\text{m} \pm 9\mu\text{m}$). Unfortunately, despite high sample sizes ($n=25$) none of the parameters could reach the level of significance. The spine morphology however seems to be unchanged; neither spine density (0.727 ± 0.02 in wild-type to 0.767 ± 0.03 in mutant [$1/\mu\text{m}$]), nor mean length (2.161 ± 0.04 in wild-type to 2.180 ± 0.06 in mutant [μm]) show genotype-dependent differences (**Fig.28, D**).

Taken together, in LRRK2-deficient neurons we observed a tendency towards an increase in branching and network complexity marked by increasing numbers of higher order neurites. Also specifically *in vivo* a general increase in neurite length seems to be present but fails to reach significance.

4.4.3.5 *Lrrk2* R1441C tubulin cells comprise hyperacetylated tubulin *in vitro* and *in vivo*

Since our model systems did not show as clear-cut results in regard to neurite outgrowth as other groups published (MacLeod *et al.*, 2006; Plowey *et al.*, 2008; Sämman *et al.*, 2009), compensatory mechanisms have to be taken into account. It might be possible, that under the more physiological situation of expressing mutated LRRK2 life long at an endogenous level enables the cell to adapt to this burden more efficiently, as compared to the situation, where expression vectors are being transfected. One possibility to compensate a slightly deregulated microtubular network would be, to modify its physiological properties induced by posttranslational modifications of tubulin. Therefore we analysed the composition of the microtubular network in more detail and

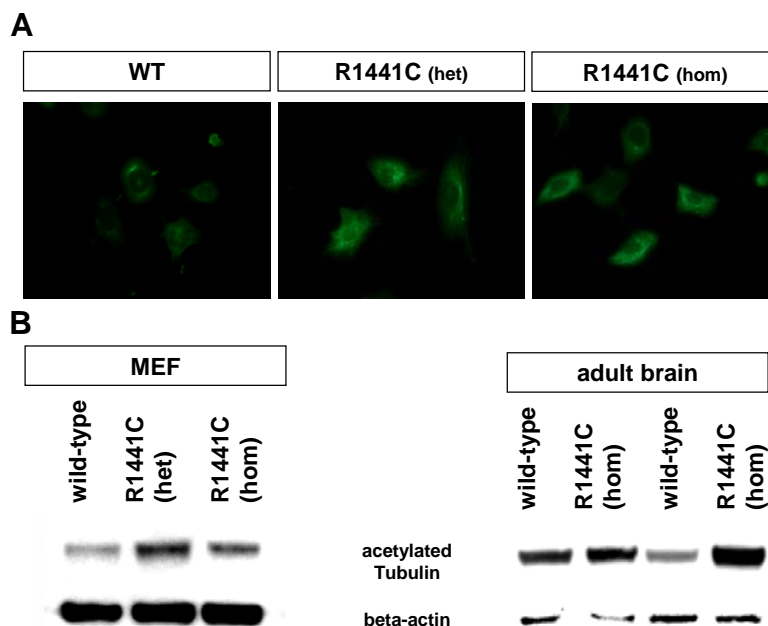


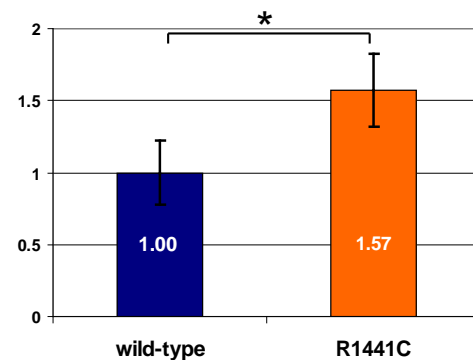
Figure 29: *Lrrk2* R1441C cells show elevated levels of acetylated microtubules *in vitro* in embryonic fibroblast as well as *in vivo* in the adult brain.

A) Immunocytochemistry using an anti-acetylated tubulin antibody on wild-type, *Lrrk2* R1441C embryonic fibroblasts nicely demonstrates a higher signal intensity on heterozygous and homozygous MEF lines compared to wild-type cells. **B)** Western blot analysis on MEF-lysates confirms the observation of higher amounts of this posttranslational modified tubulin fraction. **C)** Also *in vivo*, in brain lysates from 4 month old *Lrrk2* R1441C animals, an initial Western blot analysis suggest elevated levels (see also **Fig.30**).

looked by ICC for different subsets of posttranslational modified microtubules (PTM).

Strikingly, in *Lrrk2* R1441C derived MEF cells we could clearly detect both in heterozygote and homozygote fibroblasts already qualitatively a higher amount of acetylated tubulin, whereas staining for tyrosinated tubulin or total tubulin did not show considerable differences (data not shown). This result could be confirmed by Western blot analysis on protein lysates (**Fig.29, A-B**). It has to be considered, that microtubules in general are highly dynamic and especially PTMs play a crucial role during mitotic events like the formation of the spindle apparatus (Gundersen and Bulinski, 1986; Hyman and Karsenti, 1996). Hence, for both ICC and protein preparation, growth status and density of the cells had to be considered carefully, in regard to minimize possible normal variations between different cultures irrespective of their genotype. But this hyperacetylation of alpha-tubulin could not only be detected *in vitro* but also *in vivo*. When checking protein lysates prepared from whole brains of young wild-type and R1441C knock-in mice via western blot, a similar increase could be detected (**Fig.29, C**).

Figure 30: Quantitative studies revealed a significant increase in the amount of acetylated tubulin of about 50% in the adult brain of *Lrrk2* R1441C mice compared to wild-type littermates. Western blot analysis was performed with total brain lysates from young (4 month) animals *Lrrk2* R1441C knock-in mice. Depicted is the relative amount of acetylated tubulin in R1441C animals normalized to actin and compared to wild-type levels (n=6, Student's t-test: p=0.048, data is expressed as mean \pm SEM).



After quantification by *ImageJ* (Abramoff *et al.*, 1984), a significant (Student's t-test: p=0.048) increase by 1.57-fold (\pm 0.25) in the relative amount of acetylated tubulin compared to wild-type levels could be confirmed *in vivo* (**Fig.30**). The pattern of acetylated tubulin in the adult brain of wild-type and R1441C knock-in mice was checked via IHC and by performing Western blots of brain lysates derived from different brain regions (data not shown). No obvious differences in the distribution and intensity could be detected, suggesting that the hyperacetylation is not limited to a specific region or

neuronal subpopulation the adult central nervous system and therefore might represents a more general cellular effect.

5.4.2.3 Tubulin hyperacetylation in R1441C neurons can be further enhanced by HDAC-6 inhibition

The posttranslational modification of microtubules is a highly dynamic and reversible process (Hammond *et al.*, 2008), so either the enhancement of acetylation or the inhibition of deacetylation could come into consideration to be the cause for this hyperacetylation. Since the enzyme responsible for tubulin acetylation has not yet been identified (Fukushima *et al.*, 2009), we have focused on the process of deacetylation. In this case, HDAC-6 (Hubbert *et al.*, 2002) is known to be in charge of mediating the reaction. Here Trichostatin A (TSA) as a inhibitor of HDACs (Brehm *et al.*, 1998) was used, to test the hypothesis that the disruption of the HDAC-6 dependent deacetylation could be the reason for the observed hyperacetylation. In this regard, altered or enhanced binding of LRRK2 to the acetylation site could protect acetylated alpha-tubulin from its deacetylation.

Wild-type and R1441C primary hippocampal neurons were treated with TSA in a concentration of 50 μ M. After 3 hours, the cells were scrapped of and

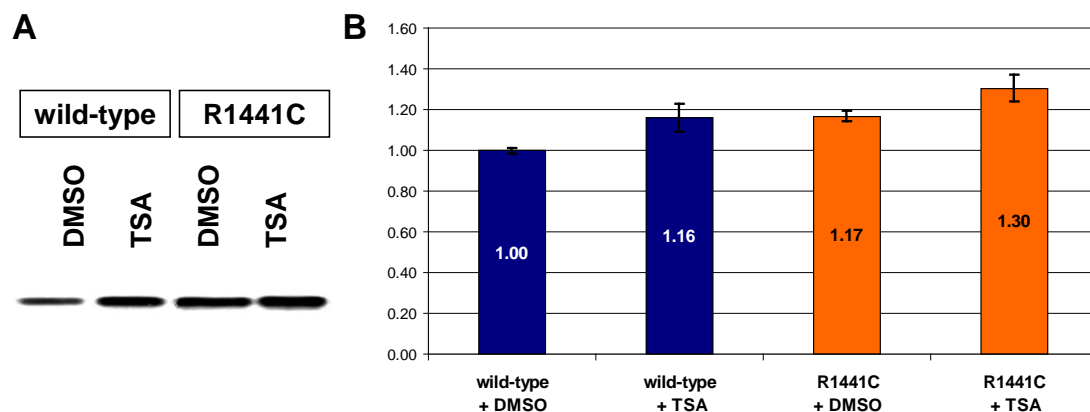


Figure 31: The *in vitro* inhibition of tubulin deacetylation by the deacetylase-inhibitor Trichostatin A (TSA) induces a comparable degree of hyperacetylation in both wild-type and *Lrrk2* R1441C neurons. Primary hippocampal neurons (DIV21) prepared from wild-type and *Lrrk2* R1441C littermates were treated with TSA [50 μ M] or solvent (DMSO). **A**) After 3 hours, the cells were analysed by Western blot for acetylated tubulin. **B**) The relative amount of acetylated tubulin was quantified using *ImageJ* and normalized with total tubulin as well as beta-actin. Level of acetylated tubulin in wild-type neurons treated with DMSO is set to 1 (n=3; genotype differences: p=0.0054 DMSO; p=0.0983 TSA; p=0.2959 increase, data is expressed as mean \pm SEM).

further prepared for Western blot analysis. Immunodetection for acetylated tubulin was performed and normalized with total tubulin as well as beta-actin (**Fig.31**). From the subsequent quantification, we obtained several results: As a result the relative amount of acetylated tubulin was increased in the TSA-treated group compared to the DMSO control group in both wild-type (16% increase, $\pm 6\%$) and mutant (13% increase, $\pm 6\%$) neurons proving the inhibition of tubulin deacetylation. The R1441C control group showed as expected a significant higher basal level of acetylated tubulin compared to the wild-type control group (17% increase, $p=0.0054$). After HDAC-6 inhibition, wild-type neurons reach the acetylation level of mutant neurons of about 1.17-fold. But R1441C neurons can be further hyperacetylated by TSA treatment until they show about 30% higher levels compared to wild-type neurons. Thereby, the relative increase caused by the treatment is similar between both genotype groups ($p=0.29$).

Taken together, this *in vitro* data confirms, that tubulin hyperacetylation takes place in R1441C neurons. The cause for this hyperacetylation is not the disruption of the HDAC-6 dependent deacetylation since in this case no further increase of the acetylation level of mutant neurons would have occurred. Therefore other still unknown molecular mechanisms are responsible for the hyperacetylation. Interestingly, even though the general binding-

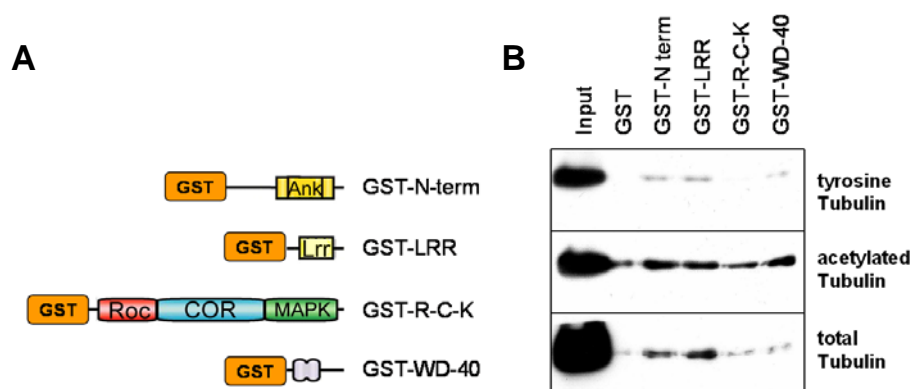


Figure 32: LRRK2 protein can bind to tubulins and shows a strong preference for acetylated tubulin representing the stable fraction of microtubules. This protein-protein interaction was demonstrated by a GST pull-down assay in collaboration with Dr. Piccoli. **A)** Schematic representation of the different GST-tagged LRRK2 domains used as bait in the pull-down assay on total brain lysates from adult wild-type mice. **B)** The identification of the interaction partners has been carried out by Western blot analysis for different tubulin modifications. **Abbr.:** N-term, N-terminal region; LRR, leucine-rich repeat domain; R-C-K, Roc- COR- and kinase-domain; WD-40, C-terminal region including the WD40-domain.

ability of human LRRK2 to microtubules has been demonstrated already by others (Gandhi *et al.* (2009), we could show in collaboration with Dr. Giovanni Piccoli from the institute of human genetics of the Helmholtz Zentrum Munich via GST pull-down assay that the binding of LRRK2 is highly specific for acetylated tubulin (**Fig.32**) since the binding to other PTMs like tyrosine tubulin was nearly not detectable. Also in case of total tubulin, levels were conspicuously low compared to the input levels; most probably these are only representing the included acetylated tubulin fraction. The binding ability to tubulin was more pronounced in case of the *N-terminal*- and *leucine-rich repeats*-constructs and most clear-cut, at least for acetylated tubulin, for the *WD40*-construct (**Fig.32**). Since acetylation and also other modifications occur after tubulin polymerisation (Greer *et al.*, 1985), we can assume also for LRRK2 a specific binding to polymeric microtubules. Nevertheless, we could not pinpoint a specific binding site in the LRRK2 protein, maybe due to strong dimerization of the constructs with tubulin-bound endogenous LRRK2.

5.4.2.4 LRRK2 and the cold-stability of the microtubular network

Evidence for an association of *Lrrk2* with microtubular organisation was given by further results of the collaborative search for LRRK2 binding partners by GST pull-down assay. Amongst them, the microtubule-associated protein STOP (Stable tubulin-only polypeptide; also known as *Mtap6*) has been identified as a potential LRRK2 binding partner (Piccoli *et al.*, 2011). It has been shown, that microtubules are drug-resistant, cold-stable and become detyrosinated if associated with active STOP proteins (Bosc *et al.*, 1996; Guillaud *et al.*, 1998; Baratier *et al.*, 2005). In addition, STOP proteins mediate neurite extension and are involved in synaptic transmission of dopaminergic neurons (Andrieux *et al.*, 2002; Brun *et al.*, 2005).

The expression of STOP protein was checked via IHC in the wild-type and mutant R1441C knock-in animals and revealed a quite ubiquitous expression throughout the adult brain which is in line with published data (Couégnas *et al.*, 2005). Based on that, coexpression of STOP and LRRK2 can be assumed for many if not all brain regions. Also the total level of protein expression in the adult brain was not altered in different protein fractions prepared from

wild-type and *Lrrk2* R1441C adult brain (Fig.35). Due to the association of STOP with the cold-stability of microtubules we now additionally tested for microtubular cold stability in R1441C primary neurons. A time course experiment of cold-induced microtubule destabilisation was performed. Fully mature (DIV14) primary hippocampal neurons of both genotypes were fixed after certain time (10 min, 40 min, 120 min) of cold exposure (4°C). Subsequently, double ICC for acetylated tubulin and tyrosine tubulin has been performed (Fig.33, a). Thereby acetylated tubulin represents the more stable and tyrosine tubulin the unstable fraction of microtubules (Bulinski and Gundersen, 1991; for reviews see Perdiz *et al.*, 2011). The ratio of unstable to relatively stable microtubules served as an indication for cold-induced destabilisation. The wild-type as well as the R1441C neurons show a nearly identical decline in the ratio of unstable to stable microtubules (Fig.33, b). Although we did not observe genotype differences, the slightly with time increasing differences prompted us to extend the incubation time to 3 hours. In addition, previous to the fixation the cells have been treated with a mild detergent solution (Digitonin) for permeabilization. This allows washing monomeric or oligomeric tubulin out of the cells prior to the fixation. Therefore,

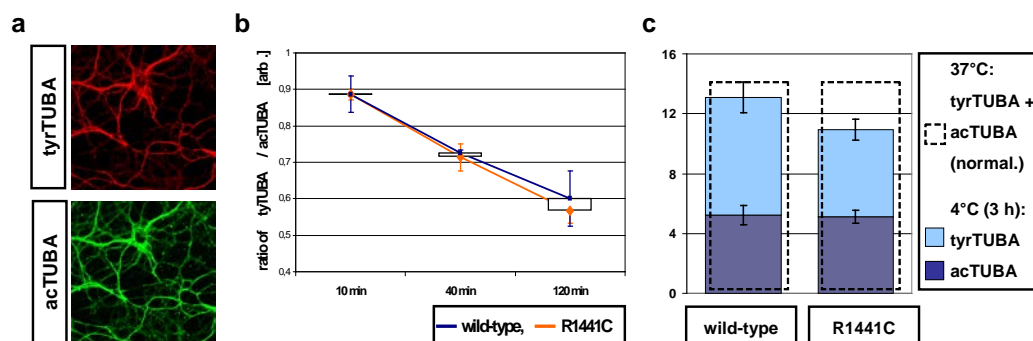


Figure 33: The microtubular cytoskeleton in *Lrrk2* R1441C hippocampal neurons show reduced cold-stability marked by the significant higher loss of tyrosine tubulin - representing the less stable and more dynamic subpopulation of microtubules - after cold treatment compared to wild-type neurons. The content of posttranscriptional modified microtubules has been determined by ICC and subsequent quantification of the relative fluorescent intensity. **a)** Exemplified pictures of a double ICC for tyrosine- (tyrTUBA) and acetylated alpha-tubulin (acTUBA). **b)** Time course experiments for 10, 40 and 120 minutes of cold-treatment (4°C) indicated only a nonsignificant trend of reduced cold-labile tyrosine tubulin normalized to the more cold-stable acetylated tubulin fraction. **c)** Looking for absolute values (arbitrary units) after 3 hours cold treatment and subsequent wash-out of monomeric tubulin, the content of tyrosine tubulin was significantly lower in R1441C cells. The sum of fluorescents of both fractions (tyrTUBA + acTUBA) at 37°C has been used for normalization (arbitrary units; n=3; genotype differences p=0.011 for tyrTUBA).

the subsequent quantification after double ICC for acetylated tubulin and tyrosine tubulin should only detect polymerized tubulin. The sum of acetylated and tyrosine tubulin at 37°C after washing has been taken to normalize the relative fluorescent values of both genotypes. The quantification revealed that the total amount of stable and unstable fraction was lower in R1441C neurons after the cold treatment (**Fig.33, c**). While the relative content of acetylated tubulin was quite similar between wild-type (5.21 ± 0.66) and mutant (5.12 ± 0.44), the relative amount of the unstable fraction represented by tyrosine tubulin was significantly ($p=0.011$) lower in R1441C cells (5.82 ± 0.68) compared to wild-type neurons (7.88 ± 1.02). This result indicates, that the putative minor alterations in the microtubular network of *Lrrk2* R1441C neurons can be demonstrated only under extreme conditions.

5.4.3 LRRK2 function at the synapse

The role of LRRK2 as a multifunctional protein seems not to be limited to the cytoskeleton since evidence arise, linking LRRK2 with a whole variety of cellular processes (Hatano *et al.*, 2007; Shin *et al.*, 2007). As an example from the second group of protein interactors which are involved in synaptic transmission, the N-ethylmaleimide-sensitive fusion protein (NSF) has been identified as a LRRK2 binding partner by Giovanni Piccoli by the means of GST pull-down assays (Piccoli *et al.*, 2011).

5.4.3.1 LRRK2 protein colocalizes with NSF in synaptosomes

NSF is an ATPase and belongs to the so called AAA (ATPases-Associated with a variety of cellular Activities) ATPase family. It is one of the most prominent component of the SNARE (SNAP-REceptor) complexes, controlling and executing vesicle fusion with target membranes in general (Zhao *et al.*, 2007) and neurotransmitter release in particular (Söllner and Rothman, 1994). The synaptic localisation of NSF could be nicely demonstrated by ICC in primary hippocampal neurons, showing a spotted distribution of the protein along the dendrites and the soma (**Fig.34**). To demonstrate the colocalization of LRRK2 and NSF in the synapses we had to chose a non-immunocytochemical method since no fully reliable antibody against LRRK2 working

reliable in ICC or IHC was available (see 5.1.3). Therefore, we established a procedure to purify synaptosomes out of brain lysates (see 7.2.1.7), based on different existing protocols for subcellular fractionation (Villasana *et al.*, 2006; Dosemeci *et al.*, 2006). All resulting fractions (input, supernatant 1,

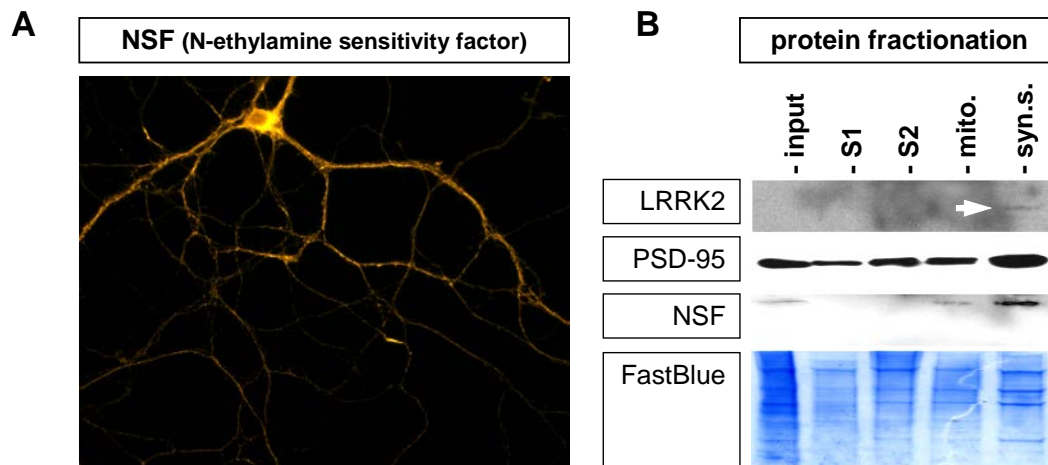


Figure 34: The synaptic protein and LRRK2 binding partner NSF is colocalized with LRRK2 in the synaptosomal fraction after subcellular fractionation. **A**) Immunocytochemistry for NSF (N-ethylmaleimide-sensitive fusion protein) in primary hippocampal neurons demonstrates the synaptic localization in primary neurons by a spotted distribution of the protein along the dendrites and the soma. **B**) Fractionation of brain lysates demonstrates synaptosomal colocalisation of NSF with LRRK2 (white arrow). Western blot analysis of protein fractions (input; **S1**, supernatant 1; **S2**, supernatant 2; **mito.**, mitochondrial fraction; **syn.s.**, synaptosomal fraction).

supernatant 2, mitochondrial fraction and the synaptosomal fraction) were analysed by Western blot for enrichment of fraction-specific marker proteins (e.g. PSD-95 for synaptosomes, see Fig.34) to verify the purification. The synaptosomal fraction itself consists out of a crude particulate fraction containing presynaptic and postsynaptic vesicularized components together with presynaptic and postsynaptic plasma membranes joined together by various structures of the synaptic cleft (Whittaker, 1993). It is therefore not possible to discriminate between pre- and postsynaptic structures. We could confirm the localisation of NSF in the synaptosomal fraction which is marked by PSD-95 (Postsynaptic density protein 95) enrichment (Hunt *et al.*, 1996). LRRK2 could be detected in that very same fraction too, indicating a subcellular colocalization of both proteins. It has to be pointed out, that LRRK2 Western blotting did not always show this clear-cut result of exclusive synaptosomal localization. Other blots did exhibit a more broad distribution of LRRK2 protein in several fractions but with main emphasis on the synaptosomal fraction. By this

technique, we further checked whether the expression of the pathological R1441C variant of LRRK2 is sufficient to induce alterations in the expression level and subcellular distribution of identified LRRK2 binding partners. Neither in case of the synaptosomal protein NSF, nor of the cytoskeletal proteins STOP significant alterations could be detected (**Fig.35**).

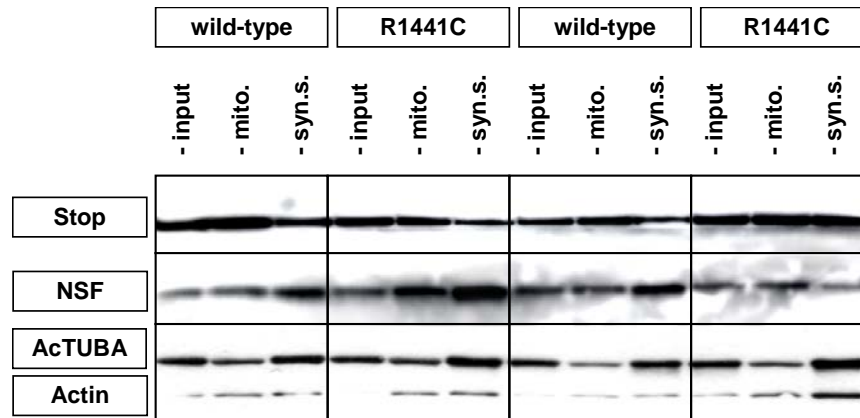


Figure 35: Relative levels and subcellular distribution of binding partners of LRRK2 are not markedly altered between wild-type and *Lrrk2* R1441C mice – except the previously described tubulin hyperacetylation. Fractionation of brain lysates from *Lrrk2* R1441C mice and wild-type littermates analysed by Western blot for different LRRK2 interactors. Equal loading was approved by ponceau staining (not shown). **Abbr.:** AcTUBA, acetylated alpha-tubulin; **mito.**, mitochondrial fraction; **syn.s.**, synaptosomal fraction.

5.4.3.2 Synaptic function: Exocytosis and endocytosis cycles in R1441C neurons

Presumably, the putative alterations in *Lrrk2* R1441C mice could be so gentle, that differences in regard to the composition of the synapse might not be visible. But any rather small alteration at this crucial functional site of the neuron should have an effect onto aspects of the synaptic transmission itself. Concentrating on NSF's role in controlling and executing vesicle fusion with target membranes (Zhao *et al.*, 2007), we looked at exocytosis- and endocytosis-events of synaptic vesicles in *Lrrk2* R1441C neurons. For neurotransmission, synaptic vesicles which are docked to the active zone, release their neurotransmitter into the synaptic cleft (exocytosis) and subsequently are getting recycled by an endocytosis process (Südhof, 1995). We used and adapted a published protocol from Matteoli *et al.*, 1992, where the antibody binding *in vitro* using living neurons was utilised, to quantify these cycling events (Matteoli *et al.*, 1992; Mundigl *et al.*, 1993; Kraszewski *et al.*,

1995). In short, the principle of this functional exo-endocytosis assay is based on the binding of an antibody given to the living neurons for a certain time. During the exocytosis of a synaptic vesicle, the luminal part of synaptotagmin 1, a transmembrane synaptic vesicle protein gets exhibited at the cell surface. Thereby, a monoclonal antibody present in the medium and directed against this part of the protein can bind. After 4 minutes of the assay, the cells get briefly washed, fixed with PFA, permeabilized with Triton X-100 and stained by double-IHC for the internalized synaptotagmin and another synaptic vesicle marker (synaptophysin) for the total vesicle pool. The ratio of vesicles stained by synaptotagmin versus the number of synaptophysin positive vesicles gives the rate of exo-endocytosis activity for a certain neuron within the time of the assay (see 7.2.3.2 and Fig.58). The ratio of synaptotagmin-positive to the total number of vesicles was determined in wild-type neurons to 32.12% ($\pm 3.43\%$), meaning that approximately one third of all detected synaptic vesicles underwent an exo-/endocytosis cycle within the 4 minutes of the assay. This basal value fits to the range of published data using a comparable loading time (Bacci *et al.*, 2001). The basal exo-/endocytosis rate in R1441C neurons was with a value of 34.65% ($\pm 2.52\%$) only slightly and non-significantly higher

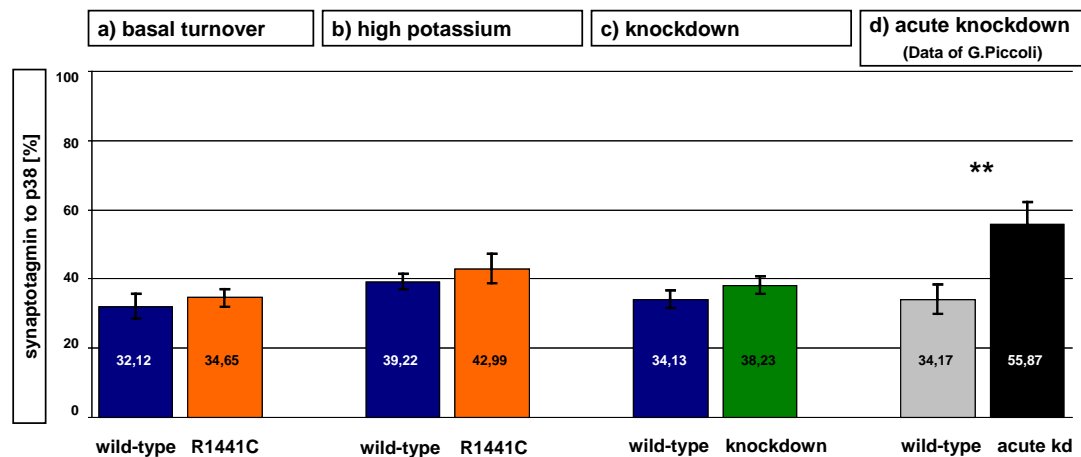


Figure 36: Neither the expression of mutated LRRK2 on endogenous levels, nor the constitutive loss of LRRK2 protein is sufficient to induce synaptic alterations. Only the acute knockdown of *Lrrk2* significantly increases the synaptic vesicle turnover. Results of the exo-/endocytosis assay: The bars indicate the percentage of total vesicles of a certain neuron which underwent an exocytosis- and endocytosis-event during 4 minutes of the assay: Quantifications for hippocampal neurons prepared from *Lrrk2* R1441C mice under basal (a) and evoked condition (b), for neurons prepared from *Lrrk2* knockdown mice (c) and for wild-type neurons with and without an acute viral knockdown of *Lrrk2* performed by G.Piccoli (d) (data is expressed as mean \pm SEM; $n > 25$; asterisks: $p < 0.01$).

compared to wild-type neurons (**Fig.36, a**). The evoked activity in a depolarizing high-potassium buffer was enhanced in both genotypes to a similar degree. Again, in this case the mutant neurons exhibit a slightly, non-significant higher ratio of 42.99% ($\pm 4.30\%$) in comparison to the value of 39.22% ($\pm 2.19\%$) in wild-type neurons (**Fig.36, b**). Furthermore, also neurons prepared from *Lrrk2* knockdown mice have been tested by this assay. Wild-type neurons of this line did reach comparable levels as their counterparts of the knock-in line of 34.17% ($\pm 4.15\%$). The LRRK2-depleted neurons did show a slight but nonsignificant increase of vesicle turnover rate to 38.23% ($\pm 2.67\%$) (**Fig.36, c**). Altogether, this assay was not sufficient to proof putative small alterations in the dynamics of exo-endocytosis in *Lrrk2* R1441C knock-in and knockdown neurons, the reason of which may be again compensatory mechanisms in case of neurons in which modified *Lrrk2* expression is in place for a long time. Therefore we set out in collaboration with G. Piccoli and M. Ueffing to examine the effect onto synaptic transmission in an acute knockdown using lentiviral mediated infection of primary neurons with a siRNA directed against *Lrrk2* (Bauer *et al.*, 2009). To minimize the chances for any kind of possible compensatory mechanisms, the neurons have been infected with the virus at DIV10 and assayed at DIV18. Strikingly, under basal conditions LRRK2-depleted neurons did show a significant ($p < 0.01$) increase of nearly two fold in their basal synaptic vesicle turnover rate from 34.17% ($\pm 4.15\%$) in non-treated to 55.87% ($\pm 6.21\%$) in viral infected neurons (**Fig.36, d**). By his further studies, Giovanni Piccoli could show - partially in collaboration with us - that *Lrrk2* silencing not only alters vesicle recycling dynamics but also affects their kinetics and thereby induces a redistribution of vesicles at the presynaptic site. Furthermore, electrophysiological recordings indicated alterations in evoked postsynaptic currents (Piccoli *et al.*, 2011). These results suggest that LRRK2 modulates synaptic vesicle trafficking and distribution in neurons and in consequence participates in regulating the dynamics between vesicle pools inside the presynaptic bouton.

5.5 The morphological analysis of the *Lrrk2* R1441C line

The morphological analysis of the *Lrrk2* R1441C knock-in mouse line as a genetic model for PD predominantly has to answer the question about presence of pathological hallmarks of PD such as Lewy bodies in the brain and are there age-related changes in regard to the dopaminergic or other neurotransmitter systems? To address these questions we analysed young (4 month), mid-aged (12-14 month) and fully aged animals (> 24 month).

5.5.1 The development of the CNS in *Lrrk2* R1441C mice

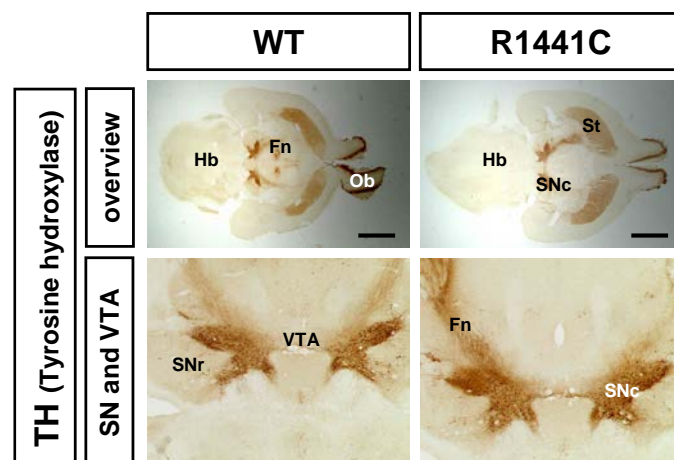
Using Nissl-staining we could show that the gross morphology of the CNS from *Lrrk2* R1441C knock-in mice is not altered (n=5). Neither the total size, nor the size of the different brain compartments or the dimensions of the ventricles are altered in mutant animals (data not shown). Also the stratifications of the cortex, the folding of the cerebellar lobes or the fibre bundles innervating the brain are set up properly.

Concerning the dopaminergic system we did not find any differences between wild-type and mutant animals in their qualitative amount of dopaminergic neurons within the substantia nigra of young animals (n: wt=5, mut=5). The same holds true for dopaminergic neurons in the VTA and olfactory bulb (data not shown). Also the connectivity of the dopaminergic neurons in the substantia nigra to the forebrain via the *fibrae nigrostriatales* seems not to be

Figure 37:

The development of the dopaminergic system is not markedly disturbed in *Lrrk2* R1441C mice.

Pictures from DAB-Immunohistochemistry for the marker *tyrosine hydroxylase* (TH) on young *Lrrk2* R1441C animals illustrating the dopaminergic system. **Abbr.:** **Fn**, *Fibrae nigrostriatales*; **Mb**, mid-brain; **Ob**, olfactory bulb; **SNc**, substantia nigra pars compacta; **SNr**, substantia nigra pars reticulata; **St**, striatum. Number of animals: 5/5 (wt/mut). Scale bars represent 2mm.



disturbed in these mice as demonstrated by immunohistochemistry for the dopaminergic marker *tyrosine hydroxylase* (TH). The innervation of the striatum, depicted by the dense network of axonal nerve terminals, shows the same level of immuno-reactivity in wild-type as well as in mutant mice (**Fig.37**). From this we can conclude, that the *Lrrk2* R1441C point mutation did not influence the proper setup of the dopaminergic system.

Based on the first results from the behavioural screen of young *Lrrk2* R1441C knock-in mice, showing a depression- and anxiety-related phenotype (see **5.6.1.3**), which resembles a major non-motor symptom of PD, we were in particular interested in the setup of the serotonergic system. Several studies have demonstrated the widespread influence of serotonergic forebrain projections on behavioural aspects like sleep, anxiety, locomotion and cognition of rodents (Briley *et al.*, 1990; Lucki, 1998; Ramboz *et al.*, 1998) and also in humans, disruption of this transmitter system is implicated in a variety of mental and mood disorders e.g. major depression (Brown and Linnoila, 1990).

Therefore IHC for the neurotransmitter serotonin (5-HT) itself have been performed on paraffin sections of young wild-type and *Lrrk2* R1441C knock-in mice. By using DAB as the chromophore, it was possible to generate a very intense staining, which also depicts minor axonal nerve terminals in distal projection areas. Looking for the soma of 5-HT positive neurons, they can be found nearly exclusively in several nuclei located in the hindbrain namely the raphe nuclei (Hornung, 2003). No obvious qualitative differences, neither in

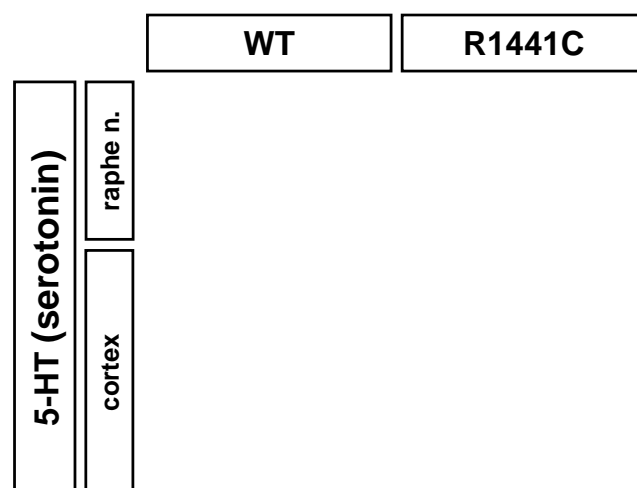


Figure 38: The development of the serotonergic system is not markedly disturbed in *Lrrk2* R1441C mice.

DAB-Immunohistochemistry using an antibody directed against serotonin (5-hydroxytryptamine, 5-HT) on young (4 month) *Lrrk2* R1441C animals. Illustrated are the serotonergic neurons in the dorsal raphe nuclei and the serotonergic innervation of the cortex (layers I-III). Number of animals: 5/5 (wt/mut). Scale bars represent 20µm (raphe nucleus) and 100µm (cortex.).

regard to their amount, nor to the size and morphology of these neurons could be detected in young knock-in mice (**Fig.38**). When looking for the axonal nerve terminals, we focused on the prefrontal cortex. Interestingly it has been shown that in this brain region during development the dopaminergic and the serotonergic system compete for the innervation of functional territories (Cunningham *et al.*, 2005). The overall staining intensity of the prefrontal cortex was comparable between wild-type and mutant mice. Also by comparing the average length and density of single immunopositive fibres, no obvious alterations of the serotonergic innervation could be detected (**Fig.38**). In summary, the general CNS architecture of young *Lrrk2* R1441C knock-in mice is not altered. We could show that there are no significant differences in the morphology of both the dopaminergic and serotonergic system between wild-type and mutant mice. Nevertheless, these results could serve as a necessary reference point for the further studies in aged animals.

5.5.2 Pathology of mid-aged *Lrrk2* R1441C mice

Lrrk2 R1441C knock-in animals at an age of at least twelve month were used to look for early signs of PD pathology since their appearance is age-related and therefore not expected to be seen in young animals. The most prominent pathological hallmarks of PD are the manifestation of Lewy bodies and Lewy neurites in the diseased brain. These eosinophilic, intracytoplasmic, proteinaceous inclusions are mainly consisting of α -synuclein (Spillantini *et al.*, 1997; Mezey *et al.*, 1997) and arise predominately in the substantia nigra of the midbrain but also in other brain regions like the medulla oblongata or cerebral cortex (Braak *et al.*, 2003).

Immunohistochemistry (IHC) for α -synuclein has been performed since it is the most common approach to detect Lewy bodies and neurites. For the DAB immunohistochemistry on free-floating brain sections, we were using a monoclonal antibody (4D6 #ab1903) which already has been shown to detect murine α -synuclein in IHC (Ekstrand *et al.*, 2007). The obtained staining depicted both in wild-type and mutant animals weaker signal in midbrain and hindbrain; medium to stronger signal could be seen in the forebrain with main emphasis on cortex and striatum (**Fig. 39**), reflecting the endogenous expres-

sion of α -synuclein (Abeliovich *et al.*, 2000). Using higher magnifications in various parts of the brain, neither round-shaped intracellular staining, nor heavy stained cellular extensions, corresponding to Lewy bodies and Lewy neurites respectively, could be detected.

In PD and in particular in a variety of patients with *LRRK2*-linked PD, neurofibrillary tangles (NFT) composed of hyperphosphorylated tau could be detected (Zimprich *et al.*, 2004; Gilks *et al.*, 2005; Giordana *et al.*, 2007). Consequentially, we were interested if also in ageing *Lrrk2* R1441C knock-in mice NFTs develop. Therefore we performed IHC using a phospho-specific antibody to detect tau protein which is pathologically hyperphosphorylated at threonine 205 in NFTs. (phosphoT205; #ab4841). It has been shown, that this residue is one of the sites which is phosphorylated in hyperphosphorylated tau found in NFTs (Augustinack *et al.*, 2002). The resulting ubiquitous and weak staining was similar between the genotypes both in regard to general level and pattern of expression (Fig. 39). Regions of more intense staining in

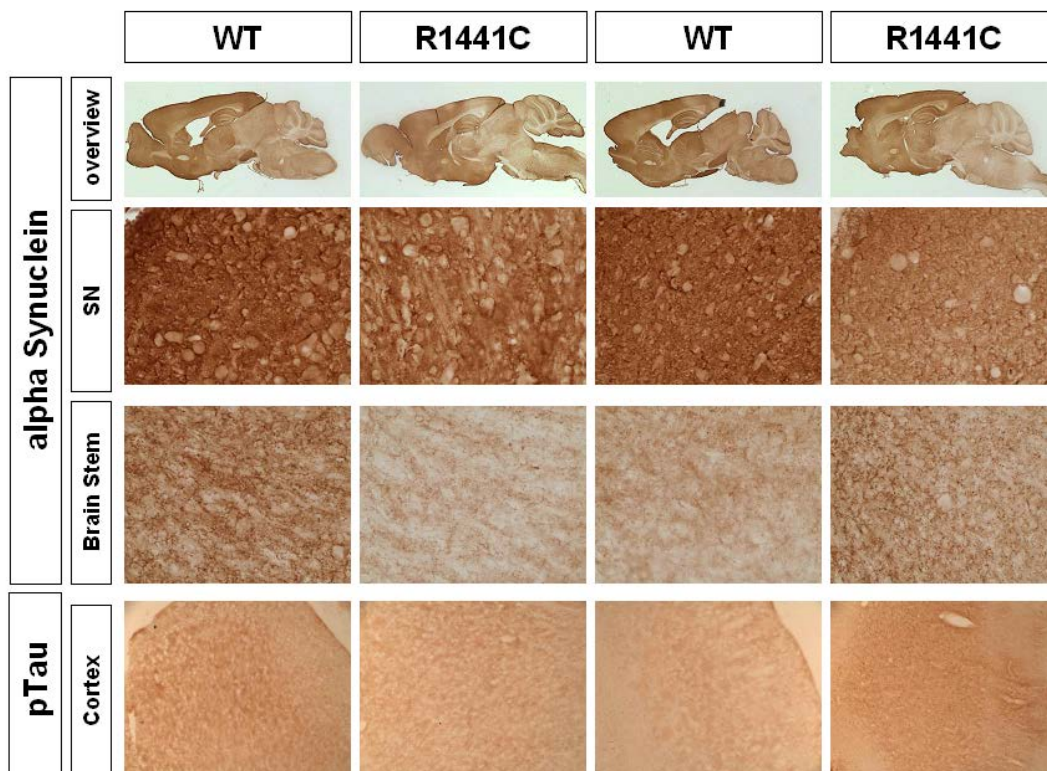


Figure 39: Mid-aged *Lrrk2* R1441C mice do not show signs of pathological aggregations and inclusion bodies found in PD patients. Pictures from DAB-Immunohistochemistry (DAB-IHC) on >12 month old *Lrrk2* R1441C animals for detecting SNCA (4D6, #ab1903) and phosphorylated Tau (phosphoT205, #ab4841) in the whole brain and in different areas of special interest: the substantia nigra, brain stem and cortex. Number of animals: males (wt/mut): 2/2.

some sections of one mutant mouse could be identified as enhanced background around lesions in the tissue caused during the process of cutting. Pictures with higher magnification from various brain regions (e.g. cortex) depicted only a slight signal, equally distributed in the soma of all cells. No intra- or extracellular agglomerations could be detected.

In conclusion, mid-aged *Lrrk2* R1441C knock-in mice neither show common forms of PD inclusions like Lewy bodies, nor more *LRRK2*-specific forms like neurofibrillary tangles.

5.5.3 Pathology of fully aged *Lrrk2* R1441C mice

The next step was the morphological and pathological analysis of fully aged *Lrrk2* R1441C knock-in as well as *Lrrk2* knockdown mice. In these animals we looked for the general morphology and as in the stages before we did not detect any significant differences in regard to size, size of different brain compartments or of the ventricles (data not shown). To survey the morphological condition of the dopaminergic system, we have chosen a different

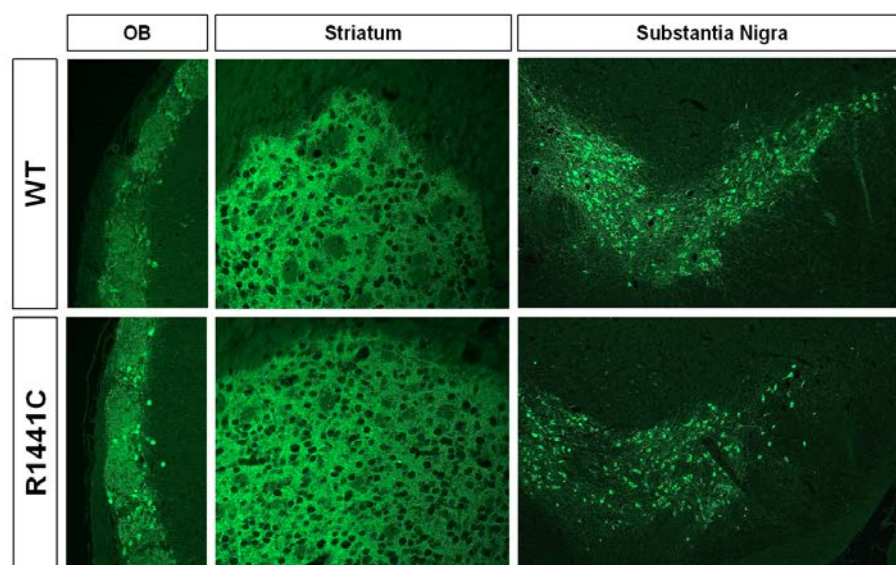


Figure 40: No dopaminergic degeneration can be observed in fully-aged (23 month) *Lrrk2* R1441C mice. Neither in the olfactory bulb nor in the nigrostriatal dopaminergic system, obvious differences to wild-type littermates have been found. Pictures from fluorescent immunohistochemistry for *tyrosine hydroxylase* (TH) as a marker for dopaminergic neurons on aged *Lrrk2* R1441C animals (23 month) illustrating the dopaminergic system in the glomerular layer of the olfactory bulb, the axonal sprouting in the striatum and the mid-brain dopaminergic system in the substantia nigra and the VTA.

approach than for young animals. Instead of DAB-IHC, a fluorescent IHC using TH as a marker was performed on paraffin sections (**Fig.40**) in order to assess better for the innervation of the target areas (e.g. the striatum), by the dopaminergic neurons - a morphological parameter known to be affected before the dopaminergic neurons in the substantia nigra succumb to neuronal death (Lin *et al.*, 2010). Confocal pictures of IHC for TH in wild-type and *Lrrk2* R1441C knock-in striata have been quantified using the *ImageJ* software (Abramoff *et al.*, 1984), but no significant differences in regard to total fluorescence could be detected (data not shown). Only the amount of TH positive neurites in the R1441C substantia nigra could be slightly reduced in comparison to wild-type, this observation could not yet be quantified due to a lack of animals. In addition, no obvious differences in regard to approximate cell number and neurite density could be observed in the dopaminergic neurons of the olfactory bulb (**Fig.40**).

We also checked again for the most prominent pathological feature of PD, *Lewy bodies* and *Lewy neurites* in the dopaminergic neurons. And once again, neither *Lewy bodies* nor *Lewy neurites* could be detected in the brain of R1441C mice. The staining pattern was similar between wild-type and mutant animals. However, even though the overall intensity of α -synuclein expression seemed to be similar, a detailed view onto the striatum depicted a slight increase of immunoreactivity in the *Lrrk2* R1441C knock-in mouse (**Fig.41**).

In order to confirm a possible differential regulation of α -synuclein in the brain of aged *Lrrk2* R1441C knock-in animals, we checked the expression on the

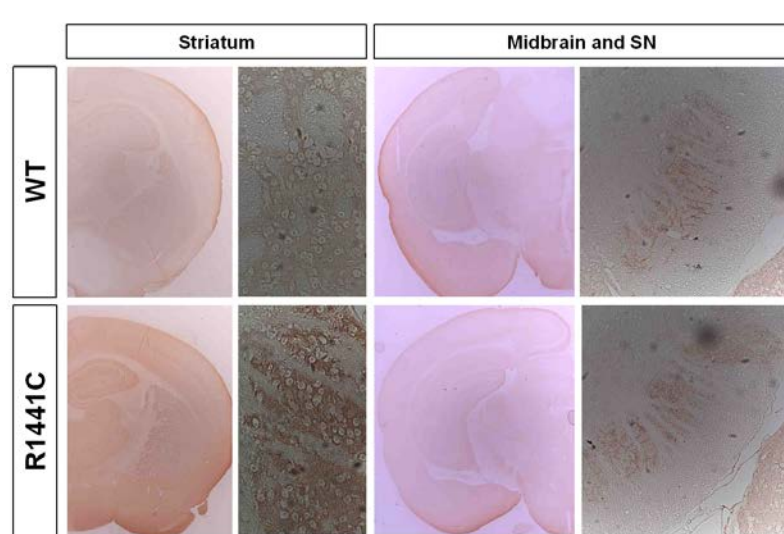


Figure 41:
In fully-aged *Lrrk2* R1441C (23 month old) mice, again no pathological α -synuclein aggregations or *Lewy bodies* can be found. Pictures from DAB-IHC for α -synuclein on aged *Lrrk2* R1441C animals detecting neurodegenerative aggregates or inclusion bodies (23 month).

mRNA level. Therefore, three different *in situ* hybridisation (ISH) probes were cloned from murine cDNA. Probe one and three were located in the 5' and 3' untranslated region of the transcript respectively, both overlapping with probe two, which is spanning the whole coding region of α -synuclein. All three probes were tested on wild-type brain sections and did show an identical pattern of expression, which is in line to already published data (Abeliovich *et al.*, 2000). Additionally, to α -synuclein also the patterns and levels of *Lrrk2* mRNA have been checked via ISH in aged *Lrrk2* knock-in brains (Fig.42, A). The analysis demonstrated neither severe alterations in the pattern of *Lrrk2* expression during ageing, nor any differences in the *Lrrk2* mRNA levels between wild-type and *Lrrk2* R1441C animals in the striatum as on of the most prominent expression domains (wild-type: 100.0% \pm 1.9%; R1441C: 99.7% \pm 4.0%). The same holds true for the general expression of α -synuclein in the adult cortex (wild-type: 100.0% \pm 3.3%; R1441C: 103.7% \pm 3.7%) (Fig.42, B).

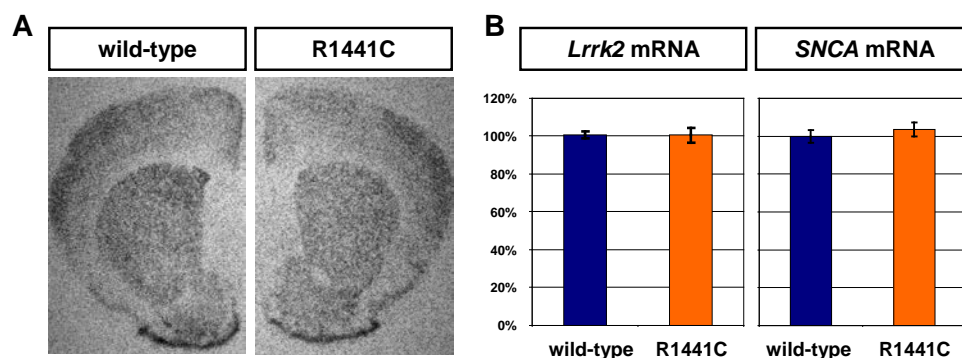


Figure 42: The expression pattern and levels of the dominant inherited PD-associated genes *Lrrk2* and α -synuclein are not altered in the brain of aged (24 month) *Lrrk2* R1441C mice compared to wild-type littermates. **A)** Autoradiographic images illustrating α -synuclein (*SNCA*) mRNA expression in coronal sections of the aged murine forebrain depicted by radioactive *in situ* hybridisation (ISH). **B)** Quantification results of *Lrrk2* mRNA in the striatum and α -synuclein (*SNCA*) mRNA in the aged cortex.

Taken together, the morphological analysis of the *Lrrk2* R1441C knock-in mouse line did not reveal any pronounced genotype differences neither in young, nor in old animals. The general development of the CNS is not changed by the insertions of the pathogenic point mutation. We could also not detect overt age-related neurodegeneration of the dopaminergic system, inclusion bodies or other pathological hallmarks of PD. Nevertheless, since

our functional analysis suggests a distinct role of LRRK2 protein in cellular functions like cytoskeletal organisation and synaptic transmission, we still could expect at least small alterations in the behaviour of these animals.

5.6 Behavioural analysis

Parkinson's disease is characterized by numerous behavioural symptoms ranging from obvious disturbances like resting tremor, to less apparent disorders such as depression or bipolar disorders (Lemke *et al.*, 2004) over to extremely cryptic alterations like a decrease in general motivation (Cools, 2008). To assess as many Parkinson-related behavioural features as possible, we created a special test battery for the behaviour analysis of our mice. Each known symptom of the disease has to be engaged by a set of test, preferably covering as many aspects as possible (Sedelis *et al.*, 2001). Taking into account, that PD is an age-dependent, progressive neurodegenerative disease, we had to test both young and aged animals. For this purpose, large cohorts of animals classified into four groups (wild-type and mutants of both genders) were needed. To deal with the high variability generally common to behavioural tests, every group was aimed to consist out of at least 10 to 15 individuals. In order to ensure a preferably high comparability, only groups of littermates from either heterozygous x heterozygous breeding in the case of the *Lrrk2* knock-in line, or wt x heterozygous breeding in the case of the *Lrrk2*-knockdown line have been used. Since already one allele expressing the *Lrrk2*-shRNA results in a high degree of LRRK2 protein depletion (see 5.3, Fig.23), heterozygous *Lrrk2*-knockdown mice were used, whereas for the knock-in line only homozygous carriers of the R1441C mutation were compared to their wild-type littermates.

5.6.1 Analysis of young *Lrrk2* R1441C and *Lrrk2* knockdown mice

The cohort of *Lrrk2* R1441C knock-in mice was tested at young age, on the one hand to look for initial phenotypes, on the other hand as a reference point to reveal age-dependent phenotype when testing aged animals. The mice

performed seven behavioural tests, starting at an age of 4 month and ending the tests at an age of 12 month.

In case of the *Lrrk2* knockdown line, the analysis of young mice was even more vital and much more promising since we did not primarily expected an age-dependent phenotype. The mice were tested at an age of 4 to 11 month by the same seven behavioural tests we used for the young *Lrrk2* R1441C knock-in mouse line.

5.6.1.1 Motor behaviour of the *Lrrk2* mouse lines

For revealing possible motor deficits, the open field test and rotarod test have been used. Overall locomotion, as determined by the total distance travelled during the open field test was not changed between wild-type and R1441C mice (data not shown). Only female mutant mice showed a slight decrease, which became a tendency when only the distance travelled on the periphery (Fig.43) was taken into account (t-test: $p=0.06$).

Using the accelerating rotarod we could not detect general problems of the mice in regard to motor coordination, although the mutant mice showed a slightly reduced performance (Fig.43). The only differences could be observed between male wild-type and mutant mice during the second trial, where wild-type mice performed highly significant better ($p<0.01$ trial 2 vs. trial 1 and 3). During the third trial, instead of improving, wild-type males performed worse and comparable to R1441C mice. Male mutants slightly but significantly

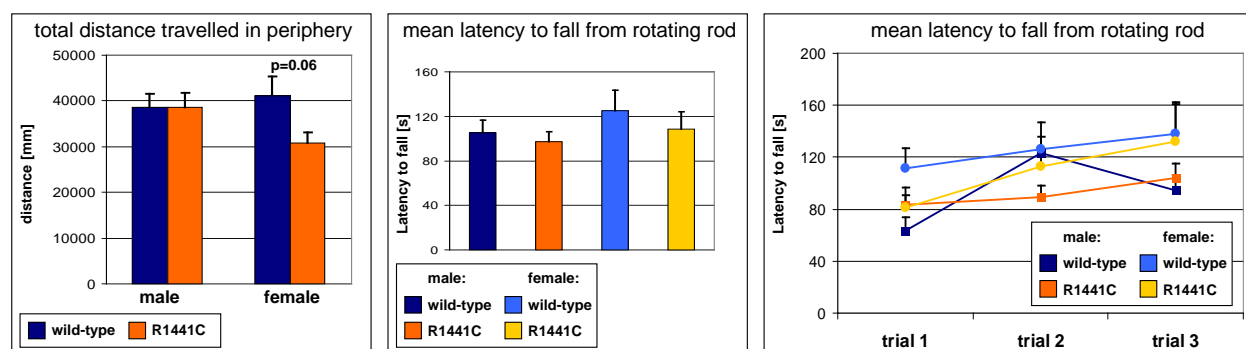


Figure 43: Young *Lrrk2* R1441C animals show only minimal alterations in their general motor performance: Selected results of the Open field and the accelerating rotarod test: the total distance travelled in periphery indicates the general motor activity and is slightly decreased in mutant females ($p=0.06$). The latency to fall from the rotating rod indicating the motor coordination is not changed. In addition also the learning ability of the mice, studied in a time-course from trial 1 to 3, is not altered. Numbers of animals tested: males: wt=13, mutant=19; females: wt=9, mutant=11 (data is expressed as mean \pm SEM).

improved their performance in the third trial ($p < 0.05$ trial 3 vs. trial 1 and 2). Female R1441C mice did not perform different from wild-type and both genotypes improved significantly until trial 3 (Student's t-test: $p < 0.05$). It has to be noticed, that at the time of the rotarod tests, male mutants exhibited a small but significant increase in body weight compared to the control animals; female R1441C mice showed the same trend (data not shown). In summary, although R1441C female mice show a tendency of reduced locomotion and both mutant genders show slightly less motor coordination, these differences are not significant.

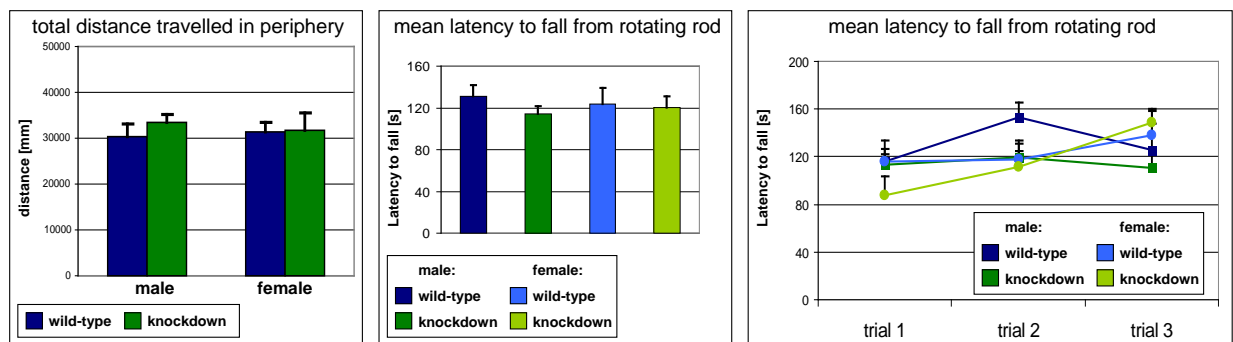


Figure 44: The general motor performance of young *Lrrk2* knockdown animals is not altered. Selected results of the Open field and the accelerating rotarod test: the total distance travelled in periphery indicates the general motor activity, the latency to fall from the rotating rod motor coordination. In addition, the learning ability of the mice can be studied in a time-course from trial 1 to 3. None of the parameters do show significant changes between wild-type and mutant mice. Numbers of animals tested: males: wt=10, mutant=22; females: wt=11, mutant=13 (data is expressed as mean \pm SEM).

For the *Lrrk2* knockdown line, the total distance travelled during the open field test was the same between wild-type and mutant mice, indicating that the overall locomotion is not changed (Fig.44). In case of the motor coordination tested by the accelerating rotarod, no significant difference could be detected, although there is an indication that knockdown males fall slightly earlier from the rod than their wild-type littermates (Fig.44). Both wild-type and mutant males fail to improve over the three trials, whereas the females of both genotypes significantly increase their performance ($p < 0.01$) during the test. At the time of the rotarod tests, mutant and control animals exhibited comparable body weights. Taken together, no differences either in locomotion or in motor coordination could be detected in young *Lrrk2* knockdown mice.

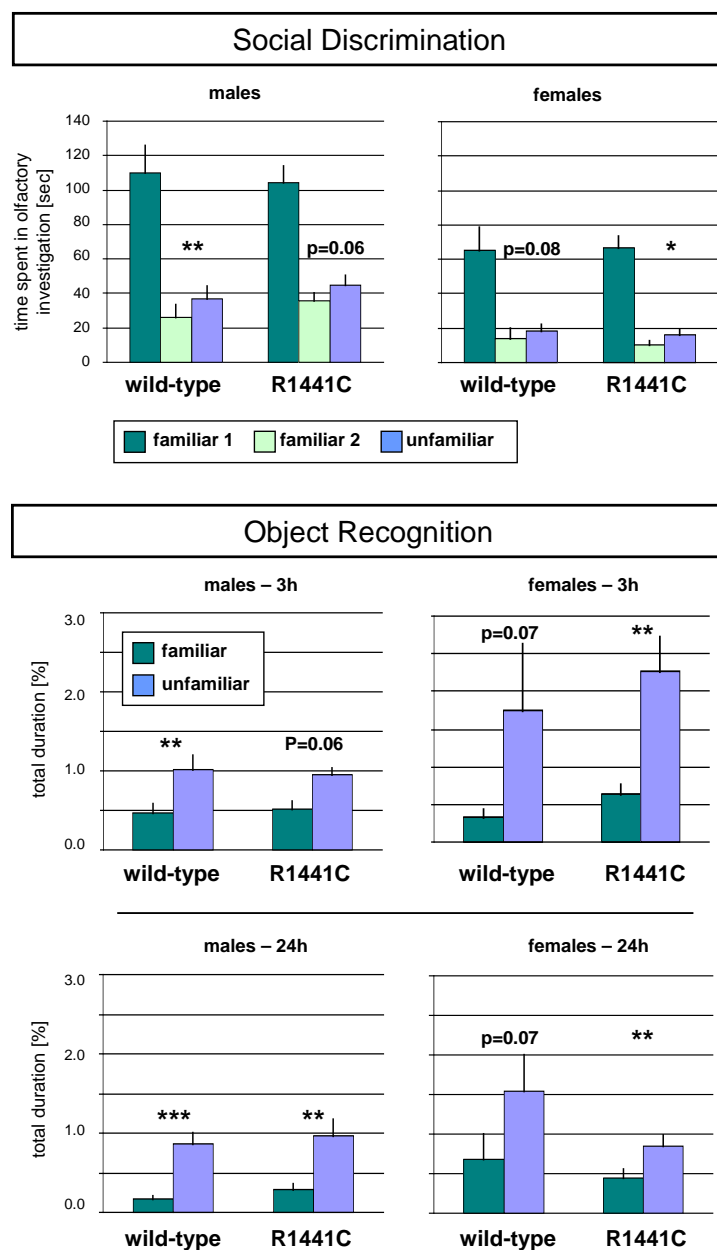
Combined, both *Lrrk2* mouse lines at least in young animals do exhibit normal motor skills.

5.6.1.2 Cognition and memory in the *Lrrk2* mouse lines

Besides the common motor dysfunctions, PD is also characterized by several non-motor symptoms like cognitive impairments or memory defects (Sollinger *et al.*, 2010). To analyze both the cognitive functions and the short-term and social memory, we tested the animals in regard to their ability to discriminate between familiar and unfamiliar objects and social partners.

Figure 45:
Cognitive function and memory performance are un-altered in young *Lrrk2* R1441C mice.

Results of the social discrimination and object recognition test. The social discrimination test paradigm is based on determine the absolute time [sec] a mouse spends with olfactory investigation of fellow mice. In case the mouse significantly spends less time with investigating the familiar mouse during the second phase of the test (familiar 2) compared with the unfamiliar control, indicates correct recognition and memory function of the tested animal. Similar principles are valid for the object recognition test. Numbers of animals tested: males (wt/mut): 8/16; females (wt/mut): 7/9 (data is expressed as mean \pm SEM).



During the sample phase of the social discrimination test, wild-type and R1441C mice spent the same time with olfactory investigating the familiar mouse. During the test phase all animals, irrespective of genotype and gender, spent more time exploring the unfamiliar mouse, albeit significance was not reached for every condition (**Fig.45**). Even more clear-cut were the results of the object recognition test. The animals of both genotypes spent significantly more time with the unfamiliar object at both time points (**Fig.45**). Only for wild-type females significance could not be reached due to the high variability in the time spent with the unfamiliar object. Taken together,

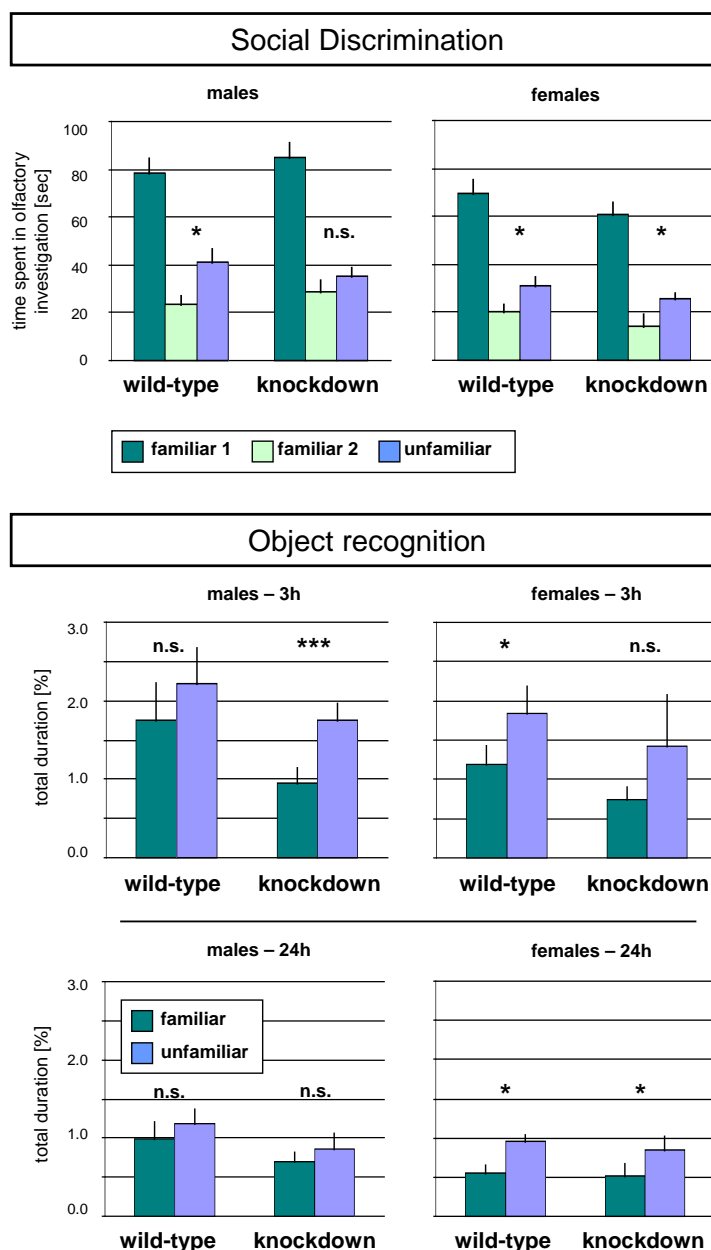


Figure 46: Cognitive function and memory performance is not changed in young *Lrrk2* knockdown animals.

Results of the social discrimination and object recognition test. In the object recognition test paradigm, the temporal ratio [%] in which the mouse is investigating an object during the course of the test is measured. Spending significantly higher proportions with exploring the unfamiliar object indicate correct recognition and memory function. Similar principles are valid for the social discrimination test (data is expressed as mean \pm SEM). Numbers of animals tested: males (wt/mut): 8/16; females (wt/mut): 7/9.

alterations in the cognitive functions and the short-term and social memory can be excluded for young *Lrrk2* R1441C mice.

Also for the *Lrrk2* knockdown animals, no abnormalities could be detected by the social discrimination test. The olfactory investigation was not significantly different between the genotypes during the sample phase. Wild-type as well as *Lrrk2* knockdown animals spent significantly more time in exploring the unfamiliar mouse during the test phase. Only for mutant males, significance could not be reached, although they exhibit a clear tendency (**Fig.46**). And again during the object recognition test, a tendency for spending more time in investigating the unfamiliar object was obvious in both wild-type and *Lrrk2* knockdown mice. In general, the animals could after 3 hours as well as after 24 hours discriminate between familiar and unfamiliar objects. Admittedly not for all groups and time points significance could be reached, but a clear trend towards more interest into the unfamiliar object could be observed (**Fig.46**).

This result indicates that young *Lrrk2* knockdown mice have no problems in regard to their cognitive functions and memory. Taken together, neither the expression of the pathogenic form, nor the loss of LRRK2 protein causes cognitive or memory dysfunction in young animals.

5.6.1.3 Depression- and anxiety-like behaviour

Depression represents one of the most prominent non-motor PD symptom occurring in more than 60% of the patients (Martínez-Martín and Damián, 2010). Since depression is such a complex mood disorder and displays a high interconnection especially with anxiety (Hettema, 2008; Bessa *et al.*, 2009) we did not only look for depression-like behaviour, but used also some aspects of the open field test to determine the anxiety-related behaviour of our animals. In their environment, mice fear novel and open spaces and therefore generally avoid the centre of the open field arena. This natural behaviour can be used in this test to measure anxiety-like behaviour (Bouwknicht *et al.*, 2008; Hasegawa *et al.*, 2009). In case of the *Lrrk2* R1441C animals, no differences compared to wild-type littermates could be observed except a slight but non-significant increase in the time the R1441C females spent in the 16% centre of the arena (**Fig.47**).

One of the most common assays to study depression-like behaviour in rodents are the tail suspension test and the forced swim test (Trullas *et al.*, 1989; Cryan *et al.*, 2005). R1441C females depict a distinct and significant increase ($p=0.020$) in the latency to immobility of far more than two-fold compared to wild-type littermates (**Fig.47**). The main readout value – the total duration of immobility – was consequential clearly decreased, but unfortunately did not reach the level of significance. Nevertheless, this first result of a decrease in depression-like behaviour at least in R1441C females could be confirmed by the results of the forced swim test. As expected, the mutant females spent significant more time with swimming ($p<0.05$) and less time with floating ($p<0.05$). The results of the male mice show a tendency towards the same direction (**Fig.47**). Since body mass might influence the test results, the weight of all mice has been determined again and previous noticed differences

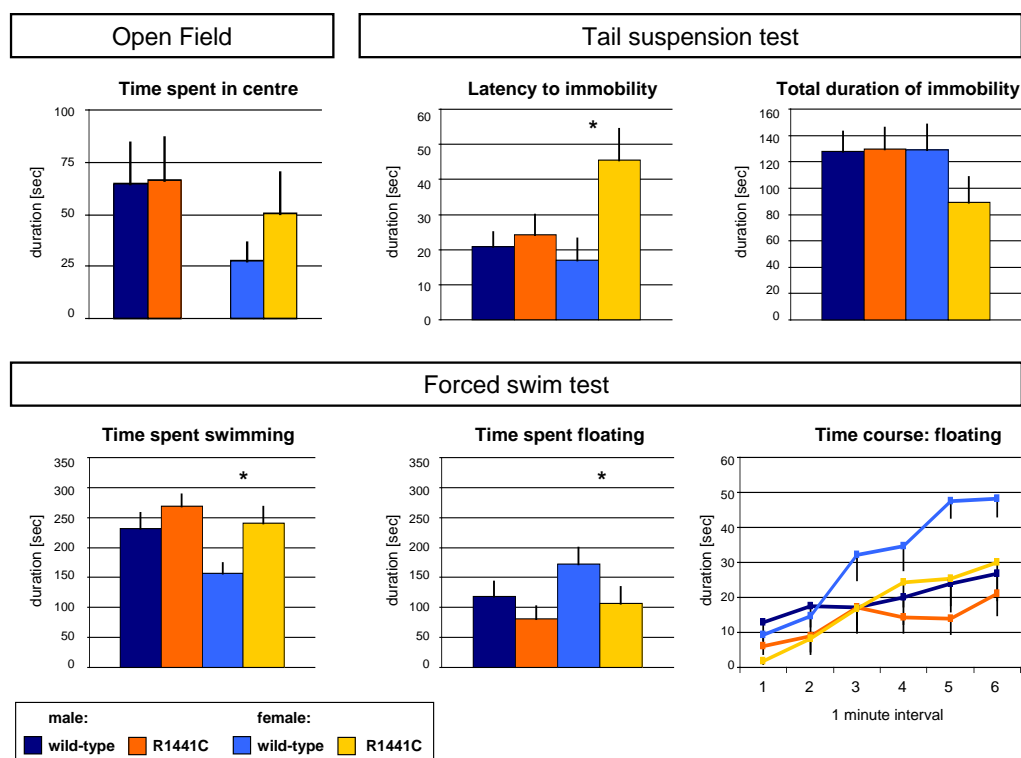


Figure 47: *Lrrk2* R1441C females show a reduced anxiety- and depression-related behaviour. While mutant females in the open field test show only a slight tendency for spending more time in the centre, during the tail suspension test mutant females show a significant increase of far more than two-fold in the latency to immobility compared to wild-type littermates ($p=0.020$). Also the forced swimming test revealed that at least mutant females significantly spent more time with floating and less time with swimming ($p<0.05$ for both). The Numbers of animals tested: males (wt/mut): 10/22; females (wt/mut): 11/13 (data is expressed as mean \pm SEM).

between the genotypes could not be seen at the time of the test (data not shown). In summary we observed a subtle tendency in one and significant changes in two other related tests, suggesting a decrease in anxiety and depression-like behaviour in young R1441C females.

Similar results could also be observed in the *Lrrk2* knockdown line. Although the open field revealed identical overall locomotion of wild-type and knockdown mice, the anxiety-related aspects of this test displayed clear-cut behavioural differences between the genotypes. While female mutant just show a very slight tendency towards it, male *Lrrk2* knockdown mice spent significantly ($p < 0.05$) more time in the centre of the test arena (**Fig.48**). After a short period of orientation where both genotypes behave almost identical, wild-type animals tend to avoid the centre while knockdown mice do not so

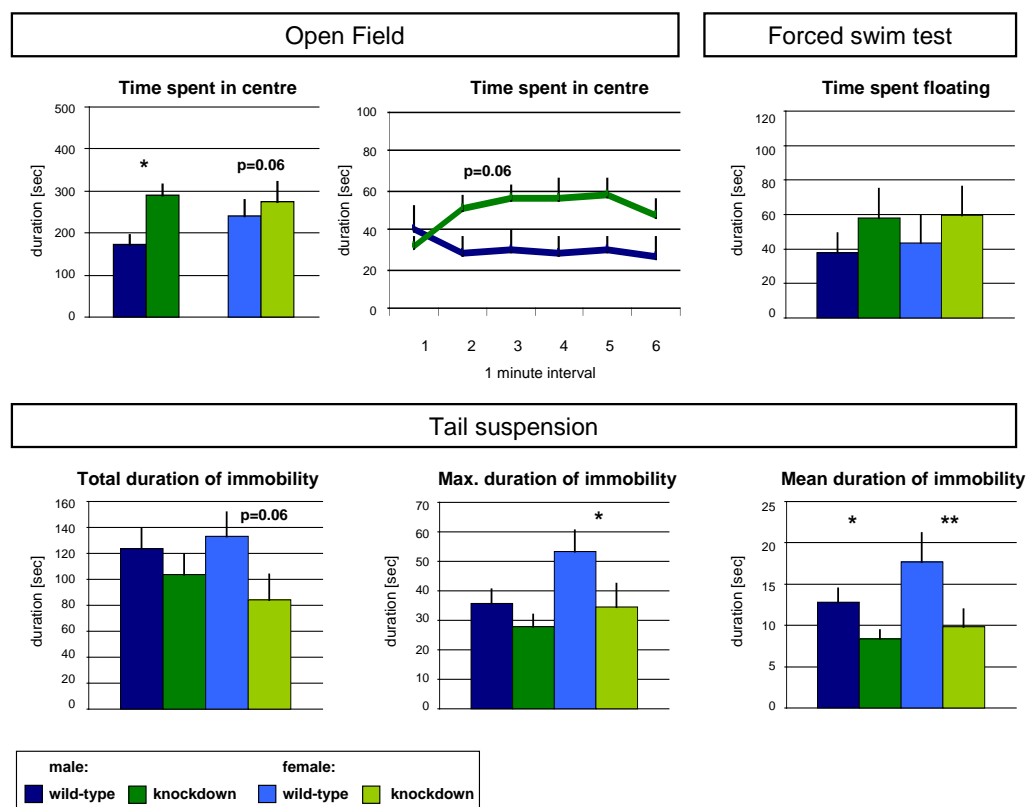


Figure 48: Anxiety and depression-related behaviour is reduced in *Lrrk2* knockdown animals. During the open field test, *Lrrk2* knockdown mice spent significantly ($p < 0.05$ males, $p = 0.06$ females) more time in the centre of the test arena suggesting reduced anxiety. No genotype differences have been revealed in the forced swimming test. Results of the tail suspension test demonstrate a significant reduction in the total, maximal and mean duration of immobility. Numbers of animals tested: males (wt/mut): 10/22; females (wt/mut): 11/13 (data is expressed as mean \pm SEM).

and even increase their time spent in the centre. According to the open-field exposure paradigm (Prut and Belzung, 2003), this behaviour has to be interpreted as a reduction in anxiety-related behaviour at least in male *Lrrk2* mice.

The forced swim test revealed no significant changes; nevertheless the trend is directed towards less floating of mutant mice compared to their wild-type littermates (**Fig.48**). The time spent with swimming was almost identical between the different genotypes (data not shown). Genotype-dependent alterations of the body mass were also not observed (data not shown).

In the tail suspension test, as like the knock-in line, *Lrrk2* knockdown animals showed a tendency for the decrease in total duration of immobility ($p=0.06$). When looking to the maximum and mean duration of immobility, at least female mutants show a clear-cut and significant reduction ($p<0.05$ and $p<0.01$) (**Fig.48**). The results of the male mice show a trend towards the same direction. In summary, young *Lrrk2* knockdown males show a reduced anxiety-like behaviour in the open field, whereas knockdown females exhibit a decrease in depression-like behaviour evaluated by the tail suspension test.

Taken together, for both the young *Lrrk2* R1441C knock-in as well as the *Lrrk2* knockdown line significant changes in two to three related tests did show significant changes in anxiety and depression-like behaviour. Interestingly, the results are suggesting a decrease in these behavioural aspects for both lines. This could indicate similar molecular alterations induced by the loss of the protein as well as the expression of its pathological mutated form.

5.6.2 Odour discrimination in aged *Lrrk2* R1441C and *Lrrk2* knockdown mice

Since hyposmia (olfactory dysfunction) is one of the most widespread non-motor symptoms and is occurring very early in the course of the disease, it is actually also used for prediction and diagnosis of PD (for review see Haehner *et al.*, 2009). Based on this our colleague Lisa Glasl established an odour discrimination paradigm by which several parameters can be addressed: First of all the sensitivity of the mouse to detect an assigned odour in increasing

dilutions, next the ability to discriminate between certain degrees of a binary mixture of two different odours has been determined. In a final step the capacity to recognize the assigned odour again was checked after additional 8-10 weeks following the training (olfactory memory). Shortly, the assay was performed as follows: during the three days of the training phase, each mouse has been assigned to a personal odour. Therefore either methyl trans-cinnamate (“strawberry”) or Phenethylacetate (“apple”) has been used. In the test phase, food deprived mice had to identify their assigned odour in order to get small pieces of chocolate as a reward (Glasl *et al.*, in preparation).

Old *Lrrk2* R1441C animals at an age between 24 and 27 month have been tested in this regard. In the binary mixture paradigm, both genotypes have no problem to identify the sole odour, but already in a 70%-mixture, *Lrrk2* R1441C exhibit a significant lower performance. Also in the more challenging mixtures, the mutant animals do produce more failures compared to their wild-type littermate. The identical performance of both genotypes at the 50%-mixture indicates the correct operation of the test (**Fig.49, a**). Furthermore, also the total odour sensitivity is depleted in old *Lrrk2* R1441C animals. While wild-type animals could recognize their assigned odour until a dilution step around no.25, mutant animals did fail already at a dilution step about no.22 to no.23, indicating a decrease of 4- to 8-fold. These results fairly reach the level

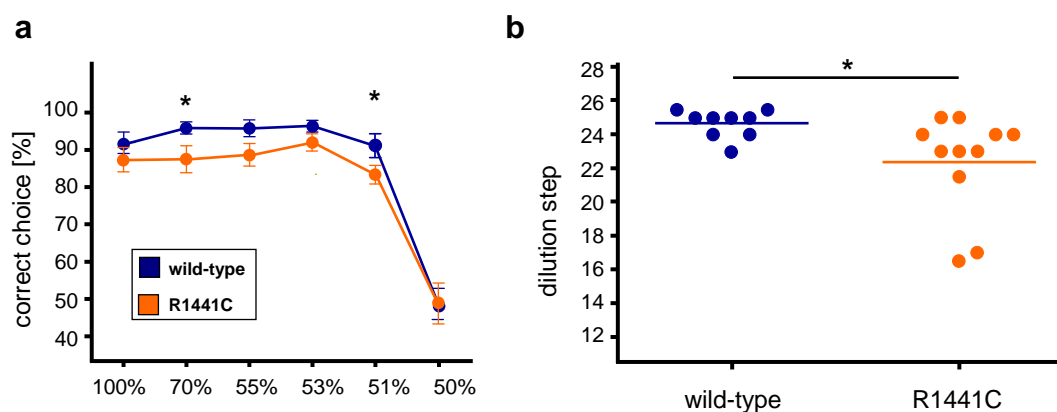


Figure 49: Aged *Lrrk2* R1441C mice display significantly reduced olfaction in an odour discrimination and sensitivity test paradigm. a) Discrimination of binary odorant mixtures (“apple” and “strawberry”) is reduced in mutant mice significantly at least in two mixtures (70% and 51%; $p < 0.05$). **b)** The general olfactory sensitivity, defined by the maximal dilution step an individual mouse could absolve, is significantly ($p = 0.04$) reduced in aged *Lrrk2* R1441C knock-in mice. Numbers of animals tested: wt/mut: 9/11 (genders pooled, data expressed as mean \pm SEM).

of significance ($p < 0.05$), although it has to be mentioned that for both tests the results from males and females had to be pooled due to the low number of wild-type females (**Fig.49, b**). During the third phase of this test, which addresses the olfactory memory of the animals, no additional deficits could be seen in this mouse line (data not shown). Nevertheless, the odour discrimination paradigm clearly did demonstrate significant olfactory deficits in old *Lrrk2* R1441C animals compared to their littermates.

Aged animals between 24 and 27 month of the *Lrrk2* knockdown line have been tested in a similar way. Only the binary mixtures of 53% and 51% of the female group haven't yet been included into the odour discrimination part of the test. Possibly due to this fact, only a trend of reduced olfaction could be observed in the binary discrimination part for this group (**Fig.50, a**). Apart from

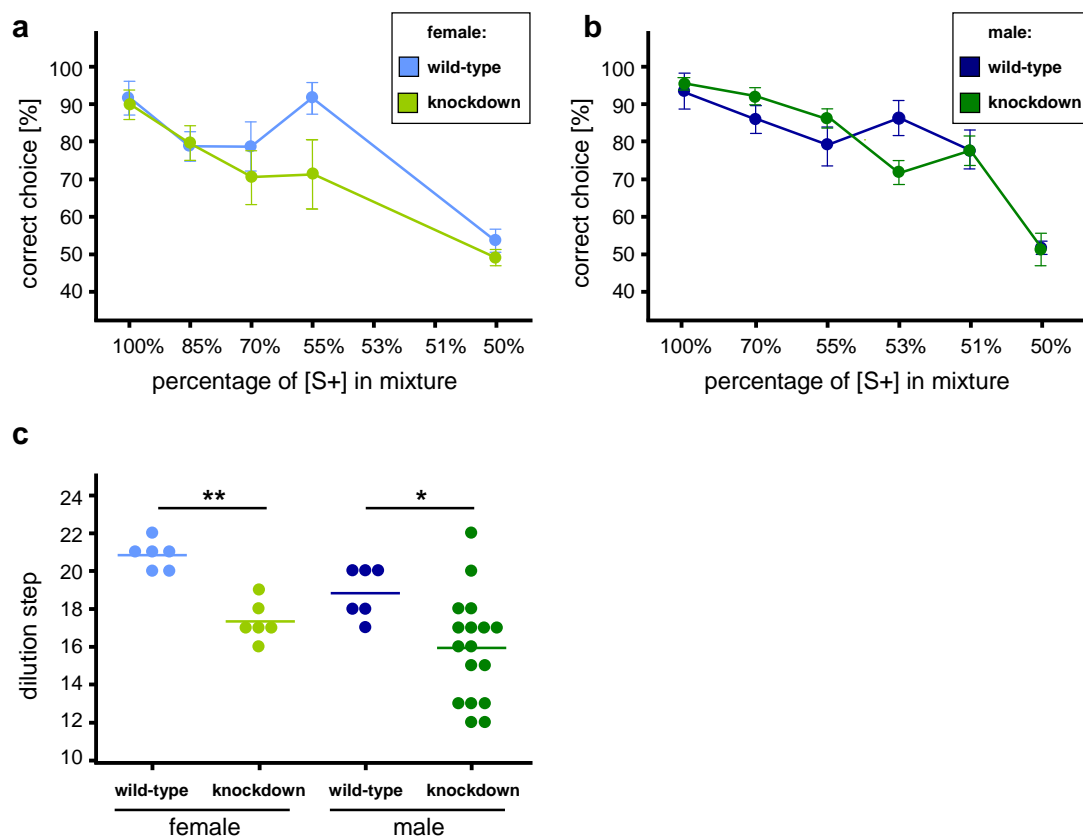


Figure 50: Both male and female *Lrrk2* knockdown mice display significantly reduced olfaction in age. Results of the olfaction discrimination and sensitivity test: **a**) and **b**) discrimination of binary odorant mixtures in female and male mice respectively **C**) The general olfactory sensitivity, defined by the maximal dilution step an individual mouse could absorb is significantly diminished in *Lrrk2* knockdown mice of both genders ($p < 0.01$ for females; $p < 0.05$ for males). Numbers of animals tested: males (wt/mut): 6/17; females (wt/mut): 6/6 (data is expressed as mean \pm SEM).

that, the male mutant mice did perform the test for the 53%-mixture significantly worse than their wild-type littermates. Puzzling, for all other mixtures no differences could be observed (**Fig.50, b**). Both in the female and male group, the identical performance of the different genotypes at the 50%-mixture indicates the correct operation of the test. More clear-cut is the result of the odour sensitivity test in both *Lrrk2* knockdown females and males. First of all we can observe that wild-type females did perform the test much better than the corresponding male animals. Nevertheless, in both genders the mutant littermates produce significantly more failures than control animals do. Mutant male mice reach fail approximately 3, female mice up to 4 dilution steps earlier to correctly recognize their assigned odour. This indicates a reduction of their odour sensitivity by the 8- to 16-fold compared to their wild-type littermates (**Fig.50, c**).

Again the third part of this test, addressing the olfactory memory of the animals, did not reveal any alterations in this mouse line (data not shown). Clearly the odour sensitivity paradigm did demonstrate significant olfactory deficits also in old *Lrrk2* knockdown animals.

Taken together, the observed reduced olfactory performance of both the *Lrrk2* R1441C and the *Lrrk2* knockdown line do recapitulate nicely one of the pre-motor symptoms known from PD patients.

5.6.3 Gait analysis of aged *Lrrk2* R1441C and *Lrrk2* knockdown mice

Olfactory deficits have been shown to be a promising approach for the presymptomatic diagnosis of PD. Nevertheless, also hyposmia does have limitations in its predictive power which makes it necessary to assess also other possible early PD symptoms like depression or initial and subtle motor dysfunctions (for review see Postuma and Montplaisir, 2009). Since we could not demonstrate severe motor disturbances in young animals by the accelerating rotarod (see **5.6.1.1**), we have chosen a more sensitive approach for the diagnosis of subtle changes in the gait of fully-aged animals. Therefore the automated *CatWalk*TM (Noldus, Wageningen, Netherlands) apparatus, allowing the recording and quantification of multiple gait parameters, has been

utilized. So far this technique has not only been used for animal models of nerve injury or pain, but also for movement disorders of the CNS including PD (Hampton and Amende, 2010; Vandeputte *et al.*, 2010).

For this assay, the mice are placed on a glass walkway, where the paw contacts are visualized, recorded and computerized analysed (for a sample picture see figure 54, upper left). In case of the *Lrrk2* R1441C knock-in line, 28 month old animals have been used (n=6/8). The most striking genotype differences could be found in regard to their step sequence patterns and inter paw coordination (**Fig.51**). The percentage of time, in which the animals move in a cruciate step sequence pattern (RF-LF-RH-LH) was significantly reduced from about 20% in wild-type mice to 8.3% in R1441C knock-in mice ($p < 0.05$). The most common pattern in wild-type mice is the alternate step sequence pattern (LF-RH-RF-LH) (Hamers *et al.*, 2006), which did not show significant changes. In addition to that, also the coordination between different paws is

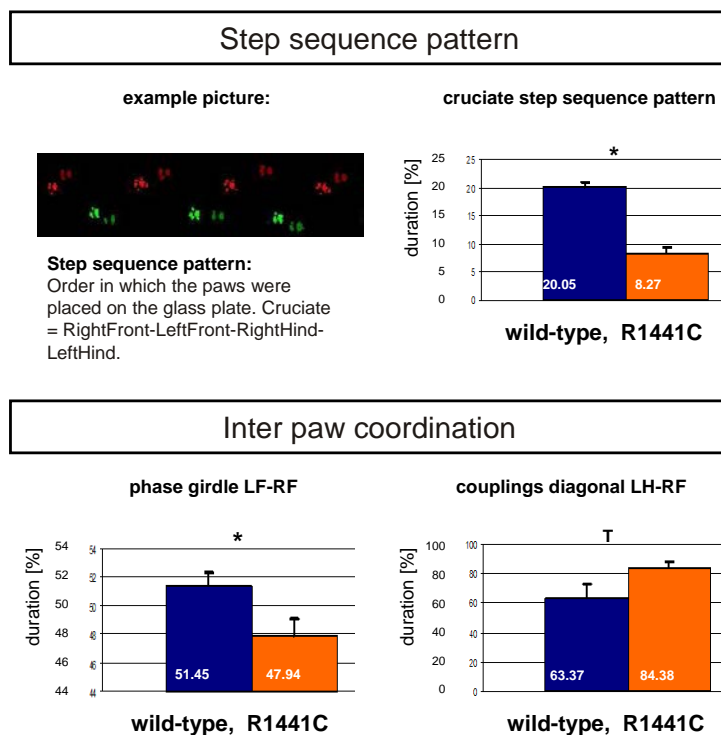


Figure 51: Gait analysis of fully aged (28 month) *Lrrk2* R1441C animals revealed significant alterations in several aspects of the analysis.

Mutant animals show a reduced percentage of using a cruciate step sequence pattern ($p < 0.05$) in the automated *CatWalk*TM analysis. Also the inter paw coordination is disturbed: The temporal coordination and thereby correlation between the girdle pair left-front (LF) and right-front (RF) is significantly reduced ($p < 0.05$). In addition, a trend ($T < 0.08$) towards increased coupling of the diagonal pair left-hind (LF) and right-front (RF) paw could be observed. Numbers of animals tested: males: wt = 5, mutant = 5; females: wt = 1, mutant = 3; genders were pooled (data is expressed as mean \pm SEM).

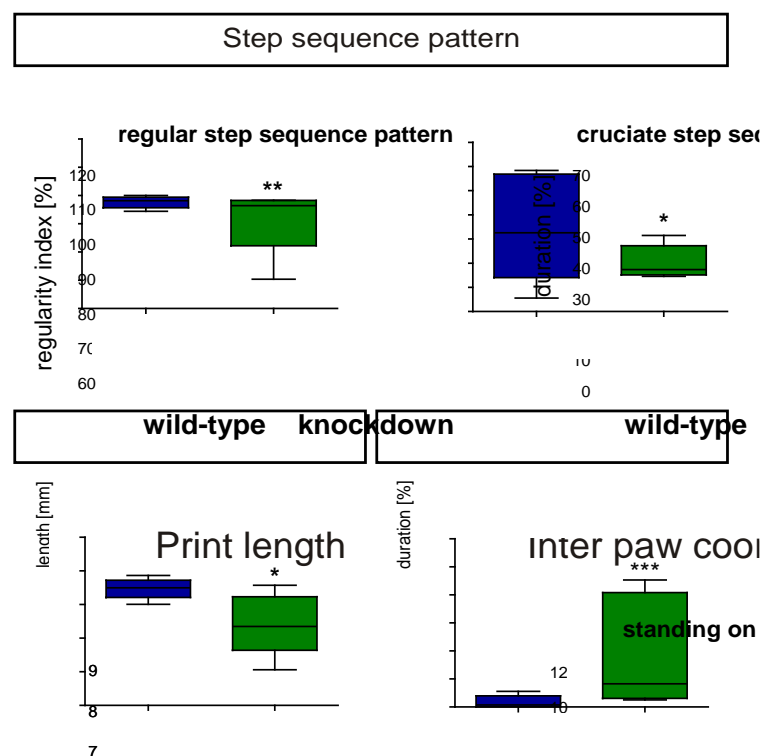
disturbed. A value of around 50% in the phase of the pair left-front (LF) and right-front (RF) (termed girdle pair in contrast to lateral and diagonal pair) would indicate a proper temporal correlation and coordination of these limbs. In mutant animals we observed a significant ($p < 0.05$) reduction to 47.9%. Together with the observed trend ($T < 0.08$) towards increased coupling of the diagonal pair left-hind (LF) paw and right-front (RF) paw, we can conclude slight alterations (**Fig.51**) in the coordination of gait in these animals.

Lrrk2 knockdown animals ($n=14/26$) were tested at a slightly younger age around 24 month. But again, like for the *Lrrk2* R1441C knock-in line, the most striking genotype differences have been identified in their step sequence patterns and inter paw coordination (**Fig.52**). Interestingly, in this mouse line the wild-type animals do show a higher ratio of the cruciate step sequence pattern of 32.5%; nonetheless we did observe a significant reduction to 18% in LRRK2-depleted animals ($p < 0.05$). In this case, even the overall time in which the mice do show any step sequence pattern and which is defined as the regulatory index is slightly but highly significant ($p < 0.01$) reduced from

Figure 52:

Fully aged *Lrrk2* knock-down animals revealed several significant alterations during gait analysis.

Results from the automated *CatWalk™* analysis of fully aged (24 month) *Lrrk2* knockdown animals: Mutant animals show a reduced percentage of using both a regular step sequence pattern ($p < 0.01$) and a cruciate step sequence pattern ($p < 0.05$). The physical print length is shorter in mutant animals ($p < 0.05$), whereas in the inter paw coordination, they stand significantly more on the girdle pairs compared to wild-type animals ($p < 0.005$). Numbers of animals tested: males: wt = 4, mutant = 15; females: wt = 10, mutant = 11; genders were pooled (data is expressed as mean \pm SEM).



98% in wild-type, to 96% in mutant mice. Alterations of the inter-paw coordination in these animals is indicated by the significantly longer time LRRK2-depleted mice stand on the girdle pairs compared to wild-type animals ($p < 0.005$). Additionally, the print length is reduced from 7.5 mm in wild-type to 6.25 mm in *Lrrk2* knockdown animals ($p < 0.05$), indicating a more tiptoed gait in these animals (**Fig.52**).

Taken together, in both the *Lrrk2* R1441C knock-in as well as knockdown line, minor nevertheless significant changes in several parameters of the automated *CatWalk*TM gait analysis could be detected. Strikingly, both lines did show depletions in identical features like the cruciate step sequence pattern and the inter paw coordination. A higher degree of gait instability can be observed only in toxin-induced lesion models of PD accompanied with severe dopaminergic degeneration (Byler *et al.*, 2009). Therefore we could interpret the observed phenotypes as presymptomatic alterations independent from neurodegeneration.

By summing up the results of this behaviour analysis, it is remarkable that young *Lrrk2* R1441C knock-in as well as the *Lrrk2* knockdown animals only show significant changes in two to three related tests suggesting a reduced anxiety and depression-like behaviour. Other tests for memory, cognitive and motor functions did not show significant alterations. On the other side in fully aged animals of both lines indeed we could detect phenotypes like reduced olfaction and gait alterations which resemble early, non-motor symptoms of PD. Strikingly, all phenotypes could be detected in both lines and did point towards the same direction. Taken the results of our functional analysis of *Lrrk2* R1441C knock-in cells into account, from which a distinct but not vital role of LRRK2 protein in cellular functions like cytoskeletal organisation and synaptic transmission can be assumed, it is not surprising that we could not detect overt age-related neurodegeneration of the dopaminergic system, inclusion bodies or other pathological hallmarks of PD. It seems that LRRK2 dysfunction does not affect overtly dopaminergic survival, but rather subtly affects all neurons, of which dopaminergic neurons are most sensitive and succumb earlier to cell death when challenged (according to multiple hit theory).

6 Discussion

6.1 Analysis of *Lrrk1* and *Lrrk2* expression

6.1.1 Expression during embryogenesis

In the beginning of the project, the only published data about the expression of *Lrrk2* was a Northern blot analysis showing the expression of a 9 kb transcript in various human tissues like heart, liver and kidney; in addition many regions of the adult brain did show *LRRK2* expression (Paisán-Ruíz *et al.*, 2004). By the qualitative technique of RT-PCR, *Lrrk1* and *Lrrk2* mRNA could be detected from early embryonic stages onwards; in the case of *Lrrk2* even from embryonic stem cells onwards. In general, the expression level of both *Lrrk* mRNA's appeared to be rather low. Therefore we have decided to determine the murine expression in particular by means of radioactive *in situ* hybridisation (ISH) as an extremely sensitive technique (see 7.2.2.2; Dagerlind *et al.*, 1992). Nevertheless also with this method robust signals of both *Lrrk1* and *Lrrk2* mRNA could not be depicted before midgestation stage E10.5 (Fig. 9). Since also the distribution of both transcripts is rather ubiquitous until this embryonic stage, a very specific role of the genes during early embryogenesis seems not to be highly likely. In general, for detecting weak expression domains like the *Lrrk2* expression in the substantia nigra (SN) of the adult brain or the expression of *Lrrk1* in the olfactory bulb, comparable longer exposure times for the ISH had to be chosen. This finding is in line with the results of quantitative RT-PCR we performed for various regions of the adult brain and for *Lrrk1* and *Lrrk2* qPCR results published by Biskup and colleagues, showing considerable lower levels compared to nominally expressed genes like *TATA binding protein* which served as control (see 5.1.3, Biskup *et al.*, 2007). Also in fibroblasts and neurons which have been *in vitro* differentiated from a LRRK2-GFP knock-in ES cell line, the level of murine LRRK2 protein appeared to be quite low (data not shown).

With ongoing organogenesis, the overall mRNA level of both genes increases and their expression patterns are getting more distinct. The involvement of *Lrrk1* or *Lrrk2* in the development of certain organs and tissues seems to be

possible due to their well-defined domains of high and in several cases dynamic expression. Organs like kidney, lung and heart, but also tissues like the chondral structures of the skull and vertebrae, or the developing teeth show prominent expression of either *Lrrk1* or *Lrrk2* mRNA. Interestingly no real overlap of strong expression domains of these two genes could be observed. Even if both are highly expressed in the same organ like the kidney, the pattern of robust expression is quite distinct from each other. In contrast to the situation in rat where *Lrrk1* mRNA could be detected in the developing brain and neural tube (Westerlund *et al.*, 2008/1), we could show that neither *Lrrk1* nor *Lrrk2* is expressed in the neuronal tissue of the murine CNS during embryonic development. Admittedly, this finding is in conflict with published data of quantitative RT-PCR on embryonic brain tissue of the mouse, showing a low expression of both genes from E11.5 onwards (Biskup *et al.*, 2007). But the strong expression of both genes in the meninges, tightly surrounding the complete CNS can explain this discrepancy. Non-radioactive ISH published by Zechel and colleagues even claimed a higher expression of *Lrrk2* in the developing cortex from mid-gestation embryos onwards (Zechel *et al.*, 2010). Since all other reported expression domains outside the embryonic brain, e.g. the mesenchyme surrounding the forming digits or the developing kidney match nicely to our data, it remains elusive where this difference arises from. In general it has to be mentioned that in this work we tested six overlapping and not overlapping riboprobes instead of only two, and did obtain identical results (see 5.1.1 and Fig.7). Moreover we instead used considerable longer probes and did avoid the 3' part of the transcript which contains the GTPases domain conserved throughout the Ras superfamily (Wennerberg *et al.*, 2005) and the serine/threonine kinase domain similar to mitogen-activated protein kinases (Paisán-Ruíz *et al.*, 2004; Guo *et al.*, 2007; Zechel *et al.*, 2010). Altogether, based on our findings a role of *Lrrk1* and *Lrrk2* in the embryonic development of the murine CNS is not likely. The proper brain development in *Lrrk2* knockdown mice nicely supports this conclusion.

6.1.2 *Lrrk2* mRNA expression in the adult CNS

Already during embryogenesis, but especially in the adult brain the expression pattern of *Lrrk2* differs quite conspicuously from the expression of other PD related genes like *Parkin*, *PINK1* and *DJ-1*. While these genes show a rather uniform and ubiquitous distribution in the CNS (Kühn *et al.*, 2004; Taymans *et al.*, 2006; Bader *et al.*, 2005), *Lrrk2* mRNA is not only ubiquitously expressed on a low level throughout the brain, but also depicts various regions of high and dynamic expression (**Fig.13**) which allows a deeper insight into the possible functions of LRRK2 in the CNS. First of all it has to be noticed that *Lrrk2* expression is not limited to neurons but also can be found to a lower extend in different glial cells of the murine brain. This result has been confirmed in human tissue by Miklossy and colleagues using RT-PCR on different tissue extracts and cell lines (Miklossy *et al.*, 2006). Initially it has been discussed, whether the substantia nigra pars compacta, which is the most affected brain region in PD patients, does express *Lrrk2* mRNA. While we could show a comparable low level of expression in this area, Melrose and colleagues could not detect any *Lrrk2* mRNA in the murine SN in their expression analysis (Galter *et al.*, 2006; Melrose *et al.*, 2006). Nevertheless, later on other studies confirmed our result of a minor but clearly detectable level of expression of *Lrrk2* in that area (Simón-Sánchez *et al.*, 2006; Higashi *et al.*, 2007/1; Han *et al.*, 2008). The highest levels of *Lrrk2* mRNA in the adult brain can be found in the striatum, piriform cortex, olfactory tubercle, hippocampus and in various areas of the neocortex. First of all it is striking that all these structures are located in the murine forebrain. The most out-standing region is undoubtedly the striatum since this is the only domain of strong *Lrrk2* expression which is an integral part of the basal ganglia circuit. Interestingly it is also the only expression domain, where a conspicuous postnatal increase of expression can be observed (**Fig.12**). But not only the striatum but virtually all target areas of dopaminergic innervation, like the cortex and the olfactory bulb exhibit elevated levels of *Lrrk2* mRNA. Based on these results, a postsynaptic role of LRRK2 in the function of the basal ganglia circuit could be assumed. Further more it has to be pointed out, that *Lrrk2* is expressed in all regions of adult neurogenesis in the rodent brain, which could suggest also a role in this

fascinating but until now not fully de-ciphered mechanism. The expression in the subventricular zone (SVZ) has been confirmed by Melrose and colleagues by showing the coexpression of LRRK2 with PSA-NCAM as a marker for neuroblasts in the SVZ (Melrose *et al.*, 2007).

Besides the spatial, also the temporal distribution of LRRK2 expression can give hints for its possible functions. Remarkable in this regard, is the congruent occurrence of dopaminergic synaptogenesis in the striatum during the first postnatal weeks (Mensah *et al.*, 1982) and the upregulation of *Lrrk2* expression in this region during this time span. This raises the questions whether LRRK2 protein is directly involved in the process of synaptogenesis, whether LRRK2 is needed to built up the synaptic machinery or whether the protein is getting simply more abundant by the increase of neuronal complexity per se. Not only the dynamic mRNA expression, but also the observed discrepancy between *Lrrk2* mRNA and protein level in the adult striatum is conspicuous. Both immunohistochemistry (IHC) using the antibody NB300-267, and Western blot analysis using a non-commercial antibody (1E11) revealed significantly less LRRK2 protein expression in the striatum compared to the high mRNA level revealed by ISH (**Fig.16**). The antibody NB300-267 later on was published by others to work in IHC at least in human tissue (Milosevic *et al.*, 2009). However, this result has to be interpreted cautiously since at least immunohistochemically all available antibodies directed against LRRK2 had difficulties in detecting the endogenous murine LRRK2 (Biskup *et al.*, 2007). It has been discussed by other groups, whether a widespread distribution of LRRK2 protein might be a hint for a pronounced transport of the protein (Melrose *et al.*, 2007), but in particular for the striatum, this explanation seems not highly likely: The medium spiny projection neurons in general do not project to far distant brain areas which means that despite intraneuronal protein transport, LRRK2 would not be transported out of the region to a great extend. A more straightforward explanation may be the posttranscriptional regulation of *Lrrk2* expression by specific microRNAs in the adult brain. MicroRNAs have been shown to play a role not only in general developmental processes like cell fate determination, but also in very specific mechanisms like synaptic development and function (Corbin *et al.*, 2009). We have already identified several candidate microRNAs which are predicted to

target *Lrrk2* mRNA, but further studies are necessary to pinpoint *Lrrk2*-specific microRNAs with region-specific expression.

In contrast to the widespread and informative expression pattern of *Lrrk2*, its paralog *Lrrk1* is barely expressed in the adult murine CNS. The only domain where small amounts of *Lrrk1* mRNA can be detected in neuronal tissue is limited to the mitral cell layer of the olfactory bulb (**Fig.14**); no very prominent expression of *Lrrk2* can be observed in this layer. Interestingly, the neurons of this structure – the mitral cells – are receiving the input of the olfactory nerves projecting from the olfactory epithelium. Therefore, the apical dendrites of the mitral cells terminate in glomeruli of the glomerula layer of the olfactory bulb where they form synapses with the incoming olfactory axons (Barlow and Mollon, 1982). Great care has been taken to verify the results of the ISH. Different probes located in different parts of the *Lrrk1* mRNA have been cloned and did show identical expression patterns and almost identical signal levels on embryonic sections, suggesting their functionality and specificity. All of the probes exhibited equal or even lower signal levels compared to their corresponding sense-probes (see 7.2.2.2) all-around the adult brain. To exclude the possibility of a subtle, ubiquitous expression of *Lrrk1* mRNA below the detection level of the radioactive *in situ* hybridisation, a RT-PCR analysis has been performed which widely supports this result of almost no neuronal *Lrrk1* in postnatal and adult mice. Altogether it has to be concluded, that *Lrrk1* is almost absent from the murine CNS. This finding fits quite well to published data of quantitative RT-PCR showing conspicuously lower levels of *Lrrk1* mRNA in the total brain of adult mice compared to *Lrrk2* (Korr *et al.*, 2006; Biskup *et al.*, 2007). It has to be mentioned that Westerlund and colleagues showed minor levels of *Lrrk1* mRNA to be widely till ubiquitously expressed in the adult rat CNS by means of non-radioactive *in situ* hybridisation (Westerlund *et al.*, 2008/1). Whether this discrepancy can be explained by species differences or the use of different detection techniques remains elusive. On the contrary Taylor and colleagues published data of quantitative RT-PCR from different mouse brain areas, were they could show low levels of *Lrrk1* expression throughout the brain; the only region showing elevated expression levels is the olfactory bulb (Taylor JN *et al.*, 2007). Assuming that the ubiquitous lower level results from the expression of *Lrrk1* in the meninges

and choroid plexus, this publication is fully supporting the data presented here.

Altogether it is surprising, that despite their high degree of homology and their comparable similar expression patterns during development, the adult brain almost exclusively expresses *Lrrk2*. We can conclude from this analysis that highly redundant functions or compensatory effects between the two paralogs *Lrrk1* and *Lrrk2* can be neglected, at least for the adult murine brain. This conclusion is supported by data from patients: linkage analysis or sequencing of the *Lrrk1* gene in sporadic could not identify any pathological mutations segregating with the disease (Taylor JN *et al.*, 2007; Haugarvoll *et al.*, 2007). The limited expression of *Lrrk1* in the olfactory bulb is nevertheless remarkable. This very specific part of the rodent brain does not belong to the basal ganglia circuit which is affected in PD, but very much like the domains of high *Lrrk2* expression like the striatum and the cortex, also the olfactory bulb is innervated by dopaminergic nerve terminals. One distinct region in the olfactory bulb, referred to as the periglomerular layer, even harbours dopaminergic neurons (McLean and Shipley, 1988).

6.1.3 LRRK2 protein expression in the adult CNS

The drawback of no available antibody suitable for immunohistochemistry (IHC) made it difficult to get further insights into the expression of LRRK2 on the protein level. We tested a whole variety of commercial and self-made antibodies in different immunohistochemical approaches (**Fig.15**). Some of the antibodies did work in Western blot analysis and did also show reduced or diminished LRRK2 levels in knockdown lysates (data not shown; **Fig.23, b**) but in IHC nearly all failed to show either any staining or a reduction of the staining on knockdown tissue. NB300-267 was the only antibody which did show a moderate reduction on knockdown tissue which suggests at least partial specificity. Unfortunately we could not confirm this result with a later batch of this antibody. In general, also other groups did recognize that the quality of available antibodies raised against murine LRRK2 is extremely poor. While several antibodies do recognize human LRRK2 even in IHC (Higashi *et al.*, 2007), only a few ones directed against mouse LRRK2 did recognize the

endogenous protein in Western blot analysis (Melrose *et al.*, 2007; Biskup *et al.*, 2007). Therefore, the problems we had to establish an immunohistochemical staining of LRRK2 protein are reasonable albeit not understood. It seems that murine LRRK2 protein is *per se* difficult to detect in its endogenous levels on tissue. One could argue for a role of the protein within a putative complex of several interaction partners since in this confirmation, the antigen is not accessible for the antibody. Nevertheless, an antibody working well in IHC would be an important tool to unravel the physiological role of LRRK2 (Biskup and West, 2008; Zechel *et al.*, 2010). We are therefore following another strategy to circumvent this problem by analyzing the cellular and sub-cellular distribution of a GFP-tagged form of the endogenous LRRK2 protein in differentiated ES cells and the adult mouse brain (work in progress). Preliminary results from ES cells, *in vitro* differentiated into neurons revealed a punctuated but rather uniform cytosolic distribution of the protein (data not shown). In addition, for studying the pattern of LRRK2 protein distribution in the adult mouse brain, we performed Western blot analysis using the polyclonal antibody 1E11 on lysates prepared from different brain regions. Interestingly we could detect LRRK2 protein in virtually all brain regions except the olfactory bulb, which is in line with previously published data based on a different antibody (Melrose *et al.*, 2007). In parallel, the contralateral side of each brain region was used to prepare cDNA from total RNA preparations. This cDNA was later used to quantify the amount of *Lrrk2* mRNA by quantitative real time PCR. By setting the sum of the relative levels of protein and mRNA to 100%, we could not only show that the protein levels do correlate in most of the regions quite well to the respective mRNA level, but could also demonstrate that in distinct regions like the striatum and the brain stem we do detect only about half of the amount of protein that one could expect (**Fig.16**). Strikingly, the hypothetical 1:1 correlation of relative mRNA to protein levels can be observed in various brain regions of moderate or low *Lrrk2* expression like diencephalon, cerebellum or midbrain. In the end the fact remains that on the mRNA level, the striatum shows the highest level of *Lrrk2* expression, whereas on the protein level cortical regions did show the highest levels in the adult CNS (**Fig.16**).

These observations can be explained by several facts (for reviews see Greenbaum *et al.*, 2003). First of all this could be based on potentially different turnover rates of the LRRK2 protein in different brain regions. Unfortunately, up to now there are no studies available which could argue for such differences in the adult rodent brain. The only information we have up to now is, that the general half-life of LRRK2 protein is relatively long (West *et al.*, 2005). We did exclude the possibility, that LRRK2 protein synthesized in the striatum is subsequently transported into other brain compartments, since the medium spiny neurons are known to have rather local projections in the murine CNS (Shi *et al.*, 1994). The most reasonable explanation for these discrepancies would be a post-transcriptional regulation of *Lrrk2* expression. This has been already presumed by other groups at least in distinct cell lines (Biskup *et al.*, 2007). Since microRNAs are more and more seen to play a role in brain function and neurodegenerative diseases (for reviews see Saugstad, 2010), we thought about a possible regulation of *Lrrk2* expression by this non-coding RNA species; for example in case of alpha-synuclein (*SNCA*), a regulation via *microRNA-7* has been demonstrated recently (Junn *et al.*, 2007). Also for *Lrrk2*, regional expressed microRNAs could explain the observed discrepancies between mRNA and protein levels if we assume a translational repression. It is discussed whether the mammalian microRNAs predominantly decrease their target mRNA levels (Guo *et al.*, 2010) or rather act as translational repressors. For distinct microRNAs, the binding of to Argonaute (*Ago*) proteins has been shown to inhibit translation (Kiriakidou *et al.*, 2007). Interestingly, in a *Drosophila* model, LRRK2 itself is involved in translational repression via *Ago2* (Gehrke *et al.*, 2010).

Based on the results of our detailed expression analysis we are currently working on the identification of specific microRNAs targeting *Lrrk2*. Preliminary results nevertheless could exclude the *SNCA* targeting *microRNA-7* also to regulate *Lrrk2* expression (data not shown).

6.1.4 *Lrrk2* expression in the adult striatum

To further characterize the *Lrrk2* expressing neurons in more detail, fluorescent and non-fluorescent double *in situ* -/ immunohistochemistry (ISH-IHC)

had to be used to bypass the limitations set by the available LRRK2 antibodies. Nevertheless also this technique bears disadvantages. Since the detection level of the non-radioactive ISH did not reach the level of the radioactive one, we are only able to make statements for cells that robustly express *Lrrk2*. Weak expressing cells might not be detected by this technique. To exclude the possibility that the chromophore used for ISH might interfere with the subsequent IHC we used different fluorescent and non-fluorescent substrates. Furthermore we only used markers and antibodies giving a strong and distinct signal to prevent additional detection problems in the course of the IHC. Like the radioactive ISH already revealed (**Fig.11, C**), *Lrrk2* is expressed predominantly but not exclusively neuronal indicated by the high overlap with the pan-neuronal marker NeuN (**Fig.17**). In summary, *Lrrk2* expression in the murine CNS is on the one side not limited to specific neuronal or glial cell types. Also other groups have identified *Lrrk2* mRNA in a whole variety of cell types either by double IHC using self-made antibodies against human or mouse LRRK2 protein, or by RT-PCR from sorted cell-populations. Thus far, expression was found predominately in neurons and interneurons of various types; but also in astrocytes, in microglia and oligodendroglia (Miklossy *et al.*, 2006; Higashi *et al.*, 2007/1; Melrose *et al.*, 2007; Han *et al.*, 2008).

We have focused our view onto the striatum as one of the most outstanding *Lrrk2* expressing regions and as the target area of nigrostriatal dopaminergic innervation which is affected in PD. Detailed ISH-IHC studies in this area revealed a high degree of coexpression with DARPP-32 (dopamine and cAMP regulated phosphoprotein 32) used as a marker for the medium-size spiny neurons (MSN). This result is not surprising since these cells make up 95% of all neurons in the striatum (Tepper *et al.*, 2004), were *Lrrk2* is highly expressed in neurons. We observed robust *Lrrk2* expression in about 70% of all dopamine receptor D1 (DR-D1) and in about 60% of all DR-D2 positive neurons (**Fig.17**). Firstly, this surprising result indicates that *Lrrk2* expression is not prone for either the D₁-like, or the D₂-like family of dopamine receptors, represented by their most abundant members DR-D1 and DR-D2. If this were the case, we would have to see a nearly total overlap with at least one of the two markers. Whether *Lrrk2* plays a pivotal role rather in the direct or in the indirect striatonigral pathway can not be fully answered by this experiment

since up to now, the molecular characterisation of these pathways is still under debate. To answer this question, markers exclusively expressed in neurons of the direct or indirect pathway, like enkephalin and substance P (Cuello *et al.*, 1981) would have to be used for ISH-IHC in addition. In general, the direct pathway is more associated with the DR-D1, the indirect with the DR-D2 (Gerfen *et al.*, 1990). On the other side, data is still puzzling whether both receptors are coexpressed in nearly half of the MSN (Surmeier *et al.*, 1996) or to a much smaller content suggested by the analysis of BAC-reporter mice (Matamales *et al.*, 2009; Valjent *et al.*, 2009).

Nevertheless, recent studies utilize DR-D1 and DR-D2 driven Cre-lines to distinguish between distinct functional pathways in the striatum (Bateup *et al.*, 2010). Taken together, our results suggest that altered or disrupted activity of LRRK2 in the striatum is highly likely to affect both the direct as well as the indirect pathway of the basal ganglia circuit (see **3.1.2**).

With this expression analysis we provided further insights in the pattern of expression of both *Lrrk* genes. This work exhibits the first complete analysis of murine *Lrrk1* and *Lrrk2* mRNA expression covering numerous stages from ES cells, embryonic development till the postnatal and adult brain. In contrast to the published works of all other groups we used radioactive labelled riboprobes (Dagerlind *et al.*, 1992) which are ensuring highest quality and resolution levels and an extremely high detection level. Next we could demonstrate the quantitative distribution of LRRK2 protein in the adult brain and detected conspicuous discrepancies between relative mRNA and protein levels in distinct regions of the brain. Furthermore we present first quantitative analysis of *Lrrk2* mRNA in DR-D1- and DR-D2-expressing medium spiny neurons of the striatum. In case of *Lrrk1*, the extremely limited expression in adult brain impedes redundant functions to its paralog *Lrrk2* at least in the CNS. This could explain for the first time, why no PD-associated mutations could be identified in the *Lrrk1* locus up to now (Haugarvoll *et al.*, 2007).

6.2 Generation of the *Lrrk2* R1441C knock-in mouse model

The effects of a recessive PD mutation like *Parkin*, *DJ-1* or *PINK1* is based on the loss-of-function of the respective protein and a knock-out mouse is the ideal approach to produce a rodent PD model. In case of a dominant PD mutation, the situation is much more complex. To implement the proposed gain-of-function mechanism, several approaches are possible. In the case of alpha-synuclein, multiple mouse models have been generated which are based on different tactics like the ubiquitous or cell type specific overexpression of wild-type protein under the control of exogenous promoters, the expression of pathogenically mutated forms of the protein or any other combination (Buchman and Ninkina, 2008). In case of our *Lrrk2* PD mouse model, the paradigm was used to create a model which is as close to the situation of the patients as possible. Therefore, one of the pathogenic mutations known from PD patients, should be inserted into the endogenous murine *Lrrk2* gene. This strategy is based on the fact, that LRRK2 is highly conserved between human and mouse. Due to this one can expect that the molecular effects of the observed point mutations should have a similar impact whether in human or in murine LRRK2 protein. The initial identification of pathogenic mutations in the human *LRRK2* gene segregating with PARK8-linked PD was performed in two independent families from North America and Spain (Zimprich *et al.*, 2004; Paisán-Ruiz *et al.*, 2004) and revealed the three point-mutations R1441C, R1441G and Y1699C. Two mutations occurred at the same position within the catalytic Roc-GTPase domain, while the third is located in the COR domain for which virtually no functional data was available. On the basis of this, the pathogenic point mutation R1441C was chosen for our *Lrrk2* disease model. Furthermore in patients the ultimate result of both mutations, G2019S - the most prominent mutation known so far - and R1441C, is a very similar, in some cases indistinguishable form of familial PD (Gandhi *et al.*, 2009). In addition to the insertion of the pathogenic point mutation R1441C, the respective exon 31 was flanked by *Lox-P* (locus of X-over P1) sites, allowing its deletion by Cre (Cyclization Recombination) recombinase. This would lead to the in-frame deletion of a 73 amino-acid long C-terminal part of the Roc-GTPase domain which will result in the putative functional

disruption of this domain. This approach provides an *in vivo* read-out for the function of the GTPase domain and allows the dissection of the *one protein – two enzymes* idea (see 3.4.1). Altogether, the targeting strategy enables to simulate both the gain- and loss-of-function with minimal modifications of the endogenous *Lrrk2* locus.

6.3 Functional analysis

We established fibroblast cell lines to obtain an easy tool for studying the possible effects of mutated LRRK2 on basic cellular processes. Those immortalized cell lines bear the advantage of being easy to handle and can be cultivated and treated for a long time. On the other hand, these cells do have the drawback of slight clonal variations between the different lines (Franco *et al.*, 2001), making it necessary to compare preferably different lines per genotype group. Most of the *in vitro* analyses published during the course of this work by other groups, did use various cellular systems where human or murine *Lrrk2* - either as wild-type or different mutated forms - are getting exogenously expressed. But this does not resemble the physiological situation in human PD patients and additionally several groups did observe cytotoxic effects induced by the overexpression of any *Lrrk2* form (Greggio *et al.*, 2006; MacLeod *et al.*, 2008; personal communication). Our model, in contrast, provides the opportunity to study the impact of *Lrrk2* mutations without artificial intrusions like transfections or viral infections avoiding the simultaneous expression of both endogenous and exogenous protein. In addition, MEF cells prepared from our *Lrrk2* knockdown mouse model have been extremely useful for the verification of various *Lrrk2* antibodies (see 5.1.3). The initial analysis of R1441C expressing MEF (mouse embryonic fibroblast) cells revealed no obvious changes, regarding morphology, cell cycle duration general viability and sensitivity to oxidative stress. This supports the idea of Santpere and Ferrer, that the cytotoxic effects of LRRK2 observed by different groups (Greggio *et al.*, 2006; Smith *et al.*, 2006; Iaccarino *et al.*, 2007) are simply caused by the massive and non-physiological overexpression of *Lrrk2* regardless to its endogenous role (Santpere and Ferrer, 2009). Next we put our focus on the cytoskeleton in these cells, since both sequence analysis as

well as preliminary *in vitro* results suggested a role for LRRK2 in the regulation of the cytoskeleton and axonal transport (Bosgraaf *et al.*, 2002; Dächsel *et al.*, 2007; Higashi *et al.*, 2007/1).

Although we could not detect clear manifestations of markedly altered cytoskeletal morphology or pharmacological stability, in *Lrrk2* R1441C derived MEF (mouse embryonic fibroblast). Nevertheless, the first hint for a raised level of acetylated tubulin resulted from this analysis. Immunocytochemistry (ICC) for different posttranslational modified microtubules (PTMs) in *Lrrk2* MEF cells revealed an increase in the amount of acetylated tubulin which could also be confirmed via Western blot analysis of crude cell lysates. Remarkably, no overt differences could be seen between heterozygote and homozygote R1441C MEF lines, which might be based on the truly dominant mechanism of pathological *Lrrk2* mutations. Besides these *in vitro* results, also *in vivo* a hyperacetylation of tubulin could be shown in protein lysate prepared from young wild-type and *Lrrk2* R1441C mouse brains. For narrowing down the site of interest, we prepared brain lysates from different brain regions (data not shown) and analysed them in the same way. None of the brain regions did show significantly more or less tubulin hyperacetylation compared to wild-type. Also immunohistochemistry (IHC) using an specific antibody directed against acetylated tubulin, did not reveal any significant hotspots in the adult mouse brain but rather a quite homogenous distribution (data not shown). Together with the original identification in the non-neuronal MEF cell lines, this would suggest that the observed tubulin hyperacetylation is not limited to a distinct region or cell type and could occur in every *Lrrk2* expressing cell.

Next, we were looking if this hyperacetylation has also an impact on distinct cellular processes like neurite outgrowth since the fundamental process of axonal and dendritic generation and elongation is dependent on a variety of mechanisms; amongst them the cytoskeleton and in particular the actin and tubulin network do play the central role (Bouquet and Nothias, 2007). Especially the dynamical stabilisation and destabilisation of microtubules has been shown to be crucial during this process (Baas *et al.*, 1993; Kurachi *et al.*, 1999). This is achieved primarily by a higher degree of posttranslational

modifications of the microtubular network during neurite outgrowth (Black *et al.*, 1980, Bulinski and Gundersen, 1991, Georges *et al.*, 2008).

Based on this, we did look in more detail onto the neurite outgrowth process *in vitro*. First of all, the expression of *Lrrk2* in primary hippocampal and cortical neurons had to be confirmed. We could detect *Lrrk2* mRNA from the first checked time point (DIV4) onwards by qualitative RT-PCR (data not shown). On the protein level, a gradual increase of LRRK2 protein could be observed from DIV4 till DIV20 by western blot in these cultures (Piccoli *et al.*, 2011). This is in line with the results of our expression analysis, suggesting the first prominent *Lrrk2* expression in the murine forebrain to show up during late embryogenesis and early postnatal stages.

No unambiguous significant difference could be detected between wild-type and both *Lrrk2* R1441C and *Lrrk2* knockdown neurons respectively, by analysing different parameters like number and length of primary as well as secondary and tertiary neurites. In addition, for the R1441C line also different days (1, 2 and 5) after cell preparation have been analysed for detecting also putative transient effects during the development of the neurite network. Due to this we found the mean number of secondary neurites in R1441C neurons to be markedly reduced at DIV5; unfortunately this result did not reach the level of significance due to an elevated degree of variation. This degree of variation could not be eliminated since we had to prepare single cultures from each embryo separately in contrast to the published data where mostly one single wild-type culture gets transfected or transduced with different constructs. Hence by our experimental set-up, the natural variation between single primary cultures from embryos of a mixed genetic background, outruns minor genotype-dependent differences. In case of the *Lrrk2* knockdown neurons, we could nevertheless show a tendency (Student's t-test: $p=0.06$) towards an increase in the number of secondary neurites. This result encouraged us to go one step further and to analyze the dendritic branches of neurons in the basal ganglia circuit in adult knockdown animals. Therefore we performed the classical Golgi-Staining with which randomly entire single neurons are getting stained. We decided to analyse the medium-size spiny neurons (MSNs) of the striatum, based on following reasons. On the one side, this target area of nigrostriatal dopaminergic innervation shows the highest

level of Lrrk2 mRNA in the basal ganglia circuit. On the other side, this population is highly homogenous since about 95% of all neurons in the striatum are MSNs making the analysis more straightforward. We observed tendencies towards a general increase in neurite length and towards an increasing numbers of higher order neurites. Unfortunately, despite high sample sizes, like in the *in vitro* study these alterations failed to reach significance. Nevertheless it is remarkable, that both *in vitro* in primary hippocampal neurons, as well as *in vivo* in MSNs of the striatum, a similar trend can be observed.

In total our results are in line with published data: it has been proposed for example by MacLeod and colleagues, that the expression of pathologically mutated LRRK2 decreases, whereas the knockdown of LRRK2 increases the complexity of the neurite network; at least a tendency towards this direction could be observed also in our *ex vivo* system. Strikingly, the effects of pathogenic mutations in the kinase domain like G2019S have been shown to be far more drastically compared to the slight reduction in R1441C overexpressing neurons (MacLeod *et al.*, 2006). Subsequent publications therefore exclusively used the G2019S mutation to demonstrate neurite outgrowth deficits (Plowey *et al.*, 2008; Sämann *et al.*, 2009; Dächsel *et al.*, 2010). The instance, that we did only see subtle changes may be explained not only by the fact that we did express murine LRRK2 on an endogenous level instead of transducing and overexpressing human LRRK2, but also by the use of different species (*Rattus norvegicus* versus *Mus musculus*) as a source for the preparation of primary neurons. Supposing that altered intracellular transport is at least partially causative for the slight alterations observed, one could as well speculate that the pathologically mutated LRRK2 slows down the intracellular transport but is in turn nearly completely compensated by tubulin hyperacetylation mediated transport acceleration (Reed *et al.*, 2006). On the other side, if the knockdown of LRRK2 slightly accelerates this process, this could favour the formation of a more complex neurite network and explain why we see more pronounced alterations in the knockdown situation. Since the speed of intracellular transport has to increase with the length of an axon (Miller and Samuels, 1997), in our *ex vivo* approach, genotype differences would be more pronounced in older cultures with

already long but still elongating neurites. Altogether, LRRK2 seems to be – directly or indirectly - involved in the mechanism of neurite outgrowth, but its concrete role remains elusive.

Following that line, since microtubules have already been identified as a direct LRRK2 binding partner (Gandhi *et al.*, 2008; Gillardon, 2009) we wondered whether the LRRK2 interaction is specific for acetylated tubulin. In collaboration with Giovanni Piccoli from the institute of human genetics of the Helmholtz Zentrum Munich we could show by GST pull-down assay that LRRK2 binds acetylated tubulin with high affinity. Binding levels of other posttranslational modified tubulins were extremely low which suggests a specific binding of LRRK2 only to acetylated tubulins or microtubules respectively. Next we wanted to investigate the process of tubulin acetylation and deacetylation in *Lrrk2* R1441C neurons and utilized again the *ex vivo* system of primary hippocampal neurons to do so. First of all we ensured that also in these cells, hyperacetylation can be observed in R1441C carriers. Following that, we focused on a possible molecular pathway by which LRRK2 is involved in tubulin acetylation. Unfortunately this process is poorly understood so far (Fukushima *et al.*, 2009); the enzyme, catalyzing the acetylation of microtubule is still unknown (for reviews see Perdiz *et al.*, 2011), also it has been speculated that the N-acetyltransferase complex ARD1-NAT1 might be a good candidate (Ohkawa *et al.*, 2008). In contrast, both HDAC6 (histone deacetylase 6) and SIRT2 (human Sir2 ortholog) have been shown to act as microtubule deacetylase (Hubbert *et al.*, 2003; North *et al.*, 2003). Based on their expression profiles in the rodent brain, HDAC6 seems to be more abundant in neurons, whereas SIRT2 can be found predominantly in glia cells (Southwood *et al.*, 2007). Nevertheless, also a cooperation of both proteins in the process of tubulin deacetylation is discussed (Nahas *et al.*, 2007). Of course also the role of SIRT2 is of high interest in regard to the observed phenotype. Unfortunately, highly specific inhibitors of the second known tubulin deacetylase SIRT2 like B2 or AKG2 (Outeiro *et al.*, 2007) were not commercially available; in ongoing experiments, nicotinamide (Green *et al.*, 2008) or a knockdown of SIRT2 by RNA interference are planned to be used. Hence, we utilized the HDAC6 inhibitor Trichostatin A (TSA) to see whether it is possible to further increase the level of acetylated tubulin (Brehm *et al.*,

1998). Interestingly, inhibition of HDAC6 in wild-type neurons elevated the amount of acetylated tubulin to a similar level as observed in untreated *Lrrk2* R1441C neurons. Nevertheless, TSA treatment of mutant neurons further increased the hyperacetylation of microtubule. From this one can conclude that the hyperacetylation is not caused by an inhibition of HDAC6 since in this case no further increase should have been observed. The relative increase upon treatment was comparable between both genotypes, suggesting that also partial inhibition of HDAC6 should not be the predominant molecular mechanism leading to hyperacetylated microtubule in *Lrrk2* R1441C neurons. In general, the mechanism by which dysfunctional or deregulated LRRK2 contributes to the acetylation of microtubule remains elusive. The demonstrated direct binding of protein to acetylated tubulin could physically inhibit its deacetylation. On the other side it has been shown that alpha-tubulin is specifically and exclusively acetylated at residue lysine in position 40, which is located in the inner lumen of microtubule (Nogales *et al.*, 1999). Together with the fact that acetylation occurs after tubulin polymerisation (Greer *et al.*, 1985), this suggests that deacetylation (and acetylation) is limited to the tips of microtubule where the lumen is accessible. Constant binding of a large scaffold protein like LRRK2 with its multiple binding sites and dimerisation capacity, seems not to be likely at that position. More reasonable would be a direct or indirect role for LRRK2 in the regulation of acetylation or deacetylation respectively. Interestingly, no acetylase or deacetylase has yet been identified to bind LRRK2 protein (personal communication) although both LRRK2 and HDAC6 have been identified as components of Lewy bodies (Kawaguchi *et al.*, 2003). It has been reported, that *in vitro* overexpression of tau inhibits HDAC6 function leading to an increase in acetylated tubulin and a decrease of proteasome-induced autophagy (Perez *et al.*, 2009). HDAC6 deficient mice exhibit elevated levels of acetylated microtubule, but interestingly do not show any other overt phenotype and also no changes in basal microtubule stability. From this the authors concluded, that the effects of tubulin hyperacetylation can be compensated on mice kept under standard laboratory conditions (Zhang *et al.*, 2008). Furthermore, acetylation of microtubules increases the recruitment of kinesin-1 and enhances the anterograde transport of JIP1 (JNK-interacting protein 1) in neurons (Reed *et al.*, 2006).

Strikingly in Huntington's disease (HD), the inhibition of HDAC6 by TSA can compensate for deficits in axonal transport (Dompierre *et al.*, 2007).

For the second tubulin deacetylase SIRT2 no knockout mouse model has been published, but the inhibition of SIRT2 in both a cell culture and a *Drosophila* PD model can rescue the toxic effects of alpha-synuclein overexpression (Outeiro *et al.*, 2007). It is discussed that inhibition of SIRT2 can induce the formation of few large alpha-synuclein inclusion bodies instead of many small ones (Garske *et al.*, 2007). Also in slow Wallerian degeneration mice SIRT2-mediated tubulin deacetylation is involved in both microtubule hyperacetylation and resistance to axonal degeneration (Suzuki and Koike, 2007). Interestingly, most recent Min and colleagues reported that in different tauopathies the acetylation of the microtubular binding protein tau inhibits its degradation and thereby can promote the formation of inclusions (Min *et al.*, 2010). Hence we are starting to analyse the acetylation state of other proteins than tubulin to see, whether we have a more general impairment of acetylation in our *Lrrk2* mouse models. Commonly, an imbalanced general homeostasis of protein acetylation seems to play a role in a variety of neurodegenerative diseases (Saha and Pahan, 2006), but the exact mechanisms are still unknown (Gan and Mucke, 2008).

In case of the microtubule, both HDAC6 and SIRT2 are regulating the stability of the network by microtubule acetylation and deacetylation (Matsuyama *et al.*, 2002; Suzuki and Koike, 2007) although the linkage between microtubular stability and acetylation is still not completely clarified. Depolarized microtubules have been shown to be selectively toxic for dopaminergic neurons (Ren *et al.*, 2005). The selectivity of Rotenone toxicity is based on the negative effect of Rotenone-induced microtubule disassembly onto transport mechanisms whereas Parkin can protect dopaminergic neurons by its ability to stabilize microtubules (Ren *et al.*, 2009).

An additional hint for the involvement of microtubular organisation in the aetiology of *Lrrk2*-linked PD came from the identification of the microtubule-associated protein STOP (Stable tubulin-only polypeptide) as a LRRK2 binding partner (Piccoli *et al.*, 2011). Based on this, we continued to look for subtle changes in the stability of the microtubular network in R1441C mice despite of the negative results obtained from general drug stability or neurite

outgrowth assays. Binding of STOP protein to microtubules mediates not only drug-resistance but also cold-stability in addition to their detyrosination (Bosc *et al.*, 1996; Guillaud *et al.*, 1998; Baratier *et al.*, 2005). Depolymerisation at low temperature is a normal feature of most microtubules; only distinct population exhibit a stronger resistance. This seems to have nothing to do with the need of the cell for cold-stable microtubule per se; nevertheless this physical feature can be used as a marker for specific subgroups of microtubule stabilized by certain factors like STOP proteins (Wallin and Strömberg, 1995). Under basal conditions, we could not detect any differences in regard to expression levels, pattern and subcellular localisation of STOP, neither in primary neuronal cultures nor in the brain of R1441C animals. In STOP knockout mice, cold stability of the microtubules is suppressed, leading to the complete loss of the microtubular network in primary neurons after cold treatment (0°C) (Andrieux *et al.*, 2002). We never observed similar drastic effects in R1441C primary neuronal cultures. Therefore it was necessary to determine the relative loss of unstable microtubules represented by tyrosine tubulin compared to acetylated tubulin. Thereby we could detect significantly less unstable microtubules in *Lrrk2* R1441C neurons, but only after 3hrs of cold treatment. This result could indicate that under physiological conditions, minor changes in cytoskeletal organisation can easily be compensated, but not longer under the harsh conditions of extended cold treatment. In future, to further elucidate that question, preparations of polymeric microtubules from mutant and wild-type cells or mice could be used to determine their physical properties. Since mouse models with more drastic alterations of the microtubular network like the HDAC6 or STOP knockout mice, did not exhibit any changes in the basal stability of microtubules, it is highly likely that subtle alterations like the hyperacetylation of tubulin in the *Lrrk2* R1441C knock-in mouse can be compensated just as well.

However, STOP knockout mice despite not having detectable defects in brain anatomy they do show clear-cut synaptic defects like impaired plasticity accompanied with depleted synaptic vesicle pools (Andrieux *et al.*, 2002). Interestingly also specific alterations in the dopaminergic system, like an increase in evoked dopamine release, can be observed in STOP deficient

mice (Brun *et al.*, 2005). Together with the identification of NSF as a binding partner for LRRK2 (Piccoli *et al.*, 2011), this advised us to look closer also for a putative role of LRRK2 in the mechanisms of synaptic transmission. The N-ethylmaleimide-sensitive fusion protein (NSF) as one of the most important members of the SNARE (SNAP-REceptor) complexes is heavily involved in various events where vesicles have to fuse with target membranes (Zhao *et al.*, 2007). Hence in neurons, it is predominantly located in the pre-synapse to regulate and execute the release of neurotransmitter (Söllner and Rothman, 1994), but also a role in autophagosome fusion during autophagy events are known (Ishihara *et al.*, 2001). IHC in adult mouse brain (data not shown) or ICC of primary neurons prepared from *Lrrk2* R1441C mice did not reveal any changes. So we utilized the technique of subcellular fractionation (Villasana *et al.*, 2006; Dosemeci *et al.*, 2006) to pin-point the colocalisation with LRRK2 with NSF in the synaptosomal fraction of wild-type brain lysates. This colocalisation with NSF is reasonable, since the association of LRRK2 with lipids or lipid-associated proteins has been already reported (Biskup *et al.*, 2006; Hatano *et al.*, 2007). During the course of these experiments, Shin and colleagues published related results, by showing the interaction and colocalisation of LRRK2 with Rab5b in synaptosomal fractions (Shin *et al.*, 2008). Although the comparison of different fractions from wild-type and R1441C mice did exhibit differences in the distribution of NSF, we can not conclude any genotype effect since these results did show a high variation between different samples. For the future, higher sample sizes are recommendable since the used method of differential centrifugation implies certain technical-based variations between different samples. Nevertheless, this technique provided an additional hint for a possible functional interaction of LRRK2 with NSF.

The fact that for the first time during this work, the function of an LRRK2 interactor was well described, allowed us to look for changes of a distinct cellular mechanism in the *Lrrk2* R1441C mouse line. We have put our main focus on the well described role of NSF in controlling and executing vesicle fusion with target membranes (Zhao *et al.*, 2007). Therefore we established and utilized an assay for quantifying exocytosis and endocytosis events of synaptic vesicles based on several reasons. On the one side our primary

hippocampal neurons prepared from *Lrrk2* R1441C knock-in gives us the opportunity to study this mechanism in the living cell, which implies a higher relevance to the *in vivo* situation. Next, the process of synaptic vesicle release marks one of the ultimate events in the information processing of a neuron which is dependent on a variety of upstream events. Last but not least, it is known for a couple of PD rodent models like for example in *Parkin*-deficient mice (Kitada *et al.*, 2009), that impairments in dopamine release can only be observed if the system is evoked or challenged. In this regard, this *ex vivo* system combines the advantages of easy accessibility of *in vitro* systems with a higher physiological relevance to the *in vivo* situation. We used and adapted a published protocol from Matteoli and colleagues based on the specific binding of antibodies to the inner lumen of fused vesicles (Matteoli *et al.*, 1992; Mundigl *et al.*, 1993). The tests revealed that within the 4 minutes of the assay 32% of all detected synaptic vesicles underwent an exo-endocytosis cycle in wild-type cells, which is basically in the expected range known from literature (Bacci *et al.*, 2001), indicating the correct progress of the assay. The rate of 34.5% observed for *Lrrk2* R1441C knock-in neurons was nearly identical. Like indicated before, we put our main emphasis for detecting significant impairments not onto the basal level, but onto the evoked activity of these cells. We could indeed detect a clear increase of exo-/endocytosis events in wild-type cells depolarized by high amounts of potassium, nevertheless only a slight and nosignificant additional increase could be observed in R1441C knock-in neurons. In parallel, we performed the very same assay together with our collaborators in neurons, where LRRK2 gets acutely knocked down by lentiviral-delivered short hairpin RNA interference (Bauer *et al.*, 2009). Utilizing the same primary neurons and experimental setup, they could detect a significant increase in exo-/endocytosis events both in basal as well as in evoked conditions (Piccoli *et al.*, 2011). At the same time Shin and colleagues published very similar results. Also in their system, the acute knockdown of LRRK2 revealed increased rates of exocytosis. But in addition, the overexpression of both wild-type or pathogenic forms of LRRK2 did influence the rate of endocytosis (Shin *et al.*, 2008). Strikingly, when we used primary hippocampal neurons from both wild-type and *Lrrk2* knockdown embryos (*ex vivo*), we could not detect any significant differences in both

basal as well as in evoked conditions (**Fig.36**). The technical difference between the two systems of course is obvious. The acute approach is based on the differential treatment of a single culture. By contrast, in case of the *ex vivo* approach, several cultures derived from single embryos of one litter had to be prepared and analysed. Thereby we included an additional and maybe considerable source of variation. Nevertheless, first of all biological factors have to be taken into account. In case of the observed differences between our R1441C knock-in neurons and the overexpression experiments published by Shin and colleagues, one has to keep in mind that both wild-type and mutated LRRK2 did influence the level of endocytosis. In contrast to the published model with its ten- to fifteen-fold overexpression of LRRK2 protein, in our system we study the effects of pathogenic point mutations on the endogenous level. Since a whole bunch of publications did report a cytotoxic effect in case of LRRK2 overexpression, these results have to be taken with care. Our finding, that only the acute knockdown of LRRK2 significantly increases the exo-/endocytosis rate could be taken as a further hint, that compensatory mechanisms play a pivotal role.

Interestingly, the further analysis of acutely LRRK2 deprived neurons revealed not only alterations in evoked postsynaptic currents accompanied by a redistribution of synaptic vesicles, but also enhanced kinetics of these vesicles due to acute *Lrrk2* silencing (Piccoli *et al.*, 2011). The enhanced motility of the vesicles could be perfectly in line with a general enhanced intracellular trafficking as we already discussed earlier. Together this data indicates that LRRK2 is involved in the mechanisms of synaptic vesicle exo-/endocytosis but endogenous levels of pathogenic LRRK2 is not sufficient to imbalance the system under basal conditions. For future experiments it might be crucial to find a suitable modifier or stressor to tease out putative subtle impairments.

6.4 Dopaminergic system, histological analysis

To cope with the progressive and age-related characteristic of PD, at least three groups of different age have been used for histological analysis. The analysis of young *Lrrk2* R1441C knock-in animals was performed to exclude

developmental alterations and like expected, no overt alterations in the general setup of the central nervous system could be detected. Not only the dopaminergic but also the serotonergic system has been studied in detail in this group and both did not show overt changes. For the dopaminergic system, which is naturally in the central focus in this mouse model, this analysis is essential. The 'multiple hit theory', which claims that the combination of multiple factors like low-penetrance mutations, environmental insults or stress are only in combination responsible for the final outbreak of the disease (Carvey *et al.*, 2006; Sulzer, 2007). Following that, also marginal developmental depletion of TH-positive neurons could be already the first hit. Nevertheless, for the *Lrrk2* R1441C knock-in line, this has to be neglected.

Due to the diagnosed changes in regard to anxiety-related behaviour in young animals, we also took a deeper look onto the serotonergic system. It has been shown, that developmental changes in the serotonergic innervation of cortex and hippocampus are sufficient to cause perturbations in anxiety (Briley *et al.*, 1990; Lucki, 1998; Ramboz *et al.*, 1998; Hohmann *et al.*, 2007) and that during development the dopaminergic and the serotonergic system compete for the innervation of functional territories (Cunningham *et al.*, 2005) in these regions. Therefore we did not only look for the prominent serotonergic nuclei like the raphe nuclei, but also for their projections and innervation of the cortex. Both, the serotonergic neurons itself and their projections into the cortex did not exhibit alterations between wild-type and R1441C knock-in mice. Nevertheless, to exclude also subtle differences not only in the innervation but also in the release of different neurotransmitter, HPLC analysis or even *in vivo* micro-dialysis should be used. This could be a promising approach especially in aged animals. Several genetic PD rodent models, like for example *Parkin* knockout mice (Goldberg *et al.*, 2003), do not show dopaminergic cell loss but alterations in the evoked release of dopamine or other neurotransmitter.

Animals with an age of 24 month have been analysed for the dopaminergic marker TH both for the total level of expression and as well as for the pattern of TH-positive fibres in the adult brain. The data suggests no significant alterations in the amount of dopaminergic innervation of the striatum. Also the TH-positive neurons in both midbrain and olfactory bulb are not depleted in

fully aged *Lrrk2* R1441C knock-in mice. In case of the dopaminergic nerve terminals the data obtained from patients is puzzling: stable amounts, reductions and even increases of the dopaminergic innervation has been reported (Porritt *et al.*, 2005; Chou *et al.*, 2008). Potentially, the stage of the disease plays a critical role. If we look in general onto published results from other genetic PD rodent models, one could expect only minor changes in the amount of dopaminergic cells and neurites at the most. Only for one alpha-synuclein overexpressing mouse line, small albeit robust depletion of midbrain dopaminergic neurons have been reported (Masliah *et al.*, 2000), whereas other models based on *DJ-1*, *PINK1* or *Parkin* do show slightest till no reduction of TH-positive neurons. Massive cell loss, accompanied by severe motor defects can only be observed either in toxin-induced lesion models using 6-OHDA, MPTP and Rotenone, or in genetic models based on genes involved in the development and maintenance of dopaminergic neurons like the *Pitx3* aphakia mouse (Hwang *et al.*, 2003) or the (*En1*^{+/-}; *En2*^{-/-}) mice (Terzioglu and Galter, 2008). But at least *Pitx3*-based mouse models do have the drawback, that the observed cell loss is neither age-dependent, nor slowly progressing.

The histological analysis could also not identify some of the typical inclusion bodies known from PD patients like Lewy bodies (LBs), Lewy neurites (LNs) and neurofibrillary tangles (NFT) or Tau-pathology in *Lrrk2* R1441C knock-in mice up to 24. Once again, these results are very much in line with published results from other rodent PD models. Only for BAC transgenic mouse overexpressing high levels of mutated LRRK2, two groups recently described a hyperphosphorylation of Tau and identified neurites positive for the antibody AT8 directed against pathologically folded forms of human Tau protein (Li Y. *et al.*, 2009; Melrose *et al.*, 2010). In case of Lewy body-pathology, amongst the other PARK-gene models, only in alpha-synuclein overexpressing mice, inclusion bodies with LB resemblance can be found. In contrast to dopaminergic cell death, toxin-induced lesion models completely fail to mimic this cardinal pathological feature of PD.

Another related finding from PD patients is the upregulation of alpha-synuclein in dopaminergic neurons of the Substantia nigra (Gründemann *et al.*, 2008). While performing IHC to identify alpha-synuclein positive inclusion bodies, no

obvious differences between wild-type and R1441C mice also referring to general level or pattern of expression could be detected. We confirmed this result on the mRNA level by performing ISH on aged wild-type and R1441C brain slices. Westerlund and colleagues even proposed a co-regulation of LRRK2 and alpha-synuclein due to their observation that *Lrrk2* mRNA is upregulated in an alpha-synuclein overexpressing mouse model (Westerlund *et al.*, 2008/2). Therefore we repeated the alpha-synuclein ISH on aged wild-type and *Lrrk2* knockdown brains, to check for a possible differential regulation of alpha-synuclein in a *Lrrk2*-depleted brain but did not observe any differences (data not shown). Together with the fact that also unchanged levels of *Lrrk2* mRNA have been reported in alpha-synuclein knockout mice (Westerlund *et al.*, 2008/2), a co-regulation of LRRK2 and alpha-synuclein seems not to be likely in mouse.

Taken together, our mouse model does not recapitulate the major pathological key-features of PD, but is thereby in line with findings from other *Lrrk2* mouse models. To trigger the formation of inclusion bodies, protein aggregates or considerable dopaminergic cell death, the expression of pathogenic LRRK2 protein on an endogenous level seems to be not sufficient (Tong *et al.*, 2009; Tong *et al.*, 2010). For this, a massive, unphysiological overexpression of pathological forms of LRRK2 is necessary (Li Y. *et al.*, 2009; Melrose *et al.*, 2010; Li. *et al.*, 2010). Also the loss of *Lrrk2* does not lead to PD pathology; further, LRRK2-depleted mice do not show enhanced sensitivity to a treatment with the PD-inducing toxin MPTP (Andres-Mateos *et al.*, 2009).

6.5 Behavioural analysis

The absence of a pathological manifestation of PD in our *Lrrk2* models might explain why the mice do not show obvious motor deficits or dysfunctions as it can be observed in patients. Nevertheless this is in agreement with a variety of published mouse models of PD (for reviews see Dawson *et al.*, 2010) and does not imply the absence of any other behavioural alteration.

But which symptoms we could expect to find in our *Lrrk2* PD models is in dependence of the situation in PD patients. There, neuropsychiatric manifestations of the disease are diagnosed for more than 70% of cases (Ring and

Serra-Mestres, 2002). Amongst them, depression or bipolar disorders are the most frequent indications occurring in about 50% of all PD patients and is often accompanied with anxiety disorders. The underlying mechanism leading to depressive symptoms in PD patients is not yet clear. From the physiological point of view, disturbances not only of the dopaminergic but also of the serotonergic and noradrenergic system have been taken into account (Taylor TN *et al.*, 2009). On the other side of course also the diagnosis of a severe and disabling chronic illness like PD itself, can contribute to this manifestation of the disease. Similar to depression, also the symptoms of anxiety disorders observed in PD patients have been mechanistically linked to impairments of the serotonergic and noradrenergic neurotransmitter system. In addition, also disturbances in global cognitive performance have been correlated with depressive symptoms in PD (Fernandez *et al.*, 2009). Apart from these neuropsychiatric manifestations, also the cognitive and motor symptoms like tremor at rest, rigidity of the skeletal muscles, bradykinesia and postural instability have to be taken into account (Shulman *et al.*, 1996; Bloem *et al.*, 2001; Berardelli *et al.*, 2001). Based on this, seven different behavioural tests have been chosen for our PD test battery. Deficits in the cognitive function were analysed by the odour preference test and by aspects of the odour discrimination test, social discrimination and object recognition test. Open field, tail suspension and the forced swimming test were utilized to address the depression- and anxiety-related behaviour. The open field test and the accelerating rotarod have been used to address subtle motor impairments. Our behavioural test battery accommodates PD being a complex disease and set-ups of this kind are getting more and more the minimum requirement for a thorough behavioural characterization of PD mouse models (for reviews see Taylor TN *et al.*, 2010).

As mentioned before, we did not see overt motor impairments in young LRRK2 knockdown and R1441C animals. The rotarod test, focusing on the coordination and synchronisation of both fore and hind limbs did not reveal an initial motor phenotype in both lines. The only significant difference could be detected in male *Lrrk2* knockdown mice during trial 2 (**Fig.44**), but was rather caused by a remarkable increased performance of the wild-type litter-mates if compared to all other trials or gender groups. Accordingly, values for latency

to fall from the rotarod did match to knockdown levels in trial 3 again. Since increased body weight does have a negative impact in this test, we have to be aware that R1441C animals are slightly heavier than their wild-type littermates. Significant reduction in rotarod performances has been observed in at least some PD models like in overexpressors of human Y39C alpha-synuclein, in VMAT-2 deficient mice and in 6-OHDA lesion models (Field *et al.*, 2006). The earliest manifestation of this motor impairment could be detected in at least 15 month old transgenic animals (Colebrooke *et al.*, 2006; Zhou *et al.*, 2008), therefore it was not surprising for us, to detect only minor till no changes in the young *Lrrk2* cohorts.

In the open field test paradigm, the total distance each mouse travels in the arena regardless to the localisation can be taken as readout for locomotion activity. The only tendency of reduced locomotor activity was found for female R1441C mice in the periphery of the open field. Various other genetic rodent models do exhibit reduced locomotor activity, but only when the animals were challenged by drugs like amphetamine (Goldberg *et al.*, 2005); dopamine receptor D2 knockout mice do exhibit hypokinesia also under basal conditions (Baik *et al.*, 1995). Therefore it should be considered for the future to test the general locomotion of both *Lrrk2* lines in mice after specific pharmacological stimulation.

In general cognitive functions, in short-term and social memory, neither of the two *Lrrk2* mouse lines did show distinct impairments. With object recognition and social discrimination, two independent tests have been used, which differ in regard to the used objects. Nevertheless, both lines do not show any difficulties to memorize and discriminate between objects or social partners (**Fig.45** and **Fig.46**). Only for two other rodent PD models, memory and cognitive function deficits have been reported: for the *Pitx3* deficient aphakia mouse (Ardayfio *et al.*, 2008) and for a 6-OHDA lesion model (De Leonibus *et al.*, 2007).

While young *Lrrk2* knockdown mice show a significant decrease in both depression-like behaviour as well as anxiety, young R1441C mice do exhibit only a significant reduction in depression-like behaviour. We used the forced swim test and tail suspension test, which comprise the most commonly used assays in this regard (Trullas *et al.*, 1989; Cryan *et al.*, 2005). The *Lrrk2*

knockdown animals did not show any significant changes in the forced swim test, whereas *Lrrk2* R1441C mice do spent significantly more time with swimming and less time with floating. This result reached the level of significance only for female mice. The second test, the tail suspension test confirmed this finding - at least in females - of a reduced depression-like behaviour in young R1441C animals. In this test, also *Lrrk2* knockdown animals exhibit a significant decrease of depression-like behaviour. Using the natural avoidance of the centre in the open field test, we could also show a decrease of anxiety related behaviour in knockdown males, which supports the finding that both lines do show analogue behavioural changes. Naturally it was surprising to see, that these alterations indicate a reduction of depression and anxiety-like behaviour and not an increase, as it could be observed in patients. Comparison with other murine PD models is difficult in this regard, since only for two models, changes in the depressive-like behaviour have been reported; on the one side mice with a heterozygote deletion of *Engrailed1*, a homeobox transcription factor involved in development and maintenance of dopaminergic neurons (Wurst *et al.*, 1994; Sonnier *et al.*, 2007), on the other side a 6-OHDA lesion mouse, modelling premotor stages of PD (Tadaiesky *et al.*, 2008). Both models do show, according to the situation in humans, an increase of depressive-like behaviour using the forced swim test. On the other side, since they are predominately used to test the effects of antidepressants, one has to keep in mind, that the relevance of these tests for basal conditions is still discussed (Cryan and Slattery, 2007; Bessa *et al.*, 2009). One possibility for the future would be to treat our animals with certain antidepressants and to look for impairments in the reaction upon these drugs. In addition also the data of aged *Lrrk2* knockdown and R1441C animals might be useful to clarify these discrepancies between the human and rodent situation. It could be speculated, that putative impairments can be compensated or even overcompensated in young animals.

Both, *Lrrk2* R1441C and knockdown animals did show significant reductions in olfaction skills at an age between 24 and 27 month and both, the ability to discriminate between binary mixtures and the maximal sensitivity for a certain odour is diminished. While *Lrrk2* R1441C mice have depicted already a distinct 4- to 8-fold decrease in olfactory sensitivity compared to wild-type

littermates, the *Lrrk2* knockdown animals did perform even worse. Unfortunately in case of the *Lrrk2* R1441C line, both genders had to be pooled due to the lack of enough wild-type females. Therefore only for the knockdown line sex-differences became evident suggesting in general a better performance of aged females of both genotypes; this finding is in line with the situation in humans where the general performance is higher in women and also their normal age-dependent depletion does start later compared to men (Fernandez *et al.*, 2009). The question arises, if this observed phenotype is age-related in one or both lines. Unfortunately, young cohorts of both lines have been tested only for general olfaction (data not shown) where they did perform comparable to wild-type. But of course, this was just a qualitative and no quantitative test to exclude anosmia and also old *Lrrk2* R1441C and knockdown mice can smell, albeit to a lesser extent (hyposmia). Since the absolute social discrimination test is highly dependent also from the olfaction skill of the tested animals and both lines did not show significant impairments, it could be speculated that this phenotype of *Lrrk2* mouse models is indeed age-dependent. To definitively answer that question, it is essential to repeat this elaborated olfaction test battery in young and mid-aged animals. Similar olfactory deficits were reported for a PD mouse model where alpha-synuclein is getting overexpressed pan-neuronal under the Thy-1 promoter. Also alpha-synuclein inclusions have been identified in the olfactory bulb of these mice (Fleming *et al.*, 2008). In addition, dopamine receptor D2, as well as dopamine transporter knockout mice do exhibit a comparable hyposmia (Tillerson *et al.*, 2006). But what might be the underlying mechanism, leading to this olfaction phenotype? Data from PD patients is puzzling; a pure neurodegenerative mechanism seems not to be highly likely since also increasing numbers of dopaminergic neurons in the post-mortem olfactory bulb have been reported (Huisman *et al.*, 2004). On the other hand, the olfactory bulb has been reported to be one of the first regions to depict pathological features of PD (Braak *et al.*, 2006). But even in the above mentioned murine alpha-synuclein model, olfaction deficits occur before dopaminergic cell loss and motor impairments can be observed (Fleming *et al.*, 2008). The simple loss of the dopaminergic system seems not to be a sufficient explanation. Accordingly, the analysis of TH positive neurons in the olfactory bulb of the

Lrrk2 R1441C did not reveal overt differences (data not shown). Our own focus in regard to this phenotype is also directed onto a putative role of impaired adult neurogenesis which has been linked to olfactory function and learning. A subset of neurons within the olfactory bulb, regular undergoes apoptosis and are getting replaced by newly generated cells (Petreanu and Alvarez-Buylla, 2002). Therefore we started to study the adult neurogenesis in both *Lrrk2* mouse lines. Further on, also the olfactory epithelium, harbouring the receptor cells, could be affected. It is known that olfactory receptor neurons do express the dopamine receptor D2 and that dopamine depresses the synaptic inputs into the olfactory bulb (Hsia *et al.*, 1999). This would imply that either impairments in the release of dopamine or an increase of the total number of dopaminergic neurons in the olfactory bulb might be responsible for the hyposmia. But also completely different mechanisms might be involved. Interestingly, the receptors of olfactory epithel neurons are clustered in special organelles referred to as primary cilia (McEwen *et al.*, 2009). These cilia are characterized by a classical 9+2 composition of microtubules in the axoneme and show a high degree of acetylated tubulin enrichment (Wang and Brautigan, 2008). Disturbances in the composition of these cilia have been linked to various forms of olfactory dysfunction (Jenkins *et al.*, 2009). But if LRRK2 - directly or indirectly - might interfere with the cilia function in olfactory epithel neurons has to be clarified. Last but not least, the *olfactory vector hypothesis* has to be mentioned: according to this theory, neurodegenerative diseases are caused by the incorporation of xenobiotics via the olfactory mucosa (Doty, 2008). But if PARK genes like *Lrrk2* can increase the susceptibility for this mechanism seems not to be likely. Altogether, the observed reduced olfactory performance does recapitulate nicely one of the pre-motor symptoms known from PD patients. Interestingly a recent study did confirm olfactory deficits (Schweitzer *et al.*, unpublished data) in the very same family where the pathogenic *Lrrk2* mutation R1441C has been originally identified. Last but not least, the gait analysis could also detect subtle motor alterations in aged *Lrrk2* R1441C knock-in as well as knockdown mice. As observed in several other tests, both lines did show comparable changes in similar if not identical parameters like the cruciate step sequence pattern and the inter paw coordination; additionally in *Lrrk2* knockdown animals, also a print length

reduction could be observed. The automated *CatWalk*TM gait analysis provides a convenient tool for analysing numerous aspects of this complex behaviour and is sensitive enough to detect also subtle changes. Interestingly, it has been shown that alternative methods of movement analysis, like for example the treadmill gait analysis, fail to detect presymptomatic motor impairments in genetic as well as toxin-induced mouse models of neurodegenerative disorders (Guillot *et al.*, 2008).

In PD patients, severe gait disturbances are one of the major hallmarks. On the other side, gait changes in the initial phase of the disease are less pronounced and also less well studied. Nevertheless, inconsistency timing of gait, reduced swing times and increased left/right swing asymmetry could be identified in early PD (Baltadjieva *et al.*, 2006). This suggests, that slight gait pattern alterations appear early in the presymptomatic phase of the disease (Hausdorff *et al.*, 1998). Naturally it is not easy to compare the bipedal locomotion of human patients with quadrupedal rodents, but strikingly also our mouse models did show distinct gait pattern alterations. In both lines, the most striking changes is a significant decreased percentage of the cruciate step sequence pattern (RF-LF-RH-LH). The same holds true for the *Lrrk2* knockdown animals; additionally they do show a slight but highly significant reduction of the percentage in which the animals do show any step sequence pattern known as the regulatory index (Hamers *et al.*, 2006). Wild-type rodents prefer the regular step pattern (LF-RH-RF-LH) and use this pattern in about 80% of cases (Cheng *et al.*, 2006). Therefore we can conclude, that old *Lrrk2* R1441C knock-in mice do not exhibit a severe gait phenotype, but start to avoid more rare step sequence patterns like the cruciate pattern. The knockdown animals show a similar, nevertheless slightly more severe gait phenotype, since also their regulatory index is diminished. Interestingly, the avoidance of the cruciate step sequence pattern seen in both lines has also been reported for a 6-OHDA rat lesion model (Vlamings *et al.*, 2007). Of course the overall gait alterations are not as pronounced compared with toxin-induced lesion models of PD where they are caused by a massive loss of dopaminergic neurons (Amende *et al.*, 2005; Byler *et al.*, 2009). Therefore we could interpret the observed phenotypes as presymptomatic alterations independent from neurodegeneration but nevertheless associated to the

dopaminergic system. Strikingly, our conclusions have been corroborated by recent findings from human *LRRK2* G2019S carriers. Intriguingly, also asymptomatic mutation carriers exhibit alterations in several aspects of their gait under challenging conditions. This can be interpreted as an endophenotype of the *LRRK2* mutation or an early presymptomatic manifestation of PD which could also serve as a biomarker (Mirelman *et al.*, 2011). Genetically *Lrrk2* mouse models of early PD like the present ones could be extremely useful to clarify these questions.

6.6 Concluding remarks

The scope of the present study was to create a Parkinson's disease mouse model for further exploring the aetiology of PD and to get closer insights into the physiological roles of the *Lrrk2* gene in health and disease.

We started with the analysis of the murine expression pattern of both *Lrrk2* and its paralog *Lrrk1* in *Mus musculus*. By this we could show the first complete analysis of murine *Lrrk1* and *Lrrk2* mRNA expression covering numerous stages from ES cells, embryonic development till the postnatal and adult brain. We concluded that both genes may not play major roles in the overall development of the brain. Further, we could show for the first time that *Lrrk2* is highly expressed in both dopaminergic populations of the striatum and thereby possibly affecting both the direct and indirect pathway within the basal ganglia circuitry. The limited expression of *Lrrk1* in adult brain can explain for the first time, why no PD-associated mutations can be found and that redundant functions to its paralog *Lrrk2* in the adult brain have to be excluded. Next, we managed to insert the pathological mutation R1441C, observed in Parkinson's disease patients, into the murine *Lrrk2* gene, without influencing the endogenous expression pattern or level. The functional analysis could show, that LRRK2 is involved in cytoskeletal modification and stability, possibly also in neurite outgrowth, and definitely in synaptic transmission and vesicle trafficking. The detailed analysis of both the *Lrrk2* R1441C knock-in as well as the *Lrrk2* knockdown line revealed a variety of changes, predominately in functions and mechanisms related with non-motor symptoms observed in Parkinson's disease patients (**Fig.53**). Adequate to

		Lrrk2 R1441C	Lrrk2 knockdown
functional analysis	neurite outgrowth		
	<i>in vitro</i>	↓ (T)	↑ (T)
	<i>in vivo</i>	n.d.	↑ (T)
	microtubule		
	acetylation	↑ (*)	n.d.
	basal stability	→	n.d.
	cold stability	↓ (*)	n.d.
	exo-/ endocytosis		
	basal	→	→
evoked	→	→	
morphological analysis	dopaminergic neurodeg.		
	SNpc	→	→
	striatal innervation	→	→
	olfactory bulb	→	n.d.
	serotonergic neurodeg.	→	n.d.
	inclusion bodies	→	→
behaviour (young)	motor performance	→	→
	cognition and memory	→	→
	depression and anxiety	↓ (*)	↓ (*)
behaviour (aged)	olfaction	↓ (*)	↓ (*)
	gait analysis	↓ (*)	↓ (*)

Key:		
	→	not changed/detected
	↑ (T)	slightly increased
	↑ (*)	increased
	↓ (T)	slightly decreased
	↓ (*)	decreased
	n.d.	not determined

Figure 53: Schematic overview of the findings from the functional, morphological and behavioural analysis of both the *Lrrk2* R1441C as well as the *Lrrk2* knockdown mouse line.

these findings, both lines did exhibit neither any overt neurodegeneration, nor pathological hallmarks of PD like inclusion bodies in the morphological analysis. If we compare the results of the two lines, it is remarkable that on the functional level, altered LRRK2 function in the R1441C line rather leads to opposing effects compared to the loss of the protein (e.g. contradictory trends in the neurite outgrowth assay). But strikingly on the behavioural level both

lines performed in a similar manner and did show a very high overlap in regard to the identified phenotypes (e.g. depression- and anxiety-related behaviour or olfaction). This might indicate that LRRK2 dysfunction and loss of LRRK2 alters distinct cellular processes in a contrary way, but the general impairment of these processes results in a similar dysfunction on the behavioural level. Based on the multiple hit theory LRRK2 dysfunction does not exclusively affect dopaminergic survival, rather impairs distinct cellular mechanisms in a whole variety of neurons, of which dopaminergic neurons are most sensitive and therefore degenerate previous to all other, resulting in Parkinson's disease. This initial analysis of our two *Lrrk2* mouse lines provided us first hints what these mechanisms could be, but further studies are necessary to identify the definite role of LRRK2 in the aetiology of Parkinson's disease. Furthermore, both lines nicely mimic early, non-motor symptoms as observed in PD patients and can therefore be seen as valid mouse models of presymptomatic Parkinson's disease.

7 Materials and Methods

7.1 Materials

7.1.1 Chemicals

Chemical	Supplier
α - ³² P-dCTP	Amersham
β -Mercaptoethanol	Sigma, Gibco
[α -thio ³⁵ S]-UTP	Amersham
1 kb+ DNA Ladder	Invitrogen
3,3'-diaminobenzidine (DAB)	Sigma
acetic acid	Merck
acetic anhydride	Sigma
agarose (for gel electrophoresis)	Gibco Life Technologies, Biozym
ammonium acetate	Merck
ampicillin	Sigma
Ampuwa	Fresenius
antifade solution, Aqua Poly/Mount	Polysciences Inc.
ascorbic acid	Sigma
B-27 supplement	Gibco
bicine	Fluka
boric acid	Merck
bovine serum albumin (BSA, 20 mg/ml)	NEB, Sigma
bromphenol blue	Sigma
calcium chloride	Sigma
carrier DNA	Sigma
chlorobutanol	Sigma
Complete [®] Mini (protease inhibitors)	Roche
cresyl violet acetate	Sigma
Criterion [™] XT Bis-Tris-gels	BioRad
dextran sulphate	Sigma
dithiotreitol (DTT)	Roche
DMEM	Gibco
DMSO	Sigma

dNTP (100 mM dATP, dTTP, dCTP, dGTP)	MBI
EDTA	Sigma
EGTA	Sigma
Eosin Y	Sigma
ethanol absolute	Merck
ethidiumbromide	Fluka
ethylene glycol	Sigma
FastBlue B	Sigma
fetal calf serum (FCS)	PAN
Ficoll 400	Sigma
formamide	Sigma
gelatine	Sigma
glucose	Sigma
glycerol	Sigma
HBSS	Gibco
HEPES	Gibco
hydrochloric acid (HCl)	Merck
hydrogen peroxide, 30%	Sigma
isopropanol	Merck
kanamycin	Sigma
Lipofectamin™ 2000	Invitrogen
magnesium chloride (MgCl ₂ ·4H ₂ O)	Merck
Mannitol	Sigma
MEM nonessential aminoacids	Gibco
MES hydrate	Sigma
methanol	Merck
mineral oil	Sigma
MOPS	Sigma
Neurobasal medium	Gibco
Neurofect™, transfection agent	Invitrogen
Nonidet P40 (NP-40)	Fluka
normal goat serum (NGS)	Gibco
NuPAGE® Novex Bis-Tris gels, 10% (protein)	Invitrogen
Opti-MEM® I Reduced-Serum medium	Invitrogen
Orange G	Sigma
PBS (for cell culture)	Gibco
PIPES	Sigma

polyvinylpyrrolidone 40 (PVP 40)	Sigma
ponceau red	Sigma
potassium chloride (KCl)	Merck
potassium ferricyanide ($K_3Fe(CN)_6$)	Sigma
potassium ferrocyanide ($K_4Fe(CN)_6 \cdot 3H_2O$)	Sigma
potassium hydroxide (KOH)	Sigma
potassium phosphate ($KH_2PO_4 \cdot H_2O$, K_2HPO_4)	Roth
protease inhibitor	Roche
Quick Start Bradford Protein Assay	Bio-Rad
RapidHyb buffer	Amersham
RNaseZAP [®]	Sigma
Roti-HistoKit [®] II	Roth
Roti-Histol [®]	Roth
saccharose	Sigma
salmon sperm DNA	Fluka
SeeBlue [®] Plus2 Prestained protein ladder	Invitrogen
skim milk powder	BD Biosciences
SmartLadder DNA marker	Eurogentec
sodium acetate (NaOAc)	Merck, Sigma
sodium chloride (NaCl)	Merck
sodium citrate	Sigma
sodium desoxycholate	Sigma
sodium dodecylsulfate (SDS)	Merck
sodium hydroxide (NaOH)	Roth
sodium phosphate ($NaH_2PO_4 \cdot H_2O$, Na_2HPO_4)	Sigma
spermidin	Sigma
sucrose	Sigma
triethanolamine	Merck
TriReagent	Sigma
Tris (Trizma-Base)	Sigma
Triton X-100	Biorad
Trizol	Invitrogen
tRNA	Roche
trypsin	Gibco
tryptone	BD Biosciences
Tween 20	Sigma

7.1.2 Enzymes

Enzyme	Supplier
DNase I (RNase-free)	Roche
Klenow fragment of DNA Polymerase I	NEB
PCR-Mastermix 5x	Eppendorf, Rediprime
proteinase K	Roche
restriction enzymes	Roche, MBI, NEB
RNA polymerases (T3, T7, SP6)	Roche
RNase A	Serva
RNasin RNase inhibitor	Roche
T4 DNA ligase	NEB

7.1.3 Commercial kits

Kit	Company
DNA Maxi Prep Kit	Qiagen
DNA Mini Prep Kit	Qiagen
ECL Detection Kit	Amersham
FD Rapid GolgiStain™	FD Neurotechnologies
PCR Purification Kit	Qiagen, Promega
QIAquick Gel Extraction Kit	Qiagen
RediPrime DNA Labeling Kit	Amersham
RNeasy Mini Kit	Qiagen
RNeasy Midi Kit	Qiagen
SuperScript First-Strand Synthesis System for RTPCR	Invitrogen
TOPO-TA Cloning Kit	Invitrogen
Vectastain Elite ABC Kit	Vector Labs
Wizard PCR Purification Kit	Promega
Wizard Genomic DNA Purification Kit	Promega

7.1.4 Solutions

General solutions:	Composition:
loading buffer (5x) for agarose gels (DNA):	15% Ficoll 400 200 mM EDTA 1 - 2% orange G
loading buffer (10x) for MOPS agarose gels (RNA):	50% Glycerol 1 mM EDTA, pH 8.0 0.25% Bromphenole blue 0.25% Xylene cyanol FF in RNase free water
paraformaldehyde solution (PFA, 4%):	4% PFA w/v in PBS
PBS (1x):	171 mM NaCl 3.4 mM KCl 10 mM Na ₂ HPO ₄ 1.8 mM KH ₂ PO ₄ pH 7.4
SSC (saline sodium citrate, 20x):	3 M NaCl 0.3 M sodium citrate pH 7.0
sucrose solution	10% - 25% sucrose w/v in PBS
TAE (10x):	0.4 M Tris base 0.1 M acetate 0.01 M EDTA
TBE (10x):	0.89 M Tris base 0.89 M boric acid 0.02 M EDTA
TBS (10x):	0.25 M Tris-HCl pH 7.6 1.37 M NaCl
TBS-T (1x):	1 x TBS 0.05% Tween 20
TE (Tris-EDTA):	10 mM Tris-HCl pH 7.4 1 mM EDTA
Tris-HCl:	1 M Tris base pH 7.5

Solutions for cell culture work:	Composition:
----------------------------------	--------------

Dissection medium:	48,4 ml HBSS (Gibco) 500 µl HEPES (1M, Gibco) 600 µl MgSO ₄ (1M) 500 µl Penicillin/Streptomycin (100x) total volume 50ml
--------------------	---

Culture medium:	48 ml Neurobasal (Gibco) 1 ml B-27 (Gibco) 500 µl L-Glutamine 500 µl Penicillin/Streptomycin (100x) total volume 50ml
-----------------	---

ES cell medium:	10% FCS (PAN) 1x MEM nonessential aminoacids 0.1 mM β-mercaptoethanol 1500 u/ml LIF in DMEM
-----------------	---

feeder medium:	10% FCS in DMEM
----------------	--------------------

KCl solution	1 M KCl in H ₂ O, sterile filtered
--------------	--

freezing medium (2x):	50% FCS (PAN) 20% DMSO in DMEM
-----------------------	--------------------------------------

gelatin solution:	1% gelatin in H ₂ O
-------------------	-----------------------------------

Solutions for Southern blot analysis:	Composition:
---------------------------------------	--------------

Lysis buffer:	0.1 M Tris pH 8.5 5 mM EDTA 0.2% SDS 0.2 M NaCl 0.1 mg/ml Proteinase K
---------------	--

Church buffer:	0.5 M Na ₂ HPO ₄ 0.5 M NaH ₂ PO ₄ 1% BSA 7% SDS 1 mM EDTA pH 8.0 0.1 mg/ml salmon sperm DNA
----------------	--

Denaturation solution:	0.5 M NaOH 1.5 M NaCl
------------------------	--------------------------

Neutralizing solution:	0.1 M Tris-HCl pH 7.5 0.5 M NaCl
------------------------	-------------------------------------

Stripping solution:	0.4 M NaOH
---------------------	------------

Wash solution I, II, III:	2 x SSC, 0.5 x SSC, 0.1 x SSC, 0.1% SDS
---------------------------	--

Solutions for Western blot analysis: Composition:

Blocking solution milk:	4% skim milk powder in TBS-T
-------------------------	---------------------------------

Tris glycine blotting buffer (10x):	0.25 M Tris 1.92 M glycine
-------------------------------------	-------------------------------

Tris glycine blotting buffer (1x):	10% 10 x blotting buffer 10% methanol
------------------------------------	--

Laemmli buffer (5x):	313 mM Tris-HCl pH 6.8 50% glycerol 10% SDS 0.05% bromphenolblue 25% β -mercaptoethanol
----------------------	---

RIPA buffer:	50 mM Tris-HCl pH 7.4 1% NP-40 0.25% sodium desoxycholate 150 mM NaCl 1 mM EDTA 1 tablet protease inhibitor in 50 ml H ₂ O
--------------	---

NuPAGE transfer buffer (10x, for NuPAGE gels):	250 mM bicine 250 mM bis-tris 10 mM EDTA 0.05 mM chlorobutanol
--	---

NuPAGE transfer buffer (1x, for NuPAGE gels):	1 x transfer buffer 10% methanol
---	-------------------------------------

MOPS running buffer (10x, for Criterion gels):	500 mM MOPS 500 mM Tris 1% SDS 10 mM EDTA adjust to pH 7.7
--	--

10X MOPS:	0,2 M 3-Morpholinopropan-sulfonsäure 50 mM Natriumacetat 10 mM EDTA
-----------	---

MES running buffer (10x, for NuPAGE gels):	500 mM MES 500 mM Tris 1% SDS 10 mM EDTA adjust to pH 7.2
--	---

Solutions for <i>in situ</i> hybridisation: (radioactive and non-radioactive)	Composition:
chamber fluid	50% formamide 2x SSC
hybridisation mix	50% formamide 20 mM Tris-HCl, pH 8.0 300 mM NaCl 5 mM EDTA, pH 8.0 10% dextrane sulphate 0.02% Ficoll-400 0.02% PVP-40 0.02% BSA 0.5 mg/ml tRNA 0.2 mg/ml carrier DNA 20 mM DTT
NTE buffer (5x)	0.5 M NaCl 10 mM Tris-HCl, pH 8.0 5 mM EDTA, pH 8.0
proteinase K buffer	50 mM Tris-HCl, pH 7.6 5 mM EDTA pH 8.0
triethanolamine solution	0.1 M triethanolamine adjust to pH 8.0
ammonium acetate stock solution (10x):	3 M NH ₄ OAc
PK buffer (2x):	100 mM Tris 10 mM EDTA pH 8.0
PBT:	1 x PBS 0.05% Tween-20
5 x NTE:	2.5 M NaCl 50 mM Tris 8.0 25 mM EDTA
10 x TN:	1 M Tris 1.5 M NaCl Solve TN 1h at 60°C
TNT:	1 x TN 0.05 % Tween-20
TNB:	1 x TN 0.5 % Blocking reagent (NEN)
TMN (or MTN):	0,1 M Tris 0,1 M NaCl 0,05 M MgCl ₂ -6H ₂ O
Maleat buffer:	150 mM NaCl 100 mM Maleinsäure pH 7.5
cresylviolet staining solution (Nissl):	0.5% cresylviolet

2.5 mM sodium acetate
 0.31% acetic acid
 ad 500 ml H₂O
 filter before use

Solutions for Immunohistochemistry:	Composition:
Cryo-protection solution:	30% ethylene glycol 30% glycerol 0.1M PBS
PBS-T:	PBS 1% Tween-20
TBS-T:	TBS 1% Tween-20
Blocking solution:	10% fetal bovine serum in TBS-T
DAB stock solution:	1% DAB in Tris-HCl, pH 7.4

7.1.5 Instrumentation

Instrument	Company
autoclave	Aigner, type 667-1 ST
balances	Sartorius, LC6201S, LC220-S
hybridisation tubes	ThermoHybaid
cassettes for autoradiography	Amersham, Hypercassette
centrifuges	Sorvall, Evolution RC; Eppendorf, 5415D, 5417R; Heraeus, Varifuge 3.0R, Multifuge 3L-R
chambers for electrophoresis (DNA)	MWG Biotech; Peqlab
confocal microscope	Zeiss LSM 510
cryostat	Mikrom, HM560
developing machine	Agfa, Curix 60
digital camera	Zeiss, AxioCam MRc
DNA sequencer	Applied Biotech, DNA Analyzer 3730
freezer (-20°C)	Liebherr
freezer (-80°C)	Heraeus HFU 686 Basic
fridges (4°C)	Liebherr
gel- and blotting system "Criterion"	BioRad

gel- and blotting system "Xcell SureLock™ Mini-Cell"	Invitrogen
glass pipettes	Hirschmann
glassware	Schott
homogenizer	Ika, Ultra Turrax T25 basic
hybridisation ovens	Memmert, UM 400; MWG-Biotech, Mini 10; ThermoElectron, Shake'n'Stack
ice machine	Scotsman, AF 30
incubators (for bacteria)	New Brunswick Scientific, innova 4230
incubators (for cells)	Heraeus
laminar flow	Nunc Microflow 2
light source for microscopy	Leica KL 1500
liquid szintillation counter	Hidex, Triathler
luminometer	Berthold, Orion I
magnetic stirrer / heater	Heidolph, MR3001
microscope	Zeiss Axioplan 2
microwave oven	Sharp R-937 IN
Neubauer counting chamber	Brand
paraffin embedding machine	Leica, EG1160
PCR machine	Eppendorf, MasterCycler Gradient
pH-meter	InoLab, pH Level 1
photometer	Eppendorf, Biophotometer 6131
pipetteboy	Eppendorf, Easypet; Hirschmann, Pipettus akku
pipettes	Gilson; Eppendorf
power supplies for electrophoresis	Consort, E443; Pharmacia Biotech, EPS200; Thermo, EC250-90, EC3000-90
radiation monitor	Berthold, LB122
rotating rod apparatus	Bioseb, Letica LE 8200
shaker	Heidolph, Promax 2020
slide warmer	Adamas instrument, BV SW 85
sonifier	Branson sonifier, cell disrupter B15
stereo microscope	Zeiss, Stemi SV6
thermomixer	Eppendorf, comfort
ultramicrotom	Microm, HM 355S
UV-DNA/RNA-crosslinker	Scotlab, Crosslinker SL-8042; Stratagene, UV-Stratalinker 1800

UV-lamp	Benda, N-36
vortex	Scientific Industries, Vortex Genie 2
water bath	Lauda, ecoline RE 112; Leica, HI1210; Memmert, WB7
water conditioning system	Millipore, Milli-Q biocel

7.1.6 Antibodies

Antigen:	Species:	Company:
5-HT	rabbit (polyclonal)	ImmunoStar #20080
Acetylated-Tubulin	mouse (monoclonal)	Sigma T6793
alphaSynuclein	mouse (monoclonal)	abcam - ab1903
beta III tubulin	rabbit (polyclonal)	abcam - ab18207
Darpp32	rabbit (monoclonal)	abcam - ab40801
Dopamine D1 Receptor	rabbit (polyclonal)	Calbiochem 324390
Dopamine D2 Receptor	rabbit (polyclonal)	Chemicon - AB5084P
LRRK1 (C –terminal)	rabbit (polyclonal)	Abgent - AP7098a
LRRK1 (N-terminal)	rabbit (polyclonal)	Abgent - AP7098b
LRRK2	rabbit (polyclonal)	Novus NB300-267
pDarpp32 (Thr34)	rabbit (monoclonal)	Cell Signalling #2304
STOP	mouse (monoclonal)	Chemicon - MAB5524
Synaptophysin/P38	mouse (monoclonal)	Synaptic Systems (101011)
Synaptotagmin 1 (luminal)	rabbit (polyclonal)	Synaptic Systems (105102)
Tau (phospho T205)	rabbit (polyclonal)	abcam - ab4841
Tyrosin-Tubulin	mouse (monoclonal)	Sigma T9028

For further LRRK2-directed antibodies see: **5.1.3** and **Fig.15**. All secondary antibodies used in this work were obtained from *Jackson ImmunoResearch Laboratories*.

7.2 Methods

7.2.1 Methods in Molecular biology

7.2.1.1 General methods working with DNA

Sterile precipitation of plasmid DNA

To the digested plasmid DNA, 0.1 volume of a sterile 3M sodium acetate (NaOAc) solution was added to achieve a final NaOAc-concentration of 0.3M. After three times the volume of 100% Ethanol (EtOH) were added to the solution, the mixture was vortexed and incubated at -20°C for at least a couple of hours to precipitated the DNA quantitatively. The DNA was pelleted by centrifugation with 14.000 x g for 30 min. The pellet was washed with 70% EtOH, air dried in a laminar flow and solved in an appropriate amount of sterile H₂O.

Concentration measurement of nucleic acids

The concentration of aqueous nucleic acid solutions was determined photometrical by measuring the optic density (OD) at a wavelength of 260 nm. The OD of different, appropriate dilutions of a nucleic acid solution was measured utilizing a photometer. An OD₂₆₀ value of 1 corresponds to 50 µg/ml of double stranded or 37 µg/ml of single stranded DNA respectively. In case of RNA, an OD₂₆₀ of 1 corresponds to a concentration of 40 µg/ml (Sambrook *et al.* 1989).

Oligonucleotide primer

All oligonucleotide primer used in this work, were designed using the online tool *primer3* (Rozen and Skaletsky 2000). The oligonucleotides were either produced by Mr. Utz Linzner using the Applied Biosystems 394 DNA/RNA synthesizer[®], or obtained commercially by Sigma or MWG Biolabs. After delivery, the lympholized nucleotides were solved in an appropriate volume of sterile H₂O and diluted to a working-concentration of 10mM.

Isolation of genomic DNA

Cut mouse tail tips were incubated in lysis buffer for 4 hours till overnight at 55°C until they were completely digested. In case of DNA preparation from mouse embryos or cells, the tissue was put into lysis buffer and incubated for 3 hours at 55°C. Genomic DNA from cells and mouse tissue was isolated using Promega's Wizard genomic DNA purification kit following the manufacturer's instructions. The obtained pellet was resuspended in 25-250 µl H₂O or TE-buffer.

Restriction digests of DNA

For the restriction digests of plasmid-DNA and cDNA, reaction conditions, amount of enzyme and type of buffer were applied following manufacturer's instructions. Samples were digested for 2 hours till overnight at 37°C (unless other temperature was recommended for the enzyme). For each µg of DNA and for each restriction site in the plasmid 1 u of enzyme were used. For the digestion of genomic DNA a separate protocol was used (see 7.2.1.5).

Gel electrophoresis of DNA fragments

Separation of DNA fragments according to their size was performed via gel electrophoresis. For this, DNA samples were run on agarose gels at a concentration of 0.8 to 2 % in TAE buffer and stained by adding ethidium bromide to the gel. Samples were loaded onto the gel after mixing them with 5x loading buffer; the 1kb+ ladder[®] or the Smart Ladder[®] were used as length standard and a voltage of 80- 120 V was applied for 30 min to several hours depending on the sizes of the DNA fragments to be separated. Pictures of the gels were taken on a UV desk with short wave UV radiation at 254 nm and photographed using a gel documentation system.

Isolation of DNA fragments from agarose gels

DNA fragments of a specific size were isolated from agarose gels by visualizing the bands on a long wave UV radiation (366 nm) device to prevent damage of the DNA. The band of interest was then cut out with a clean scalpel as precise as possible. The purification of the DNA was performed using the Qiagen Gel Extraction Kit following manufacturer's instructions.

7.2.1.2 General methods working with RNA

Working with RNA requires special care to avoid the rapid degradation by RNases. Glassware was baked at 200°C for 2 hours; instruments were incubated in concentrated NaOH or RNaseZAP[®] and subsequently washed with fresh MilliQ water.

RNA extraction from cells and tissues

Cells were trypsinised and pelleted by centrifugation. Mice were asphyxiated with CO₂, decapitated, and the brain was dissected removing bones and meninges. The whole brain or dissected parts of it were immediately frozen on dry ice or liquid nitrogen to prevent degradation of RNA. Tissue was processed directly or stored at -80°C. Disruption of the tissue has been carried out using either an electric homogenizer or mortar and pestle. Total RNA was extracted with RNeasy Mini Kit from Qiagen following manufacturer's protocol. RNA concentration was determined using a photometer, where an OD₂₆₀ of 1 corresponds to 40 µg RNA per ml. RNA quality was controlled by electrophoresis. Isolated RNA was stored at -80°C if not processed immediately.

RNA agarose gels

RNase free 1xMOPS buffer containing 1% agarose was heated in a microwave oven and let cool down to 60°C. 3% Formaldehyde (37.5%) and ethidium bromide was added and filled into a thoroughly cleaned gel chamber. After gel run, the quality of the RNA was estimated by evaluating the range of longer RNA fragments and by comparing the ratio of the 18- and 28-S ribosomal bands.

Reverse transcription (RT) of mRNA into cDNA

To perform RT-PCR, mRNA from different tissues was transcribed by the reverse transcriptase SuperScript-II into cDNA. Approximately 1 µg of total RNA were incubated with random hexamer primers, dNTPs, SuperScript-II, and the corresponding buffers at 42°C following manufacturer's instructions. Identical reactions without SuperScript-II were used as negative control. The

RNA template was digested by RNase-H incubation. 1 μ l cDNA was used for semiquantitative RT PCR analysis.

7.2.1.3 General methods working with bacteria

Generation of chemical competent bacteria

E.coli bacteria of the strain DH5 α were cultivated on a LB agar plate without antibiotics overnight at 37°C. One single colony was inoculated to 5 ml LB medium and again incubated overnight on a shaker. 4 ml of this culture were added to 400 ml of fresh LB medium and incubated on a shaker for several hours. When the cell suspension reached an absorption value of 0.375 at 590 nm, but not higher than 0.4, bacteria were transferred to prechilled 50 ml tubes, chilled on ice for 5-10 min and centrifuged (1,600xg for 7 min at 4°C). Each pellet was carefully resuspended in 10 ml ice-cold CaCl₂ solution. Cells were centrifuged again (1,100x g, 5 min, 4°C) and each pellet was resuspended in 2 ml ice-cold CaCl₂ solution. Bacteria were then ready for direct transformation or were aliquoted and frozen at -80°C.

Transformation of competent bacteria

Single aliquods of 50 μ l competent bacteria suspension were carefully thawed on ice and approximately 25 ng of plasmid DNA were added. The sample was mixed carefully and incubated on ice for 10 min. After a heat shock (60 sec at 42°C) and short chilling on ice, 500 μ l of SOC medium was added. Bacteria were incubated at 37°C for 60 min gently shaking. Then the transformed bacteria were plated on LB plates containing an appropriate antibiotic and incubated overnight at 37°C.

7.2.1.4 The polymerase chain reaction

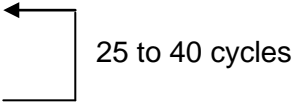
For amplification of DNA fragments from miscellaneous templates like genomic DNA, cDNA or vector DNA, polymerase chain reaction (PCR) was performed. About 20-400 ng of DNA template were used with the appropriate primers diluted from a 100 pmol/ μ l stock solution. Either an appropriated 10x

PCR-buffer together with a Taq-polymerase, or a 5x PCR mastermix has been used in a total reaction volume of 25 μ l.

PCR-Reaction (example):

template	1-5 μ l
2 mM dNTP's	2 μ l
10 x PCR-buffer	3 μ l
forward primer (10 pmol/ μ l)	1 μ l
reverse primer (10 pmol/ μ l)	1 μ l
Taq polymerase (10 U/ μ l)	0.5 μ l
ultrapure H ₂ O	12.5-16.5 μ l
total volume	25 μ l

After initial denaturation of the template DNA into single strands at 95°C, the PCR was performed for 25 to 35 cycles, each consisting of the following steps:

Step	Temperature	Time	
1. Denature:	94°C	3 min.	
2. Denature:	94°C	30 sec.	
3. Annealing:	55-65°C	45 sec.	
4. Elongation:	72°C	1 min.	
5. Elongation:	72°C	10 min.	

After the final elongation phase for 10 min at 72°C, the samples were chilled at 4°C until processing. For optimal results the cycle times and the annealing temperature were adjusted for each primer pair. PCR products were separated on a 0.8% 1.2% agarose gel in 1x TAE visualized on a UV desk with short wave UV radiation (254 nm), and photographed for documentation

Triplex genotyping PCR for the *Lrrk2* R1441C knock-in line

Standard genotyping polymerase chain reactions need two different reactions for each sample to discriminate not only between wild-type and mutant but also between the heterozygote or homozygote state. For more efficient genotyping, we established a triplex PCR for the genotyping of the *Lrrk2* R1441C knock-in line. By this method it is possible to amplify two different products within one single reaction. The 5' primer is used for both products.

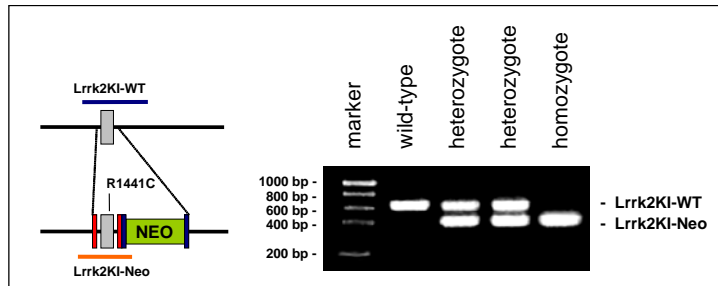


Figure 54: The *Lrrk2* R1441C knock-in line is genotyped by triplex PCR. Scheme (left) and example (right) of the triplex genotyping PCR using the primers *Lrrk2KI-left*, *Lrrk2KI-right WT* and *Lrrk2KI-right Neo*.

At the 3' end, 'Lrrk2KI-right Neo' is located in the neomycin resistance cassette which is present only in the mutant allele. The primer *Lrrk2KI-right WT* located in intron 32 is only functional in the wild-type allele, since in the mutant case, the distance to the 3' primer is too big for efficient amplification in the given elongation time. The wild-type allele gives rise to a 626 bp product; the mutant allele gives rise to a 442 bp product. If the conditions and relative amounts of the single primers are properly chosen, in the heterozygote state both products are amplified.

10 x PCR-Mastermix		10 µl
ultrapure H ₂ O		12 µl
<i>Lrrk2KI-left</i>	(10 pmol/µl)	0.8 µl
<i>Lrrk2KI-right WT</i>	(10 pmol/µl)	1 µl
<i>Lrrk2KI-right Neo</i>	(10 pmol/µl)	0.2 µl
genomic DNA		1 µl
total volume		25 µl

In this case, a commercial PCR-Mastermix has been used. Also the three primers were used premixed in the following ratio: 40% of primer *Lrrk2KI-left*, 50% of primer *Lrrk2KI-right WT* and 10% of primer *Lrrk2KI-right Neo* (Fig.54, left). This composition guarantees the equal amplification efficiency of both products and prevents false negative results.

PCR-Program:

Step	Temperature	Time	
1. Denature:	94°C	5 min.	
2. Denature:	94°C	30 sec.	← 33 cycles
3. Annealing:	58.5°C	30 sec.	
4. Elongation:	72°C	1 min.	
5. Elongation:	72°C	5 min.	

PCR products were separated on a relatively high concentrated agarose gel (1.2% to 1.5%) to ensure the proper separation of both products (**Fig.54**). The relatively small difference in size of both products is chosen intentional again to avoid any preferences for either product.

Quantitative real-time PCR (qPCR)

For determine quantitatively gene expression level, the TaqMan® mouse gene expression assays for murine Lrrk2 (Mm00481934_m1) purchased from AB Biosystems (Foster, CA), were used. This assay consists of two unlabeled primers together with an associated dye-labeled TaqMan® probe. The dye consist out of 6-carboxyfluorescein (6-FAM) linked to the 5' end and a nonfluorescent quencher (NFQ) at the 3' end. As an internal control gene, β -actin was used (Actb, 4352933E, Applied Biosystems). To compensate for variations in PCR amplification efficiency, each cDNA sample was amplified in 3 independent PCR reactions. PCR reaction was set up as followed: 9 μ l of diluted cDNA (about 90 ng); 10 μ l of 2 \times Taqman Master Mix, no UNG; 1 μ l of Taqman gene expression assay; in 20 ml reaction volume. The qPCR was performed using the ABI PRISM 7900 Sequence Detection System and data was acquired using SDS 2.0 software (Applied Biosystems). The program resembled 95°C for 10 min followed by 40 cycles of 95°C for 15 sec and 60°C for 1 min. The PCR reaction exploits the 5' nuclease activity of the DNA polymerase system to cleave a TaqMan® probe during PCR. During elongation, the cleavage of the dye-labeled probe separates the reporter dye at the 5' end and the quencher dye at the 3' end of the probe. This separation results in increased fluorescence of the reaction. The cycle number at which each PCR reaction reached a significant threshold (Ct) during the logarithmic phase of the amplification was used as a relative measurement of transcript expression. Results for qPCR were normalized to the housekeeping gene β -actin and relative mRNA expression was evaluated by the comparative Ct method (Livak and Schmittgen, 2008).

7.2.1.5 Southern blot analysis

In this work, the technique of Southern blot analysis has been used exclusively for genotyping ES cells, MEF cells, primary neurons or mice. For

genotyping the *Lrrk2* knock-in line, either the *Lrrk2KI* 3'-SB (see 5.2.2) or *Lrrk2KI* 5'-SB probe have been used (Fig.55). For the *Lrrk2*-knockdown line, either the ROSA-5' or the Neo probe have been used. Approximately 20 µg of genomic DNA were digested with 10 to 20 units of the appropriate restriction enzyme in a total volume of 30 µl. Spermidine (3.3 mM) was added to the sample for better restriction accuracy and DNA was digested overnight at 37°C. Digested DNA was separated on a 0.8% agarose gel in TBE buffer for 14 to 20 hours at 30 to 70 V, depending on the size of the gel apparatus and the required grade of separation. After the run, the gels were documented to ensure the complete digestion of the genomic DNA. Gels were rinsed in water to wash off removing TBE buffer, and incubated in 0.25 M HCl for 30 min at RT under gentle agitation. Partial depurination by HCl leads to a mild fragmentation of the DNA and subsequently to a better blotting efficiency of larger fragments. Afterwards, gels were rinsed in water again. To denature DNA strands, gels were agitated 2 times for 20 min in denaturation solution, rinsed in water again, and agitated again for 2 times 20 min in neutralization solution to bring the gel back to neutral pH. Single stranded DNA was then blotted overnight via capillary transfer onto a positive charged nylon membrane using 20x SSC. After DNA transfer the membrane was briefly rinsed with 2x SSC and additionally UV cross-linked. If not used for immediate hybridisation, the membrane was stored dry at 4°C. After crosslinking the membrane was prehybridized at 65°C for at least one hour in a hybridisation tube containing approximately 10 ml Rapid-Hyb™ Buffer or Church Buffer to reduce unspecific binding of the probe. The DNA probe consists of a 200 to 500 bp long appropriated fragment of genomic DNA which has been cloned into any vector. After the fragment is excised and gel-purified, 50-200 ng of the probe has been labelled with α -³²P-dCTP using the Rediprime II kit following manufacturer's instructions. For purification, the radioactive labelled probe was centrifugated through a Microspin S-300 column; by this, left over nucleotides and radioactively labeled DNA fragments with a size less than about 100 bp have been removed. To determine the labeling efficiency, the activity of 1 µl of cleaned up probe was measured in a liquid scintillation counter. For hybridisation Church buffer were applied. Before hybridisation,

the membrane was incubated with Church buffer for at least one hour at 65°C in a hybridisation tube. For hybridisation the radioactive labeled DNA probe (300,000 to 600,000 cpm/ml hybridisation buffer) was denatured at 95°C, chilled on ice and added to the hybridisation buffer. Finally, the membrane was hybridized at 65°C for 5 hours to overnight. The membrane was washed several times with wash solution I, II and III. Carefully, with Increasing stringency of the buffers and increasing temperature from RT to 65°C, the membrane was cleaned from unspecific bound probe. The number of washing steps and appropriate use of the different washing buffers were adjusted by determining the amount of radiation left on the membrane after each washing step. Subsequent, the membrane was covered in transparent foil to keep it humid and exposed to an autoradiography film for maximal three days at -80°C. To increase the intensity of weak signals, the Biomax MS film was used together with the Biomax screen. This combination intensified the signal six times compared to a conventional film without enhancer screen. Finally, the film can be developed using a developing machine.

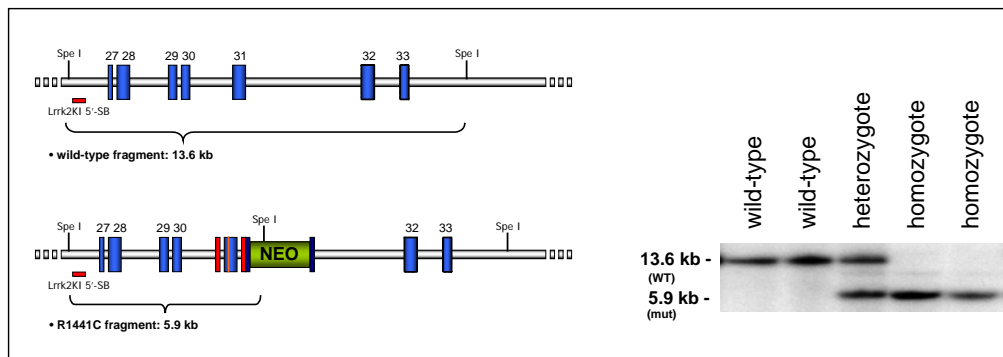


Figure 55: Schematic illustration of the Lrrk2 R1441C 5'-Southern blot principle used to verify correct recombination in ES cell clones and for routine genotyping. The probe *Lrrk2KI 5-SB* (red) does recognize a 13.6kb big fragment created by *Spe I* digestion (upper left). After insertion of the *Lrrk2* knock-in construct, an additional *Spe I* restriction site in the neomycine resistance cassette shortens this fragment to 5.9 kb, which allows discriminating between the wild-type and R1441C allele (lower left). A example of a *Lrrk2* R1441C 5'-Southern blot is depicted on the right. The corresponding 3' Southern blot principle is illustrated in 5.2.2, Fig.20.

7.2.1.6 Western blot analysis

Sample preparation and measurement of protein concentration

The preparation of protein samples for Western blot analysis should be performed at preferable low temperatures to avoid degradation. Therefore, the

dissection has to be performed as quickly as possible; the tissue samples were kept on ice for further processing or snap frozen in liquid nitrogen. In the case of *in vitro* assays, cells were homogenized by pipetting in an adequate amount of RIPA buffer. Cell debris in the homogenate was removed by centrifugation for 15 min at 4°C (13,000 rpm). In case of mouse tissue, the samples were homogenized in an adequate amount of RIPA buffer either with a small motor-driven pestle, or via an electrical homogenizer (Ika, Ultra Turrax T25 basic) depending on the total sample volume. For 1 g of tissue approximately 10 µl of buffer were used. DNA in the homogenate was sheared by sonification and cell debris was pelleted by centrifugation. The supernatant was removed and stored at -80°C. For determination of protein concentration with the BCA protein assay kit, 1 µl of the protein solution was mixed with 49 µl of RIPA buffer as diluent and 1 ml of BCA working reagent was added. Samples were incubated at 37°C in a water bath for 30 min, cooled down to RT and absorption was measured at 562 nm in a photometer. A BSA standard curve has to be included in each measurement. To correlate the absorption to the protein concentration mathematically, the slope of the linear part of the standard curve can be used.

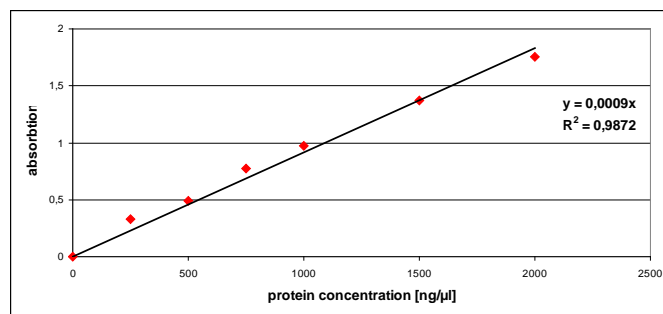


Figure 56: Example of a BSA standard curve for the determination of the protein concentration. To determine the protein concentration, the slope of the linear part of the standard curve can be used.

Gel electrophoresis and blotting

Proteins were separated by SDS polyacrylamide gel electrophoresis (SDS-PAGE) according to their size. Commercial available, precasted gel systems from Invitrogen (NuPAGE® Novex) and Biorad (Criterion™XT) have been used. An appropriated amount of protein solution (1 to 100 µg for each lane) were mixed with 5x Laemmli buffer (Laemmli, 1970), denatured at 95-100°C for 5 min, chilled on ice and loaded onto the gel. As molecular weight marker 5 µl of a commercial available standard like SeeBlue® Plus2 were loaded. After running the gel at 200V for 1-1.5 hours, the gel was blotted on a PVDF

membrane, which has been activated by soaking in 100% methanol. Blotting was performed at 30 V for 1 hour with the module from Invitrogen or at 50 V for 2 hours at RT to overnight at 4°C with the Biorad apparatus. Gel and Membrane can be transiently stained with various dyes like Ponceau red or FastBlue B to verify the blotting of the proteins.

Immunochemical detection of proteins

To ensure specific binding of the used antibodies, the membrane has to be blocked with a solution of 4% skim milk powder (5% BSA for phosphoproteins) in TBS-T for half an hour (RT) to overnight (4°C) prior to the incubation the first antibody directed against the protein of interest. The time of incubation (from half an hour at RT to overnight at 4°C) in either blocking solution or pure TBS-T and the concentration of the first antibody has to be determined for each assay. Also the subsequent washing in TBS-T of the membrane is highly dependent on the used antibody and protein (in general 15 to 60 min by changing the TBS-T three to four times). Incubation with the second, horseradish-peroxidase-conjugated antibody has been carried out for 45 to 60 min in TBS-T and washed again with TBS-T for three to four times). The detection reaction was initiated with ECL detection reagent following manufacturer's instructions and the membrane was exposed to a chemiluminescent film for 5 sec to several minutes depending on the signal intensity. Several films with different exposure times were then developed with a developing machine. For quantification, several films of each membrane have been scanned and band intensity was determined by the image processing and analysis software *ImageJ* (Abramoff *et al.*, 1984).

7.2.1.7 Protein fractionation

Instead of using total protein lysates from cells or tissue, subcellular fractions can be prepared to address certain questions (Whittaker, 1965). This technique is based on the separation of subcellular components by a series of centrifugation steps with increasing speed and density of the medium; the organelles that have sedimented to are recovered in the pellet, solved again and is than centrifuged again at higher speed to sediment the next-largest organelles. Therefore, we established a procedure to purify synaptosomes

out of mouse brain based on existing protocols (Villasana *et al.*, 2006; Dosemeci *et al.*, 2006).

Solutions:

0.32 M sucrose:	5,48g sucrose (MW 342.3) ad 50 ml
0.8 M sucrose:	13,70g sucrose ad 50 ml
40 mM Tris	2 mL 1M Tris (pH 8) ad 50 ml

Freshly prepared adult mouse brains were homogenized in 1ml of 0.32 M sucrose in a 1 mM MgCl₂ solution, containing a protease inhibitor cocktail using a glass homogenizer. The homogenate was transferred into a 15ml Falcon Tube containing another 9 ml of the same 0.32 M sucrose solution and then was distributed into ten 1,5ml microcentrifuge tube and centrifuged at 470 g for two minutes using a fixed angle rotor. All centrifugation steps were carried out in a chilled microcentrifuge at 4°C. The resultant supernatant is defined as input. For fractionating, it was decanted into another microcentrifuge tube and centrifuged at 10,000 g for 10 minutes using the same rotor to obtain a mitochondria- and synaptosome-enriched pellet (=P2) overlaid with supernatant (=S1). The (P2) pellet was resuspended with a pipet in 500µl of a 0.32 M sucrose solution. 750 µl of a 0.8 M sucrose solution in another microcentrifuge tube was carefully overlaid with this suspension. After the samples were centrifuged for 15 minutes at 9100g using either a fixed angle rotor or better a swinging bucket rotor, the myelin/light membrane layer at the interface between the 0.32 M and the 0.8 M sucrose layer was carefully removed with a 1000µl pipet and discarded. The 0.32 M sucrose layer was removed completely and defined as supernatant 2 (=S2). The 0.8M sucrose layer was transferred into another microcentrifuge tube together with some loose parts of the pellet containing the synaptosomes. Left behind is the harder mitochondrial pellet (=mito.). Collected synaptosomes in 0.8M sucrose were diluted with 20 mM HEPES (pH 7) to obtain a final sucrose concentration of 0.4 M. An equal volume (double of HEPES volumen) of a 150 mM KCl solution containing 2% Triton X-100 was added and samples were agitated in cold for 15 minutes prior to centrifugation at 20,800g for 45 minutes using a fixed angle rotor. Resulting pellets were washed in a 75 mM

KCl solution containing 1% Triton X-100 and centrifuged again at 20,800g for further 30 minutes using the same rotor. Subsequently, pellets were washed once again by resuspending in 20 mM HEPES and centrifugated as before. Finally, the pellets were resuspended in 20 to 100 μ l Tris-solution (pH 7.4) obtaining the synaptosomal fraction (syn.s.). All fractions (input, S1, P1, S2, P2, mitochondrial fraction, synaptosomal fraction) were analysed by Western blot for enrichment of fraction-specific marker proteins (e.g. cytochrome C, PSD-95, see Fig.57).

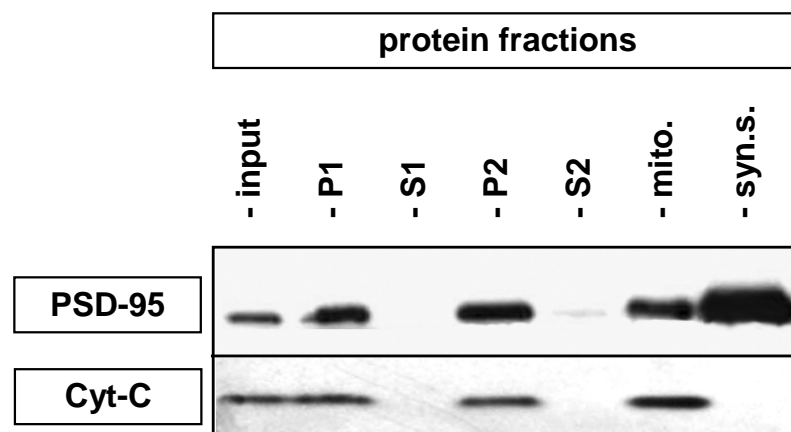


Figure 57: Subcellular fractions of brain lysates from adult brain. Western blot analysis of different fraction-specific marker proteins: Cytochrome-C as a marker for mitochondria, PSD-95 as a marker for synaptosomes. **Abbr.:** mito., mitochondrial fraction; P1/2, pellet 1/2; S1/2, supernatant 1/2; syn.s., synaptosomal fraction.

7.2.1.8 HPLC analysis

Sample preparation for the high performance liquid chromatography (HPLC) analysis should be performed at preferable low temperatures to avoid the degradation of the molecules of interest. Therefore, the dissection has been performed as quick as possible; the tissue was snap frozen in liquid nitrogen; all subsequent steps have been performed on ice. Tissue samples were weighed and carefully thawed on ice. To each sample 500 μ l extraction buffer was added before they were homogenized using a motor-driven pestle. Additional 500 μ l of extraction buffer were added, samples were mixed via pipetting, and centrifuged at 14.000 rpm and 4°C for 15-20 min. Supernatants were sterile filtered using a 0,2 μ m filter and stored at -80°C. For measurements of protein content cell pellets were washed with 500 μ l water (MiliQ) and centrifuged at 14.000 rpm and 4°C for 10-15 min. After that, the pellets

were suspended in 200 µl 0,1M Tris-HCl, pH 8.0 and thoroughly homogenized using the motor-driven pestle. 50 µl of the protein suspension were mixed with 50 µl 6N NaOH and further diluted with water in the range of 1:5 to 1:20, depending on the intensity of reaction color in bradford reagent. From each reaction batch, 10 µl per sample were mixed with 1 ml of the bradford reagent, incubated for 5 min at RT; finally the optical densities at a wavelength of 595 nm was measured in a photometer. The HPLC run kindly was performed by Brigitte Nuscher at the Adolf-Butenandt-Institute of the Ludwig-Maximilians-University Munich.

7.2.2 Histological methods

7.2.2.1 Perfusion and cutting

Mice were asphyxiated with CO₂ and the thoracic cavity was opened to dissect the heart. A blunt needle was inserted through the left ventricle into the ascending aorta and the right atrium was snipped. Using a pump vessels were rinsed with PBS until the liver became pale and then perfusion was carried out with 4% paraformaldehyde (PFA)/PBS for approximately 5 min (10 ml/min). After perfusion was complete the mouse was decapitated and the brain was dissected removing bones and meninges. For postfixation the brain was kept in 4% paraformaldehyde/PBS for 1 hour at RT to overnight at 4°C, depending on the subsequent procedure. For Embryo preparation pregnant mice were asphyxiated with CO₂ and Embryos were taken out and rinsed in cold PBS. The Embryos were decapitated and the brain was dissected removing bones and meninges and incubated in 4% PFA overnight at 4°C.

Cryo sections

After perfusion brains were postfixed for 1 hour at RT and equilibrated in 20% sucrose solution o/n at 4°C. For immunohistochemistry of phosphorylated proteins, solutions for perfusion were used ice-cold, brains were postfixed overnight at 4°C and 25% sucrose solution was used. Brains were frozen on dry ice or at 20°C and fixed on an object holder with freezing medium. On a cryostat slices of 30 or 40 µm were cut and collected in PBS. For storage longer than overnight the slices were kept in cryoprotection solution at -20°C.

Paraffin sections

After perfusion brains were postfixed for 1-2 hours at RT, dehydrated in an ascending ethanol scale, and equilibrated and embedded in paraffin. Using an automated embedding machine, the program is as follows:

Step	Solution	Temperature	Time (min)
Dehydration:	30% EtOH	RT	90
	50% EtOH	RT	90
	75% EtOH	RT	90
	85% EtOH	RT	90
	95% EtOH	RT	90
	100% EtOH	RT	90
	100% EtOH	RT	60
Clarification:	RotiHistol [®]	RT	60
	RotiHistol [®]	RT	60
Paraffination:	50% RotiHistol [®] / 50% paraffin	65°C	60
	paraffin	65°C	60
	paraffin	65°C	480
Embedding:	paraffin	65°C to RT	

Paraffin embedded brain tissue was first mounted on a tissue cassette with paraffin and fixed on the microtome. 8 µm thick sections were cut and put into a water bath (37-42°C) for flattening. Sections were mounted on slides and dried on a heating plate and/or in an incubator at 37°C. Slides with slices were stored at 4°C or used immediately.

7.2.2.2 *In situ* hybridisation on paraffin sections (radioactive)

For the detection of mRNA expression on brain sections, radioactive ISH on paraffin section was performed. During the whole procedure RNase free solutions and materials were used to avoid degradation of the mRNA and the RNA probe.

Synthesis of ³⁵S labelled RNA probes

Radioactively labelled RNA probes for *in situ* hybridisation were generated by *in vitro* transcription with an appropriate RNA polymerase in the presence of [α -thio³⁵S]- UTP. As templates, plasmids containing part of the cDNA of the gene to analyze and promoters for the RNA polymerases T7 and SP6 were

linearised shortly behind the end of the cDNA sequence with an appropriate restriction enzyme. A 1x transcription reaction was composed as follows:

3 µl	10x transcription buffer
3 µl	dNTP mix (rATP/rCTP/rGTP 10mM each)
1 µl	0.5 M DTT
1 µl	RNasin (RNase inhibitor; 40 u/µl)
1.5 µg	linearised plasmid DNA template
7 µl	[α-thio- ³⁵ S]-UTP (12.5 mCi/mM)
x µl	H ₂ O (total volume is 30 µl)
1 µl	RNA polymerase (T7 or SP6; 20 u/µl)
30 µl	total volume

The reaction was incubated at 37°C for 3 hours in total. After the first hour another 0.5 µl of RNA polymerase was added to facilitate the transcriptional process. After transcription the DNA template was destroyed by adding 2 µl of RNase-free DNase I and incubation at 37°C for 15 min. Probes were purified with the RNeasy Mini Kit following manufacturer's instructions and activity was measured with a liquid scintillation counter. The probe was stored at -20°C up to five days.

Hybridisation

The hybridisation temperature is about 25°C under the melting temperature of the probe. Before hybridisation paraffin sections were dewaxed and pre-treated as follows:

Day 1

2 x 15 min	Rotihistol
2 x 5 min	100 % Ethanol
5 min	70 % Ethanol
3 min	DEPC-H ₂ O
3 min	PBS/DEPC
20 min	4 % PFA/PBS
2 x 5 min	PBS/DEPC
7 min	20 µg/ml Proteinase K in Proteinase-K-buffer
5 min	PBS/DEPC
20 min	4 % PFA/PBS
5 min	PBS/DEPC
10 min	200 ml of rapidly stirring 0.1 M triethanolamine-HCl (pH 8) (TEA)
2 x 5 min	2x SSC
1 min	60 % Ethanol/DEPC

1 min	70 % Ethanol/DEPC
1 min	95 % Ethanol/DEPC
1 min	100 % Ethanol

Slides were air dried and used immediately for prehybridisation. For prehybridisation slides were incubated with Hyb-mix (without labelled riboprobe) for 1 h at hybridisation temperature. For hybridisation the following protocol was used:

- Make appropriate amount of hybridisation mix containing 35000 to 70000 cpm/ μ l. Use 90 to 100 μ l hybmix per slide (3,5 to 7 Million counts per slide).
- heat hybridisation mix containing the probe to 90 °C for 2 min.
- put shortly on ice, then on RT.
- after prehybridisation remove coverslip and as much liquid as possible. Go on immediately with hybridisation to avoid drying out!
- Take 90 to 100 μ l of hybridisation mix containing 35000 to 70000 cpm/ μ l per slide, drop the solution on the slide and put coverslip carefully on it.
- Place slides carefully into a hybridisation chamber containing hybridisation chamber fluid to avoid drying out of the hybridisation mix.
- Incubate in an oven at 55-68°C for overnight (up to 20 hours).
- Hybridisation temperature is about 25C under the melting temperature of the probe, the higher the less background.

Day 2

4 x 5 min	RT	4xSSC
20 min	37 °C	NTE (20 μ g/ml RNaseA)
2 x 5 min	RT	2xSSC/1 mM DTT
10 min	RT	1xSSC/1 mM DTT
10 min	RT	0,5xSSC/1mM DTT
2 x 30 min	64 °C	0,1xSSC/1 mM DTT
2 x 10 min	RT	0,1xSSC
1 min	RT	30 % Ethanol in 300 mM NH ₄ OAc
1 min	RT	50 % Ethanol in 300 mM NH ₄ OAc
1 min	RT	70 % Ethanol in 300 mM NH ₄ OAc
1 min	RT	95 % Ethanol
2 x 1 min	RT	100 % Ethanol

Slides were air dried and exposed to an autoradiography film (BioMax MR) for 2 days. For a detailed analysis slides were dipped with a photo emulsion (diluted 1:1 with water) and stored at 4°C in the dark for an appropriate time depending on the signal intensity (estimated by the results from the film; in general 4 weeks). For developing, slides were equilibrated for 1 h to RT, developed for 5 min, rinsed in water and fixed for 7 min. After rinsing the slides for 25 min in floating tap water, remaining emulsion on the backside was scratch with a razor blade and slides were counterstained with cresyl violet.

Nissl staining (cresyl violet)

Nissl staining of Paraffin sections was performed according to the following protocol:

- Staining: 1-5 min cresyl violet staining solution
- Rinse: H₂O
- Clearing: 1 min 70% Ethanol until slide is clear
10-60 sec 96% Ethanol + 0.5% acetic acid
- Dehydration: 2 x 1 min 96% Ethanol
2 x 2 min 100% Ethanol
- 2 x 10 min xylol

Slides were lidded immediately with DPX and dried o/n under the hood.

7.2.2.3 *In situ* hybridisation on paraffin sections (DIG-labelled probes)

Probe labelling

20 µg of the probe containing plasmid were digested for at least 3h with appropriate restriction enzymes and for antisense probes. Upon heat inactivation the digestion was checked by electrophoresis on an agarose gel and the probe is cleaned up with the Wizard SV Gel & PCR Clean up kit (Promega) according to manufacturer's protocol. The purified probe can be stored at – 20°C and is used for reverse transcription:

Reverse transcription mix:

1 µg	linearised DNA (purified probe)
2 µl	10 x Transcription buffer (Roche)
2 µl	10 x DIG labeling Mix (Roche)
0.5 µl	RNase Inhibitor (Roche)
2 µl	T7, T3 or Sp6 RNA Polymerase
x µl	RNase free water (fill up to 20 µl)
20 µl	total volumen

The reverse transcription mix was incubated for 3h at 37°C RNase free DNaseI (Roche) was added to eliminate the DNA-template. The reaction was stopped by adding EDTA and stored at -80°C or the RNA probe was immediately purified with the RNeasy Mini kit. The reverse transcription products are checked on an agarose gel and the DIG-labelled control RNA kit (Roche) was used to ensure efficient DIG labelling of the probe.

Pre-treatment of Paraffin sections for ISH with DIG labelled probes:

Time	Treatment
2 x 20 min	Xylol
2 x 5 min	100 % Ethanol
5 min	95 % Ethanol
5 min	70 % Ethanol
3 min	H2O (RNase free)
3 min	PBS
20 min	4 % PFA in PBS
2 x 5 min	PBS
2 min	60 % Ethanol
2 min	70 % Ethanol
2 min	95 % Ethanol
2 min	100 % Ethanol
	Air-dry

*Protocol for ISH with DIG labelled probes on Paraffin sections:*Day 1:

cycles	time	reagent	temp
5	5 min	0.6 % H ₂ O ₂ /MeOH; no detergent	24 °C
7	5 min	PBS	
2	5 min	0.2 N HCl	
4	5 min	PBS	
1	5 min	Proteinase buffer	
2	10 min	Proteinase K 20 µg/ml	
7	5 min	PBS	

2	10 min	4 % PFA	
7	5 min	PBS	
1	15 min	Hyb. Mix + DTT 1.5 mg/ml	24 °C
1	30 min	Hyb. Mix	64 °C
1	6 h	Dig-Probes (150-) 300 ng/ml	64 °C

Day 2

cycles	time	reagent	temp
5	5 min	5 x SSC preheated (90 min in advance) to 64 °C	64 °C
5	10 min	Formamide I (2x SSC in 50 % Formamide)	
5	12 min	Formamide II (1x SSC in 50 % Formamide)	
4	8 min	0,1 x SSC	25 °C
4	5 min	NTE pH 7.6	
4	7 min	Iodacetamide, 20 mM	
4	5 min	NTE	
2	5 min	TNT pH 7.6	
3	10 min	4% Sheep Serum (filter 0.45 µm)	
4	5 min	TNT	
2	10 min	TNB blocking	
2	5 min	TNT	
2	5 min	Maleat Wash	
2	10 min	Maleat blocking	
2	5 min	Maleat Wash	
2	5 min	TNT	
3	5 min	TMN (no Levamisol)	
4	5 min	TNT	
4	10 min	TNB blocking	
2	30 min	Anti DIG-POD (1:600 or 0.2925 U/µl)	
6	5 min	TNT	
1	30 min	Tyramid-Biotin 1: 50 in TSA	
6	5 min	Maleat Wash	
2	30 min	Neutravidin-AP (Pierce; 31002) 1:750/2.85 µg/ml in MWB	
6	5 min	Maleat Wash	
4	5 min	TNT	
2	5 min	TMN	
2	15 min	NBT-BCIP in TMN + (+ 0.5 mg/ml Levamisol, BCIP 0.15ug/ml, NBT 0.4 ug/ml)	
4	5 min	Water I + 0.05 % Tween	
1	5 min	NTE	
1	20 min	4%PFA	
4	5 min	Water II	

7.2.2.4 Immunohistochemistry on paraffin sections

Immunohistochemistry on Paraffin sections was performed in glass cuvettes (about 250 ml per cuvette) except blocking, antibody incubations, the ABC-

reaction and the DAB-staining. As blocking solution 10% FCS with 0.05% Triton-X in 1x PBS was used. Primary and secondary antibodies were diluted in 10% FCS in 1x PBS. The DAB working solution was prepared by adding 1 ml DAB stock solution and 15 μ l H₂O₂ (30%) to 19 ml 0.1M Tris-HCl, pH 7.4 immediately before use.

Day 1

1. dewaxing	Min. 45 min	Rotihistol or Xylol	
2. Rehydration	2 x 5 min	Ethanol 100%	
3.	2 x 5 min	Ethanol 96%	
4.	2 x 5 min	Ethanol 70%	
5. Rinse	10 min	Aqua dest	
6. wash	3 min	0.01 M Na-citrat, pH 6.0	
7. Antigen retrieval	5 min	Microwave at 100%	<u>Attention:</u> Times have to be determined for each microwave
8.	10 min	Cooling down	
9.	3 min	Microwave at 70%	
10.	20 min	Cool down	
11. wash	2 x 5 min	0.1M PBS	
12. destruction of endogenous peroxidases	5 min	0.1% H ₂ O ₂ / PBS	Add H ₂ O ₂ directly before use
13. wash	2 x 5 min	0.1M PBS	
14. blocking	1 hr	Blocking reagent	RT; humid chamber
15. 1st antibody	Over night	1st antibody	4°C; humid chamber

Day 2

1. wash	3 x 5 min	PBS	
2. 2nd antibody	1 hr	2nd antibody	RT; humid chamber,
3. wash	3 x 5 min	PBS	
4. intensifying	30 min	ABC-solution	RT; humid chamber
5. wash	2 x 5 min	PBS	
6. wash	5 min	0.1M Tris-HCl	
7. DAB-staining		DAB-working solution	humid chamber; Control intensity under microscope
8. stop staining	2 x 5 min	PBS	
9. dehydration	2 x 5 min	Ethanol 70%	
10.	2 x 5 min	Ethanol 96%	
11.	2 x 5 min	Ethanol 100%	
12.	2 x 5 min	Rotihistol or Xylol	
13. embedding		Rotihistokitt or DPX	

7.2.2.5 Immunohistochemistry on frozen sections (free floating)

In cryoprotection solution stored free-floating sections (40 μ m in thickness) were first washed in 1x TBS, 6 x 15 min at RT or overnight at 4°C. Further

steps were performed gently shaking at RT in 6-well or 12-well plates. Sections were blocked for 1h in 5% normal goat serum (NGS) in 0,2% Triton X100 in PBS (PBST) and incubated overnight with the primary antibody in 5% NGS in PBST overnight at 4°C on a shaker. The next day sections were washed 3 x 15min with PBST and incubated 45 min with a fluorescence-dye labelled secondary antibody in 5% NGS in PBST. Finally sections were washed 3 x 15 min in PBST and 3 x 10 min 1x PBS. During the second PBS washing step DAPI is added to PBS to label the DNA as counterstaining. Sections were mounted on slides, air-dried, and lidded with Aqua Poly/Mount (Polysciences, Inc.). During all steps the exposure of fluorescent dyes to bright light was reduced to a minimum.

7.2.2.6 Documentation of histological results

All histological results on slides were documented using the following microscopes: the light microscope Zeiss, Axioplan 2 (objective 5x – 100x); the binocular microscope: Zeiss, Stemi SV 6 (planobjective S 1.0x); the fluorescent microscope Zeiss, Axiovert 200M (objective 5x – 100x); the confocal microscope Zeiss, LSM 510 (objective 5x – 64x). Pictures were taken using the digital cameras AxioCam MRC/HRC controlled by the software Axiovision 3.1 and 4.0 respectively. Subsequently, the pictures were optimized using the editing program Adobe-Photoshop® (version 7.0) basically exclusive by changing contrast and brightness. Anatomical structures were identified and termed following the designations taken from the histological atlases „The atlas of mouse development“ (Kaufmann, 1992), „Atlas of the prenatal mouse brain“ (Schambra *et al.*,1992) and „The mouse brain in stereotactic coordinates“ (Franklin and Paxinos, 1997).

7.2.3 Methods in cell culture

7.2.3.1 Mouse embryonic fibroblasts

In general Mouse embryonic fibroblasts (MEFs) were grown on plain cell culture dishes in a 37°C incubator under a 5% CO₂ atmosphere. The DMEM culture medium was supplied with 10% FCS and 1% of a penicillin and streptomycin antibiotic mixture. Cell density and condition was controlled

regularly and cells were splitted every 2-7 days depending on their growth rate. For best conditions cells were kept at 40-90% confluency.

Generation of MEF cell lines

For the generation of MEF cell lines, appropriate breeding pairs were set up. 12-15 days after fertilization, female mice were asphyxiated with CO₂. Uteri were taken out, put in 1x PBS and cooled on ice. Since dissection has to be done under the microscope, all instruments and surroundings were cleaned thoroughly with 100% ethanol, dissection was performed in petridishes filled with sterile 1x PBS. Embryos were dissected out of the uterus; their heads were excised from the rest of the body and collected for genomic DNA extraction and genotyping. Torsos were opened ventrally, and all inner organs and blood vessels were removed under the microscope. Residual tissue was immediately transferred under a sterile cell culture hood and collected in 6-well cell culture plates. The tissue was minced with scalpels, while using a fresh, sterile scalpel for every embryo. 1 ml of medium, containing 50% FCS, was added to every well, and cell culture dishes were put in a 37°C incubator with a 5% CO₂ atmosphere. On the next day, medium was changed; one day later, large tissue parts were removed from the cultures and medium was changed. Over the next 7 days, the FCS content of the medium was gradually reduced from 50% to 10%. In case of highly diverse distribution of cell densities, cells were tryplated by trypsination and seeding onto fresh 6-well dishes without dilution. Cell confluency was controlled every day and as soon as the fibroblasts were grown dense enough, cells were splitted onto 10 cm dishes. The exact time point of splitting was chosen independantly for every single cell line in regard to its cell density. MEF cells density and condition was controlled every 1-2 days. They were splitted every 1-7 days depending on the cell density, trying to keep them always between 40% and 90% confluency. When MEFs were highly confluent or starting to grow on top of each other, they were splitted to a desired amount of fresh cell culture plates.

Immortalization of MEF cell lines

Primary MEF cell cultures grow nicely and with a high growth rate until about 5-15 passages after MEF cell preparation from the embryo. Soon their growth

rate slows down dramatically until cell densities are very low and all cells die. To work with established cell lines, which can be passaged over a very long period time without extinction, primary MEF cells can be immortalized.

3T3 cells

For immortalization of primary MEF cell lines, two different methods were used. The first method was modified from the 3T3 method (Todaro & Green, 1963). Primary fibroblast cultures were controlled every day and splitted every 3-6 days according to their growth rate. Usually 5-15 passages after MEF cell-generation, the growth rate of fibroblasts slows down very fast, until they die. To prevent cell death and to high dilution of cells, MEFs were either splitted or tryplated every 3-10 days for a time period of at least 6 months. During this time, spontaneous mutation can occur, leading to cancerous growth behavior of the cells and thus immortalization. A negative effect of this method is, that one cannot be sure what kind of spontaneous mutation might have occurred in the cells genome, and cell lines might show a great variety. Hence different cell lines, can prove not be genetically equal, although they underwent the same protocol. It is therefore not always convenient to compare e.g. knockout and control cell lines which were immortalized by this method. Therefore we decided to use another immortalization method in parallel.

SV40 largeT antigen transfection

For this kind of immortalization, MEFs were transfected with SV40 largeT antigen (Jensen et al., 1963; Koprowski et al., 1963) via LipofectaminTM 2000. For this purpose, MEFs were splitted on 6 cm cell culture dishes and grown until they reached 70-90% confluency. 5 µg of sterile DNA (SV40 largeT antigen, unlinearized plasmid) was added to 500 µl of Opti-MEM[®] I Reduced-Serum medium (1x), 12,5 µl LipofectaminTM 2000 were added to another 500 µl of Opti-MEM[®] I Reduced-Serum medium (1x), and both were incubated for 5 min at RT. The two solution were pipetted together, mixed gently and incubated for 20 min at RT so that LipofectaminTM 2000 could form complexes with the DNA. Medium was removed from cell culture dishes, they were washed with 1x PBS and supplied with 4 ml fresh, prewarmed medium and 1 ml of the transfection mix, and put back into a 37°C incubator

under 5% CO₂ atmosphere. Medium was changed the next day. Established MEF cell lines of both methods of immortalization were cultured for at least 4 to 6 months until they reached passages between 35 and 55, before they were used for any kinds of experiments.

7.2.3.2 Primary neuronal cultures from mouse tissue

For functional studies in neurons, no established neuronal cell lines or artificial differentiated progenitor cell lines have been used, but the most straight forward method of directly cultivating postmitotic neurons in primary culture. This approach allows not only studying the nervous system at a single cell level but also the complex interaction of the neurons with their neighbouring cells in a complex network. Drawback of this model is the limitation in cultivation time, since unlike established cell lines, primary cultures can in general not be cultivated for very long periods but have to be prepared consistently.

Pretreatment of coverslips

In general, primary neurons were cultivated in 24-well culture dishes on top of round coverslips (12 mm in diameter, Marienfeld). This method allows to fix the cells after cultivation and to use them for performing immunocytochemistry (ICC). Since cell adhesion is one of the most critical steps in the cultivation of neurons, the coverslips have to be pretreated very carefully. For cleaning the surface, coverslips have been incubated in concentrated nitric acid overnight and washed extensively for at least one day in ddH₂O which has to be changed as often as possible. After the coverslips have been distribute into 24-well plates, the last cleaning step was performed for 3 hours till overnight in 70% EtOH followed by washing with ddH₂O again for three times. 1 mg/ml poly-D-lysine has been dissolved in sterile water (or PBS); this stock solution can now be stored in 500 µl or 1 ml aliquots at -20°C. For coating, this stock solution has been diluted with water (or PBS) in a ratio of 1:20 to obtain a 50µg/ml working solution. For each well of a 24-well culture dish, 300µl is sufficient to overlay and coat one 12mm coverslip (~7,5 µg poly-D-lysine per cm²). Now the plates had to be incubated for 3 hours till overnight. Then the liquid must be aspirate and the wells carefully rinsed with 500 µl water for 2 to

3 times. After that, the coverslips were allowed to dry completely. Now the plates can be used directly or stored dry at 4°C for some weeks in a sterile wrapping.

Preparation of primary neurons

For the generation of MEF cell lines, appropriate breeding pairs were set up. 12-15 days after fertilization, female mice were asphyxiated with CO₂. Uteri were taken out, put in 1x PBS and cooled on ice. Since dissection has to be done under the microscope, all instruments and surroundings were cleaned thoroughly with 100% ethanol, dissection of the uterus was performed in petridishes filled with sterile 1x PBS. Embryos were dissected out of the uterus and stored in a 50 ml tube in cold dissection medium on ice. The desired brain regions have been isolated from single embryos and stored in 1.5 ml reaction tube again in dissection medium and stored on ice. For genotyping, one limb of each single embryo has been collected. All subsequent steps have been carried out under the laminar flow to ensure a sterile environment. The tissue has been washed 2 to 3 times with prewarmed Trypsin (0.02%) and then incubated for 10-15 min at 37°C with 1 ml Trypsin to disrupt the tissue structure. Alternatively to Trypsin, 2mg/ml Papain can be used. Subsequently, the tissue has to be washed carefully for three times with culture medium - Trypsin should have enough time to dissociate out of the tissue. Trituration was performed using a glass Pasteur pipette with the tip fire polished and narrowed to about half of the original diameter. The tissue is dispersed by carefully pipetting the tissue within 1ml of culture medium up and down. After undispersed pieces have settled down for 30 seconds or 1 min, the supernatant has been carefully transferred into a new tube. The amount of living cells in each preparation from a single embryo has been determined by counting in a Neubauer counting chamber after staining non-viable cells with Trypan Blue. For seeding, 300 µl of culture medium containing 3.5 to 5.0·10⁴ cells has been pipettet into each coated well of a 24-well culture dish and incubated at 37°C under a 5% CO₂ atmosphere. After 4 days, half of the medium has been changed. Neurons can be cultivated up to 3 to 4 week under optimal conditions.

Exocytosis / Endocytosis assay

When synaptic transmission is taking place, a neurotransmitter-filled synaptic vesicle fuses with the plasma membrane (**Fig. 58, A: a,b**), by neuroexocytosis mediated by the SNARE complex, the neurotransmitter gets released (**Fig. 58, A: c**). By this, the lumen of the vesicle is now exposed to the outside of the neuron. Synaptotagmin 1 is a synaptic vesicle protein and acts as a calcium receptor during exocytosis (Brose *et al.*, 1992) and consists out of a long cytoplasmatic part, an intramembran domain and a short N-terminal part in the lumen of the vesicle (**58, A: c**). Polyclonal antibodies, directed against the lumenal part of synaptotagmin 1 in the medium of fully mature (>DIV14) and living primary neurons, can only bind their epitope, when this part of the protein is exhibited to the cell surface during exocytosis (**58, A: c,d**).

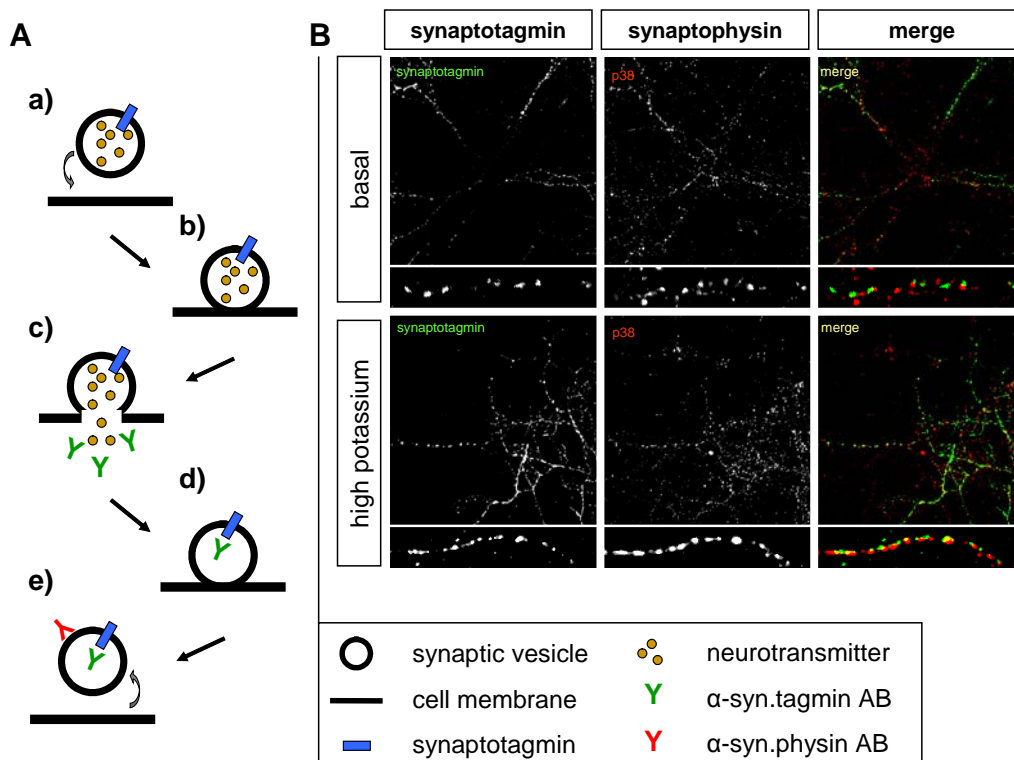


Figure 58: Principle and example pictures of the exo-/endocytosis assay. **A)** Schematic representation of the principles of the exo/endocytosis assay. **a** and **b**, fusion of a synaptic vesicle with the cell membrane; **c**, exocytosis releases the neurotransmitter and exposures of the epitope to the antibody; **d**, endocytic recycling of the vesicle internalizes the antibody; **e**, after washing and fixation, in addition the total pool of vesicles is stained by IHC. **B)** Representative confocal picture of hippocampal neurons after double IHC under basal and evoked (high potassium) conditions.

Therefore, the more synaptic vesicles undergo a cycle of exo- and endocytosis during antibody exposure, the more vesicles have bound synaptotagmin 1 antibody. With the next round of endocytosis, the antibody is getting internalized together with the synaptic vesicle. After a certain time, the neurons are getting briefly washed, fixed, permeabilized and subsequently counterstained for synaptophysin (58, A: e). This membrane protein is another marker for synaptic vesicles with until now unspecified function in synaptic vesicles biogenesis (Pennuto *et al.*, 2002). A representative result is depicted in figure 60B; while synaptophysin staining detects all synaptic vesicles of a neuron, positive signals for synaptotagmin can only be found in vesicles, which underwent a cycle of exo- and endocytosis during the time of antibody exposure. The ratio of vesicles stained by synaptotagmin versus the number of synaptophysin positive vesicles gives the rate of exo-endocytosis activity for a certain neuron. If the neurons are getting partially depolarized by high levels of potassium in the medium, also the exo-endocytosis activity is getting stimulated indicating the functionality of this assay. For further verification, neurotoxins like tetrodotoxine (TTX) for inhibition or bicucullin (Bic) for enhanced excitation of the neurons was used (data not shown).

For the assay, *Lrrk2* R1441C knock-in and knockdown primary hippocampal neurons have been used after at least two weeks of maturation to ensure a functionally neuronal network within the culture. For each condition, one well of a 24-well culture plate has been used from each wild-type or mutant cell line. Initially, the cells have been washed two times with prewarmed DMEM for some seconds, to habituate the neurons and to ensure equal starting conditions for each line. The assay starts by giving DMEM medium, for basal conditions supplemented with anti-synaptotagmin-1 antibody in a concentration of 1:200 to the cells. For evoked conditions, the medium is in addition supplemented with 90mM KCl. Loading of the antibody was performed for 4 minutes at room temperature under the laminar flow. Subsequently, the cells were washed with fresh DMEM medium for some seconds to remove unbound antibody and fixed with 4% paraformaldehyde solution. After double ICC for synaptotagmin and synaptophysin was performed, pictures were taken at a confocal microscope. The number of

positive vesicles was evaluated using the particle analysis function of the image processing software *ImageJ* (Abramoff *et al.*, 1984).

Neurite Outgrowth assay

For every assay, several primary hippocampal cultures of each genotype were prepared in a couple of 24-well plates. Wells were fixed with paraformaldehyde at DIV1, -2 and -5 respectively, to study the progress of neurite outgrowth. To visualize the cell morphology and to discriminate between neurons and glial cells, immunohistochemistry for the neuron-specific tubulin subtype beta-III-tubulin was performed. The quantification of neurite outgrowth was performed by measuring the individual length of each neurite of a beta-III-tubulin positive cell displaying a healthy morphology. The length of primary, secondary and in case of the *Lrrk2* knockdown neurons also tertiary neurites have been determined using the image processing and analysis software *ImageJ* (Abramoff *et al.*, 1984). Also the total numbers and the numbers of primary, secondary and tertiary neurites have been taken into account.

7.2.4 Methods in ES cell culture

7.2.4.1 Embryonic stem cells

Since totipotency also includes the cells ability to differentiate into extra-embryonic tissue, embryonic stem (ES) cells are defined as pluripotent (Smith *et al.*, 1988). They built up the inner mass of blastocysts from which they can be isolated directly for *in vitro* cultures (Evans and Kaufman, 1981). TBV2, the mouse ES cell line used for the generation of the *Lrrk2* R1441C knock-in mouse line, was created at the Institute of Developmental Genetics of the Helmholtz Zentrum München by Veronique Blanquet and originates from the mouse strain 129SvEv/Tac. The mouse ES cell line IDG3.2, used for the generation of the *Lrrk2* knockdown mouse line, originates from the F1 generation of the mouse strains C57Bl/6J and 129SvEv/Tac. These cell lines are able and tend to differentiate into divergent cell types *in vivo* as well as *in vitro*. Nevertheless it is possible to cultivate ES cells and keep them in an undifferentiated state when they are cultivated under special conditions. Therefore, the ES cultivating medium was supplemented with the Leukemia

inhibiting factor or LIF (Williams *et al.*, 1988). In addition, specially tested fetal calf serum (FCS) was used, and ES cells were grown on a monolayer of confluent feeder cells at 37°C and 5% CO₂. The cells were used not only for the generation of genetically modified mice, but also for test experiments and *in vitro* differentiation into different cell types of interest. Whereas ES cells for mouse generation were always grown on a monolayer of feeder cells, ES cells for transient experiments were grown on gelatine coated cell culture dishes without feeder cells. Therefore the dish was overlaid with 1% gelatin solution, after a short time the solution was sucked off again and the plates were shortly dried before ES cells were plated.

7.2.4.2 Preparation of feeder cells

The supporting feeder cells which are necessary for cultivate ES cells in an undifferentiated state are mouse fibroblast cells which have been mitotically inactivated by mitomycin c treatment. These fibroblasts are prepared from embryos of the transgenic mouse strain C57Bl/6J-Tg(pPGKneobpA)3Ems/J at the age of E14.5 to E16.5, since they have to be neomycin resistant in order to survive the selection procedure which ES cells have to undergo for screening. Primary fibroblasts were expanded for two passages and grown on 10 cm cell culture dishes until 100 % confluency is achieved. For mitotical inactivation, the cells were incubated with medium containing 10 µg/ml mitomycin c for 2 hours at 37°C. After intensive washing with PBS, feeder cells were trypsinized and plated onto a fresh culture dish or frozen at -80°C (in 1x freezing medium) for later use. Feeder cells were plated at a density of 2 to 2.5 x 10⁴ cells per cm² at least several hours prior to plating of ES cells.

7.2.4.3 Splitting of ES cells

During expansion, the ES cells were splitted every two days to avoid confluent growing which would enhance differentiation of the cells. The medium was sucked off, cells were washed with PBS (0.05%) and trypsinized for 5 min at 37°C until cells detached from the surface. An equal amount of medium, containing a trypsin inhibitor stopped the reaction and the suspension was triturated carefully by pipetting up and down until a single cell suspension has been achieved. For determination of the total cell number, 10 to 20 µl of cell

suspension were pipetted in a Neubauer counting chamber and ES cells were counted using a microscope. The cell number of one quadrant multiplied by the factor $1 \cdot 10^4$ corresponded to the number of cells in one millilitre of cell suspension. The suspension was seeded onto one or several fresh culture dishes depending on the desired amount of cells per dish and the experimental objective.

7.2.4.4 Freezing and thawing of ES cells

For short term storage (up to 2-3 months), ES cells were stored -80°C . Long term storage has been carried out in liquid nitrogen. For this, cells were trypsinized as described in 7.2.4.3, gently centrifuged at 1200 rpm for 4 minutes. After that, the cells were resuspended in ice cold 1x freezing medium, and 2 ml was pipetted into a prechilled cryovial. Vials were frozen in a freezing container at -80°C allowing a slow temperature decline. After one or two days, the vials were transferred into liquid nitrogen for long term storage. For freezing of cells on multi-well plates, cells were trypsinized and then resuspended with a small amount of medium. The same volume of ice cold 2x freezing medium was added. Plates were wrapped in cellulose and frozen at -80°C . In this case, the cellulose should prevent the very fast freezing of the cells.

For thawing, cells were transferred into a 37°C warm water bath as quick as possible. Directly after the suspension is liquid, fresh medium has been added to dilute the DMSO-containing freezing medium. Cells were centrifuged at 1200 rpm for 4 minutes and resuspended in an appropriate volume of fresh medium and plated on dishes with or without feeder cells. For small volumes of frozen cells or cells frozen on multi-well plates, cells were diluted in a larger volume of medium and plated out directly. For this procedure, it is necessary to change the medium as quick as possible after the cells are attached to the surface.

7.2.4.5 Electroporation of ES cells

The method of choice to import DNA into ES cells is the electroporation. By this method, the cell membrane is permeabilized transiently by short electrical pulses, allowing DNA attached on the outer surface to enter the cell. Circular

plasmid DNA stays transiently in the cell while linear DNA fragments can also be integrated into the genome either by random or homologous integration. Cotransfection of a specially designed circular plasmid together with an expression vector for an integrase results in integration of a defined fragment of the circular plasmid into the genome of the cell, according to the recombination event catalyzed by the integrase (e.g. for the recombinase-mediated cassette exchange).

Cells were harvested from their culture dishes by trypsination, centrifuged at 1,200 rpm for 5 min, washed with PBS, centrifuged again and resuspended. For each sample to be electroporated, $7 \cdot 10^6$ cells in 800 μ l chilled PBS have been used. A maximum of 50 μ g of linearized and sterile precipitated DNA (see 5.2.2) has been pipetted to the cell suspension and was transferred into an electroporation cuvette. The electroporation has been performed with containing the DNA to be electroporated. A maximum of 50 μ g of total DNA was used for 240 V and 500 μ F for 6 ms. In case of the *Lrrk2* R1441C knock-in mouse line $1 \cdot 10^8$ cells were mixed with 120 μ g of the linearized plasmid pLrrk2-knock-in and electroporated with a single electric pulse for 0.1 msec with 0.8 kV and 3 μ F. For transient experiments, where the transfection efficiency has to be as high as possible, a voltage of 320 V was used for 3 ms. After transfection, cells were allowed to recover for 10 to 20 min on ice. Subsequently, the mixture was diluted with ES culture medium and plated on 4-5 fresh 10cm culture dishes. Cells were grown for two days at 37°C before selection for resistant ES cell clones can be started.

7.2.4.6 Selection of recombinant ES cell clones

For the selection of clones where recombination did occur, two days after the transfection the specific antibiotic or an analogon was added to the medium. Selection with the neomycin analog Geneticin (G418) is based on the expression of a neomycin resistance gene located on the targeting vector after its integration into the genome. Transiently transfected cells loose the vectors with time and die together with non-transfected cells after a certain time of selection. The antibiotic G418 has been used at a concentration of 140 μ g/ml. Selection medium was applied for one week until round, light-breaking, and prominent colonies had formed and most of the single, non-proliferating cells

have died and detached from the plate. Colonies were picked with a 20 μ l pipette from the culture dish containing some PBS into a 96-well plate. By adding 50 μ l of trypsin to each well, colonies were dissociated and after a maximum time of 10 min, the reaction was stopped by adding 50 μ l of ES culturing medium. Cells were then triturated by pipetting and plated on a fresh 96-well plate with feeder cells in a total volume of 300 μ l medium. Medium was changed the next day to remove dead cells and cell debris. The cells had to be expanded into larger wells as soon as they reach about 80% confluency. Cells on 24-well plates were splitted onto several plates with feeder cells and plates coated with gelatin. Cells on a feeder layer were frozen at -80°C in 1x freezing medium or further expanded, and the ES cells on gelatin coated plates were cultivated until they are total confluent. This material could then be used for DNA extraction and genotyping of the according duplicate.

7.2.4.7 Screening for correctly recombined ES cell clones

Gelatine coated plates have been used for cultivating the cells for DNA extraction because of two reasons. On the one hand it is not necessary to keep the cells in the pluripotent ES cell state since this does not influence the genomic DNA; on the other hand, co-purified DNA out of the fibroblast cells would disturb the results of the genotyping. ES cells were grown to confluence, washed twice with PBS, and either directly used for DNA extraction or dried and frozen at -20°C for further analysis. Extraction of the DNA has been carried out directly in the multi-well dish using Promega's Wizard genomic DNA purification kit[®] following the manufacturer's instructions. Screening for homologous recombination events has been performed by Southern blotting as described in 7.2.1.5.

7.2.5 Animal husbandry

7.2.5.1 Animal facilities

All mice were kept and bred in the Helmholtz Zentrum Munich animal facilities in accordance with national and institutional guidelines. Mice were group-housed (if not mentioned else) with five mice per cage at maximum in open cages and maintained on a 12 hours light/dark cycle with food and water ad

libitum. The temperature was kept to $22 \pm 2^\circ\text{C}$ and relative humidity $55 \pm 5\%$. For breeding, single or double matings were set up and pups were weaned at an age of three weeks. At weaning mice got earmarks for identification. For subsequent genotyping, the tip of the tail (3 to 5 mm) was removed.

7.2.5.2 Blastocyst injection and embryo transfer

For the production of mouse blastocysts (E3.5), female C57BL/6J mice were superovulated to increase the number of ovulated oocytes. Superovulation was performed with PMSG (pregnant mare's serum gonadotropin), an analogon of the follicle-stimulating hormone (FSH) and hCG (human chorionic gonadotropin) an analogon of the luteinizing hormone (LH) (Stewart and Allen, 1995). The hormones were injected intraperitoneally (i. p.) at noon, starting with 7.5 units of PMSG to induce maturation of the follicles. 48 hours later 7.5 u of hCG, which initiates the ovulation of the oocytes, were injected. Directly after the injection of hCG, female mice were mated with one male of the same strain for 24 hours. The uteri of pregnant females were dissected 3 days post coitum and blastocysts were flushed out with M2 medium. One isolated blastocyst were fixed with a capillary of the micromanipulator and with a second capillary 10-20 mutant ES cells were injected into the blastocoel, where they will contribute to the inner cell mass. Pseudo-pregnant CD1 females were used as foster mothers for these early embryos. The pseudo-pregnancy was achieved by mating the females to sterile, vasectomized males. As anaesthesia for the embryo transfer normally 0.25 ml of 1% ketamine and 0.1% rompun in isotonic saline solution was used in a body weight dependent dosis. The retroperitoneal cavity of the foster mother was opened and ovaries and uterus were dissected. To avoid dehydration of the cornea and therefore prevent blindness of the mice, the eyes were kept wet with 0.9% NaCl during surgery. The proximal sides of the uterus were perforated with a thin cannula and up to 10 manipulated blastocysts per side were transferred to the uterus via this opening. The surgery field was closed again with clips and the foster mothers were kept on a warm plate until awakening.

7.2.5.3 Establishment of new genetically modified mouse lines

About two weeks (16 days) after the blastocysts have been transferred into foster mothers, chimeric mice were born, which consist partly of cells derived from the blastocyst used for injection and partly of cells derived from the genetically manipulated ES cells. Since the wild-type cells from the blastocyst code for black fur color and the modified ES cells code for agouti fur color, chimeric mice showed a mixture of black and agouti fur. The higher degree of agouti the higher is the contribution of the genetically manipulated ES cells to the chimera. Chimeras were mated to wild-type C57Bl/6J mice to obtain offspring with germline transmission of the modified allele. Mice, which have received the modified allele from their chimeric parent, were identified by genotyping via southern blotting (see 7.2.1.5).

7.2.6 Behavioural analysis

7.2.6.1 Tail suspension test

The tail suspension test was performed by fixing the animal's tail tip fixed with adhesive tape on the edge of a slit of a hard plastic cube, letting the mouse hang head down. For 6 min, activity and immobility behaviour was observed by a trained observer using a hand-held computer. Data were analyzed with respect to duration and frequency of activity or immobility periods; total duration, mean and maximum time of each behaviour aspect and latency to the first immobility period.

7.2.6.2 Accelerating rotarod

The motor coordination and balance was assessed using a rotating rod apparatus. The rod diameter was approx. 4.5 cm made of hard plastic material covered by soft black rubber foam with lane widths of 5 cm. The test phase consisted of three trials, interrupted by 15 min intervals. Three mice per trial were placed on the rod leaving an empty lane between two mice. The rod was initially rotating at constant speed (4 rpm) to allow positioning of all mice in their respective lanes. Once all mice were positioned, the trial was started and the rod accelerated from 4 rpm to 40 rpm in 300 sec. The latency and the speed at which each mouse fell off the rod were measured. Passive rotations

were counted as a fall off and the mouse was removed from the rod carefully. Subsequent each trial, the apparatus was disinfected and dried carefully.

7.2.6.3 Forced swim test

The procedure of the forced swimming was adapted from Ebner et al. (Ebner *et al.* 2002). The swimming apparatus consisted of a cylindrical glass beaker with 24.5 cm in diameter filled with water ($25 \pm 1^\circ\text{C}$) to a depth of 20 cm which was renewed before the next mouse was tested. Inside the cylinder, the mice are not able to climb or jump out, thus they are forced to swim. A trained observer recorded the animal's behaviour in moderate lighting conditions for 6 min with a handheld computer according to one of the following behaviours: struggling, defined as movements during which the forelimbs broke the water's surface; swimming, defined as movement of the animal induced by movements of the fore and hind limbs without breaking the water surface; and floating, defined as the behaviour during which the animal used limb movement just to keep its equilibrium without any movement of the trunk. After each trial, the mouse was dried with a tissue and put into a new cage.

7.2.6.4 Open field test

For initial testing the explorative behaviour of the animals, the open field test was used. The test is composed out of a 1 m² hard plastic arena with 25 cm high walls where the tested animal was put in one corner. Its movement in the open field was recorded by a camera for 10 min. For evaluation, the time the mouse spent in the centre area which is defined as the inner most 16% or 45% of the plane. Also the time in which the animal stayed close to the walls was considered. The open field was disinfected after each animal was tested.

7.2.6.5 Object recognition test

For testing recognition memory, the object recognition test utilizes the animal's tendency to interact more with an unfamiliar than with a familiar object (Bevins and Besheer, 2002). The object recognition test is carried out in a disinfected, empty cage. During three 5 min sample phases with intervals of 15 min, two equal metal cubes were presented to the mice. 3 hours after

the end of the third sample phase, the test animal was put again into the test area for a test phase of 5 min. At this time point, one of the now familiar metal cubes is exchanged by an unfamiliar plastic cube. 24 hours after the end of the last sample phase the animal was tested again for 5 min. In the second test phase one of the two objects in the cage was again the familiar metal cube; the second one was a counter of blue colour. The time the animal spent exploring each of the two different objects was documented during each of the two test phases. Mice with an intact recognition memory show significantly longer investigation duration of the unfamiliar object compared to the familiar one.

7.2.6.6 Social discrimination test

To test the social memory of the mice, the social discrimination procedure based on the previously described protocol by Engelmann *et al.* was used (Engelmann *et al.*, 1995). As a stimulus adult ovariectomised female mice were used to exclude additional sexual stimuli. Briefly, test animals were separated by transferring them to fresh cages 2 hours before starting the session. The social discrimination procedure consisted of two 4 min exposures of stimulus animals to the test animal in the test animal's home cage. During the first exposure one stimulus animal was exposed to the test animal, and after a retention interval of 2 hours, this stimulus animal was re-exposed to the test animal together with an additional, previously not presented stimulus animal. During each exposure the duration of investigatory behaviour of the test animal towards the stimulus animals was recorded by a trained observer blind to the genotype with a hand-held computer. Mice with an intact social memory show significantly longer investigation duration of the unfamiliar stimulus compared to the familiar one.

7.2.6.7 Odour preference test

This test, in contrast to the odour discrimination test, only determines whether the animals are in general able to smell and to between two different odours. The odours are on the one hand neutral litter (no odour) or used litter (odour) where a smelling mouse should show a preference to the odorous litter, due to their normal social behaviour. The test environment of the odour preference

test consists of an empty, disinfected cage with two holes in the bottom. In one of the holes an eppendorf tube with clean cage litter is placed (no odour), the second hole contained a tube filled with used litter from a cage of mice, unfamiliar to the test animal (odour). The test animal was put into the cage for 10 min, and the time it spent with olfactory exploration of the two tubes was determined and analysed.

7.2.6.8 Odour discrimination test-battery

Training and tests are carried out in a standard mouse cage (29.5cm x 18.5cm, height: 13cm); during each trial, one quarter of the cage is separated from the rest by a plexiglas screen. Two different odours are being used: Methyl trans-cinnamate (“strawberry”) and Phenethylacetate (“apple”). The odours are presented to the mouse in two small boxes ($\varnothing=3\text{cm}$, height: 1cm) filled with litter and separated by a small plexiglas screen. Every mouse is assigned to one personal odour (S+). During the training phase, food deprived animals do have to learn at three consecutive days to dig for small pieces of chocolate in small litter-filled boxes: On day one, the chocolate is placed on top of the litter – visible for the mouse; on the second day, one piece is placed on top one half buried a third one totally buried in the litter; on day three, only one piece is buried at the bottom of the box. If mice do not learn to dig for the chocolate until day three, an extra training day has to be inserted for these animals. The conditioning of the mice for a special odour is carried out for two days with 12 trials per day. The mice have to choose between two boxes; one box contains litter with a specific odour (S+), one box litter just with the solvent. For the first 6 correctly absolved trials, only S+ contains chocolate, for the following 6 trials both boxes contain the food.

For the odour discrimination test, the solvent is exchanged by another odour (S-) for which the mouse is not conditioned. Again for the first 6 correctly absolved trials only S+, for the following 6 trials also the S- box contains chocolate. After two days, the boxes contain mixtures of both odours ([S+]:[S-]: 100:0; 85:15; 70:30; 55:45; 53:47; 51:49, 50:50). Both boxes do contain chocolate, but the mouse is only allowed to dig for the food in the S+ box (12 trials for each mixture per day; 18 trials in case of 53:47 and 51:49). During

the odour sensitivity test, the mice have to discriminate between the solvent-containing box and the box with its specifically trained odour (S+) but in decreasing concentration. None of the boxes contain chocolate; the mouse receives the chocolate directly via forceps after digging in the correct box. Each mouse has to absolve three to five dilution steps each day according to the following scheme:

Dilution Stage	#1	#2	#3	#4	#5	#6	#8	...	#25
Concentration [S+]	5%	2.5%	1.25	0.62	0.31	0.155	0.03875	...	$3 \cdot 10^{-7}$

After three correct trials, the stage is absolved; if two mistakes are made in a row, the mouse has to return to the previous stage. Every mouse will reach its individual maximum stage, which is assumed as its sensitivity level.

7.2.6.9 Gait analysis

The *CatWalk*TM (Noldus; Wageningen, Netherlands) setup allows measuring several features of the dynamics of locomotion, including stride length, limb base of support and interlimb coordination (Hamers *et al.*, 2001). The mice have to cross a walkway made of Plexiglas walls spaced 10.5 cm apart with a glass floor (122 × 15 × 1cm). They are filmed from a ventral perspective while they pass the walkway. Light from an encased white fluorescent tube (117 cm long) is reflected onto the glass floor. Paw contact with the floor interrupts the light and is recorded by a camera. The *CatWalk*TM program automatically acquires, compresses, stores, and analyzes the gait parameters. Data analysis was performed by interactively categorizing and labeling the signals (right/left fore/hind paw, nose, abdomen, tail, and artifact). The position, size, and intensity of these pixels were analyzed and facilitated by using false colours for the display (for a sample picture see 5.6.3, Fig.51, upper left). From this, multiple parameters have been calculated: intensity of the paws (signal depends on the degree of contact between a paw and the glass plate and increases with increasing pressure), print length (length of the complete print),

print width (width (vertical direction) of the complete paw print), print area (surface area of the complete print), stand (duration of contact of a paw with the glass plate in a step cycle), swing (duration of no contact with the glass plate in a step cycle), swing speed (speed of the paw during swing), stand index (measure for the speed at which the paw loses contact with the glass plate), stride length (the distance between successive placements of the same paw), angle (estimate of the angle (in degrees) of the paw axis relative to the horizontal plane).

8 References

- Abeliovich A, Flint Beal M (2006).** Parkinsonism genes: culprits and clues. *J Neurochem* **99**(4), 1062-72.
- Abeliovich A, Schmitz Y, Fariñas I, Choi-Lundberg D, Ho WH, Castillo PE, Shinsky N, Verdugo JM, Armanini M, Ryan A, Hynes M, Phillips H, Sulzer D, Rosenthal A (2000).** Mice lacking alpha-synuclein display functional deficits in the nigrostriatal dopamine system. *Neuron* **25**(1), 239-52.
- Abramoff MD, Magelhaes PJ, Ram SJ (2004).** Image Processing with ImageJ. *Biophot Int* **11**(7), 36-42.
- Abysalh JC, Kuchnicki LL, Larochelle DA (2003).** The identification of pats1, a novel gene locus required for cytokinesis in Dictyostelium discoideum. *Mol Biol Cell* **14**(1), 14-25.
- Adams JR, van Netten H, Schulzer M, Mak E, Mckenzie J, Strongosky A, Sossi V, Ruth TJ, Lee CS, Farrer M, Gasser T, Uitti RJ, Calne DB, Wszolek ZK, Stoessl AJ (2005).** PET in LRRK2 mutations: comparison to sporadic Parkinson's disease and evidence for presymptomatic compensation. *Brain* **128**, 2777-85.
- Albin RL, Young AB, Penney JB (1989).** The functional anatomy of basal ganglia disorders. *Trends Neurosci* **12**(10), 366-75.
- Amende I, Kale A, McCue S, Glazier S, Morgan JP, Hampton TG(2005).** Gait dynamics in mouse models of Parkinson's disease and Huntington's disease. *J Neuroeng Rehabil* **2**, 20.
- Anand VS, Reichling LJ, Lipinski K, Stochaj W, Duan W, Kelleher K, Pungaliya P, Brown EL, Reinhart PH, Somberg R, Hirst WD, Riddle SM, Braithwaite SP (2009).** Investigation of leucine-rich repeat kinase 2: enzymological properties and novel assays. *FEBS J* **276**(2), 466-78.
- Andres-Mateos E, Mejias R, Sasaki M, Li X, Lin BM, Biskup S, Zhang L, Banerjee R, Thomas B, Yang L, Liu G, Beal MF, Huso DL, Dawson TM, Dawson VL (2009).** Unexpected lack of hypersensitivity in LRRK2 knock-out mice to MPTP (1-methyl-4-phenyl-1,2,3,6-tetrahydropyridine). *J Neurosci* **29**(50), 15846-50.
- Andrieux A, Salin PA, Vernet M, Kujala P, Baratier J, Gory-Fauré S, Bosc C, Pointu H, Proietto D, Schweitzer A, Denarier E, Klumperman J, Job D (2002).** The suppression of brain cold-stable microtubules in mice induces synaptic defects associated with neuroleptic-sensitive behavioral disorders. *Genes Dev* **16**(18), 2350-64.
- Ardayfio P, Moon J, Leung KK, Youn-Hwang D, Kim KS (2008).** Impaired learning and memory in Pitx3 deficient aphakia mice: a genetic model for striatum-dependent cognitive symptoms in Parkinson's disease. *Neurobiol Dis* **31**(3), 406-12.
- Augustinack JC, Schneider A, Mandelkow EM, Hyman BT (2002).** Specific tau phosphorylation sites correlate with severity of neuronal cytopathology in Alzheimer's disease. *Acta Neuropathol* **103**(1), 26-35.
- Avale ME, Faure P, Pons S, Robledo P, Deltheil T, David DJ, Gardier AM, Maldonado R, Granon S, Changeux JP, Maskos U (2008).** Interplay of beta2 nicotinic receptors and dopamine pathways in the control of spontaneous locomotion. *Proc Natl Acad Sci USA* **105**(41), 15991-6.

- Avila J, Pérez M, Lim F, Gómez-Ramos A, Hernández F, Lucas JJ (2004).** Tau in neurodegenerative diseases: tau phosphorylation and assembly. *Neurotox Res* **6(6)**, 477-82.
- Baas PW, Ahmad FJ, Pienkowski TP, Brown A, Black MM (1993).** Sites of microtubule stabilization for the axon. *J Neurosci* **13(5)**, 2177-85.
- Bacci A, Coco S, Pravettoni E, Schenk U, Armano S, Frassoni C, Verderio C, De Camilli P, Matteoli M (2001).** Chronic blockade of glutamate receptors enhances presynaptic release and downregulates the interaction between synaptophysin-synaptobrevin-vesicle-associated membrane protein 2. *J Neurosci* **21(17)**, 6588-96.
- Bader V, Ran Zhu X, Lübbert H, Stichel CC (2005).** Expression of DJ-1 in the adult mouse CNS. *Brain Res* **1041(1)**, 102-11.
- Baik JH, Picetti R, Saiardi A, Thiriet G, Dierich A, Depaulis A, Le Meur M, Borrelli E (1995).** Parkinsonian-like locomotor impairment in mice lacking dopamine D2 receptors. *Nature* **377(6548)**, 424-8.
- Ballatore C, Lee VM, Trojanowski JQ (2007).** Tau-mediated neurodegeneration in Alzheimer's disease and related disorders. *Nat Rev Neurosci* **8**, 663-672.
- Baltadjieva R, Giladi N, Gruendlinger L, Peretz C, Hausdorff JM (2006).** Marked alterations in the gait timing and rhythmicity of patients with de novo Parkinson's disease. *Eur J Neurosci* **24**, 1815
- Banker G, Goslin K (1998).** Culturing Nerve Cells, second edition. *The MIT Press*, Cambridge, Massachusetts
- Baratier J, Peris L, Brocard J, Gory-Fauré S, Dufour F, Bosc C, Fourest-Lieuvin A, Blanchoin L, Salin P, Job D, Andrieux A (2006).** Phosphorylation of microtubule-associated protein STOP by calmodulin kinase II. *J Biol Chem* **281(28)**, 19561-9.
- Barlow HB, Mollon JD (1982).** The senses. *Cambridge University Press*.
- Baskys A, Bayazitov I, Zhu E, Fang L, Wang R (2007).** Rab-mediated endocytosis: linking neurodegeneration, neuroprotection, and synaptic plasticity? *Ann N Y Acad Sci* **1122**, 313-29.
- Bateup HS, Santini E, Shen W, Birnbaum S, Valjent E, Surmeier DJ, Fisone G, Nestler EJ, Greengard P (2010).** Distinct subclasses of medium spiny neurons differentially regulate striatal motor behaviors. *Proc Natl Acad Sci USA* **107(33)**, 14845-50.
- Bauer M, Kinkl N, Meixner A, Kremmer E, Riemenschneider M, Förstl H, Gasser T, Ueffing M (2009).** Prevention of interferon-stimulated gene expression using microRNA-designed hairpins. *Gene Ther* **16(1)**, 142-7.
- Belin AC, Westerlund M (2008).** Parkinson's disease: a genetic perspective. *FEBS J* **275(7)**, 1377-83.
- Bella J, Hindle KL, McEwan PA, Lovell SC (2008).** The leucine-rich repeat structure. *Cell Mol Life Sci* **65(15)**, 2307-33.
- Benitez-King G, Ramírez-Rodríguez G, Ortíz L, Meza I (2004).** The neuronal cytoskeleton as a potential therapeutic target in neurodegenerative diseases and schizophrenia. *Curr Drug Targets CNS Neurol Disord* **3(6)**, 515-33.
- Berardelli A, Rothwell JC, Thompson PD, Hallett M (2001).** Pathophysiology of bradykinesia in Parkinson's disease. *Brain* **124(11)**, 2131-46.

- Berg D, Schweitzer K, Leitner P, Zimprich A, Lichtner P, Belcredi P, Brussel T, Schulte C, Maass S, Nagele T (2005).** Type and frequency of mutations in the LRRK2 gene in familial and sporadic Parkinson's disease. *Brain Dec* **128**, 3000-11.
- Bessa JM, Mesquita AR, Oliveira M, Pêgo JM, Cerqueira JJ, Palha JA, Almeida OF, Sousa N (2009).** A trans-dimensional approach to the behavioral aspects of depression. *Front Behav Neurosci* **3**, 1.
- Bevins RA, Besheer J (2006).** Object recognition in rats and mice: a one-trial non-matching-to-sample learning task to study 'recognition memory'. *Nat Protoc* **1(3)**, 1306-11.
- Bilen J, Bonini NM (2005).** Drosophila as a model for human neurodegenerative disease. *Annu Rev Genet* **39**, 153-71.
- Biskup S, Mueller JC, Sharma M, Lichtner P, Zimprich A, Berg D, Wüllner U, Illig T, Meitinger T, Gasser T (2005).** Common variants of LRRK2 are not associated with sporadic Parkinson's disease. *Ann Neurol* **58(6)**, 905-8.
- Biskup S, Moore DJ, Celsi F, Higashi S, West AB, Andrabi SA, Kurkinen K, Yu SW, Savitt JM, Waldvogel HJ, Faull RL, Emson PC, Torp R, Ottersen OP, Dawson TM, Dawson VL (2006).** Localization of LRRK2 to membranous and vesicular structures in mammalian brain. *Ann Neurol* **60(5)**, 557-69.
- Biskup S, Moore DJ, Rea A, Lorenz-Deperieux B, Coombes CE, Dawson VL, Dawson TM, West AB (2007).** Dynamic and redundant regulation of LRRK2 and LRRK1 expression. *BMC Neurosci* **8**, 102.
- Biskup S, West AB (2008).** Zeroing in on LRRK2-linked pathogenic mechanisms in Parkinson's disease. *Biochim Biophys Acta*.
- Blach-Olszewska Z, Leszek J (2007).** Mechanisms of over-activated innate immune system regulation in autoimmune and neurodegenerative disorders. *Neuropsychiatr Dis Treat* **3(3)**, 365-372.
- Black MM, Baas PW, Humphries S (1989).** Dynamics of alpha-tubulin deacetylation in intact neurons. *J Neurosci* **9(1)**, 358-68.
- Blandini F, Nappi G, Tassorelli C, Martignoni E (2000).** Functional changes of the basal ganglia circuitry in Parkinson's disease. *Prog Neurobiol* **62(1)**, 63-88.
- Bloem BR, van Vugt JP, Beckley DJ (2001).** Postural instability and falls in Parkinson's disease. *Adv Neurol* **87**, 209-23.
- Bonifati V, Rizzu P, van Baren MJ, Schaap O, Breedveld GJ, Krieger E, Dekker MC, Squitieri F, Ibanez P, Joesse M, van Dongen JW, Vanacore N, van Swieten JC, Brice A, Meco G, van Duijn CM, Oostra BA, Heutink P (2003).** Mutations in the DJ-1 gene associated with autosomal recessive early-onset parkinsonism. *Science* **299(5604)**, 256-9.
- Bosc C, Cronk JD, Pirollet F, Watterson DM, Haiech J, Job D, Margolis RL (1996).** Cloning, expression, and properties of the microtubule-stabilizing protein STOP. *Proc Natl Acad Sci USA* **93(5)**, 2125-30.
- Bosgraaf L, Russcher H, Smith JL, Wessels D, Soll DR, Van Haastert PJ (2002).** A novel cGMP signalling pathway mediating myosin phosphorylation and chemotaxis in Dictyostelium. *EMBO J* **21(17)**, 4560-70.
- Bosgraaf L, Van Haastert PJ (2003).** Roc, a Ras/GTPase domain in complex proteins. *Biochim Biophys Acta* **1643(1-3)**, 5-10.

- Bouquet C, Nothias F (2007).** Molecular mechanisms of axonal growth. *Adv Exp Med Biol* **621**, 1-16.
- Bouwknicht JA, Spiga F, Staub DR, Hale MW, Shekhar A, Lowry CA (2007).** Differential effects of exposure to low-light or high-light open-field on anxiety-related behaviors: relationship to c-Fos expression in serotonergic and non-serotonergic neurons in the dorsal raphe nucleus. *Brain Res Bull* **72(1)**, 32-43.
- Bozzi Y, Borrelli E (2006).** Dopamine in neurotoxicity and neuroprotection: what do D2 receptors have to do with it? *Trends Neurosci* **29(3)**, 167-74.
- Braak H, Del Tredici K, Rub U, de Vos RA, Jansen Steur EN, Braak E (2003).** Staging of brain pathology related to sporadic Parkinson's disease. *Neurobiol Aging* **24**, 197-211.
- Braak H, Rüb U, Del Tredici K (2006).** Cognitive decline correlates with neuropathological stage in Parkinson's disease. *J Neurol Sci* **248(1-2)**, 255-8.
- Brehm A, Miska EA, McCance DJ, Reid JL, Bannister AJ, Kouzarides T (1998).** Retinoblastoma protein recruits histone deacetylase to repress transcription. *Nature* **391(6667)**, 597-601.
- Bretscher A, Chambers D, Nguyen R, Reczek D (2000).** ERM-Merlin and EBP50 protein families in plasma membrane organization and function. *Annu Rev Cell Dev Biol* **16**, 113-43.
- Briley M, Chopin P, Moret C (1990).** Effect of serotonergic lesion on "anxious" behaviour measured in the elevated plus-maze test in the rat. *Psychopharmacology* **101**, 187-189.
- Brill MS, Ninkovic J, Winpenny E, Hodge RD, Ozen I, Yang R, Lepier A, Gascón S, Erdelyi F, Szabo G, Parras C, Guillemot F, Frotscher M, Berninger B, Hevner RF, Raineteau O, Götz M (2009).** Adult generation of glutamatergic olfactory bulb interneurons. *Nat Neurosci* **12(12)**, 1524-33.
- Brose N, Petrenko AG, Südhof TC, Jahn R (1992).** Synaptotagmin: a calcium sensor on the synaptic vesicle surface. *Science* **256(5059)**, 1021-5.
- Brown GL, Linnoila MI (1990).** CSF serotonin metabolite (5-HIAA) studies in depression, impulsivity, and violence. *J Clin Psychiatry* **51(Suppl)**, 31-41.
- Brun P, Bégou M, Andrieux A, Mouly-Badina L, Clerget M, Schweitzer A, Scarna H, Renaud B, Job D, Suaud-Chagny MF (2005).** Dopaminergic transmission in STOP null mice. *J Neurochem* **94(1)**, 63-73.
- Buchanan SG, Gay NJ (1996).** Structural and functional diversity in the leucine-rich repeat family of proteins. *Prog Biophys Mol Biol* **65**, 1-44.
- Buchman VL, Ninkina N (2008).** Modulation of alpha-synuclein expression in transgenic animals for modelling synucleinopathies--is the juice worth the squeeze? *Neurotox Res* **14(4)**, 329-41.
- Bulinski JC (2007).** Microtubule modification: acetylation speeds anterograde traffic flow. *Curr Biol* **17**, R18-R20.
- Bulinski JC, Gundersen GG (1991).** Stabilization of post-translational modification of microtubules during cellular morphogenesis. *Bioessays* **13(6)**, 285-93.
- Byler SL, Boehm GW, Karp JD, Kohman RA, Tarr AJ, Schallert T, Barth TM (2009).** Systemic lipopolysaccharide plus MPTP as a model of dopamine loss and gait instability in C57Bl/6J mice. *Behav Brain Res* **198(2)**, 434-9.

- Canli T, Lesch KP (2007).** Long story short: the serotonin transporter in emotion regulation and social cognition. *Nat Neurosci* **10(9)**, 1103-9.
- Carballo-Carbajal I, Weber-Endress S, Rovelli G, Chan D, Wolozin B, Klein CL, Patenge N, Gasser T, Kahle PJ (2010).** Leucine-rich repeat kinase 2 induces alpha-synuclein expression via the extracellular signal-regulated kinase pathway. *Cell Signal* **22(5)**, 821-7.
- Carland FM, McHale NA (1996).** LOP1: a gene involved in auxin transport and vascular patterning in Arabidopsis. *Development* **122(6)**, 1811-9.
- Carvey PM, Punati A, Newman MB (2006).** Progressive dopamine neuron loss in Parkinson's disease: the multiple hit hypothesis. *Cell Transplant* **15(3)**, 239-50.
- Chandra S, Fornai F, Kwon HB, Yazdani U, Atasoy D, Liu X, Hammer RE, Battaglia G, German DC, Castillo PE, Südhof TC (2004).** Double-knockout mice for alpha- and beta-synucleins: effect on synaptic functions. *Proc Natl Acad Sci USA* **101(41)**, 14966-71.
- Chandra S, Gallardo G, Fernández-Chacón R, Schlüter OM, Südhof TC (2005).** Alpha-synuclein cooperates with CSPalpha in preventing neurodegeneration. *Cell* **123(3)**, 383-96.
- Chandran JS, Lin X, Zapata A, Höke A, Shimoji M, Moore SO, Galloway MP, Laird FM, Wong PC, Price DL, Bailey KR, Crawley JN, Shippenberg T, Cai H (2008).** Progressive behavioral deficits in DJ-1-deficient mice are associated with normal nigrostriatal function. *Neurobiol Dis* **29(3)**, 505-14.
- Chang L, Jones Y, Ellisman MH, Goldstein LS, Karin M (2003).** JNK1 is required for maintenance of neuronal microtubules and controls phosphorylation of microtubule-associated proteins. *Dev Cell* **4(4)**, 521-33.
- Chen S, Spiegelberg BD, Lin F, Dell EJ, Hamm HE (2004).** Interaction of Gbetagamma with RACK1 and other WD40 repeat proteins. *J Mol Cell Cardiol* **37(2)**, 399-406.
- Chen L, Ding Y, Cagniard B, Van Laar AD, Mortimer A, Chi W, Hastings TG, Kang UJ, Zhuang X. (2008).** Unregulated cytosolic dopamine causes neurodegeneration associated with oxidative stress in mice. *J Neurosci* **28(2)**, 425-33.
- Cheng H, Almström S, Giménez-Llort L, Chang R, Ove Ogren S, Hoffer B, Olson L (1997).** Gait analysis of adult paraplegic rats after spinal cord repair. *Exp Neurol* **148(2)**, 544-57.
- Chenu F, David DJ, Leroux-Nicollet I, Le Maître E, Gardier AM, Bourin M (2008).** Serotonin1B heteroreceptor activation induces an antidepressant-like effect in mice with an alteration of the serotonergic system. *J Psychiatry Neurosci* **33(6)**, 541-50.
- Chou J, Harvey BK, Ebendal T, Hoffer B, Wang Y (2008).** Nigrostriatal alterations in bone morphogenetic protein receptor II dominant negative mice. *Acta Neurochir* **101**, 93-8.
- Chung KK, Zhang Y, Lim KL, Tanaka Y, Huang H, Gao J, Ross CA, Dawson VL, Dawson TM (2001).** Parkin ubiquitinates the alpha-synuclein-interacting protein, synphilin-1: implications for Lewy-body formation in Parkinson disease. *Nat Med* **7(10)**, 1144-50.
- Cnops G, Neyt P, Raes J, Petrarulo M, Nelissen H, Malenica N, Luschnig C, Tietz O, Ditengou F, Palme K, Azmi A, Prinsen E, Van Lijsebettens M (2006).** The TORNADO1 and TORNADO2 genes function in several patterning processes during early leaf development in Arabidopsis thaliana. *Plant Cell* **18(4)**, 852-66.
- Colebrooke RE, Humby T, Lynch PJ, McGowan DP, Xia J, Emson PC (2006).** Age-related decline in striatal dopamine content and motor performance occurs in the absence of nigral cell loss in a genetic mouse model of Parkinson's disease. *Eur J Neurosci* **24(9)**, 2622-30.

- Conde C, Cáceres A (2009).** Microtubule assembly, organization and dynamics in axons and dendrites. *Nat Rev Neurosci* **10**(5), 319-32.
- Cookson MR, Hardy J, Lewis PA (2008).** Genetic Neuropathology of Parkinson's Disease. *Int J Clin Exp Pathol* **1**(3), 217–231.
- Cools R (2008).** Role of dopamine in the motivational and cognitive control of behavior. *Neuroscientist* **14**(4), 381-95.
- Corbin R, Olsson-Carter K, Slack F (2009).** The role of microRNAs in synaptic development and function. *BMB Rep* **42**(3), 131-5.
- Couégnas A, Schweitzer A, Andrieux A, Ghandour MS, Boehm N (2007).** Expression pattern of STOP lacZ reporter gene in adult and developing mouse brain. *J Neurosci Res* **85**(7), 1515-27.
- Cryan JF, Page ME, Lucki I (2005).** Differential behavioral effects of the antidepressants reboxetine, fluoxetine, and moclobemide in a modified forced swim test following chronic treatment. *Psychopharmacology* **182**(3), 335-344.
- Cryan JF, Slattey DA (2007).** Animal models of mood disorders: Recent developments. *Curr Opin Psychiatry* **20**(1), 1-7.
- Cuello AC, Del Fiacco M, Paxinos G, Somogyi P, Priestley JV (1981).** Neuropeptides in striato-nigral pathways. *J Neural Transm* **51**(1-2), 83-96.
- Cunningham MG, Connor CM, Zhang K, Benes FM (2005).** Diminished serotonergic innervation of adult medial prefrontal cortex after 6-OHDA lesions in the newborn rat. *Brain Res Dev Brain Res* **157**(2), 124-31.
- Dächsel JC, Mata IF, Ross OA, Taylor JP, Lincoln SJ, Hinkle KM, Huerta C, Ribacoba R, Blazquez M, Alvarez V, Farrer MJ (2006).** Digenic parkinsonism: investigation of the synergistic effects of PRKN and LRRK2. *Neurosci Lett* **410**(2), 80-4.
- Dächsel JC, Taylor JP, Mok SS, Ross OA, Hinkle KM, Bailey RM, Hines JH, Szutu J, Madden B, Petrucelli L, Farrer MJ (2007).** Identification of potential protein interactors of Lrrk2. *Parkinsonism Relat Disord* **13**(7), 382-5.
- Dächsel JC, Behrouz B, Yue M, Beevers JE, Melrose HL, Farrer MJ (2010).** A comparative study of Lrrk2 function in primary neuronal cultures. *Parkinsonism Relat Disord*.
- Dächsel JC, Nishioka K, Vilariño-Güell C, Lincoln SJ, Soto-Ortolaza AI, Kachergus J, Hinkle KM, Heckman MG, Jasinska-Myga B, Taylor JP, Dickson DW, Gibson RA, Hentati F, Ross OA, Farrer MJ (2010).** Heterodimerization of Lrrk1-Lrrk2: Implications for LRRK2-associated Parkinson disease. *Mech Ageing Dev*.
- da Costa CA (2007).** DJ-1: a newcomer in Parkinson's disease pathology. *Curr Mol Med* **7**(7):650-7.
- Dagerlind A, Friberg K, Bean AJ, Hökfelt T (1992).** Sensitive mRNA detection using unfixed tissue: combined radioactive and non-radioactive in situ hybridisation histochemistry. *Histochemistry* **98**(1), 39-49.
- da Silva JS, Dotti CG (2002).** Breaking the neuronal sphere: regulation of the actin cytoskeleton in neuritogenesis. *Nat Rev Neurosci* **3**(9), 694-704.
- Dauer W, Przedborski S (2003).** Parkinson's disease: mechanisms and models. *Neuron* **39**(6), 889-909.

- Dawson TM, Ko HS, Dawson VL (2010).** Genetic animal models of Parkinson's disease. *Neuron* **66**(5), 646-61
- de Lau LM, Schipper CM, Hofman A, Koudstaal PJ, Breteler MM (2005).** Prognosis of Parkinson disease: risk of dementia and mortality: the Rotterdam Study. *Arch Neurol* **62**(8), 1265-9.
- De Leonibus E, Pascucci T, Lopez S, Oliverio A, Amalric M, Mele A (2007).** Spatial deficits in a mouse model of Parkinson disease. *Psychopharmacology (Berl)* **194**(4), 517-25.
- Delić S, Streif S, Deussing JM, Weber P, Ueffing M, Hölter SM, Wurst W, Kühn R (2008).** Genetic mouse models for behavioral analysis through transgenic RNAi technology. *Genes Brain Behav* **7**(7), 821-30.
- DeLong MR, Wichmann T (2007).** Circuits and circuit disorders of the basal ganglia. *Arch Neurol* **64**(1), 20-4.
- Deng J, Lewis PA, Greggio E, Sluch E, Beilina A, Cookson MR (2008).** Structure of the ROC domain from the Parkinson's disease-associated leucine-rich repeat kinase 2 reveals a dimeric GTPase. *Proc Natl Acad Sci USA* **105**(5), 1499-504.
- de Rijk MC, Breteler MM, Graveland GA, Ott A, Grobbee DE, van der Meché FG, Hofman A (1995).** Prevalence of Parkinson's disease in the elderly: the Rotterdam Study. *Neurology* **45**(12), 2143-6.
- Devine MJ, Lewis PA (2008).** Emerging pathways in genetic Parkinson's disease: tangles, Lewy bodies and LRRK2. *FEBS J* **275**(23), 5748-57.
- Dodson MW, Guo M (2007).** Pink1, Parkin, DJ-1 and mitochondrial dysfunction in Parkinson's disease. *Curr Opin Neurobiol* **17**(3):331-7.
- Dompierre JP, Godin JD, Charrin BC, Cordelières FP, King SJ, Humbert S, Saudou F (2007).** Histone deacetylase 6 inhibition compensates for the transport deficit in Huntington's disease by increasing tubulin acetylation. *J Neurosci* **27**(13), 3571-83.
- Dosemeci A, Tao-Cheng JH, Vinade L, Jaffe H (2006).** Preparation of postsynaptic density fraction from hippocampal slices and proteomic analysis. *Biochem Biophys Res Commun* **339**(2), 687-94.
- Doty RL (2008).** The olfactory vector hypothesis of neurodegenerative disease: is it viable? *Ann Neurol* **63**(1), 7-15.
- Ebner K, Wotjak CT, Landgraf R, Engelmann M (2002).** Forced swimming triggers vasopressin release within the amygdala to modulate stress-coping strategies in rats. *Eur J Neurosci* **15**(2), 384-388.
- Ekstrand MI, Terzioglu M, Galter D, Zhu S, Hofstetter C, Lindqvist E, Thams S, Bergstrand A, Hansson FS, Trifunovic A, Hoffer B, Cullheim S, Mohammed AH, Olson L, Larsson NG (2007).** Progressive parkinsonism in mice with respiratory-chain-deficient dopamine neurons. *Proc Natl Acad Sci USA* **104**(4), 1325-30.
- Engelmann M, Wotjak CT, Landgraf R (1995).** Social discrimination procedure: an alternative method to investigate juvenile recognition abilities in rats. *Physiol Behav* **58**(2), 315-21.
- Evans M, Kaufman M (1981).** Establishment in culture of pluripotential cells from mouse embryos. *Nature* **292**, 154-6.

- Fearnley JM, Lees AJ (1991).** Ageing and Parkinson's disease: substantia nigra regional selectivity. *Brain* 114, 2283-301.
- Ferraris A, Ialongo T, Passali GC, Pellecchia MT, Brusa L, Laruffa M, Guidubaldi A, Paludetti G, Albanese A, Barone P, Dallapiccola B, Valente EM, Bentivoglio AR (2009).** Olfactory dysfunction in Parkinsonism caused by PINK1 mutations. *Mov Disord* 24(16), 2350-7.
- Fernandez HH, See RH, Gary MF, Bowers D, Rodriguez RL, Jacobson C 4th, Okun MS (2009).** Depressive Symptoms in Parkinson Disease Correlate With Impaired Global and Specific Cognitive Performance. *J Geriatr Psychiatry Neurol*.
- Field EF, Metz GA, Pellis SM, Whishaw IQ (2006).** Sexually dimorphic postural adjustments during vertical behaviour are altered in a unilateral 6-OHDA rat model of Parkinson's disease. *Behav Brain Res* 174(1), 39-48.
- Fire A, Xu S, Montgomery MK, Kostas SA, Driver SE, Mello CC (1998).** Potent and specific genetic interference by double-stranded RNA in *Caenorhabditis elegans*. *Nature* 391(6669), 806-811.
- Fleming SM, Salcedo J, Fernagut PO, Rockenstein E, Masliah E, Levine MS, Chesselet MF (2004).** Early and progressive sensorimotor anomalies in mice overexpressing wild-type human alpha-synuclein. *J Neurosci* 24(42), 9434-40.
- Fleming SM, Tetreault NA, Mulligan CK, Hutson CB, Masliah E, Chesselet MF (2008).** Olfactory deficits in mice overexpressing human wildtype alpha-synuclein. *Eur J Neurosci* 28(2), 247-56.
- Forno LS (1996).** Neuropathology of Parkinson's disease. *J Neuropathol Exp Neurol* 55(3), 259-72.
- Franklin KBJ, Paxinos G (1997).** The mouse brain in stereotactic coordinates. *Academic Press, Inc., San Diego*.
- Franco S, MacKenzie KL, Dias S, Alvarez S, Rafii S, Moore MA (2001).** Clonal variation in phenotype and life span of human embryonic fibroblasts (MRC-5) transduced with the catalytic component of telomerase (hTERT). *Exp Cell Res* 268(1), 14-25.
- Fukushima N, Furuta D, Hidaka Y, Moriyama R, Tsujiuchi T (2009).** Post-translational modifications of tubulin in the nervous system. *J Neurochem*.
- Galter D, Westerlund M, Carmine A, Lindqvist E, Sydow O, Olson L (2006).** LRRK2 expression linked to dopamine-innervated areas. *Ann Neurol* 59(4), 714-9.
- Gan L, Mucke L (2008).** Paths of convergence: sirtuins in aging and neurodegeneration. *Neuron* 58(1), 10-4.
- Gandhi S, Muqit MM, Stanyer L, Healy DG, Abou-Sleiman PM, Hargreaves I, Heales S, Ganguly M, Parsons L, Lees AJ, Latchman DS, Holton JL, Wood NW, Revesz T (2006).** PINK1 protein in normal human brain and Parkinson's disease. *Brain* 129, 1720-31.
- Gandhi PN, Wang X, Zhu X, Chen SG, Wilson-Delfosse AL (2008).** The Roc domain of leucine-rich repeat kinase 2 is sufficient for interaction with microtubules. *J Neurosci Res* 86(8), 1711-20.
- Gandhi PN, Chen SG, Wilson-Delfosse AL (2009).** Leucine-rich repeat kinase 2 (LRRK2): a key player in the pathogenesis of Parkinson's disease. *J Neurosci Res* 87(6), 1283-95.

- Garske AL, Smith BC, Denu JM (2007).** Linking SIRT2 to Parkinson's disease. *ACS Chem Biol* **2**(8), 529-32.
- Gasper R, Meyer S, Gotthardt K, Sirajuddin M, Wittinghofer A (2009).** It takes two to tango: regulation of G proteins by dimerization. *Nat Rev Mol Cell Biol*.
- Gasser T (2007).** Update on the genetics of Parkinson's disease. *Mov Disord* **22**(17), S343-50.
- Gehrke S, Imai Y, Sokol N, Lu B (2010).** Pathogenic LRRK2 negatively regulates microRNA-mediated translational repression. *Nature* **466**(7306), 637-41.
- Georges PC, Hadzimichalis NM, Sweet ES, Firestein BL (2008).** The yin-yang of dendrite morphology: unity of actin and microtubules. *Mol Neurobiol* **38**(3), 270-84.
- Gerfen CR, Engber TM, Mahan LC, Susel Z, Chase TN, Monsma FJ Jr, Sibley DR (1990).** D1 and D2 dopamine receptor-regulated gene expression of striatonigral and striatopallidal neurons. *Science* **250**(4986), 1429-32.
- Giasson BI, Lee VM (2001).** Parkin and the molecular pathways of Parkinson's disease. *Neuron* **31**(6), 885-8.
- Giasson BI, Van Deerlin VM (2008).** Mutations in LRRK2 as a cause of Parkinson's disease. *Neurosignals* **16**(1), 99-105.
- Gibb WR, Mountjoy CQ, Mann DM, Lees AJ (1989).** A pathological study of the association between Lewy body disease and Alzheimer's disease. *J Neurol Neurosurg Psychiatry* **52**(6), 701-8.
- Gilks WP, Abou-Sleiman PM, Gandhi S, Jain S, Singleton A, Lees AJ, Shaw K, Bhatia KP, Bonifati V, Quinn NP, Lynch J, Healy DG, Holton JL, Revesz T, Wood NW (2005).** A common LRRK2 mutation in idiopathic Parkinson's disease. *Lancet* **365**(9457), 415-6.
- Giordana MT, D'Agostino C, Albani G, Mauro A, Di Fonzo A, Antonini A, Bonifati V (2007).** Neuropathology of Parkinson's disease associated with the LRRK2 Ile1371Val mutation. *Mov Disord* **22**(2), 275-8.
- Gloeckner CJ, Kinkl N, Schumacher A, Braun RJ, O'Neill E, Meitinger T, Kolch W, Prokisch H, Ueffing M (2006).** The Parkinson disease causing LRRK2 mutation I2020T is associated with increased kinase activity. *Hum Mol Genet* **15**(2), 223-32.
- Gloeckner CJ, Schumacher A, Boldt K, Ueffing M (2009).** The Parkinson disease-associated protein kinase LRRK2 exhibits MAPKKK activity and phosphorylates MKK3/6 and MKK4/7, in vitro. *J Neurochem*.
- Goldberg MS, Fleming SM, Palacino JJ, Cepeda C, Lam HA, Bhatnagar A, Meloni EG, Wu N, Ackerson LC, Klapstein GJ, Gajendiran M, Roth BL, Chesselet MF, Maidment NT, Levine MS, Shen J (2003).** Parkin-deficient mice exhibit nigrostriatal deficits but not loss of dopaminergic neurons. *J Biol Chem* **278**(44), 43628-35.
- Goldberg MS, Pisani A, Haburcak M, Vortherms TA, Kitada T, Costa C, Tong Y, Martella G, Tschertter A, Martins A, Bernardi G, Roth BL, Pothos EN, Calabresi P, Shen J (2005).** Nigrostriatal dopaminergic deficits and hypokinesia caused by inactivation of the familial Parkinsonism-linked gene DJ-1. *Neuron* **45**(4), 489-96.
- Goldwurm S, Zini M, Mariani L, Tesei S, Miceli R, Sironi F, Clementi M, Bonifati V, Pezzoli G (2007).** Evaluation of LRRK2 G2019S penetrance: relevance for genetic counseling in Parkinson disease. *Neurology* **68**(14), 1141-3.

- Görner K, Holtorf E, Waak J, Pham TT, Vogt-Weisenhorn DM, Wurst W, Haass C, Kahle PJ (2007).** Structural determinants of the C-terminal helix-kink-helix motif essential for protein stability and survival promoting activity of DJ-1. *J Biol Chem* **282**(18), 13680-91.
- Grace AA (2008).** Physiology of the normal and dopamine-depleted basal ganglia: insights into levodopa pharmacotherapy. *Mov Disord* **23**, S560-9.
- Green KN, Steffan JS, Martinez-Coria H, Sun X, Schreiber SS, Thompson LM, LaFerla FM (2008).** Nicotinamide restores cognition in Alzheimer's disease transgenic mice via a mechanism involving sirtuin inhibition and selective reduction of Thr231-phosphotau. *J Neurosci* **28**(45), 11500-10.
- Greenbaum D, Colangelo C, Williams K, Gerstein M (2003).** Comparing protein abundance and mRNA expression levels on a genomic scale. *Genome Biol* **4**(9), 117.
- Greer K, Maruta H, L'Hernault SW, Rosenbaum JL (1985).** Alpha-tubulin acetylase activity in isolated *Chlamydomonas flagella*. *J Cell Biol* **101**(6), 2081-4.
- Greggio E, Jain S, Kingsbury A, Bandopadhyay R, Lewis P, Kaganovich A, van der Brug MP, Beilina A, Blackinton J, Thomas KJ, Ahmad R, Miller DW, Kesavapany S, Singleton A, Lees A, Harvey RJ, Harvey K, Cookson MR (2006).** Kinase activity is required for the toxic effects of mutant LRRK2/dardarin. *Neurobiol Dis* **23**(2), 329-41.
- Greggio E, Lewis PA, van der Brug MP, Ahmad R, Kaganovich A, Ding J, Beilina A, Baker AK, Cookson MR (2007).** Mutations in LRRK2/dardarin associated with Parkinson disease are more toxic than equivalent mutations in the homologous kinase LRRK1. *J Neurochem* **102**(1), 93-102.
- Greggio E, Zambrano I, Kaganovich A, Beilina A, Taymans JM, Daniëls V, Lewis P, Jain S, Ding J, Syed A, Thomas KJ, Baekelandt V, Cookson MR (2008).** The Parkinson disease-associated leucine-rich repeat kinase 2 (LRRK2) is a dimer that undergoes intramolecular autophosphorylation. *J Biol Chem* **283**(24), 16906-14.
- Groth AC, Olivares EC, Thyagarajan B, Calos MP (2000).** A phage integrase directs efficient site-specific integration in human cells. *Proc Natl Acad Sci USA* **97**, 5995-6000.
- Gründemann J, Schlaudraff F, Haeckel O, Liss B (2008).** Elevated alpha-synuclein mRNA levels in individual UV-laser-microdissected dopaminergic substantia nigra neurons in idiopathic Parkinson's disease. *Nucleic Acids Res* **36**(7).
- Gu L, Cui T, Fan C, Zhao H, Zhao C, Lu L, Yang H (2009).** Involvement of ERK1/2 signaling pathway in DJ-1-induced neuroprotection against oxidative stress. *Biochem Biophys Res Commun* **383**(4), 469-74.
- Guillaud L, Bosc C, Fourest-Lieuvin A, Denarier E, Pirolet F, Lafanechère L, Job D (1998).** STOP proteins are responsible for the high degree of microtubule stabilization observed in neuronal cells. *J Cell Biol* **142**(1), 167-79.
- Guillot TS, Asress SA, Richardson JR, Glass JD, Miller GW (2008).** Treadmill gait analysis does not detect motor deficits in animal models of Parkinson's disease or amyotrophic lateral sclerosis. *J Mot Behav* **40**(6), 568-77.
- Gundersen GG, Bulinski JC (1986).** Distribution of tyrosinated and nontyrosinated alpha-tubulin during mitosis. *J Cell Biol* **102**, 1118-1126.
- Guo H, Ingolia NT, Weissman JS, Bartel DP (2010).** Mammalian microRNAs predominantly act to decrease target mRNA levels. *Nature* **466**(7308), 835-40.

- Guo L, Gandhi PN, Wang W, Petersen RB, Wilson-Delfosse AL, Chen SG (2007).** The Parkinson's disease-associated protein, leucine-rich repeat kinase 2 (LRRK2), is an authentic GTPase that stimulates kinase activity. *Exp Cell Res* **313**(16), 3658-70.
- Guttman M (1992).** Dopamine receptors in Parkinson's disease. *Neurol Clin* **10**(2), 377-86.
- Haebig K, Gloeckner CJ, Miralles MG, Gillardon F, Schulte C, Riess O, Ueffing M, Biskup S, Bonin M (2010).** ARHGEF7 (Beta-PIX) acts as guanine nucleotide exchange factor for leucine-rich repeat kinase 2. *PLoS One* **5**(10).
- Haehner A, Hummel T, Reichmann H (2009).** Olfactory dysfunction as a diagnostic marker for Parkinson's disease. *Expert Rev Neurother* **9**(12), 1773-9.
- Hallberg B, Rayter SI, Downward J (1994).** Interaction of Ras and Raf in intact mammalian cells upon extracellular stimulation. *J Biol Chem* **269**(6), 3913-6.
- Hamers FP, Lankhorst AJ, van Laar TJ, Veldhuis WB, Gispen WH (2001).** Automated quantitative gait analysis during overground locomotion in the rat: its application to spinal cord contusion and transection injuries. *J Neurotrauma* **18**(2), 187-201.
- Hamers FP, Koopmans GC, Joosten EA (2006).** CatWalk-assisted gait analysis in the assessment of spinal cord injury. *J Neurotrauma* **23**(3-4), 537-48.
- Hammond JW, Cai D, Verhey KJ (2008).** Tubulin modifications and their cellular functions. *Curr Opin Cell Biol* **20**(1), 71-6.
- Hampton TG, Amende I (2010).** Treadmill gait analysis characterizes gait alterations in Parkinson's disease and amyotrophic lateral sclerosis mouse models. *J Mot Behav* **42**(1), 1-4.
- Han BS, Iacovitti L, Katano T, Hattori N, Seol W, Kim KS (2008).** Expression of the LRRK2 gene in the midbrain dopaminergic neurons of the substantia nigra. *Neurosci Lett* **442**(3), 190-4.
- Hardy J, Cai H, Cookson MR, Gwinn-Hardy K, Singleton A (2006).** Genetics of Parkinson's disease and parkinsonism. *Ann Neurol* **60**, 389-398.
- Harvey BK, Wang Y, Hoffer BJ (2008).** Transgenic rodent models of Parkinson's disease. *Acta Neurochir Suppl* **101**, 89-92.
- Hasegawa S, Furuichi T, Yoshida T, Endoh K, Kato K, Sado M, Maeda R, Kitamoto A, Miyao T, Suzuki R, Homma S, Masushige S, Kajii Y, Kida S (2009).** Transgenic up-regulation of alpha-CaMKII in forebrain leads to increased anxiety-like behaviors and aggression. *Mol Brain* **2**(1), 6.
- Hatano T, Kubo S, Imai S, Maeda M, Ishikawa K, Mizuno Y, Hattori N (2007).** Leucine-rich repeat kinase 2 associates with lipid rafts. *Hum Mol Genet* **16**(6), 678-90.
- Haugarvoll K, Toft M, Ross OA, White LR, Aasly JO, Farrer MJ (2007).** Variants in the LRRK1 gene and susceptibility to Parkinson's disease in Norway. *Neurosci Lett* **416**(3), 299-301.
- Haugarvoll K, Rademakers R, Kachergus JM, Nuytemans K, Ross OA, Gibson JM, Tan EK, Gaig C, Tolosa E, Goldwurm S, Guidi M, Riboldazzi G, Brown L, Walter U, Benecke R, Berg D, Gasser T, Theuns J, Pals P, Cras P, De Deyn PP, Engelborghs S, Pickut B, Uitti RJ, Foroud T, Nichols WC, Hagenah J, Klein C, Samii A, Zabetian CP, Bonifati V, Van Broeckhoven C, Farrer MJ, Wszolek ZK (2008).** Lrrk2 R1441C parkinsonism is clinically similar to sporadic Parkinson disease. *Neurology* **70**, 1456-60.

- Hausdorff JM, Cudkovicz ME, Firtion R, Wei JY, Goldberger AL (1998).** Gait variability and basal ganglia disorders: stride-to-stride variations of gait cycle timing in Parkinson's disease and Huntington's disease. *Mov Disord* **13**(3), 428-37.
- Healy DG, Falchi M, O'Sullivan SS, Bonifati V, Durr A, Bressman S, Brice A, Aasly J, Zabetian CP, Goldwurm S, Ferreira JJ, Tolosa E, Kay DM, Klein C, Williams DR, Marras C, Lang AE, Wszolek ZK, Berciano J, Schapira AH, Lynch T, Bhatia KP, Gasser T, Lees AJ, Wood NW; International LRRK2 Consortium (2008).** Phenotype, genotype, and worldwide genetic penetrance of LRRK2-associated Parkinson's disease: a case-control study. *Lancet Neurol* **7**(7), 583-90.
- Hemmings HC Jr, Greengard P (1986).** DARPP-32, a dopamine- and adenosine 3':5'-monophosphate-regulated phosphoprotein: regional, tissue, and phylogenetic distribution. *J Neurosci* **6**(5), 1469-81.
- Heo HY, Park JM, Kim CH, Han BS, Kim KS, Seol W (2010).** LRRK2 enhances oxidative stress-induced neurotoxicity via its kinase activity. *Exp Cell Res* **316**(4), 649-56.
- Hettema JM (2008).** What is the genetic relationship between anxiety and depression? *Am J Med Genet C Semin Med Genet* **148**(2), 140-6.
- Higashi S, Moore DJ, Colebrooke RE, Biskup S, Dawson VL, Arai H, Dawson TM, Emson PC (2007/1).** Expression and localization of Parkinson's disease-associated leucine-rich repeat kinase 2 in the mouse brain. *J Neurochem* **100**(2), 368-81.
- Higashi S, Biskup S, West AB, Trinkaus D, Dawson VL, Faull RL, Waldvogel HJ, Arai H, Dawson TM, Moore DJ, Emson PC (2007/2).** Localization of Parkinson's disease-associated LRRK2 in normal and pathological human brain. *Brain Res* **1155**, 208-19.
- Hitz C, Wurst W, Kühn R (2007).** Conditional brain-specific knockdown of MAPK using Cre/loxP regulated RNA interference. *Nucleic Acids Res* **35**(12), e90.
- Ho CC, Rideout HJ, Ribe E, Troy CM, Dauer WT (2009).** The Parkinson disease protein leucine-rich repeat kinase 2 transduces death signals via Fas-associated protein with death domain and caspase-8 in a cellular model of neurodegeneration. *J Neurosci* **29**(4), 1011-6.
- Hohmann CF, Walker EM, Boylan CB, Blue ME (2007).** Neonatal serotonin depletion alters behavioral responses to spatial change and novelty. *Brain Res* **1139**, 163-77.
- Horiuchi D, Collins CA, Bhat P, Barkus RV, Diantonio A, Saxton WM (2007).** Control of a kinesin-cargo linkage mechanism by JNK pathway kinases. *Curr Biol* **17**(15), 1313-7.
- Hornung JP (2003).** The human raphe nuclei and the serotonergic system. *J Chem Neuroanat* **26**(4), 331-43.
- Hu Y, Tong Y (2010).** A trojan horse for Parkinson's disease. *Sci Signal* **3**(116).
- Hubbard TJP, Aken BL, Beal K, Ballester B, Caccamo M, Chen Y, Clarke L, Coates G, Cunningham F, Cutts T, Down T, Dyer SC, Fitzgerald S, Fernandez-Banet J, Graf S, Haider S, Hammond M, Herrero J, Holland R, Howe K, et al (2007)** Ensembl 2007. *Nucleic Acids Res* **35**.
- Hubbert C, Guardiola A, Shao R, Kawaguchi Y, Ito A, Nixon A, Yoshida M, Wang XF, Yao TP (2002).** HDAC6 is a microtubule-associated deacetylase. *Nature* **417**(6887), 455-8.
- Huisman E, Uylings HB, Hoogland PV (2004).** A 100% increase of dopaminergic cells in the olfactory bulb may explain hyposmia in Parkinson's disease. *Mov Disord* **19**(6), 687-92.

- Huisman E, Uylings HB, Hoogland PV (2008).** Gender-related changes in increase of dopaminergic neurons in the olfactory bulb of Parkinson's disease patients. *Mov Disord* **23**(10), 1407-13.
- Hsia AY, Vincent JD, Lledo PM (1999).** Dopamine depresses synaptic inputs into the olfactory bulb. *J Neurophysiol* **82**, 1082-5.
- Hunt CA, Schenker LJ, Kennedy MB (1996).** PSD-95 is associated with the postsynaptic density and not with the presynaptic membrane at forebrain synapses. *J Neurosci* **16**(4), 1380-8.
- Hurtado-Lorenzo A, Anand VS (2008).** Heat shock protein 90 modulates LRRK2 stability: potential implications for Parkinson's disease treatment. *J Neurosci* **28**(27), 6757-9.
- Hwang DY, Ardayfio P, Kang UJ, Semina EV, Kim KS (2003).** Selective loss of dopaminergic neurons in the substantia nigra of Pitx3-deficient aphakia mice. *Brain Res Mol Brain Res* **114**(2), 123-31.
- Hyman AA, Karsenti E (1996).** Morphogenic properties of microtubules and mitotic spindle assembly. *Cell* **84**, 401-10.
- Iaccarino C, Crosio C, Vitale C, Sanna G, Carri MT, Barone P (2007).** Apoptotic mechanisms in mutant LRRK2-mediated cell death. *Hum Mol Genet* **16**(11), 1319-26.
- Imai Y, Gehrke S, Wang HQ, Takahashi R, Hasegawa K, Oota E & Lu B (2008).** Phosphorylation of 4E-BP by LRRK2 affects the maintenance of dopaminergic neurons in *Drosophila*. *EMBO J* **27**, 2432-2443
- Ishihara L, Warren L, Gibson R, Amouri R, Lesage S, Dürr A, Tazir M, Wszolek ZK, Uitti RJ, Nichols WC, Griffith A, Hattori N, Leppert D, Watts R, Zabetian CP, Foroud TM, Farrer MJ, Brice A, Middleton L, Hentati F (2006).** Clinical features of Parkinson disease patients with homozygous leucine-rich repeat kinase 2 G2019S mutations. *Arch Neurol* **63**(9), 1250-4.
- Ito G, Okai T, Fujino G, Takeda K, Ichijo H, Katada T, Iwatsubo T (2007).** GTP binding is essential to the protein kinase activity of LRRK2, a causative gene product for familial Parkinson's disease. *Biochemistry* **46**(5), 1380-8.
- Jaleel M, Nichols RJ, Deak M, Campbell DG, Gillardon F, Knebel A, Alessi DR (2007).** LRRK2 phosphorylates moesin at threonine-558: characterization of how Parkinson's disease mutants affect kinase activity. *Biochem J* **405**(2), 307-17.
- Jankovic J (2008).** Parkinson's disease: clinical features and diagnosis. *J Neurol Neurosurg Psychiatry* **79**(4), 368-76.
- Janssens S, Beyaert R (2003).** Functional diversity and regulation of different interleukin-1 receptor-associated kinase (IRAK) family members. *Mol Cell* **11**(2), 293-302.
- Jenkins PM, McEwen DP, Martens JR (2009).** Olfactory cilia: linking sensory cilia function and human disease. *Chem Senses* **34**(5), 451-64.
- Jensen F, Koprowski H, Ponten JA (1963).** Rapid Transformation of Human Fibroblast Cultures by Simian Virus. *Proc Natl Acad Sci USA* **50**, 343-348.
- Jia H, Li X, Gao H, Feng Z, Li X, Zhao L, Jia X, Zhang H, Liu J (2008).** High doses of nicotinamide prevent oxidative mitochondrial dysfunction in a cellular model and improve motor deficit in a *Drosophila* model of Parkinson's disease. *J Neurosci Res* **86**(9), 2083-90.

- Jiang Q, Ren Y, Feng J (2008).** Direct binding with histone deacetylase 6 mediates the reversible recruitment of parkin to the centrosome. *J Neurosci* **28**(48), 12993-3002.
- Jones R (2010).** The roles of PINK1 and Parkin in Parkinson's disease. *PLoS Biol* **8**(1).
- Junn E, Lee KW, Jeong BS, Chan TW, Im JY, Mouradian MM (2009).** Repression of alpha-synuclein expression and toxicity by microRNA-7. *Proc Natl Acad Sci USA* **106**(31), 13052-7.
- Kahle PJ, Neumann M, Ozmen L, Müller V, Odoj S, Okamoto N, Jacobsen H, Iwatsubo T, Trojanowski JQ, Takahashi H, Wakabayashi K, Bogdanovic N, Riederer P, Kretzschmar HA, Haass C (2001).** Selective insolubility of alpha-synuclein in human Lewy body diseases is recapitulated in a transgenic mouse model. *Am J Pathol* **159**(6), 2215-25.
- Kamata H, Honda S, Maeda S, Chang L, Hirata H, Karin M (2005).** Reactive oxygen species promote TNFalpha-induced death and sustained JNK activation by inhibiting MAP kinase phosphatases. *Cell* **120**(5), 649-61.
- Kaufman MH (1992).** The atlas of mouse development. *Academic Press Ltd., London*.
- Kaufman S (1995).** Tyrosine hydroxylase. *Adv Enzymol Relat Areas Mol Biol* **70**, 103-220.
- Kawaguchi Y, Kovacs JJ, McLaurin A, Vance JM, Ito A, Yao TP (2003).** The deacetylase HDAC6 regulates aggresome formation and cell viability in response to misfolded protein stress. *Cell* **115**(6), 727-38.
- Kingsbury AE, Daniel SE, Sangha H, Eisen S, Lees AJ, Foster OJ (2004).** Alteration in alpha-synuclein mRNA expression in Parkinson's disease. *Mov Disord* **19**(2), 162-70.
- Kiriakidou M, Tan GS, Lamprinaki S, De Planell-Saguer M, Nelson PT, Mourelatos Z (2007).** An mRNA m7G cap binding-like motif within human Ago2 represses translation. *Cell* **129**(6), 1141-51.
- Kirik D, Rosenblad C, Burger C, Lundberg C, Johansen TE, Muzyczka N, Mandel RJ, Björklund A (2002).** Parkinson-like neurodegeneration induced by targeted overexpression of alpha-synuclein in the nigrostriatal system. *J Neurosci* **22**(7), 2780-91.
- Kitada T, Asakawa S, Hattori N, Matsumine H, Yamamura Y, Minoshima S, Yokochi M, Mizuno Y, Shimizu N (1998).** Mutations in the parkin gene cause autosomal recessive juvenile parkinsonism. *Nature* **392**(6676), 605-8.
- Kitada T, Pisani A, Karouani M, Haburcak M, Martella G, Tscherter A, Platania P, Wu B, Pothos EN, Shen J (2009).** Impaired Dopamine Release and Synaptic Plasticity in the Striatum of Parkin^{-/-} Mice. *J Neurochem*.
- Klein CL, Rovelli G, Springer W, Schall C, Gasser T, Kahle PJ (2009).** Homo- and heterodimerization of ROCO kinases: LRRK2 kinase inhibition by the LRRK2 ROCO fragment. *J Neurochem* **111**(3), 703-15.
- Ko HS, Bailey R, Smith WW, Liu Z, Shin JH, Lee YI, Zhang YJ, Jiang H, Ross CA, Moore DJ, Patterson C, Petrucelli L, Dawson TM, Dawson VL (2009).** CHIP regulates leucine-rich repeat kinase-2 ubiquitination, degradation, and toxicity. *Proc Natl Acad Sci USA* **106**(8), 2897-902.
- Kobayashi N, Mundel P (1998).** A role of microtubules during the formation of cell processes in neuronal and non-neuronal cells. *Cell Tissue Res* **291**(2), 163-74.

- Koprowski H, Ponten J, Jensen F, Ravdin RG, Moorhead P, Saksela E (1963).** Transformation of cultures of human tissue infected with simian virus SV40. *Acta Unio Int Contra Cancrum* **19**, 362-367.
- Korr D, Toschi L, Donner P, Pohlenz HD, Kreft B, Weiss B (2006).** LRRK1 protein kinase activity is stimulated upon binding of GTP to its Roc domain. *Cell Signal* **18**(6), 910-20.
- Kraszewski K, Mundigl O, Daniell L, Verderio C, Matteoli M, De Camilli P (1995).** Synaptic vesicle dynamics in living cultured hippocampal neurons visualized with CY3-conjugated antibodies directed against the luminal domain of synaptotagmin. *J Neurosci* **15**(6), 4328-42.
- Kreitzer AC, Malenka RC (2008).** Striatal plasticity and basal ganglia circuit function. *Neuron* **60**(4), 543-54.
- Kühn K, Zhu XR, Lübbert H, Stichel CC (2004).** Parkin expression in the developing mouse. *Brain Res Dev Brain Res* **149**(2), 131-42.
- Kühn R, Streif S, Wurst W (2007).** RNA interference in mice. *Handb Exp Pharmacol* **178**, 149-76.
- Kumar A, Greggio E, Beilina A, Kaganovich A, Chan D, Taymans JM, Wolozin B, Cookson MR (2010).** The Parkinson's disease associated LRRK2 exhibits weaker in vitro phosphorylation of 4E-BP compared to autophosphorylation. *PLoS One* **5**(1).
- Kurachi M, Komiya Y, Tashiro T (1999).** Biophysical properties of stable microtubules in neurites revealed by optical techniques. *Cell Struct Funct* **24**(5), 405-12.
- Laemmli UK (1970).** Cleavage of structural proteins during the assembly of the head of bacteriophage T4. *Nature* **227**, 680-685.
- Langston JW, Ballard P, Tetrud JW, Irwin I (1983).** Chronic Parkinsonism in humans due to a product of meperidine-analog synthesis. *Science* **219**(4587), 979-80.
- Lee VMY, Goedert M, Trojanowski JQ (2001).** Neurodegenerative tauopathies. *Annu Rev Neurosci* **24**, 1121-1159.
- Lee Y, Jeon K, Lee JT, Kim S, Kim VN (2002).** MicroRNA maturation: stepwise processing and subcellular localization. *EMBO J* **21**(17), 4663-70.
- Lee E, Hui S, Ho G, Tan EK, Chen CP (2006).** LRRK2 G2019S and I2020T mutations are not common in Alzheimer's disease and vascular dementia. *Am J Med Genet B Neuropsychiatr Genet* **141B**(5), 549-50.
- Lee SB, Kim W, Lee S, Chung J (2007).** Loss of LRRK2/PARK8 induces degeneration of dopaminergic neurons in Drosophila. *Biochem Biophys Res Commun* **358**(2), 534-9.
- Lemke MR, Fuchs G, Gemende I, Herting B, Oehlwein C, Reichmann H, Rieke J, Volkman J (2004).** Depression and Parkinson's disease. *J Neurol* **251**, VI/24-7.
- Leng Y, Chuang DM (2006).** Endogenous alpha-synuclein is induced by valproic acid through histone deacetylase inhibition and participates in neuroprotection against glutamate-induced excitotoxicity. *J Neurosci* **26**(28), 7502-12.
- Lesage S, Brice A (2009).** Parkinson's disease: from monogenic forms to genetic susceptibility factors. *Hum Mol Genet* **18**(R1), R48-59.
- Leung IW, Lassam N (1998).** Dimerization via tandem leucine zippers is essential for the activation of the mitogen-activated protein kinase kinase kinase, MLK-3. *J Biol Chem* **273**(49), 32408-15.

- Lewis PA (2009).** The function of Roco proteins in health and disease. *Biol Cell* **101**(3), 183-91.
- Lewis SJ, Barker RA (2009).** Understanding the dopaminergic deficits in Parkinson's disease: insights into disease heterogeneity. *J Clin Neurosci* **16**(5), 620-5.
- Lewis PA, Greggio E, Beilina A, Jain S, Baker A, Cookson MR (2007).** The R1441C mutation of LRRK2 disrupts GTP hydrolysis. *Biochem Biophys Res Commun* **357**(3), 668-71.
- Li J, Yen C, Liaw D, Podsypanina K, Bose S, Wang SI, Puc J, Miliaresis C, Rodgers L, McCombie R, Bigner SH, Giovanella BC, Ittmann M, Tycko B, Hibshoosh H, Wigler MH, Parsons R (1997).** PTEN, a putative protein tyrosine phosphatase gene mutated in human brain, breast, and prostate cancer. *Science* **275**(5308), 1943-7.
- Li W, Zhang B, Tang J, Cao Q, Wu Y, Wu C, Guo J, Ling EA, Liang F (2007).** Sirtuin 2, a mammalian homolog of yeast silent information regulator-2 longevity regulator, is an oligodendroglial protein that decelerates cell differentiation through deacetylating alpha-tubulin. *J Neurosci* **27**(10), 2606-16.
- Li X, Tan YC, Poulouse S, Olanow CW, Huang XY, Yue Z (2007).** Leucine-rich repeat kinase 2 (LRRK2)/PARK8 possesses GTPase activity that is altered in familial Parkinson's disease R1441C/G mutants. *J Neurochem* **103**(1), 238-47.
- Li Y, Liu W, Oo TF, Wang L, Tang Y, Jackson-Lewis V, Zhou C, Geghman K, Bogdanov M, Przedborski S, Beal MF, Burke RE, Li C (2009).** Mutant LRRK2(R1441G) BAC transgenic mice recapitulate cardinal features of Parkinson's disease. *Nat Neurosci* **12**(7), 826-8.
- Li X, Patel JC, Wang J, Avshalumov MV, Nicholson C, Buxbaum JD, Elder GA, Rice ME, Yue Z (2010).** Enhanced striatal dopamine transmission and motor performance with LRRK2 overexpression in mice is eliminated by familial Parkinson's disease mutation G2019S. *J Neurosci* **30**(5), 1788-97.
- Lieuvin A, Labbé JC, Dorée M, Job D (1994).** Intrinsic microtubule stability in interphase cells. *J Cell Biol* **124**(6), 985-96.
- Lin CH, Tsai PI, Wu RM, Chien CT (2010).** LRRK2 G2019S mutation induces dendrite degeneration through mislocalization and phosphorylation of tau by recruiting autoactivated GSK3 β . *J Neurosci* **30**(39), 13138-49.
- Liu Z, Wang X, Yu Y, Li X, Wang T, Jiang H, Ren Q, Jiao Y, Sawa A, Moran T, Ross CA, Montell C, Smith WW (2008).** A Drosophila model for LRRK2-linked parkinsonism. *Proc Natl Acad Sci USA* **105**(7), 2693-8.
- Lohmann E, Periquet M, Bonifati V, Wood NW, De Michele G, Bonnet AM, Fraix V, Broussolle E, Horstink MW, Vidailhet M, Verpillat P, Gasser T, Nicholl D, Teive H, Raskin S, Rascol O, Destée A, Ruberg M, Gasparini F, Meco G, Agid Y, Durr A, Brice A (2003).** How much phenotypic variation can be attributed to parkin genotype? *Ann Neurol* **54**(2), 176-85
- Love S, Louis D, Ellison D (eds) (2008).** Greenfield's Neuropathology. Oxford University Press, 8th edition.
- Lucki I (1998).** The spectrum of behaviors influenced by serotonin. *Biol Psychiatry* **44**, 151-162.
- Lücking CB, Dürr A, Bonifati V, Vaughan J, De Michele G, Gasser T, Harhangi BS, Meco G, Denèfle P, Wood NW, Agid Y, Brice A; French Parkinson's Disease Genetics**

- Study Group; European Consortium on Genetic Susceptibility in Parkinson's Disease (2000).** Association between early-onset Parkinson's disease and mutations in the parkin gene. *N Engl J Med* **342**(21), 1560-7.
- MacLeod D, Dowman J, Hammond R, Leete T, Inoue K, Abeliovich A (2006).** The familial Parkinsonism gene LRRK2 regulates neurite process morphology. *Neuron* **52**(4), 587-93.
- Malhotra V, Orci L, Glick BS, Block MR, Rothman JE (1988).** Role of an N-ethylmaleimide-sensitive transport component in promoting fusion of transport vesicles with cisternae of the Golgi stack. *Cell* **54**(2), 221-7.
- Mallet N, Ballion B, Le Moine C, Gonon F (2006).** Cortical inputs and GABA interneurons imbalance projection neurons in the striatum of parkinsonian rats. *J Neurosci* **26**(14), 3875-84.
- Manfredsson FP, Lewin AS, Mandel RJ (2006).** RNA knockdown as a potential therapeutic strategy in Parkinson's disease. *Gene Ther* **13**(6), 517-24.
- Manning G, Whyte DB, Martinez R, Hunter T, Sudarsanam S (2002).** The protein kinase complement of the human genome. *Science* **298**(5600), 1912-34.
- Manning-Bog AB, Langston JW (2007).** Model fusion, the next phase in developing animal models for Parkinson's disease. *Neurotox Res* **11**(3-4), 219-40.
- Mareel MM, De Mets M (1984).** Effect of microtubule inhibitors on invasion and on related activities of tumor cells. *Int Rev Cytol* **90**, 125-68.
- Marek K, Jennings D, Tamagnan G, Seibyl J (2008).** Biomarkers for Parkinson's disease: tools to assess Parkinson's disease onset and progression. *Ann Neurol*. **64**, S111-21.
- Marín I (2006).** The Parkinson disease gene LRRK2: evolutionary and structural insights. *Mol Biol Evol* **23**(12), 2423-33.
- Marín I (2008).** Ancient origin of the Parkinson disease gene LRRK2. *J Mol Evol* **67**(1), 41-50.
- Marín I, van Egmond WN, van Haastert PJ (2008).** The Roco protein family: a functional perspective. *FASEB J* **22**(9), 3103-10.
- Martin LJ, Pan Y, Price AC, Sterling W, Copeland NG, Jenkins NA, Price DL, Lee MK (2006).** Parkinson's disease alpha-synuclein transgenic mice develop neuronal mitochondrial degeneration and cell death. *J Neurosci* **26**(1), 41-50.
- Martinez-Arca S, Coco S, Mainguy G, Schenk U, Alberts P, Bouillé P, Mezzina M, Prochiantz A, Matteoli M, Louvard D, Galli T (2001).** A common exocytotic mechanism mediates axonal and dendritic outgrowth. *J Neurosci* **21**(11), 3830-8.
- Martínez-Martín P, Damián J (2010).** Parkinson disease: Depression and anxiety in Parkinson disease. *Nat Rev Neurol* **6**(5), 243-5.
- Marsden CD (1983).** Neuromelanin and Parkinson's disease. *J Neural Transm* **19**, 121-141.
- Masliah E, Rockenstein E, Veinbergs I, Mallory M, Hashimoto M, Takeda A, Sagara Y, Sisk A, Mucke L (2000).** Dopaminergic loss and inclusion body formation in alpha-synuclein mice: implications for neurodegenerative disorders. *Science* **287**(5456), 1265-9.
- Mata IF, Wedemeyer WJ, Farrer MJ, Taylor JP, Gallo KA (2006).** LRRK2 in Parkinson's disease: protein domains and functional insights. *Trends Neurosci* **29**(5), 286-93.

- Matamales M, Bertran-Gonzalez J, Salomon L, Degos B, Deniau JM, Valjent E, Hervé D, Girault JA (2009).** Striatal medium-sized spiny neurons: identification by nuclear staining and study of neuronal subpopulations in BAC transgenic mice. *PLoS One* **4**(3).
- Matsuyama A, Shimazu T, Sumida Y, Saito A, Yoshimatsu Y, Seigneurin-Berny D, Osada H, Komatsu Y, Nishino N, Khochbin S, Horinouchi S, Yoshida M (2002).** In vivo destabilization of dynamic microtubules by HDAC6-mediated deacetylation. *EMBO J* **21**(24), 6820-31.
- Matteoli M, Takei K, Perin MS, Sudhof TC, De Camilli P (1992).** Exo-endocytotic recycling of synaptic vesicles in developing processes of cultured hippocampal neurons. *J Cell Biol* **117**, 849–861.
- McEwen DP, Jenkins PM, Martens JR (2008).** Olfactory cilia: our direct neuronal connection to the external world. *Curr Top Dev Biol* **85**, 333-70.
- McLean JH, Shipley MT (1988).** Postmitotic, postmigrational expression of tyrosine hydroxylase in olfactory bulb dopaminergic neurons. *J Neurosci* **8**(10), 3658-69.
- Meister G, Tuschl T (2004).** Mechanisms of gene silencing by double-stranded RNA. *Nature* **431**(7006), 343-349.
- Meixner A, Boldt K, Van Troys M, Askenazi M, Gloeckner CJ, Bauer M, Marto JA, Ampe C, Kinkl N, Ueffing M (2011).** A QUICK screen for Lrrk2 interaction partners--leucine-rich repeat kinase 2 is involved in actin cytoskeleton dynamics. *Mol Cell Proteomics* **10**(1).
- Melrose HL, Lincoln SJ, Tyndall GM, Dickson D, Farrer MJ (2006/1).** Anatomical localization of leucine-rich repeat kinase 2 in mouse brain. *Neuroscience* **139**(3), 791-4.
- Melrose HL, Lincoln SJ, Tyndall GM, Farrer MJ (2006/2).** Parkinson's disease: a rethink of rodent models. *Exp Brain Res* **173**(2), 196-204.
- Melrose HL, Kent CB, Taylor JP, Dachsel JC, Hinkle KM, Lincoln SJ, Mok SS, Culvenor JG, Masters CL, Tyndall GM, Bass DI, Ahmed Z, Andorfer CA, Ross OA, Wszolek ZK, Delldonne A, Dickson DW, Farrer MJ (2007).** A comparative analysis of leucine-rich repeat kinase 2 (Lrrk2) expression in mouse brain and Lewy body disease. *Neuroscience* **147**(4), 1047-58.
- Melrose HL (2008).** Update on the functional biology of Lrrk2. *Future Neurol* **3**(6), 669-681.
- Melrose HL, Dächsel JC, Behrouz B, Lincoln SJ, Yue M, Hinkle KM, Kent CB, Korvatska E, Taylor JP, Witten L, Liang YQ, Beevers JE, Boules M, Dugger BN, Serna VA, Gaukhman A, Yu X, Castanedes-Casey M, Braithwaite AT, Ogholikhan S, Yu N, Bass D, Tyndall G, Schellenberg GD, Dickson DW, Janus C, Farrer MJ (2010).** Impaired dopaminergic neurotransmission and microtubule-associated protein tau alterations in human LRRK2 transgenic mice. *Neurobiol Dis*.
- Mensah PL (1982).** An electron microscopical study of neuronal cell clustering in postnatal mouse striatum, with special emphasis on neuronal cell death. *Anat Embryol* **164**(3), 387-401.
- Metzger D, Chambon P (2001).** Site- and time-specific gene targeting in the mouse. *Methods* **24**(1), 71-80.
- Mezey E, M Dehejia A, Harta G, Tresser N, Suchy SF, Nussbaum RL, Brownstein MJ, Polymeropoulos MH (1998).** Alpha synuclein is present in Lewy bodies in sporadic Parkinson's disease. *Mol Psychiatry* **3**, 493–9.

- Mihalick SM, Langlois JC, Krienke JD (2000).** Strain and sex differences on olfactory discrimination learning in C57BL/6J and DBA/2J inbred mice (*Mus musculus*). *J Comp Psychol* **114**(4), 365-70.
- Miklossy J, Arai T, Guo JP, Klegeris A, Yu S, McGeer EG, McGeer PL (2006).** LRRK2 expression in normal and pathologic human brain and in human cell lines. *J Neuropathol Exp Neurol* **65**(10), 953-63.
- Miller KE, Samuels DC (1997).** The axon as a metabolic compartment: protein degradation, transport, and maximum length of an axon. *J Theor Biol* **186**(3), 373-9.
- Milosevic J, Schwarz SC, Ogunlade V, Meyer AK, Storch A, Schwarz J (2009).** Emerging role of LRRK2 in human neural progenitor cell cycle progression, survival and differentiation. *Mol Neurodegener* **4**, 25.
- Min SW, Cho SH, Zhou Y, Schroeder S, Haroutunian V, Seeley WW, Huang EJ, Shen Y, Masliah E, Mukherjee C, Meyers D, Cole PA, Ott M, Gan L (2010).** Acetylation of tau inhibits its degradation and contributes to tauopathy. *Neuron* **67**(6), 953-66.
- Mirelman A, Gurevich T, Giladi N, Bar-Shira A, Orr-Urtreger A, Hausdorff JM (2011).** Gait alterations in healthy carriers of the LRRK2 G2019S mutation. *Ann Neurol* **69**(1), 193-7.
- Mitsumoto A, Nakagawa Y (2001).** DJ-1 is an indicator for endogenous reactive oxygen species elicited by endotoxin. *Free Radic Res* **35**(6), 885-93.
- Miyake N, Tonoki H, Gallego M, Harada N, Shimokawa O, Yoshiura K, Ohta T, Kishino T, Niikawa N, Matsumoto N (2004).** Phenotype-genotype correlation in two patients with 12q proximal deletion. *J Hum Genet* **49**(5), 282-4.
- Mosavi LK, Cammett TJ, Desrosiers DC, Peng ZY (2004).** The ankyrin repeat as molecular architecture for protein recognition. *Protein Sci* **13**(6), 1435-48.
- Mundigl O, Matteoli M, Daniell L, Thomas-Reetz A, Metcalf A, Jahn R, De Camilli P (1993).** Synaptic vesicle proteins and early endosomes in cultured hippocampal neurons: differential effects of Brefeldin A in axon and dendrites. *J Cell Biol* **122**(6), 1207-21.
- Murata S, Chiba T, Tanaka K (2003).** CHIP: a quality-control E3 ligase collaborating with molecular chaperones. *Int J Biochem Cell Biol* **35**(5), 572-8.
- Nahas F, Dryden SC, Abrams J, Tainsky MA (2007).** Mutations in SIRT2 deacetylase which regulate enzymatic activity but not its interaction with HDAC6 and tubulin. *Mol Cell Biochem* **303**(1-2), 221-30.
- Nebreda, AR, Porras A (2000).** p38 MAP kinases: beyond the stress response. *Trends Biochem Sci* **25**, 257-260.
- Nishimune A, Isaac JT, Molnar E, Noel J, Nash SR, Tagaya M, Collingridge GL, Nakanishi S, Henley JM (1998).** NSF binding to GluR2 regulates synaptic transmission. *Neuron* **21**(1), 87-97.
- Nogales E, Whittaker M, Milligan RA, Downing KH (1999).** High-resolution model of the microtubule. *Cell* **96**(1), 79-88.
- Nolen B, Taylor S, Ghosh G (2004).** Regulation of protein kinases; controlling activity through activation segment conformation. *Mol Cell* **15**, 661-675
- North BJ, Marshall BL, Borra MT, Denu JM, Verdin E (2003).** The human Sir2 ortholog, SIRT2, is an NAD⁺-dependent tubulin deacetylase. *Mol Cell* **11**(2), 437-44.

- Nuscher B, Kamp F, Mehnert T, Odoy S, Haass C, Kahle PJ, Beyer K (2004).** Alpha-synuclein has a high affinity for packing defects in a bilayer membrane: a thermodynamics study. *J Biol Chem* **279**(21), 21966-75.
- Nussbaum RL, Polymeropoulos MH (1997).** Genetics of Parkinson's disease. *Hum Mol Genet* **6**(10), 1687-91.
- Obeso JA, Rodríguez-Oroz MC, Rodríguez M, Lanciego JL, Artieda J, Gonzalo N, Olanow CW (2000).** Pathophysiology of the basal ganglia in Parkinson's disease. *Trends Neurosci* **23**, S8-19.
- Ohkawa N, Sugisaki S, Tokunaga E, Fujitani K, Hayasaka T, Setou M, Inokuchi K (2008).** N-acetyltransferase ARD1-NAT1 regulates neuronal dendritic development. *Genes Cells* **13**(11), 1171-83.
- Olzmann JA, Li L, Chudaeu MV, Chen J, Perez FA, Palmiter RD, Chin LS (2007).** Parkinson-mediated K63-linked polyubiquitination targets misfolded DJ-1 to aggresomes via binding to HDAC6. *J Cell Biol* **178**(6), 025-38.
- Outeiro TF, Kontopoulos E, Altmann SM, Kufareva I, Strathearn KE, Amore AM, Volk CB, Maxwell MM, Rochet JC, McLean PJ, Young AB, Abagyan R, Feany MB, Hyman BT, Kazantsev AG (2007).** Sirtuin 2 inhibitors rescue alpha-synuclein-mediated toxicity in models of Parkinson's disease. *Science* **317**(5837), 516-9.
- Paisán-Ruiz C, Jain S, Evans EW, Gilks WP, Simón J, van der Brug M, López de Munain A, Aparicio S, Gil AM, Khan N, Johnson J, Martinez JR, Nicholl D, Carrera IM, Pena AS, de Silva R, Lees A, Martí-Massó JF, Pérez-Tur J, Wood NW, Singleton AB (2004).** Cloning of the gene containing mutations that cause PARK8-linked Parkinson's disease. *Neuron* **44**(4), 595-600.
- Paisán-Ruiz C, Nath P, Washecka N, Gibbs JR, Singleton AB (2008).** Comprehensive analysis of LRRK2 in publicly available Parkinson's disease cases and neurologically normal controls. *Hum Mutat* **29**(4), 485-90.
- Paisán-Ruiz C, Guevara R, Federoff M, Hanagasi H, Sina F, Elahi E, Schneider SA, Schwingenschuh P, Bajaj N, Emre M, Singleton AB, Hardy J, Bhatia KP, Brandner S, Lees AJ, Houlden H (2010).** Early-onset L-dopa-responsive parkinsonism with pyramidal signs due to ATP13A2, PLA2G6, FBXO7 and spatacsin mutations. *Mov Disord* **25**(12), 1791-800.
- Parkinson J (2002).** An Essay on the Shaking Palsy. *J Neuropsychiatry Clin Neurosci* **14**, 223-36.
- Pennuto M, Bonanomi D, Benfenati F, and Valtorta F (2003).** Synaptophysin I controls the targeting of VAMP2/synaptobrevin II to synaptic vesicles. *Mol Biol Cell* **14**, 4909-4919.
- Perez M, Santa-Maria I, de Barreda EG, Zhu X, Cuadros R, Cabrero JR, Sanchez-Madrid F, Dawson HN, Vitek MP, Perry G, Smith MA, Avila J (2009).** Tau - an inhibitor of deacetylase HDAC6 function. *J Neurochem* **109**(6), 1756-66.
- Perdiz D, Mackeh R, Poüs C, Baillet A (2011).** The ins and outs of tubulin acetylation: More than just a post-translational modification? *Cell Signal*.
- Petreaanu L, Alvarez-Buylla A (2002).** Maturation and death of adult-born olfactory bulb granule neurons: role of olfaction. *J Neurosci* **22**(14), 6106-13. 85.
- Pham TT, Giesert F, Röthig A, Floss T, Kallnik M, Weindl K, Hölter SM, Ahting U, Prokisch H, Becker L, Klopstock T, Hrabé de Angelis M, Beyer K, Görner K, Kahle PJ, Vogt Weisenhorn DM, Wurst W (2010).** DJ-1-deficient mice show less TH-positive

neurons in the ventral tegmental area and exhibit non-motoric behavioural impairments. *Genes Brain Behav.*

- Piccoli G, Condliffe SB, Bauer M, Giesert F, Boldt K, De Astis S, Meixner A, Sarioglu H, Vogt-Weisenhorn DM, Wurst W, Gloeckner CJ, Matteoli M, Sala C, Ueffing M (2011).** LRRK2 Controls Synaptic Vesicle Storage and Mobilization within the Recycling Pool. *J Neurosci* **31**(6), 2225-2237.
- Plaas M, Karis A, Innos J, Rebane E, Baekelandt V, Vaarmann A, Luuk H, Vasar E, Koks S (2008).** Alpha-synuclein A30P point-mutation generates age-dependent nigrostriatal deficiency in mice. *J Physiol Pharmacol* **59**(2), 205-16.
- Plowey ED, Cherra SJ 3rd, Liu YJ, Chu CT (2008).** Role of autophagy in G2019S-LRRK2-associated neurite shortening in differentiated SH-SY5Y cells. *J Neurochem* **105**(3), 1048-56.
- Plun-Favreau H, Klupsch K, Moiso N, Gandhi S, Kjaer S, Frith D, Harvey K, Deas E, Harvey RJ, McDonald N, Wood NW, Martins LM, Downward J (2007).** The mitochondrial protease HtrA2 is regulated by Parkinson's disease-associated kinase PINK1. *Nat Cell Biol* **9**(11), 1243-52.
- Polymeropoulos MH, Lavedan C, Leroy E, Ide SE, Dehejia A, Dutra A, Pike B, Root H, Rubenstein J, Boyer R, Stenroos ES, Chandrasekharappa S, Athanassiadou A, Papapetropoulos T, Johnson WG, Lazzarini AM, Duvoisin RC, Di Iorio G, Golbe LI, Nussbaum RL (1997).** Mutation in the alpha-synuclein gene identified in families with Parkinson's disease. *Science* **276**(5321), 2045-7.
- Postuma RB, Montplaisir J (2009).** Predicting Parkinson's disease - why, when, and how? *Parkinsonism Relat Disord* **15** Suppl 3, S105-9.
- Porritt M, Stanic D, Finkelstein D, Batchelor P, Lockhart S, Hughes A, Kalnins R, Howells D (2005).** Dopaminergic innervation of the human striatum in Parkinson's disease. *Mov Disord* **20**(7), 810-8.
- Pothakos K, Kurz MJ, Lau Y-S (2009).** Restorative effect of endurance exercise on behavioral deficits in the chronic mouse model of Parkinson's disease with severe neurodegeneration. *BMC Neurosci* **10**, 6.
- Pridgeon JW, Olzmann JA, Chin LS, Li L (2007).** PINK1 Protects against Oxidative Stress by Phosphorylating Mitochondrial Chaperone TRAP1. *PLoS Biol* **5**(7), e172
- Prut L, Belzung C (2003).** The open field as a paradigm to measure the effects of drugs on anxiety-like behaviors: a review. *Eur J Pharmacol* **463**(1-3), 3-33.
- Qin L, Wu X, Block ML, Liu Y, Breese GR, Hong JS, Knapp DJ, Crews FT (2007).** Systemic LPS causes chronic neuroinflammation and progressive neurodegeneration. *Glia* **55**(5), 453-62.
- Raeymaekers L (2000).** Basic principles of quantitative PCR. *Mol Biotechnol* **15**(2), 115-22.
- Rajput A, Dickson DW, Robinson CA, Ross OA, Dächsel JC, Lincoln SJ, Cobb SA, Rajput ML, Farrer MJ (2006).** Parkinsonism, Lrrk2 G2019S, and tau neuropathology. *Neurology* **67**(8), 1506-8.
- Ramboz S, Oosting R, Amara DA, Kung HF, Blier P, Mendelsohn M, Mann JJ, Brunner D, Hen R (1998).** Serotonin receptor 1A knockout an animal model of anxiety-related disorder. *Proc Natl Acad Sci USA* **95**, 14476-14481.

- Reed NA, Cai D, Blasius TL, Jih GT, Meyhofer E, Gaertig J, Verhey KJ (2006).** Microtubule acetylation promotes kinesin-1 binding and transport. *Curr Biol* **16**(21), 2166-72.
- Rekhter M, Staschke K, Estridge T, Rutherford P, Jackson N, Gifford-Moore D, Foxworthy P, Reidy C, Huang XD, Kalbfleisch M, Hui K, Kuo MS, Gilmour R, Vlahos CJ (2008).** Genetic ablation of IRAK4 kinase activity inhibits vascular lesion formation. *Biochem Biophys Res Commun* **367**(3), 642-8.
- Ren Y, Jiang H, Yang F, Nakaso K, Feng J (2009).** Parkin protects dopaminergic neurons against microtubule-depolymerizing toxins by attenuating microtubule-associated protein kinase activation. *J Biol Chem* **284**(6), 4009-17.
- Ren Y, Liu W, Jiang H, Jiang Q, Feng J (2005).** Selective vulnerability of dopaminergic neurons to microtubule depolymerization. *J Biol Chem* **280**(40), 34105-12.
- Ren Y, Zhao J, Feng J (2003).** Parkin binds to alpha/beta tubulin and increases their ubiquitination and degradation. *J Neurosci* **23**(8), 3316-24.
- Ring HA, Serra-Mestres J (2002).** Neuropsychiatry of the basal ganglia. *J Neurol Neurosurg Psychiatry* **72**(1), 12-21.
- Rizzu P, Hinkle DA, Zhukareva V, Bonifati V, Severijnen LA, Martinez D, Ravid R, Kamphorst W, Eberwine JH, Lee VM, Trojanowski JQ, Heutink P (2004).** DJ-1 colocalizes with tau inclusions: a link between parkinsonism and dementia. *Ann Neurol* **55**(1), 113-8.
- Robertson SD, Matthies HJ, Galli A (2009).** A closer look at amphetamine-induced reverse transport and trafficking of the dopamine and norepinephrine transporters. *Mol Neurobiol* **39**(2), 73-80.
- Rozen S and Skaletsky H (2000).** Primer3 on the WWW for general users and for biologist programmers. *Methods Mol Biol* **132**, 365-386.
- Saha RN, Pahan K (2006).** HATs and HDACs in neurodegeneration: a tale of disconcerted acetylation homeostasis. *Cell Death Differ* **13**(4), 539-50.
- Saha S, Guillily MD, Ferree A, Lanceta J, Chan D, Ghosh J, Hsu CH, Segal L, Raghavan K, Matsumoto K, Hisamoto N, Kuwahara T, Iwatsubo T, Moore L, Goldstein L, Cookson M, Wolozin B (2009).** LRRK2 modulates vulnerability to mitochondrial dysfunction in *Caenorhabditis elegans*. *J Neurosci* **29**(29), 9210-8.
- Sämman J, Hegermann J, Gromoff EV, Eimer S, Baumeister R, Schmidt E (2009).** *Caenorhabditis elegans* LRK-1 and PINK-1 act antagonistically in stress response and neurite outgrowth. *J Biol Chem*.
- Sakaguchi-Nakashima A, Meir JY, Jin Y, Matsumoto K, Hisamoto N (2007).** LRK-1, a *C. elegans* PARK8-related kinase, regulates axonal-dendritic polarity of SV proteins. *Curr Biol* **17**(7), 592-8.
- Sambrook J, Fritsch EF, Maniatis T (1989).** Molecular Cloning: A Laboratory Manual. Cold Spring Harbor Laboratory Press, 2nd Edition.
- Santpere G, Ferrer I (2009).** LRRK2 and neurodegeneration. *Acta Neuropathol* **117**(3), 227-46.
- Saugstad JA (2010).** MicroRNAs as effectors of brain function with roles in ischemia and injury, neuroprotection, and neurodegeneration. *J Cereb Blood Flow Metab* **30**(9), 1564-76.

- Schambra UB, Lauder JM, Silver J (1992).** Atlas of the prenatal mouse brain. *Academic Press, Inc., San Diego*.
- Schmittgen TD, Livak KJ (2008).** Analyzing real-time PCR data by the comparative C(T) method. *Nat Protoc* **3**(6), 1101-8.
- Schober A (2004).** Classic toxin-induced animal models of Parkinson's disease: 6-OHDA and MPTP. *Cell Tissue Res* **318**(1), 215-24.
- Schweitzer K, Wider C, Lash J, Jasinska-Myga B, Strongosky A, Hentschel K, Williams L, Wszolek Z (2009).** Olfactory dysfunction in LRRK2 R1441C mutation carriers (Family D), unpublished data, AD/PD 2009.
- Sedelis M, Schwarting RK, Huston JP (2001).** Behavioral phenotyping of the MPTP mouse model of Parkinson's disease. *Behav Brain Res* **125**(1-2), 109-25.
- Sen S, West AB (2009).** The Therapeutic Potential of LRRK2 and Alpha-synuclein in Parkinson's Disease. *Antioxid Redox Signal*.
- Sgadò P, Albéri L, Gherbassi D, Galasso SL, Ramakers GM, Alavian KN, Smidt MP, Dyck RH, Simon HH (2006).** Slow progressive degeneration of nigral dopaminergic neurons in postnatal Engrailed mutant mice. *Proc Natl Acad Sci USA* **103**(41), 15242-7.
- Shen J (2010).** Impaired Neurotransmitter Release in Alzheimer's and Parkinson's Diseases. *Neurodegener Dis* **7**(1-3), 80-83.
- Shi WX, Rayport S (1994).** GABA synapses formed in vitro by local axon collaterals of nucleus accumbens neurons. *J Neurosci* **14**(7), 4548-60.
- Shiba K, Arai T, Sato S, Kubo S, Ohba Y, Mizuno Y, Hattori N (2009).** Parkin stabilizes PINK1 through direct interaction. *Biochem Biophys Res Commun* **383**(3), 331-5.
- Shin N, Jeong H, Kwon J, Heo HY, Kwon JJ, Yun HJ, Kim CH, Han BS, Tong Y, Shen J, Hatano T, Hattori N, Kim KS, Chang S, Seol W (2008).** LRRK2 regulates synaptic vesicle endocytosis. *Exp Cell Res* **314**(10), 2055-65.
- Shulman LM, Singer C, Bean JA, Weiner WJ (1996).** Internal tremor in patients with Parkinson's disease. *Mov Disord* **11**(1), 3-7.
- Silva RM, Kuan CY, Rakic P, Burke RE (2005).** Mixed lineage kinase-c-jun N-terminal kinase signaling pathway: a new therapeutic target in Parkinson's disease. *Mov Disord* **20**(6), 653-64.
- Silvestri L, Caputo V, Bellacchio E, Atorino L, Dallapiccola B, Valente EM, Casari G (2005).** Mitochondrial import and enzymatic activity of PINK1 mutants associated to recessive parkinsonism. *Hum Mol Genet* **14**(22), 3477-92.
- Simon HH, Saueressig H, Wurst W, Goulding MD, O'Leary DD (2001).** Fate of midbrain dopaminergic neurons controlled by the engrailed genes. *J Neurosci* **21**(9), 3126-34.
- Simón-Sánchez J, Herranz-Pérez V, Olucha-Bordonau F, Pérez-Tur J (2006).** LRRK2 is expressed in areas affected by Parkinson's disease in the adult mouse brain. *Eur J Neurosci* **23**(3), 659-66.
- Simón-Sánchez J, Schulte C, Bras JM, Sharma M, Gibbs JR, Berg D, Paisan-Ruiz C, Lichtner P, Scholz SW, Hernandez DG, Krüger R, Federoff M, Klein C, Goate A, Perlmutter J, Bonin M, Nalls MA, Illig T, Gieger C, Houlden H, Steffens M, Okun MS, Racette BA, Cookson MR, Foote KD, Fernandez HH, Traynor BJ, Schreiber S, Arepalli S, Zonozi R, Gwinn K, van der Brug M, Lopez G, Chanock SJ, Schatzkin A, Park Y, Hollenbeck A, Gao J, Huang X, Wood NW, Lorenz D, Deuschl G, Chen H,**

- Riess O, Hardy JA, Singleton AB, Gasser T (2009).** Genome-wide association study reveals genetic risk underlying Parkinson's disease. *Nat Genet* **41**(12), 1308-12.
- Smith AG, Heath JK, Donaldson DD, Wong GG, Moreau J, Stahl M, Rogers D. (1988).** Inhibition of pluripotential embryonic stem cell differentiation by purified polypeptides. *Nature* **336**, 688-690.
- Smith WW, Pei Z, Jiang H, Moore DJ, Liang Y, West AB, Dawson VL, Dawson TM, Ross CA (2005).** Leucine-rich repeat kinase 2 (LRRK2) interacts with parkin, and mutant LRRK2 induces neuronal degeneration. *Proc Natl Acad Sci USA* **102**(51), 18676-81.
- Smith WW, Pei Z, Jiang H, Dawson VL, Dawson TM, Ross CA (2006).** Kinase activity of mutant LRRK2 mediates neuronal toxicity. *Nat Neurosci* **9**(10), 1231-3.
- Sollinger AB, Goldstein FC, Lah JJ, Levey AI, Factor SA (2010).** Mild cognitive impairment in Parkinson's disease: subtypes and motor characteristics. *Parkinsonism Relat Disord* **16**(3), 177-80.
- Söllner T, Rothman JE (1994).** Neurotransmission: harnessing fusion machinery at the synapse. *Trends Neurosci* **17**(8), 344-8.
- Sonnier L, Le Pen G, Hartmann A, Bizot JC, Trovero F, Krebs MO, Prochiantz A (2007).** Progressive loss of dopaminergic neurons in the ventral midbrain of adult mice heterozygote for *Engrailed1*. *J Neurosci* **27**(5), 1063-71.
- Southwood CM, Peppi M, Dryden S, Tainsky MA, Gow A (2007).** Microtubule deacetylases, SirT2 and HDAC6, in the nervous system. *Neurochem Res* **32**(2), 187-95.
- Spillantini MG, Schmidt ML, Lee VM, Trojanowski JQ, Jakes R, Goedert M (1997).** Alpha-synuclein in Lewy bodies. *Nature* **388**, 839-840.
- Stamper C, Siegel A, Liang WS, Pearson JV, Stephan DA, Shill H, Connor D, Caviness JN, Sabbagh M, Beach TG, Adler CH, Dunckley T (2008).** Neuronal gene expression correlates of Parkinson's disease with dementia. *Mov Disord* **23**(11), 1588-95.
- Stefanis L, Larsen KE, Rideout HJ, Sulzer D, Greene LA (2001).** Expression of A53T mutant but not wild-type alpha-synuclein in PC12 cells induces alterations of the ubiquitin-dependent degradation system, loss of dopamine release, and autophagic cell death. *J Neurosci* **21**(24), 9549-60.
- Stewart F and Allen WR (1995).** Comparative Aspects of the Evolution and Function of the Chorionic Gonadotrophins. *Reprod Dom Anim* **30**, 231-239.
- Storch A, Ludolph AC, Schwarz J (2004).** Dopamine transporter: involvement in selective dopaminergic neurotoxicity and degeneration. *J Neural Transm* **111**(10-11), 1267-86.
- Südhof TC (1995).** The synaptic vesicle cycle: a cascade of protein-protein interactions. *Nature* **375**, 645-53.
- Sulzer D (2007).** Multiple hit hypotheses for dopamine neuron loss in Parkinson's disease. *Trends Neurosci* **30**(5), 244-50.
- Surmeier DJ, Ding J, Day M, Wang Z, Shen W (2007).** D1 and D2 dopamine-receptor modulation of striatal glutamatergic signaling in striatal medium spiny neurons. *Trends Neurosci* **30**(5), 228-35.
- Surmeier DJ, Song WJ, Yan Z (1996).** Coordinated expression of dopamine receptors in neostriatal medium spiny neurons. *J Neurosci* **16**(20), 6579-91.

- Suzuki K, Koike T (2007).** Mammalian Sir2-related protein (SIRT) 2-mediated modulation of resistance to axonal degeneration in slow Wallerian degeneration mice: a crucial role of tubulin deacetylation. *Neuroscience* **147**(3), 599-612.
- Szargel R, Rott R, Eyal A, Haskin J, Shani V, Balan L, Wolosker H, Engelender S (2009).** Synphilin-1A inhibits seven in absentia homolog (SIAH) and modulates alpha-synuclein monoubiquitylation and inclusion formation. *J Biol Chem* **284**(17), 11706-16.
- Tadaiesky MT, Dombrowski PA, Figueiredo CP, Cargnin-Ferreira E, Da Cunha C, Takahashi RN (2008).** Emotional, cognitive and neurochemical alterations in a premotor stage model of Parkinson's disease. *Neuroscience* **156**(4), 830-40.
- Tan EK, Kwok HH, Tan LC, Zhao WT, Prakash KM, Au WL, Pavanni R, Ng YY, Satake W, Zhao Y, Toda T, Liu JJ (2010).** Analysis of GWAS-linked loci in Parkinson disease reaffirms PARK16 as a susceptibility locus. *Neurology* **75**(6), 508-12.
- Takahashi-Fujigasaki J, Fujigasaki H (2006).** Histone deacetylase (HDAC) 4 involvement in both Lewy and Marinesco bodies. *Neuropathol Appl Neurobiol* **32**(5), 562-6.
- Takahashi-Niki K, Niki T, Taira T, Iguchi-Arigo SM, Arigo H (2004).** Reduced anti-oxidative stress activities of DJ-1 mutants found in Parkinson's disease patients. *Biochem Biophys Res Commun* **320**(2), 389-97.
- Taylor JP, Mata IF, Farrer MJ (2006).** LRRK2: a common pathway for parkinsonism, pathogenesis and prevention? *Trends Mol Med* **12**(2), 76-82.
- Taylor JP, Hulihan MM, Kachergus JM, Melrose HL, Lincoln SJ, Hinkle KM, Stone JT, Ross OA, Hauser R, Aasly J, Gasser T, Payami H, Wszolek ZK, Farrer MJ (2007).** Leucine-rich repeat kinase 1: a paralog of LRRK2 and a candidate gene for Parkinson's disease. *Neurogenetics* **8**(2), 95-102.
- Taylor TN, Caudle WM, Shepherd KR, Noorian A, Jackson CR, Iuvone PM, Weinschenker D, Greene JG, Miller GW (2009).** Nonmotor symptoms of Parkinson's disease revealed in an animal model with reduced monoamine storage capacity. *J Neurosci* **29**(25), 8103-13.
- Taylor TN, Greene JG, Miller GW (2010).** Behavioral phenotyping of mouse models of Parkinson's disease. *Behav Brain Res* **211**(1):1-10.
- Taymans JM, Van den Haute C, Baekelandt V (2006).** Distribution of PINK1 and LRRK2 in rat and mouse brain. *J Neurochem* **98**(3), 951-61.
- Tepper JM, Bolam JP (2004).** Functional diversity and specificity of neostriatal interneurons. *Curr Opin Neurobiol* **14**(6), 685-92.
- Terzioglu M, Galter D (2008).** Parkinson's disease: genetic versus toxin-induced rodent models. *FEBS J* **275**(7), 1384-91.
- Thomas B, Beal MF (2007).** Parkinson's disease. *Hum Mol Genet* **16**(2), R183-94.
- Tillerson JL, Caudle WM, Parent JM, Gong C, Schallert T, Miller GW (2006).** Olfactory discrimination deficits in mice lacking the dopamine transporter or the D2 dopamine receptor. *Behav Brain Res* **172**(1), 97-105.
- Tong Y, Pisani A, Martella G, Karouani M, Yamaguchi H, Pothos EN, Shen J (2009).** R1441C mutation in LRRK2 impairs dopaminergic neurotransmission in mice. *Proc Natl Acad Sci USA* **106**(34), 14622-7.
- Tong Y, Yamaguchi H, Giaime E, Boyle S, Kopan R, Kelleher RJ 3rd, Shen J (2010).** Loss of leucine-rich repeat kinase 2 causes impairment of protein degradation pathways,

- accumulation of {alpha}-synuclein, and apoptotic cell death in aged mice. *Proc Natl Acad Sci USA* **107**(21), 9879-84.
- Tönissaar M, Philips MA, Eller M, Harro J (2004).** Sociability trait and serotonin metabolism in the rat social interaction test. *Neurosci Lett* **367**(3), 309-12.
- Todaro GJ, Green H (1963).** Quantitative studies of the growth of mouse embryo cells in culture and their development into established lines. *J Cell Biol* **17**, 299-313.
- Trullas R, Jackson B, Skolnick P (1989).** Genetic differences in a tail suspension test for evaluating antidepressant activity. *Psychopharmacology* **99**(2), 287-288.
- Tsaneva-Atanasova K, Burgo A, Galli T, Holcman D (2009).** Quantifying neurite growth mediated by interactions among secretory vesicles, microtubules, and actin networks. *Biophys J* **96**(3), 840-57.
- Unoki M, Nakamura Y (2001).** Growth-suppressive effects of BPOZ and EGR2, two genes involved in the PTEN signaling pathway. *Oncogene* **20**(33), 4457-65.
- Valente EM, Abou-Sleiman PM, Caputo V, Muqit MM, Harvey K, Gispert S, Ali Z, Del Turco D, Bentivoglio AR, Healy DG, Albanese A, Nussbaum R, González-Maldonado R, Deller T, Salvi S, Cortelli P, Gilks WP, Latchman DS, Harvey RJ, Dallapiccola B, Auburger G, Wood NW (2004).** Hereditary early-onset Parkinson's disease caused by mutations in PINK1. *Science* **304**(5674), 1158-60.
- Valjent E, Bertran-Gonzalez J, Hervé D, Fisone G, Girault JA (2009).** Looking BAC at striatal signaling: cell-specific analysis in new transgenic mice. *Trends Neurosci* **32**(10), 538-47.
- Vandeputte C, Taymans JM, Casteels C, Coun F, Ni Y, Van Laere K, Baekelandt V (2010).** Automated quantitative gait analysis in animal models of movement disorders. *BMC Neurosci* **11**(1), 92.
- van Egmond WN, Kortholt A, Plak K, Bosgraaf L, Bosgraaf S, Keizer-Gunnink I, van Haastert PJ (2008).** Intramolecular activation mechanism of the Dictyostelium LRRK2 homolog Roco protein GbpC. *J Biol Chem* **283**(44), 30412-20.
- Vasquez KM, Marburger K, Intody Z, Wilson JH (2001).** Manipulating the mammalian genome by homologous recombination. *Proc Natl Acad Sci USA* **98**(15), 8403-10.
- Vedin V, Molander M, Bohm S, Berghard A (2009).** Regional differences in olfactory epithelial homeostasis in the adult mouse. *J Comp Neurol* **513**(4), 375-84.
- Verbaan D, Boesveldt S, van Rooden SM, Visser M, Marinus J, Macedo MG, Fang Y, Heutink P, Berendse HW, van Hilten JJ (2008).** Is olfactory impairment in Parkinson disease related to phenotypic or genotypic characteristics? *Neurology* **71**(23), 1877-82.
- Verrey F, Groscurth P, Bolliger U (1995).** Cytoskeletal disruption in A6 kidney cells: impact on endo/exocytosis and NaCl transport regulation by antidiuretic hormone. *J Membr Biol* **145**(2), 193-204.
- Villasana LE, Klann E, Tejada-Simon MV (2006).** Rapid isolation of synaptoneuroosomes and postsynaptic densities from adult mouse hippocampus. *J Neurosci Methods* **158**(1), 30-6.
- Vlamings R, Visser-Vandewalle V, Koopmans G, Joosten EA, Kozan R, Kaplan S, Steinbusch HW, Temel Y (2007).** High frequency stimulation of the subthalamic nucleus improves speed of locomotion but impairs forelimb movement in Parkinsonian rats. *Neuroscience* **148**(3), 815-23.

- Von Coelln R, Thomas B, Savitt JM, Lim KL, Sasaki M, Hess EJ, Dawson VL, Dawson TM (2004).** Loss of locus coeruleus neurons and reduced startle in parkin null mice. *Proc Natl Acad Sci USA* **101**(29), 10744-9.
- Voorn P, Roest G, Groenewegen HJ (1987).** Increase of enkephalin and decrease of substance P immunoreactivity in the dorsal and ventral striatum of the rat after midbrain 6-hydroxydopamine lesions. *Brain Res* **412**(2), 391-6.
- Wallin M, Strömberg E (1995).** Cold-stable and cold-adapted microtubules. *Int Rev Cytol* **157**, 1-31.
- Wang D, Tang B, Zhao G, Pan Q, Xia K, Bodmer R, Zhang Z (2008).** Dispensable role of Drosophila ortholog of LRRK2 kinase activity in survival of dopaminergic neurons. *Mol Neurodegener* **3**, 3.
- Wang L, Xie C, Greggio E, Parisiadou L, Shim H, Sun L, Chandran J, Lin X, Lai C, Yang WJ, Moore DJ, Dawson TM, Dawson VL, Chiosis G, Cookson MR, Cai H. (2008).** The chaperone activity of heat shock protein 90 is critical for maintaining the stability of leucine-rich repeat kinase 2. *J Neurosci* **28**(13), 3384-91.
- Wang W, Brautigam DL (2008).** Phosphatase inhibitor 2 promotes acetylation of tubulin in the primary cilium of human retinal epithelial cells. *BMC Cell Biol* **9**, 62.
- Wang Y, Tang BL (2006).** SNAREs in neurons--beyond synaptic vesicle exocytosis. *Mol Membr Biol* **23**(5), 377-84.
- Wennerberg K, Rossman KL, Der CJ (2005).** The Ras superfamily at a glance. *J Cell Sci* **118**, 843-6.
- Wernig M, Zhao JP, Pruszak J, Hedlund E, Fu D, Soldner F, Broccoli V, Constantine-Paton M, Isacson O, Jaenisch R (2008).** Neurons derived from reprogrammed fibroblasts functionally integrate into the fetal brain and improve symptoms of rats with Parkinson's disease. *Proc Natl Acad Sci USA* **105**(15), 5856-61.
- West AB, Moore DJ, Biskup S, Bugayenko A, Smith WW, Ross CA, Dawson VL, Dawson TM (2005).** Parkinson's disease-associated mutations in leucine-rich repeat kinase 2 augment kinase activity. *Proc Natl Acad Sci USA* **102**(46), 16842-7.
- West AB, Moore DJ, Choi C, Andrabi SA, Li X, Dikeman D, Biskup S, Zhang Z, Lim KL, Dawson VL, Dawson TM (2007).** Parkinson's disease-associated mutations in LRRK2 link enhanced GTP-binding and kinase activities to neuronal toxicity. *Hum Mol Genet* **16**(2), 223-32.
- Westerlund M, Belin AC, Anvret A, Bickford P, Olson L, Galter D (2008/1).** Developmental regulation of leucine-rich repeat kinase 1 and 2 expression in the brain and other rodent and human organs: Implications for Parkinson's disease. *Neuroscience* **152**(2), 429-36.
- Westerlund M, Ran C, Borgkvist A, Sterky FH, Lindqvist E, Lundströmer K, Pernold K, Brené S, Kallunki P, Fisone G, Olson L, Galter D (2008/2).** Lrrk2 and alpha-synuclein are co-regulated in rodent striatum. *Mol Cell Neurosci* **39**(4), 586-91.
- Westerlund M, Belin AC, Anvret A, Håkansson A, Nissbrandt H, Lind C, Sydow O, Olson L, Galter D (2008/3).** Cerebellar alpha-synuclein levels are decreased in Parkinson's disease and do not correlate with SNCA polymorphisms associated with disease in a Swedish material. *FASEB J* **22**(10), 3509-14.
- Westermann S, Weber K (2003).** Post-translational modifications regulate microtubule function. *Nat Rev Mol Cell Biol* **4**(12), 938-47.

- Whittaker VP (1965).** The application of subcellular fractionation techniques to the study of brain function. *Prog Biophys Mol Biol* **15**, 39–96.
- Whittaker VP (1993).** Thirty years of synaptosome research. *J Neurocytol* **22**, 735–42.
- Williams RL, Hilton DJ, Pease S, Willson TA, Stewart CL, Gearing DP, Wagner EF, Metcalf D, Nicola NA, Gough NM (1988).** Myeloid leukaemia inhibitory factor maintains the developmental potential of embryonic stem cells. *Nature* **336**, 684–687.
- Williams SM, Goldman-Rakic PS (1993).** Characterization of the dopaminergic innervation of the primate frontal cortex using a dopamine-specific antibody. *Cereb Cortex* **3**(3), 199–222.
- Wood-Kaczmar A, Gandhi S, Yao Z, Abramov AY, Miljan EA, Keen G, Stanyer L, Hargreaves I, Klupsch K, Deas E, Downward J, Mansfield L, Jat P, Taylor J, Heales S, Duchen MR, Latchman D, Tabrizi SJ, Wood NW (2008).** PINK1 is necessary for long term survival and mitochondrial function in human dopaminergic neurons. *PLoS ONE* **3**(6), e2455.
- Wszolek ZK, Pfeiffer RF, Tsuboi Y, Uitti RJ, McComb RD, Stoessl AJ, Strongosky AJ, Zimprich A, Müller-Myhsok B, Farrer MJ, Gasser T, Calne DB, Dickson DW (2004).** Autosomal dominant parkinsonism associated with variable synuclein and tau pathology. *Neurology* **62**(9), 1619–22.
- Wurst W, Auerbach AB, Joyner AL (1994).** Multiple developmental defects in Engrailed-1 mutant mice: an early mid-hindbrain deletion and patterning defects in forelimbs and sternum. *Development* **120**, 2065–75.
- Xiromerisiou G, Hadjigeorgiou GM, Gourbali V, Johnson J, Papakonstantinou I, Papadimitriou A, Singleton AB (2007).** Screening for SNCA and LRRK2 mutations in Greek sporadic and autosomal dominant Parkinson's disease: identification of two novel LRRK2 variants. *Eur J Neurol* **14**(1), 7–11.
- Xun Z, Sowell RA, Kaufman TC, Clemmer DE (2007).** Lifetime proteomic profiling of an A30P alpha-synuclein Drosophila model of Parkinson's disease. *J Proteome Res* **6**(9), 3729–38.
- Yamada K, Andrews C, Chan WM, McKeown CA, Magli A, de Berardinis T, Loewenstein A, Lazar M, O'Keefe M, Letson R, London A, Ruttum M, Matsumoto N, Saito N, Morris L, Del Monte M, Johnson RH, Uyama E, Houtman WA, de Vries B, Carlow TJ, Hart BL, Krawiecki N, Shoffner J, *et al.* (2003). Heterozygous mutations of the kinesin KIF21A in congenital fibrosis of the extraocular muscles type 1 (CFEOM1). *Nat Genet* **35**(4), 318–21.**
- Yang F, Jiang Q, Zhao J, Ren Y, Sutton MD, Feng J (2005).** Parkin stabilizes microtubules through strong binding mediated by three independent domains. *J Biol Chem* **280**(17), 17154–62.
- Yang W, Chen L, Ding Y, Zhuang X, Kang UJ (2007).** Paraquat induces dopaminergic dysfunction and proteasome impairment in DJ-1-deficient mice. *Hum Mol Genet* **16**(23), 2900–10.
- Yang Y, Gehrke S, Imai Y, Huang Z, Ouyang Y, Wang JW, Yang L, Beal MF, Vogel H, Lu B (2006).** Mitochondrial pathology and muscle and dopaminergic neuron degeneration caused by inactivation of Drosophila Pink1 is rescued by Parkin. *Proc Natl Acad Sci USA* **103**(28), 10793–8.
- Yu L, Gaitatzes C, Neer E, Smith TF (2000).** Thirty-plus functional families from a single motif. *Protein Sci* **9**(12), 2470–6.

- Zechel S, Meinhardt A, Unsicker K, von Bohlen Und Halbach O (2010).** Expression of leucine-rich-repeat-kinase 2 (LRRK2) during embryonic development. *Int J Dev Neurosci* **28**(5), 391-9.
- Zeiss CJ (2005).** Neuroanatomical phenotyping in the mouse: the dopaminergic system. *Vet Pathol* **42**(6), 753-73.
- Zhang Y, Gao J, Chung KK, Huang H, Dawson VL, Dawson TM (2000).** Parkin functions as an E2-dependent ubiquitin- protein ligase and promotes the degradation of the synaptic vesicle-associated protein, CDCrel-1. *Proc Natl Acad Sci USA* **97**(24), 13354-9.
- Zhang Y, Kwon S, Yamaguchi T, Cubizolles F, Rousseaux S, Kneissel M, Cao C, Li N, Cheng HL, Chua K, Lombard D, Mizeracki A, Matthias G, Alt FW, Khochbin S, Matthias P (2008).** Mice lacking histone deacetylase 6 have hyperacetylated tubulin but are viable and develop normally. *Mol Cell Biol* **28**(5), 1688-701.
- Zhao C, Slevin JT, Whiteheart SW (2007).** Cellular functions of NSF: not just SNAPs and SNAREs. *FEBS Lett* **581**(11), 2140-9.
- Zhong N, Kim CY, Rizzu P, Geula C, Porter DR, Pothos EN, Squitieri F, Heutink P, Xu J (2006).** DJ-1 transcriptionally up-regulates the human tyrosine hydroxylase by inhibiting the sumoylation of pyrimidine tract-binding protein-associated splicing factor. *J Biol Chem* **281**(30), 20940-8.
- Zhou W, Freed CR (2005).** DJ-1 up-regulates glutathione synthesis during oxidative stress and inhibits A53T alpha-synuclein toxicity. *J Biol Chem* **280**(52), 43150-8.
- Zhou W, Milder JB, Freed CR (2008).** Transgenic mice overexpressing tyrosine-to-cysteine mutant human alpha-synuclein: a progressive neurodegenerative model of diffuse Lewy body disease. *J Biol Chem* **283**(15), 9863-70.
- Zhu XD, Sadowski PD (1995).** Cleavage-dependent ligation by the FLP recombinase. Characterization of a mutant FLP protein with an alteration in a catalytic amino acid. *J Biol Chem* **270**(39), 23044-54.
- Zimprich A, Biskup S, Leitner P, Lichtner P, Farrer M, Lincoln S, Kachergus J, Hulihan M, Uitti RJ, Calne DB, Stoessl AJ, Pfeiffer RF, Patenge N, Carbajal IC, Vieregge P, Asmus F, Müller-Myhsok B, Dickson DW, Meitinger T, Strom TM, Wszolek ZK, Gasser T (2004).** Mutations in LRRK2 cause autosomal-dominant parkinsonism with pleomorphic pathology. *Neuron* **44**(4), 601-7.

9 Appendix

9.1 The *Lrrk2* R1441C Targeting Vector

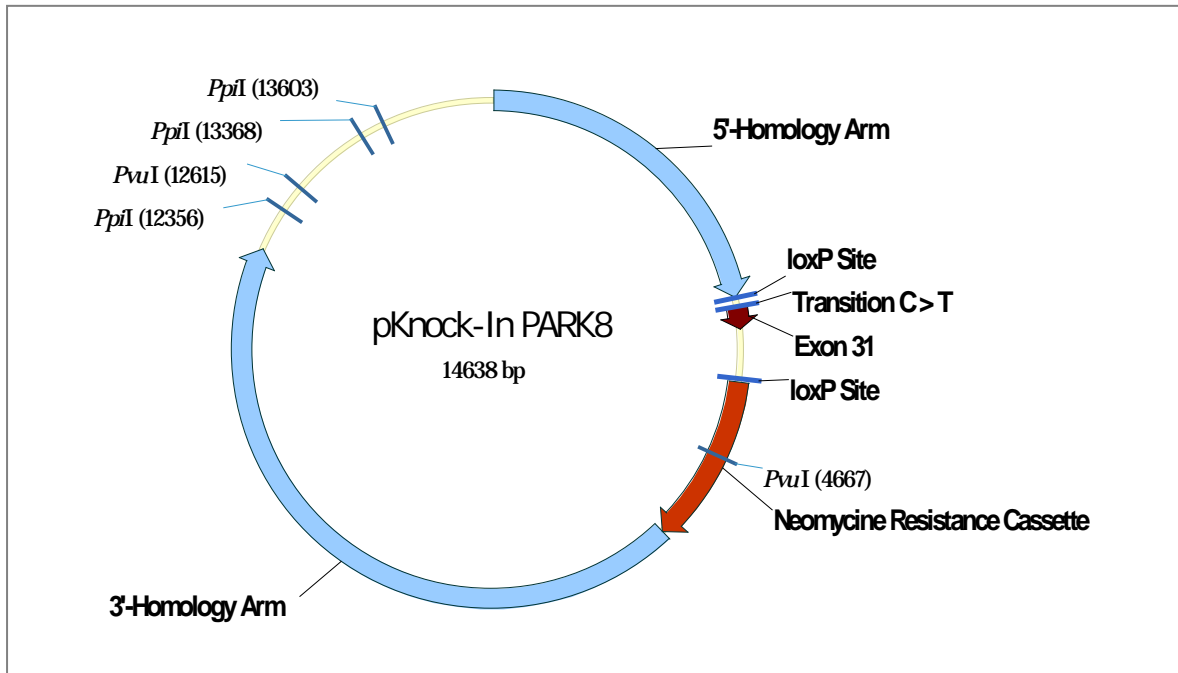


Figure 59: Schematic representation of the targeting vector *pKnock-In Park8* used for the generation of the *Lrrk2* R1441C mouse line by homologous recombination. The restriction sites *PpiI* were used for linearization.

```

2901 . . . . .GAAGG GCAAGCGTTC TCATGCTCTA TGGCAAAGGA ACAGGGAGGG GACCTAACAT CCCGGTTCCT GTGAGGACCT TCAAACGTGT TCCTTGGGCT
3001 CTGTCCTTGG GAGTTGAGCC TCTCATATAG CTCTCAAGAC GCTGCTGTGT CACACGGTTG CATTTCGAAGA TTCACACACT AGCAGCAAGG AAAGACAGCT
3101 GTTATTATGT GACTCTGAAG TCCTTGAGTC TGTCAATTGCT GCAGCACGTA GCATCCTACA TAGCAGATTT CAGCATAAAT GTAACCAAGG AGGTTTTTCC
3201 TCCCCGATAA CTTCGTATAG CATAcATTAT ACGAAGTTAT GCTAGCAGAT CTGAAACAGG AAGTGTCTTG TCTCTGTTCC CTTAGGCTTG TGCCTCTTCT
3301 TCCCGGTGA TTCTGGTGGG CACACATTTG GATGTTTCTG ATGAGAAGCA GCGAAAGCGG TGCATAAGCA AAATCAGCAA GGAACCTCCTA AATAAGCGAG
3401 GATTCCCGAC CATCCGGGAC TACCACCTTG TGAATGCCAC CGAGGAGTCA GATGCGCTGG CAAAGCTTCG GAAAACCATC ATAAATGAGA GCCTTAATTT
3501 CAAAGTGGGA GGATGGGCGC CCCTGTCAGG CTACTAGATG GTCAAAGTGG GCGAGTGTGT GCCTCTTCCA GGCTGCTAGT TAAGTAAGCC TTTCTCTTTT
3601 TGTCAATATTA TGCCTCTGCT TAGAAATGTC AGAAACCTTG AGGAGAGAGC AATTATCTGG AAATTGTAGG GTTTTTTTTT TCATAGCTCA AAACGATAAA
3701 AGTACTTTCA TTTAAAAAAT AITTTATTTAT GCCGCACTTC ATTTATAAAT CATAGAAGTG GGAATAAAAA TAAC TAGAGG ATCCTGAGAA GAAGGAGAGG
3801 AATTGCCAGG ACACCGAGAA AATCTTCCTC TCCAGGGGTT CCATCCAGAG GCTAAAAGAG AAGTGTGTGT CTGGGCCCTCC TGTCTCTGTC GACACTCGGT
3901 CCTATCTAGC ACAGAAGTTC CCACCTTCCT AACACTACAA TCCTTTCTTT AACACAGTTC CTCGTGTTGC ATAACTTCGT ATAGCATACA TTATACGAAG
4001 TTATGAAGTI CCTATTCTCT AGAAAGTATA GGAACCTCAT TCTACCGGTT AGGGGAGGCG CTTTTCCCAA GGCAGTCTGG AGCATGCGCT TTAGCAGCCC
4101 CGCTGGGCAC TTGGCGCTAC ACAAGTGGCC TCTGGCTCGC ACACATTCCA CATCCACCGG TAGGCGCCAA CCGCTCCGT TCTTTGGTGG CCCCT. . . .

```

Legend:

- 2901, base position in the targeting vector *pKnock-In Park8*;
- GAA, 5'-Homology arm (intronic sequences of *Lrrk2*);
- ATA, *loxP* site (locus x-over P1);
- GCT, linker sequence
- GCT, Exon 31 of murine *Lrrk2*;
- T, Transition C > T causing the R1441C missense mutation;
- GAA, Neomycin resistance cassette.

Figure 60: Sequence fragment of the targeting vector *pKnock-In Park8* of the critical region around *Lrrk2* exon 31. Legend depicted below sequence.

9.2 Primer Sequences

Lrrk1 in situ probes:

Product	Primer name	Primer Sequence (5'-3')
Lrrk1-ISH1	Lrrk1-ISH1 left	ccaggcctcagatggaatta
	Lrrk1-ISH1 right	cccatacgatgggatttcac
Lrrk1-ISH2	Lrrk1-ISH2 left	ggtccttgggtctccctttac
	Lrrk1-ISH2 right	gttcagtaaccggagccaaa
Lrrk1-ISH3	Lrrk1-ISH3 left	cagggcagagtacggtagga
	Lrrk1-ISH3 right	tgacggggaactcattcttc
Lrrk1-ISH4	Lrrk1-ISH4 left	cctgctggatagtcctgagc
	Lrrk1-ISH4 right	ggaggctgtctcagttccag

Lrrk2 in situ probes:

Product	Primer name	Primer Sequence (5'-3')
Lrrk2-ISH1	Lrrk2-ISH1 left	tgctgggtgttcacactctcg
	Lrrk2-ISH1 right	gggctttatagcagggttcc
Lrrk2-ISH2	Lrrk2-ISH2 left	cagcttcagaagggacaagg
	Lrrk2-ISH2 right	cagctggactgacagagacg
Lrrk2-ISH3	Lrrk2-ISH3 left	tgctctgtccactctcttgg
	Lrrk2-ISH3 right	gcaggctctctctagcatgg
Lrrk2-ISH4	Lrrk2-ISH4 left	cctgggattcagaaatgtgg
	Lrrk2-ISH4 right	ctgataccggagcactttcc
Lrrk2-ISH5	Lrrk2-ISH5 left	tgagctgaaaaacaccatgc
	Lrrk2-ISH5 right	gttccaggtggctactgagg
Lrrk2-ISH6	Lrrk2-ISH6 left	cagagcgatgatctggatagc
	Lrrk2-ISH6 right	gtgcggaagactgaaaatcg

SNCA in situ probes:

Product	Primer name	Primer Sequence (5'-3')
SNCA-ISH1	SNCA-ISH1left	ctggcagtgaggcttatgaa
	SNCA-ISH1right	gccacaacaatatccacagc
SNCA-ISH2	SNCA-ISH2/3left	gattggggaaaacaggaaga
	SNCA-ISH2right	ccttcctctgaaggcatttc
SNCA-ISH3	SNCA-ISH2/3left	gattggggaaaacaggaaga
	SNCA-ISH3right	tttgggtcttctcagccactg

Lrrk2 R1441C genotyping PCR:

Primer name	Primer Sequence (5'-3')
Lrrk2-gKI-left	gagaggaattgccaggacac
Lrrk2-gKI-rightWT	aacacaagtctcgggatgaaa
Lrrk2-gKI-rightNEO	ggggaacttctgactaggg

Lrrk2 R1441C cDNA:

Primer name	Primer Sequence (5'-3')
Lrrk2-Exon32lox-left	ttcctccccgataaacttctg
Lrrk2-Exon32lox-right	atgcaacacgaggaactgtg
Lrrk2-Exon32-left	gtgtcacacgggtgcatcttc

Lrrk2-Exon32-right-neo	gccagaggccacttgtgtag
Lrrk2-Exon32-right-WT	tcggatgattggaagacaca

Lrrk2 R1441C Southern blot probes: genotyping PCR:

	Primer name	Primer Sequence (5'-3')
Probe 5`-1	Lrrk2KI-SB5-1-left	ggaagttgagcaagatatgg
	Lrrk2KI-SB5-1-right	tccactctcctacagttgct
Probe 5`-2	Lrrk2KI-SB5-2-left	ctattaacaccccggtggttgac
	Lrrk2KI-SB5-2-right	tcgaaactgtgctagctctt
	Lrrk2KI-SB5-2a-right	aacagctcgtgtatggtgct
Probe 3`-1	Lrrk2KI-SB3-1-left	tgtgagtcatggtgactggtt
	Lrrk2KI-SB3-1-right	gtaacaaaccccaccagaa

Lrrk2 knockdown genotyping PCR:

	Primer name	Primer Sequence (5'-3')
	Lrrk2-kd-ExNeo	gttgtgccagtcatagccgaatag
	Lrrk2-kd-ExPGK	cacgcttcaaaagcgcacgctcg
	ROSA26 5'HA	aaagtcgctctgagttggtat
	ROSA26 3'HA	cacaccaggttagcctttaagcc

9.3 General abbreviations

5-HT	5-hydroxytryptamine (serotonin)
6-OHDA	6-hydroxydopamine
°C	degree Celsius
Ac	acetate
AD	Alzheimer's Disease
Amp	ampicillin
ATP	adenosine triphosphate
au	arbitrary unit(s)
bp	base pair(s)
cDNA	copy DNA
cf	compare (<i>confer</i>)
cko	conditional knockout
CMV	cytomegalovirus promotor
cpm	counts per minute
Cre	cyclization recombination enzyme (Cre recombinase)
CTP	cytidine triphosphate
DA	dopamine
DAB	3,3'-diaminobenzidine
Dat	dopamine transporter
dATP	desoxy adenosine triphosphate
dCTP	desoxy cytidine triphosphate
dGTP	desoxy guanosine triphosphate
DMEM	Dubecco's modified Eagle's medium
dNTP	desoxy nucleoside triphosphate
DOPAC	3,4-dihydroxyphenylacetic acid
DSred	trade name of the red fluorescent protein drFP583
DTT	dithiothreitol
dTTP	desoxy thymidine trisphosphate
E	embryonic day
e.g.	exempli gratia (Latin), for example (English)
<i>et al.</i>	et alii (Latin), and others (English)

EtBr	ethidium bromide
EtOH	ethanole
flp	flipase recombination enzyme
FCS	fetal calf serum
g	gram
G418	Geneticin, an analogon of neomycin
GFP	green fluoescent protein
GTP	guanosine triphosphate
h	hour
HPLC	high performance liquid chromatography
i.p.	intraperitoneally
IHC	immunohistochemistry
IMM	inner mitochondrial membrane
IMS	mitochondrial intermembrane space
IRES	internal ribosomal entry site
ISH	<i>in situ</i> hybridisation
kb	kilobase
kDa	kilodalton
kg	kilogram
Ki	knock-in
KO	knockout
l	liter
LB	lysogeny broth
LH	luteinizing hormone
loxP	locus of X-over P1
ms	millisecond
M	molar (mol/l)
μ	micro (10 ⁻⁶)
MEF	mouse embryonic fibroblast
min	minute
MPP+	1-methyl-4-phenylpyridinium ion
MPTP	1-methyl-4-phenyl-tetrahydropyridine
mRNA	messenger ribonucleic acid
mtDNA	mitochondrial DNA
n	probe number
neo	neomycin
NTP	nucleoside triphosphate
OD	optical density
o.n.	over night
P	postnatal day
PBS	phosphate buffered saline
PCR	polymerase Chain Reaction
PD	Parkinson's Disease
PFA	paraformaldehyde
pgk	phosphoglycerat kinase promotor
PMSG	pregnant mare's serum gonadotropin
PTM	posttranslational modified microtubule
RNA	ribonucleic acid
RNS	reactive nitrogen species
ROS	reactive oxygen species
RT-PCR	reverse transcriptase polymerase chain reaction
s	second
SDS	sodium dodecyle sulfat
SEM	standard error of the mean
TSA	Trichostatin A

9.4 Curriculum vitae

Name: Florian *Herbert Heinrich* Giesert
(Diplom-Biologe Univ.)

Education:

- **2006 – 2010:** Ph.D. student at the Institute of Developmental Genetics, HelmholtzZentrum Munich.
Ph.D. Thesis: *Pathogenic Mutation of Lrrk2 – a mouse model for pre-motor Parkinson’s disease*

- **1999 – 2006:** Diploma student (Biology) at the Technical University Munich.
Main subject: Genetics; Subsidiary subject: Biochemistry, Geology and Palaeontology
Final Grade: 1,3
Diploma Thesis: *Expressionsanalyse ausgewählter ESTs (Expressed Sequence Tags) und bioinformatisch vorhergesagter Gene*

- **1996 – 1998:** Diploma student (Geography) at the Ludwig-Maximilians-University Munich.

(Co-author) Publications:

- **Both Lrrk2 R1441C knock-in and Lrrk2 knockdown mice recapitulate features of pre-symptomatic Parkinson's disease.**
Giesert F*, Glasl L*, Piccoli G, Kühn R, Kloos K, Zhang J, Hafen U, Zerle J, Hofmann A, , Hölter SM, Vogt Weisenhorn DM, Wurst W. *Manuscript in preparation.*
- **Pink1-deficiency in mice recapitulates symptoms of the early phase of Parkinson's disease.**
Glasl L*, Kloos K*, Giesert F*, Roethig A, di Benedetto B, Kühn R, Zhang J, Hafen U, Zerle J, Hofmann A, Winklhofer KF, Hölter SM, Vogt Weisenhorn DM, Wurst W. *Exp Neurol, under review.*
- **LRRK2 Controls Synaptic Vesicle Storage and Mobilization within the Recycling Pool.**
Piccoli G, Condliffe SB, Bauer M, Giesert F, Boldt K, De Astis S, Meixner A, Sarioglu H, Vogt-Weisenhorn DM, Wurst W, Gloeckner CJ, Matteoli M, Sala C, Ueffing M (2011). *J Neurosci.* 31(6), 2225-2237.
- **DJ-1-deficient mice show less TH-positive neurons in the ventral tegmental area and exhibit non-motoric behavioural impairments.**
Pham TT, Giesert F, Röthig A, Floss T, Kallnik M, Weindl K, Hölter SM, Ahting U, Prokisch H, Becker L, Klopstock T, Hrabé de Angelis M, Beyer K, Görner K, Kahle PJ, Vogt Weisenhorn DM, Wurst W (2010). *Genes Brain Behav.* 9(3), 305-17.
- **A powerful transgenic tool for fate mapping and functional analysis of newly generated neurons.**
Zhang J, Giesert F, Kloos K, Vogt Weisenhorn DM, Aigner L, Wurst W, Couillard-Despres S (2010). *BMC Neurosci.* 11, 158.

Poster presentations at international conference:

- *9th International Conference AD/PD 2009. Prague, Czech Republic, March 11-15, 2009:*
Generation and Analysis of the R1441C Lrrk2 knock-in Mouse Model.
Giesert F, T. Pham TT, Röthig A, Zhang J, Vogt-Weisenhorn D, Wurst W..
- *Annual Conference of the German Genetics Society (GfG) – Genetics of Ageing. Jena, Germany, October 11-13, 2007.*
Comparative Analysis of Lrrk1 and Lrrk2 Expression in the Developing and Adult Mouse Brain.
Giesert F, Pham TT, Röthig A, Zhang J, Vogt-Weisenhorn D, Wurst W.

9.5 Acknowledgments

- First of all I want to thank my supervisor *Prof. Dr. Wolfgang Wurst* for giving me the opportunity doing my *Ph.D* in his institute and for his support during all that time.
- As well, many thanks to my second supervisor, *Dr. Daniela Vogt-Weisenhorn* for all her support and sympathy.
- Thanks to *Lisa Glasl* and *Dr. Sabine Hölter-Koch* for the behavioural analysis of the *Lrrk2* mouse lines.
- Thank you to *Dr. Giovanni Piccoli* for the nice collaboration in the *in vitro* analysis of *Lrrk2* function.
- Thanks to *Dr. Holger Prokisch* for his participation in the initiation and planing of the *Lrrk2* targeting construct.
- Thank you to *Dr. Ralf Kühn* and the transgenic unit for performing the blastocyst injections and providing us the *Lrrk2* knockdown mouse line
- Last but not least, thanks to *virtually all my colleagues* I got to know during the last years in and out of the institute for all their help and amity.

10 Selbstständigkeitserklärung

Florian Giesert
Arcisstrasse 54
80799 München

München, den _____

Sehr geehrte Damen und Herren,

hiermit erkläre ich, Florian Giesert dass die eingereichte Dissertation meine erste ist. Es gab keinen früheren Versuch eine Dissertation einzureichen oder sich einer Doktorprüfung zu unterziehen.

Ferner erkläre ich, dass die vorliegende Dissertation selbstständig und ohne unerlaubte Hilfe angefertigt worden ist. Die Dissertation wird vollständig eingereicht und wurde nicht einer anderen Prüfungskommission vorgelegt.

Florian Giesert